METHODS OF CALCULATING AERODYNAMIC LOADS ON AIRCRAFT STRUCTURES: PART I - WING-BODY INTERFERENCE EFFECTS

CHRISTOPHER J. BORLAND
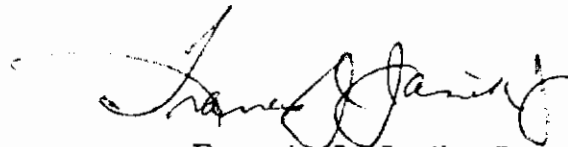
MASSACHUSETTS INSTITUTE of TECHNOLOGY

FOREWORD

This publication constitutes the first part of a three-part final report prepared under USAF Contract No. AF 33 (615)-2291. The contract was initiated under Project No. 1367, Task No. 136715. The work was performed at the Aerophysics Laboratory, Massachusetts Institute of Technology, for the Air Force Flight Dynamics Laboratory, Research and Technology Division. Mr. Charles E. Jobe monitored the project for the Air Force. The M.I.T. faculty supervisor was Prof. Morton Finston, and Dr. Leon H. Schindel was Principal Investigator. Numerical work was carried out by the author at the Computation Center, Massachusetts Institute of Technology, with the assistance of J.M. Davis and Mrs. Edith Sandy.

This report covers work conducted from October 1964 to January 1966.

The manuscript of this report was released by the author January 1966 for publication as a RTD Technical Report.

This technical report has been reviewed and is approved.

Francis J. Janik, Jr.
Chief, Theoretical Mechanics Branch
Structures Division

ii

ABSTRACT

Methods are proposed for calculating the distribution of aerodynamic loads due to mutual interference effects between wings and bodies. The methods fall into two ranges of applicability: linear, and nonlinear, with angle of attack.

Applicability of the linear loads methods to aeroelastic calculations is discussed. A computer program is presented which may be used to calculate interference loads at subsonic Mach numbers on a configuration consisting of (1) a body of any varying elliptic cross section and camber distribution, and (2) a wing with straight leading and trailing edges of any sweep angle, twist distribution, and camber distribution, located above or below the body centerline. Extension to the supersonic case is indicated. Generally good agreement with experimental data is found.

Nonlinear wing-body interference loads are also considered. Several possible methods of representing the separated flow about a wing-body combination are proposed, and analyzed by the slender body theory. Numerical procedures are outlined, and some comparisons with experimental data are made. Agreement is somewhat less than satisfactory.

Recommendations are made for further analytic extensions and improvements, and for additional experimental studies.

CONTENTS

CONTENTS (Continued)

ILLUSTRATIONS

ILLUSTRATIONS (Concluded)

SYMBOLS

$a_{\nu\eta}$ coefficients defined by Eq. (58)

a horizontal semi-axis of elliptic body

arg argument of complex number

AR aspect ratio

A_r coefficients defined by Eq. (87)

b vertical semi-axis of elliptic body

b wing total span

$b(\theta)$ wing local span

b' vortex span

$b_{\nu\nu}$ coefficients defined by Eq. (60)

$b_{\nu\eta}$ coefficients defined by Eq. (62)

$B_{\nu\eta}$ coefficients defined by Eq. (61)

$B(x)$ base area at x

c wing chord

c_r root chord

$c(y)$ local chord

c_ν local chord at the ν-th spanwise station

c_l section lift coefficient

C_L total lift coefficient

C_{L_α} lift curve slope at zero angle of attack

C_p pressure coefficient

C_m pitching moment coefficient

$F_{r,n}$ function defined by Eq. (88)

ix

F force

F function defined by Eq. (176)

f_i transformation factor, defined by Eq. (27)

$f(\theta_n)$ chordwise distribution of effective angle of attack (see Eq. 28)

$\bar{f}_{n\mu}$ coefficients defined by Eq. (66)

$g(x)$ chordwise loading parameter, defined by Eq. (24)

$\bar{g}_{\nu n}$ coefficients defined by Eq. (59)

G nondimensional vortex strength in Weissinger's procedure

G_0, G_1 functions defined by Eq. (184) and (186)

H one-half the distance between trailing elements of horseshoe vortex image

H_0, H_1 functions defined by Eq. (195) and (193)

$H(\theta, \tau)$ function defined by Eq. (87)

H_r function defined by Eq. (90)

i $\sqrt{-1}$

$I.P.$ imaginary part of complex number

ℓ elliptic parameter

ℓ integration constant in Eq. (73)

ℓ_n function defined by Eq. (88)

$\ell(x)$ chordwise loading parameter for slender wing, Eq. (25)

K source strength

L lift

$L(\xi, \tau)$ distribution function defined by Eq. (56)

$L_{\nu\mu}^{*}$ coefficients defined by Eq. (63)

SYMBOLS (Continued)

ℓ	body length
m	number of spanwise stations on the wing
M	number of trapezoidal integration intervals
M_∞	free stream Mach number
n	summation index
N	number of chordwise stations up to trailing edge
N_1	number of chordwise stations behind trailing edge
$N(x)$	normal force up to X
q	dynamic pressure $= \dfrac{\rho}{2} U_\infty^2$
r	circular body radius
r	elliptic parameter
$R.P.$	real part of complex number
S_i	velocity due to a source
s	exposed wing semi-span
s'	transformed local semi-span
t	nondimensional spanwise coordinate
t	complex variable, physical plane $= y + i z$
$\bar{t}$	complex variable, transformed plane
U_∞	free stream velocity
u	X-component of velocity perturbation
v	y-component of velocity perturbation
V_φ^*	complex flow velocity relative to vortex at s
w_η	vertical component of velocity in cross flow plane

w z-component of velocity perturbation

w upwash velocity

W_φ complex velocity at the vortex at φ

x streamwise coordinate

x_{CP} streamwise center of pressure location

x_{LE} streamwise coordinate of leading edge root

x_{TE} streamwise coordinate of trailing edge root

x_{AFT} streamwise coordinate of aft end of body

X complex variable, circle plane $= y + iz$

X_0 vortex location

X_1 image vortex location

y spanwise coordinate

y_i spanwise coordinate of i-th station

z vertical coordinate

α angle of attack

α_0 average body angle of attack

α_B local body angle of attack

$\alpha(y)_{eff}$ spanwise distribution of effective angle of attack

β $\sqrt{1 - M_\infty^2}$

Γ vortex strength

γ strength of vortex sheet element

δ cone semi-vertex angle

ϵ wing semi-vertex angle

ς	complex variable, elliptic plane $= \xi + i\eta$
ς_0, ς_1	vortex locations, wing and body
$\varsigma_0', \varsigma_1'$	separation point locations, wing and body
η	spanwise coordinate
η	vertical coordinate, elliptic plane
ϑ	chordwise distance parameter
ϑ_n	chordwise distance parameter $= \dfrac{n\pi}{m+1}$
ϑ	complex variable $= y + iz$
ϑ_0, ϑ_1	vortex locations
$\vartheta_0', \vartheta_1'$	separation point locations
λ_i	spanwise coordinate of center of box
Λ	leading edge sweep angle
$\Lambda_{c/4}$	quarter-chord sweep angle
μ, μ_1	summation index
ν	summation index
ξ	streamwise coordinate
ξ	spanwise coordinate, elliptic plane
ρ	density
σ	complex variable $= y' + iz'$
τ	nondimensional spanwise coordinate $= \dfrac{\eta}{b/2}$
τ_ν	nondimensional spanwise coordinate $= \cos\dfrac{\nu\pi}{m+1}$
$\bar{\tau}_\mu$	nondimensional spanwise coordinate $= \cos\dfrac{\nu\pi}{M+1}$
ϕ	complex potential function

SYMBOLS (Concluded)

ϕ_s complex potential of source

$\phi_{(3-D)}$ three dimensional complex potential

ϕ velocity potential

ϕ_o effective dihedral of transformed wing

ϕ_η spanwise coordinate parameter $= \cos^{-1}\tau_\eta$

$\bar{\phi}_\mu$ spanwise coordinate parameter $= \cos^{-1}\bar{\tau}_\mu$

ψ stream function

SECTION

INTRODUCTION

A recent evaluation of procedures for calculating aerodynamic load distributions for structural design (Ref. 1) has revealed significant inadequacies in available methods of predicting loads due to wing-body interference effects. The methods of former years, useful for low-speed aircraft with high aspect-ratio wings, are not readily applicable to today's high-speed low aspect-ratio aircraft and missiles. The various methods developed in recent years to handle such configurations (Refs. 2, 3, 4) may predict total loads successfully, but not load distributions, which are of primary interest to the structural designer. Other methods are not able to handle sufficiently general configurations (Ref. 5), or are not readily adaptable to aeroelastic calculations. Treatment of nonlinear interferences effects is similarly inadequate.

The present report seeks to make extensions and refinements to some of these methods, and develop new ones where needed, with a view toward presenting a unified procedure for calculating complete load distributions for combinations of general body shape and wing geometry.

1

SECTION II

BACKGROUND AND PRESENT CONTRIBUTION

This report will not attempt to present a complete history of wing-body interference calculations. The two surveys of Refs. 6 and 7 give summaries of many of the important theories. The method by Ferrari, for supersonic calculations, is essentially complete in Ref. 7. What will be presented here is an outline of the theories that have seemed most promising for extension and refinement.

The load on a wing-body combination due to interference effects may be defined as the total load on the combination, minus the sum of the load that would exist on the wing alone and on the body alone under the same flight conditions. This interference load may be divided into two parts: the additional load on the wing due to the presence of the body, and the additional load on the body due to the presence of the wing. The most promising method for calculating the distribution of interference load on the wing due to the presence of the body is the method of Gray and Schenk (Ref. 5), which is based upon the earlier work of Lennertz (Ref. 8). In this method, the load distribution on the wing is found by any convenient method, and replaced by a set of lifting horseshoe vortices. The body is then replaced by the images of these vortices so placed as to satisfy the boundary condition of no flow through the body surface. The interference load on the wing is then calculated by assuming an additional angle of attack distribution on the wing, which is just the upwash due to the image vortices, plus the upwash due to the flow about the body itself. This method gives fairly accurate results for the configurations to which it may be applied. The basic assumptions made are that 1) the body is infinitely long and straight, and 2) the body is of uniform circular cross-section.

The interference load on the body due to the presence of the wing is also known as the "body carry-over" lift because of the tendency of the wing to block the flow around the body and thus "carry" the lift back on to the body. It has, in the past, been calculated by slender body theory. A more promising approach is the "slender configuration" theory proposed in Ref. 6. This theory is, in fact, a modification of the method of Lawrence for calculating the distribution of lift on low aspect-ratio subsonic wings (Ref. 9). In Lawrence's method, an elliptic lift distribution is assumed in the spanwise direction, and the resulting one-dimensional integral equation is solved for the lift distribution in the chordwise direction. The axial lift distribution on the body is then found by evaluating the chordwise distribution at the wing centerline.

The portion of the body behind the wing is influenced not by the blocking of flow by the wing, but by the trailing sheet of vorticity which was generated by the wing lift. Multhopp's method (Ref. 7) is based on the

3

influence of this vortex sheet, but is limited to 1) infinitely long bodies of uniform cross section, 2) high aspect ratio unswept wings, and 3) very small angles of attack. Furthermore, it does not take account of the tendency of the vortex sheet to roll up into a pair of vortices located near the wing tips. Thus a method which overcomes these restrictions must be found.

The methods considered in this section have all been derived for use in subsonic flow calculations, and in the remainder of this report will be considered as limited to such work. However, many of the procedures are easily adaptable for use in supersonic calculations, and where this is feasible, the possible adaptations will be discussed.

The contributions of this report to wing-body interference theory may be summarized as follows: 1) specification of the general aeroelastic problem for a wing-body combination; 2) extension of the method of Gray and Schenk to bodies of elliptical cross section; 3) adaptation of the method of Lawrence and Flax (Ref. 6) for use in the general aeroelastic problem; 4) development of a method for calculating the effect of the vortex wake on the body, 5) development of numerical procedures for the above theories. In addition, the nonlinear effects of vortex separation on wing-body interference have been examined, and numerical procedures developed for their calculation.

The final sections of this report contain some comparisons of the theories with experimental data, and some suggestions for further study.

4

SECTION III

LINEAR WING-BODY INTERFERENCE LOADS

A. SPECIFICATION OF THE AEROELASTIC PROBLEM

In many of the earlier analyses of flight vehicles, the structure was assumed rigid, and thus had no effect on the determination of aerodynamic loads other than through the exterior shape of the vehicle. In modern structural design, however, aerodynamic analyses are usually only useful if they are applicable to the total aeroelastic problem. This may be stated as the determination of the final loads on and deflections of a deformable structure, which is subject to loads which change its aerodynamic shape, which in turn changes the loads, etc. Gray and Schenk (Ref. 5) present a matrix solution to the static aeroelastic problem for an airplane-type vehicle. Section II of Ref. 1 outlines how various aerodynamic theories may be used as input to such a solution. Since the aerodynamic methods of this report are concerned basically with this type of configuration, the methods will be specified with the aeroelastic solution in mind.

It is possible to specify the treatment of the aeroelastic problem of a wing-body combination in several ways. For example, the wing and the body may be handled separately or together in the calculation of loads and deflections. The aerodynamic input may be generated by considering the structure to be deflected in its natural mode shapes and finding the resulting loads, or by dividing the structure into "boxes" or grid elements, considering the load on one box due to the deflection of another, and superposing solutions. Each of these possible choices has inherent advantages and disadvantages. Using mode shape methods, good accuracy may be obtained with small numerical storage requirements, whereas box methods, which may include inversion of large aerodynamic influence coefficient matrices, require large amounts of numerical storage to obtain accurate results. On the other hand, some knowledge of the structure to be treated is necessary in the use of mode shape methods, while box methods may treat any configuration independent of any structural information. Investigation has shown that the current trend in the aircraft industry is toward the use of box methods, rather than mode shapes, especially for static aeroelastic calculations. Thus the methods under consideration here will be based on a box-type representation of the vehicle.

The choice of whether to treat the wing and body separately or together is less clearly defined. There seems to be no obvious trend either way in current industrial practice. Furthermore, box methods are less readily adaptable to a simultaneous treatment of the wing and the body, as the deflection of a single "box on the body" has relatively little physical significance. Methods will be chosen, therefore, which treat the wing and body separately, but which may be used for an aeroelastic treatment of the entire configuration.

Another inherent advantage of the box representation of the vehicle is that once the method is established for use in the aeroelastic problem, it may easily be adapted for analyses of generally cambered and twisted wings and cambered bodies, for the configuration used for generating aerodynamic input to the aeroelastic problem is just a special case of the general camber distribution. The only limit on the generality of twist or camber that may be treated is the number of boxes used, as the angle of attack is treated as constant over the area of each box.

B. EFFECT OF THE BODY ON THE WING

1. Method of Gray and Schenk

The method of Gray and Schenk (Ref. 5) is used to calculate the effect of the presence of an infinitely long circular body on the load distributions over a wing. It assumes that the spanwise loading on the wing alone is known along with the corresponding center of pressure distribution. The wing alone is defined to be the "exposed" wing as shown in the sketch below:
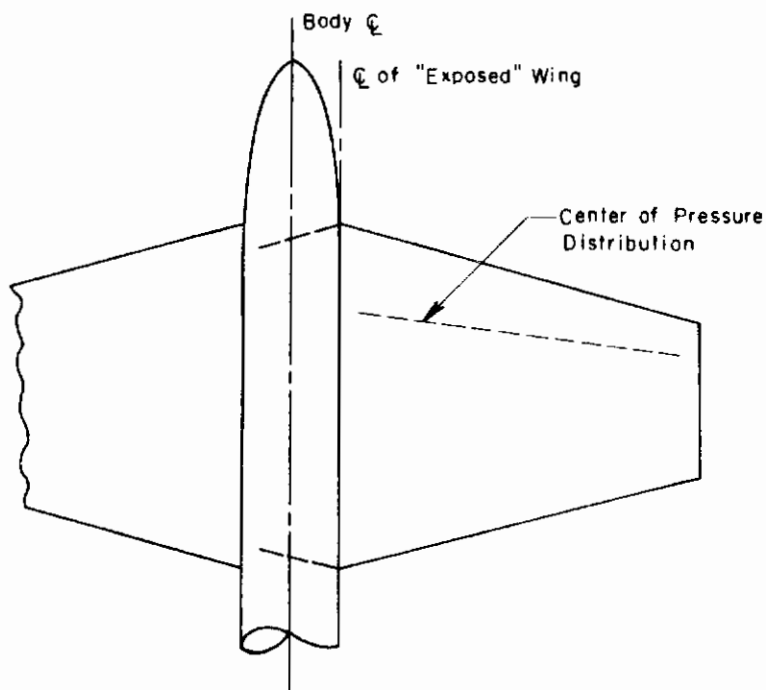
The following sketch shows typical plots of a wing spanwise loading and center of pressure.

Lift per Unit Span ----- .

$x_{c.p.}$

y

x
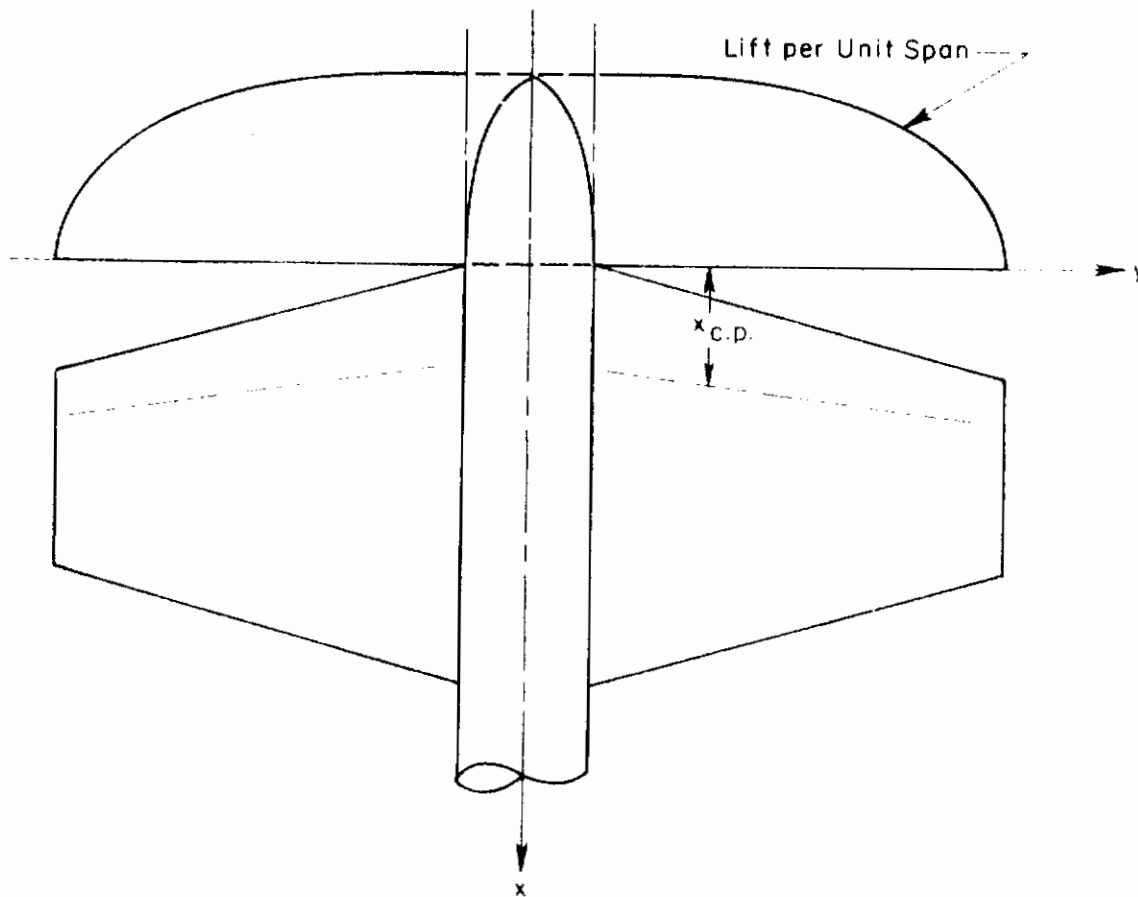
The calculation of wing load due to fuselage interference is carried out in six steps.

a. Subdivide the spanwise load distribution on the wing alone into a number of load increments.

b. Replace these step increases in load by lifting horseshoe vortices.

c. Locate the image vortices within the body.

d. Calculate the upwash distribution due to these image vortices at control points on the wing.

e. Add the upwash due to fuselage angle of attack (if any).

f. Compute the wing load due to the total distribution of upwash at certain control points on the wing. The location of the control points is a consequence of the theory used to calculate the lift distribution on the wing alone.

The extension of this theory to elliptic bodies includes the circular body as a special case.

2. Extension to Bodies of Elliptical Cross-Section

a. Description of the Method

In order to adapt the method for use with bodies of elliptical cross-section, it is necessary to find the equivalent vorticity distribution which will satisfy the boundary condition on the surface of the

7

elliptical body. As an approximation to the problem, the vorticity distribution will be replaced by a pair of image vortices within the interior of the ellipse. This approximation gives correct results for the limiting cases of the ellipse reducing to a vertical straight line and to a circle. It is felt, therefore, that for ellipses with the major axis oriented parallel to the cross-flow direction, this approximation should be a reasonable one. For ellipses oriented normal to the cross-flow, the condition of Eq. (6) below insures approximately correct results.

Some calculations of the size of the errors involved in neglecting the additional vorticity distribution (which may be considered as distributed over the body) have been made. The procedure is outlined and the results are given below.

When the complete system of image vortices is found, the well-known solution for the two-dimensional cross-flow about an elliptical body is added to account for the upwash induced by the body angle of attack

b. Calculation of the Image Vortex Positions

The positions of the image vortices within the ellipse may be found by considering the image vortices within a circle, and by a transformation which maps the circle onto the appropriate ellipse, finding the transformed position of the vortices (see sketch below).
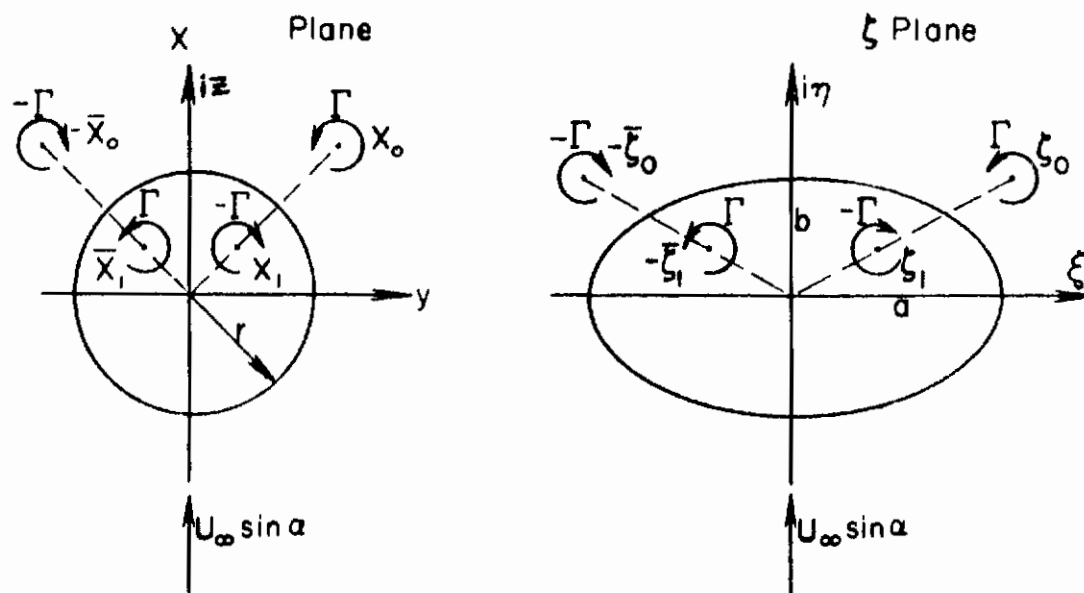
Consider a circle of radius r in the X-plane with a pair of external vortices symmetrically located at X_o and $-\bar{X}_o$, where $X = y + iz$, and bars denote the complex conjugate of quantities. This circle may be transformed to an ellipse in the $\mathcal{S}$ plane by applying the Joukowsky transformation

$$\mathcal{S} = X + k^2/X \qquad (1)$$

where $\mathscr{S} = \xi + i\eta$ and K^2 is the parameter defining the shape and orientation of the ellipse. The horizontal axis becomes $a = r + K^2/r$, and the vertical axis becomes $b = r - K^2/r$.

The external vortices at X_o and $-\overline{X_o}$ in the X plane transform to vortices at $\mathscr{S}_o$ and $-\overline{\mathscr{S}_o}$ in the $\mathscr{S}$ plane, where

$$\mathscr{S}_o = X_o + K^2/X_o \tag{2}$$

The image vortices in the X plane are located at X_1 and $-\overline{X_1}$, where

$$|X_1| = r^2/|X_o|$$

and $arg(X_1) = arg(X_o)$
That is, $X_1 = r^2/\overline{X_o}$
Since the inverse transformation is

$$X = \tfrac{1}{2}\left(\mathscr{S} \pm \sqrt{\mathscr{S}^2 - 4K^2}\right), \tag{3}$$

The positions of the image vortices become $\mathscr{S}_1$, and $-\overline{\mathscr{S}_1}$, where

$$\mathscr{S}_1 = X_1 + \frac{K^2}{X_1} = \frac{r^2}{\overline{X_o}} + \frac{K^2 \overline{X_o}}{r^2}$$

and $\mathscr{S}_o$ is given in terms of X_o by Eq. (3). Hence

$$\mathscr{S}_1 = \frac{r^4 + \tfrac{1}{4}K^2\left(\overline{\mathscr{S}_o} + \sqrt{\overline{\mathscr{S}_o}^2 - 4K^2}\right)^2}{\tfrac{1}{2}r^2\left(\overline{\mathscr{S}_o} + \sqrt{\overline{\mathscr{S}_o}^2 - 4K^2}\right)} \tag{4}$$

The positive radical has been chosen as this gives the correct position for the image vortex for the case when $K = 0$ (circle). Note that care must be used when taking the square root of the quantities including the complex conjugate $\overline{\mathscr{S}_o}$.

The image vortex position in the $\mathscr{S}$ -plane may be found in the above manner only when the image vortex in the X -plane would appear in the region between a circle of radius K about the origin and the circle of radius r . Otherwise, the transformed position of the image vortex, while it may appear within the interior of the ellipse, will be on the wrong Riemann sheet, and cannot therefore be used in calculating the downwash. Since the image vortices closer to the center of the circle have a much smaller contribution than those closer to the surface, they will simply be ignored.

This condition on the position of the image vortices in the X-plane may be stated as

$$|k| < |X| < r$$

Since $\quad |X_1| = r^2/|X_0|$

$$|X_0| = \frac{r^2}{|X_1|} \le \frac{r^2}{|k|}$$

(5)

The external vortices, then, must appear inside a circle of radius $r^2/|k|$ in the X-plane. This circle may be transformed to an ellipse in the $\mathcal{S}$-plane by the transformation $\mathcal{S} = X + k^2/X$. The horizontal axis of this ellipse is $a = r^2/|k| + (k^2/r^2)|k|$ and the vertical axis is $b = r^2/|k| - (k^2/r^2)|k|$. Thus

$$\frac{\xi_0^2}{\left(\frac{r^2}{|k|} + \frac{k^2}{r^2}|k|\right)^2} + \frac{\eta_0^2}{\left(\frac{r^2}{|k|} - \frac{k^2}{r^2}|k|\right)} \le 1$$

(6)

since $\mathcal{S}_0 = \xi_0 + i\eta_0$ is the position of the external vortex. If this condition is not satisfied by the coordinates ξ_0, η_0 of the external vortex in the $\mathcal{S}$-plane, the image vortex does not exist.

c. Calculation of Error Due to Image Vortex Approximation

If the flow about a two-dimensional circular cylinder due to a pair of symmetrically placed external vortices of strength $\mathcal{L}$ is considered, the complex potential may be written:

$$\phi(X) = -\frac{i\mathcal{L}}{2\pi} \ln(X - X_0) + \frac{i\mathcal{L}}{2\pi} \ln(X + \bar{X}_0) + \frac{i\mathcal{L}}{2\pi} \ln(X + \bar{X}_1) - \frac{i\mathcal{L}}{2\pi} \ln(X - X_1)$$

(7)

The circular cylinder has been replaced by a pair of image vortices as discussed above. The notation is defined in the sketch on page 8.

If the circle is transformed into an ellipse by the transformation $X = \frac{1}{2}(\mathcal{S} + \sqrt{\mathcal{S}^2 - 4k^2})$ the complex potential will contain terms due to the transformed external vortices, the transformed image vortices, and additional distributed vorticity. If only the flow due to the image vortices and the distributed vorticity is considered, the complex potential may be written, after some algebra, as

10

$$\phi_1(\mathcal{Y}) = \frac{-i\Gamma}{2\pi} \ln\left(1 + \frac{\sqrt{\mathcal{Y}^2 - 4K^2} - \sqrt{\mathcal{Y}_0^2 - 4K^2}}{\mathcal{Y} - \mathcal{Y}_0}\right) + \frac{i\Gamma}{2\pi} \ln(\mathcal{Y} - \mathcal{Y}_1)$$

$$+ \frac{i\Gamma}{2\pi} \ln\left(1 + \frac{\sqrt{\mathcal{Y}^2 - 4K^2} - \sqrt{\mathcal{Y}_1^2 - 4K^2}}{\mathcal{Y} - \mathcal{Y}_1}\right)$$

$$+ \frac{i\Gamma}{2\pi} \ln\left(1 + \frac{\sqrt{\mathcal{Y}^2 - 4K^2} + \sqrt{\bar{\mathcal{Y}}_0^2 - 4K^2}}{\mathcal{Y} + \bar{\mathcal{Y}}_0}\right)$$

$$- \frac{i\Gamma}{2\pi} \ln(\mathcal{Y} + \bar{\mathcal{Y}}_1) - \frac{i\Gamma}{2\pi} \ln\left(1 + \frac{\sqrt{\mathcal{Y}^2 - 4K^2} + \sqrt{\bar{\mathcal{Y}}_1^2 - 4K^2}}{\mathcal{Y} + \bar{\mathcal{Y}}_1}\right)$$

$$(8)$$

The complex potential due to the image vortices alone may be written

$$\phi_2(\mathcal{Y}) = \frac{i\Gamma}{2\pi} \ln(\mathcal{Y} - \mathcal{Y}_1) - \frac{i\Gamma}{2\pi} \ln(\mathcal{Y} + \bar{\mathcal{Y}}_1) \qquad (9)$$

In order to estimate the size of the errors involved in neglecting the distributed vorticity, the downwash in the $\eta = 0$ plane due to the images of external vortices located in the $\eta = 0$ plane will be calculated from the exact potential $\phi_1(\mathcal{Y})$ and the approximate potential $\phi_2(\mathcal{Y})$. Since

$$\frac{\partial \phi}{\partial \mathcal{Y}} = \mathcal{V} - i\omega, \qquad \omega = -I_m\left(\frac{\partial \phi}{\partial \mathcal{Y}}\right) \qquad (10)$$

For the transformed images alone:

$$W_{image} = \frac{-\Gamma}{2\pi}\left(\frac{1}{\xi - \xi_1}\right) + \frac{\Gamma}{2\pi}\left(\frac{1}{\xi + \xi_1}\right), \quad \text{since}$$

$$\mathcal{Y}_0 = \bar{\mathcal{Y}}_0 = \xi_0, \quad \mathcal{Y}_1 = \bar{\mathcal{Y}}_1 = \xi_1 \quad \text{when} \quad \eta = 0$$

$$(11)$$

11

For the transformed images plus the distributed vorticity:

$$W_{exact} = \frac{-\Gamma}{2\pi}\left\{ \frac{1}{\xi - \xi_1} - \left(\frac{1}{1 + \dfrac{\sqrt{\xi^2 - 4\kappa^2} - \sqrt{\xi_0^2 - 4\kappa^2}}{\xi - \xi_0}} \right) \times \right.$$

$$\times \left(\frac{(\xi - \xi_0)(\xi^2 - 4\kappa^2)^{1/2}\xi - (\sqrt{\xi^2 - 4\kappa^2} - \sqrt{\xi_0^2 - 4\kappa^2})}{(\xi - \xi_0)^2} \right)$$

$$+ \left[\left(\frac{1}{1 + \dfrac{\sqrt{\xi^2 - 4\kappa^2} - \sqrt{\xi_1^2 - 4\kappa^2}}{\xi - \xi_1}} \right) \left(\frac{(\xi + \xi_0)(\xi^2 - 4\kappa^2)^{1/2}\xi - (\sqrt{\xi^2 - 4\kappa^2} + \sqrt{\xi_0^2 - 4\kappa^2})}{(\xi + \xi_1)^2} \right) \right]$$

$$\left[\left(\frac{1}{1 + \dfrac{\sqrt{\xi^2 - 4\kappa^2} - \sqrt{\xi_1^2 - 4\kappa^2}}{\xi + \xi_1}} \right) \left(\frac{(\xi + \xi_1)(\xi^2 - 4\kappa^2)^{1/2}\xi - (\sqrt{\xi^2 - 4\kappa^2} + \sqrt{\xi_1^2 - 4\kappa^2})}{(\xi + \xi_1)^2} \right) \right]$$

$$\left. - \left(\frac{1}{\xi + \xi_1} \right) \right\} \tag{12}$$

The magnitude of the difference between the exact and approximate downwash expressions will be normalized with respect to the magnitude of the crossflow, $U_\infty\alpha$, for an ellipse which has been formed by transforming a cylinder of unit radius. The vortex strength, Γ will be approximated by the strength of a single equivalent lifting vortex, $\Gamma = L/\rho U_\infty$. Thus

$$\frac{\Gamma}{r} = \frac{U_\infty\alpha}{2}\frac{dC_L}{d\alpha} \cdot 1.25 \frac{b'}{r}\frac{1}{AR} \tag{13}$$

where the total span has been chosen as 1.25 times the vortex span b'. For the medium-to-high aspect ratio wings at subsonic speeds, the ratio of the lift curve slope to the aspect ratio is on the order of one. Thus

$$\frac{|W_{exact} - W_{approx}|}{U\alpha} \approx \left| \frac{W_{exact}}{\Gamma/2\pi} - \frac{W_{approx}}{\Gamma/2\pi} \right| \left(\frac{b'/r}{10} \right) \tag{14}$$

12

Calculations have been made for a vortex span-to-body radius ratio of 10 (which is reasonable for high aspect ratio subsonic configurations) for ellipses with various values of k, and various external vortex locations. Figure 1 shows the variation in normalized downwash for an ellipse with a major axis of 1.5, a semi-minor axis of .5, and an external vortex located a distance of .5 from the body. This approximates the maximum possible error, since, if the vortex lies at a distance greater than .50606, the image vortex does not exist. Figure 2 shows the same information for an ellipse which is nearly a circle, i.e., semi-major axis of 1.05, semi-minor axis of .95, and external vortex locations of .50, 1.0 and 3.5 from the body (ξ = 1.45, 1.95 and 4.45). It may be seen, in general, that the errors are much less severe for a body which is nearly a circle, and, for a given body, for external vortex locations which are inboard.

d. Calculation of the Downwash

The load distribution over the wing due to the presence of the body is found by the following steps:

1. Replace the true spanwise loading $L(y)$ by an arbitrarily divided stepwise approximation (see sketch below).
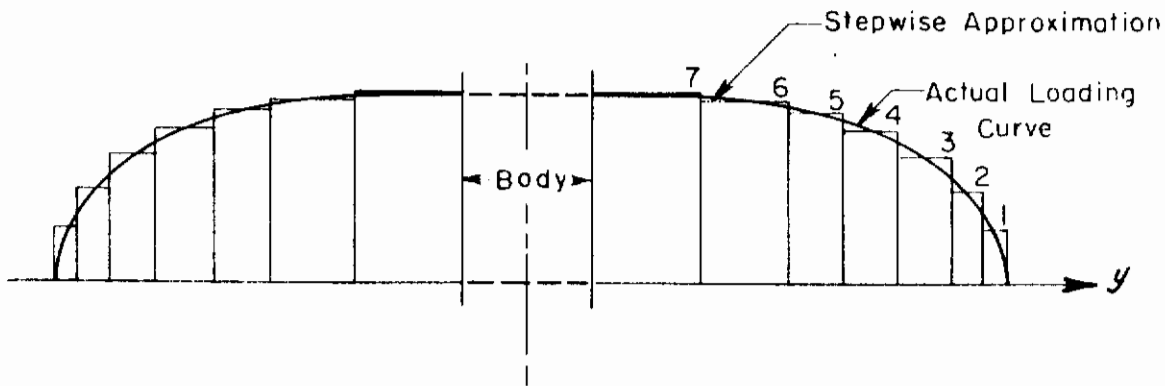
2. Replace each increment in spanwise loading by a horseshoe vortex of strength

$$\Gamma_i = \frac{1}{\rho U}\left(\frac{dL}{dy}\right)_i \tag{15}$$

(See sketch on the following page)
where ρ = free stream density
U = free stream velocity.

13
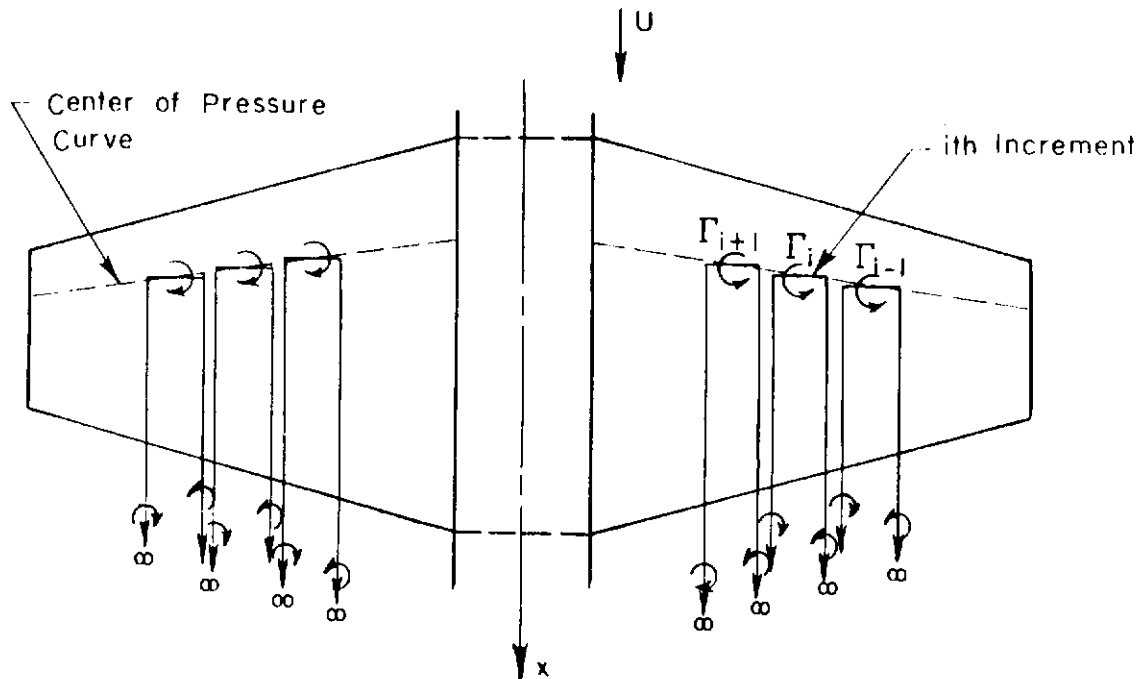
3. Find the positions $\mathcal{S}_{o_i}$ of the external trailing vortices, (see sketch below).
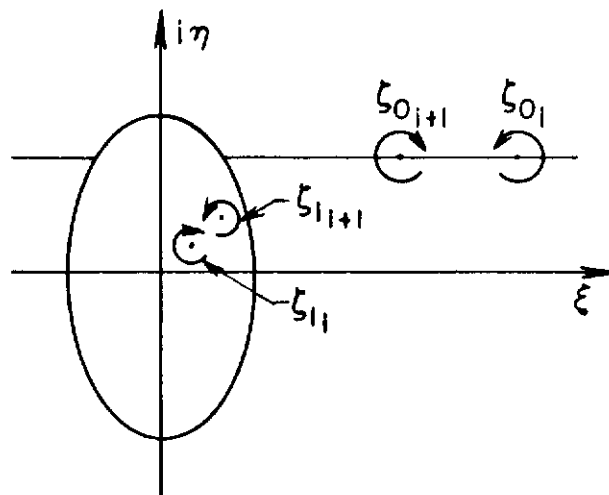
4. See if the positions $\mathcal{S}_{o_i}$ satisfy Eq. (6) and ignore those which do not.

5. Find the positions $\mathcal{S}_{i_i}$ of the image vortices by Eq. (4).

6. Connect the starting points of each pair of image vortices with a straight vortex segment approximating the image of the bound portion of the horseshoe vortex. The image vortex is assumed to begin at the same

14

axial station as the external wing vortex. The bound portion of the external horseshoe vortex is located at the local center of pressure.

7. Calculate the downwash at specified control points on the wing due to each pair of image vortices on both sides of the body.

8. Calculate the downwash induced by the angle of attack of the body.

The equations for the upwash at an arbitrary point on the wing due to the elements of the image of a horseshoe vortex and the body may be seen in Eqs. (IV-123) of Ref. 1. Note that if downwash is to be calculated the signs must be reversed.

The control points at which the downwash is calculated are chosen along a line which is one-half the local chord behind the center of pressure at each spanwise station. (The justification and consequences of this choice are discussed in the next section). The local flow angles are then determined by adding the contributions of all image vortices plus the body downwash. The spanwash angle distribution, resulting from the downwash divided by the free stream velocity, is assumed to be uniform in the chord-wise direction. Hence, the additional distribution of wing load due to wing body interference is obtained by applying one of the procedures of Ref. 1 (or other suitable methods for calculating lift distributions on wings) to this effectively twisted wing.

3. Use in Various Mach Number Regimes

For high aspect ratio subsonic wings, the method for calculating lift distributions which has proven to be the simplest to use, consistent with obtaining sufficient accuracy, is that due to Weissinger, with compressibility effects accounted for by the Prandtl-Glauert rule. For low aspect ratio subsonic wings, the Lawrence method, with the Prandtl-Glauert correction, may be used. Transonic wings may be treated by Jones' theory. Supersonic wings may be analyzed by application of the linear supersonic theory. Summaries of these theories, along with the numerical procedures to be used in their application, are given in Ref. 1.

Compressibility effects are thus incorporated into the wing-alone loading before it is subdivided to initiate the computation of wing-body interference, if the Weissinger, Lawrence, or linear supersonic theories are used. The Jones theory is independent of Mach number.

It should be noted that the incompressible vortex solution has been used to determine the angle of attack distribution due to body interference. Thus, placing the control points at one-half chord length behind the center of pressure line is justifiable only for subsonic wings, and is strictly applicable only if the wing is flat. On subsonic wings, the center of pressure is assumed to lie at the quarter-chord, and applying the boundary condition of no flow through the wing at the three-quarter chord gives the correct two-dimensional value of lift in the limit of a wing of infinite span. In the supersonic case, the point at which a bound lifting vortex induces a downwash angle matching the local wing slope will depend on Mach number and wing geometry. Since the effects of the image of the lifting vortex will

not be large, the extension of the subsonic rule to the supersonic case should not introduce a significant error.

One modification to the method should be made for supersonic calculations, however. For configurations with short forebodies and high aspect ratio wings at high Mach numbers, the Mach cone from the body nose will intersect the wing leading edge, as shown in the sketch below.
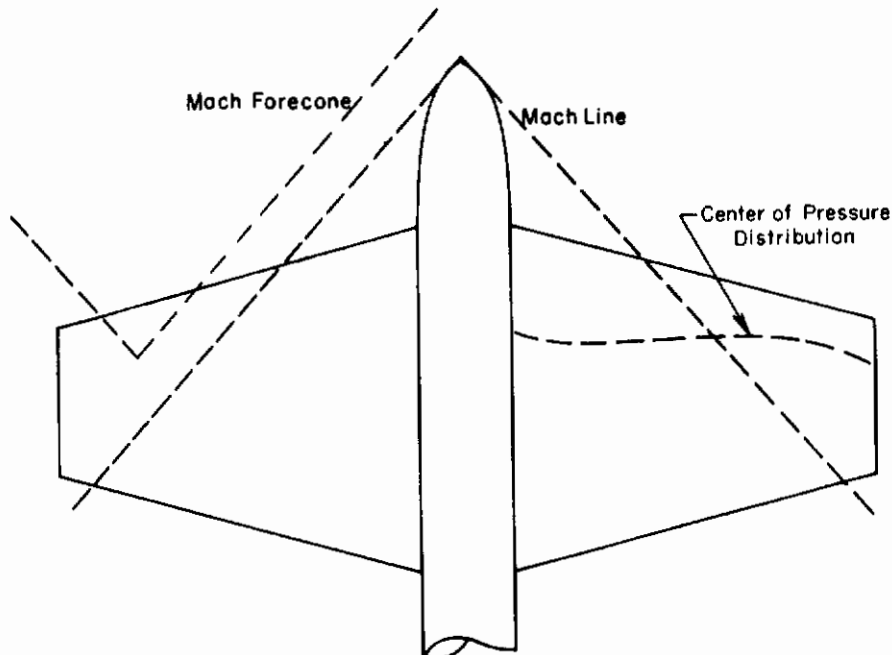
In such a case, the downwash due to the images within the body of vortices located outboard of the Mach line from the nose should be ignored. The body can have no effect on this portion of the wing, as the entire body lies outside the Mach forecone of every point on the wing located outboard of the Mach line. Similarly, the downwash at control points outboard of the Mach line is just that for the wing alone.

C. EFFECT OF THE WING ON THE BODY

1. Description of the Method

In Ref. 1, a method is described for calculating the body carry-over lift, or interference lift due to the presence of a midplane wing on a slender, circular body configuration. Slender body theory is used. This section describes a method which includes not only a better representation of the wing, but also the effect of the wake of the wing on the body. This method is applicable to configurations with bodies of varying elliptical cross-section and small general camber, with wings which may be located out of the mid-plane.

The body carry-over lift arises from two sources. The first is the blocking effect of the wing on the flow around the body. The second is the flow over the body due to the trailing vortex system in the flow field behind the wing.

The distribution of body carry-over lift is calculated in two parts. First, the segment of the body from the root of the leading edge of the wing to the root of the trailing edge is treated by an extension of the method of Lawrence (Ref. 9) for low aspect ratio subsonic wings. Compressibility effects are accounted for by a Prandtl-Glauert correction. Then the segment from the trailing edge of the wing to the aft end of the body is treated by considering the flow field due to the vortex wake of the wing. The body carry-over lift ahead of the wing is assumed negligible in the subsonic case, and zero in the supersonic case.

It should be noted that subsonic and supersonic problems will be treated by the same method. This is permitted for configurations and flight conditions where the slender body assumptions are approximately valid, since supersonic flow over a slender configuration well inside the Mach lines resembles subsonic flow. If necessary, the modified Lawrence method could be adapted to configurations not meeting these conditions by making different assumptions and transformations.

Lawrence has given a method for calculating the lift distribution on low aspect ratio subsonic wings by considering the spanwise distribution to be elliptical, and solving the resulting one-dimensional integral equation for the chordwise distribution by a numerical method. Details of the procedure of Ref. 6 for extending this method to wing-body combinations will be given below. It may be outlined as follows:
1. At each chordwise station between the leading and trailing edge of the root of the wing, transform the two-dimensional wing-body configuration to an equivalent wing plus vertical line body by a conformal mapping.
2. Calculate the chordwise lift distribution on the equivalent wing by solving Lawrence's modified integral equation.
3. Calculate the chordwide lift distribution on the original wing, and substract from the transformed wing lift to get the body carry-over lift.

The lift distribution on the aft portion of the body is calculated by assuming that the entire trailing vorticity is rolled up into a pair of concentrated vortices placed at the centroids of the vorticity distribution and beginning at the wing trailing edge. Expressions for the strength and location of this vortex pair are given below.

This approximation is, in fact, close to physical reality aft of a point approximately one or two chord lengths behind the trailing edge of the wing. It is felt, however, that allowing the single rolled-up vortex to begin at the trailing edge is a sufficiently accurate approximation. Reference 10 gives the lift distribution on a body in the presence of such a vortex. The procedure may be outlined as follows:
1. Calculate the spanwise lift distribution on the wing by any convenient means.
2. Represent this lift distribution by a single trailing vortex pair whose strength is proportional to the maximum spanwise loading and whose span produces the proper total lift.
3. Calculate the streamwise lift distribution on the body due to the presence of the vortex.

In both of the above procedures, the body carry-over lift alone is the final result. In this way, the total lift on the body may include, if desired,

17

a more accurate determination of the body-alone lift than that given by slender body theory, e.g., that given by the shock expansion method of Syvertson and Dennis, which is described in Ref. 1.

2. Body Carry-Over Lift by Lawrence's Method

The governing partial differential equation for steady irrotational incompressible flow may be solved by a superposition of elementary solutions, such as the vortex or the pressure perturbation, which satisfy the prescribed boundary conditions. For thin lifting wing problems, one approach is to replace the wing by a sheet of vorticity whose strength γ at all points ξ, η is determined such that the upwash w at a point x, y just matches the local slope of the wing, so that the boundary condition of no flow through the wing is satisfied. That is:

$$w(x, y) = -U_\infty \alpha(x, y) \tag{16}$$

where $\alpha(x, y)$ is the local slope in the streamwise direction. The upwash at a point x, y is given, in our notation, by:

$$w(x,y) = -\frac{1}{4\pi} \int_0^c \left\{ \int_{-s(\xi)}^{s(\xi)} \frac{\partial}{\partial \eta} (\gamma(\xi,\eta)) \left[\frac{1}{y-\eta} \left(1 + \frac{\sqrt{(x-\xi)^2+(y-\eta)^2}}{x-\xi} \right) \right] d\eta \right\} d\xi \tag{17}$$

assuming spanwise symmetry about the centerline.

The vortex sheet produces a discontinuity in the streamwise component of velocity over the region of the x, y plane occupied by the wing planform. The total perturbation is given by

$$\Delta u = \gamma(\xi, \eta) = u_{upper} - u_{lower} \tag{18}$$

The lifting pressure on the wing is found, by linear theory, as

$$\Delta C_p = \frac{4 u_{upper}}{U_\infty} = \frac{2 \gamma(\xi, \eta)}{U_\infty} \tag{19}$$

Thus when the integral equation for the vorticity (Eq. (17)) is solved, the distribution of lift on the wing is known. An alternate approach is to consider the pressure perturbation solution directly and write the integral equation for local upwash velocity in terms of the streamwise velocity perturbation. Thus:

$$w(x,y) = -\frac{1}{2\pi} \int_0^c \left\{ \int_{-s(\xi)}^{s(\xi)} \frac{\partial u}{\partial \eta} \left[\frac{1}{y-\eta} \left(1 + \frac{\sqrt{(x-\xi)^2+(y-\eta)^2}}{x-\xi} \right) \right] d\eta \right\} d\xi \tag{20}$$

18

Solutions to the two-dimensional integral equation are exceedingly complex, and have only been accomplished recently with the help of the digital computer (see for example, Ref. 10). In former years, the practice has been to reduce Eq. (17) or Eq. (20) to a one-dimensional integral equation, by an approximation consistent with the configuration being analyzed. Weissinger, in Ref. 11, proposed a high aspect ratio approximation (discussed in Section III-D) which is also correct for the limit of $AR = 0$. Jones, in Ref. 12, uses an approximation which reduces the integral equation to one applicable only to very low aspect ratio wings, or wings at near-transonic speeds. This is the well-known slender wing theory. Lawrence, on the other hand, uses an approximation which is correct at the limits of both high and low aspect ratios ($AR = \infty$ and 0), but gives best results for low to medium aspect ratio wings. This is the method which has been adapted for use in calculating body carry-over lift.

The integral equation for local upwash velocity in terms of the streamwise velocity perturbation for a wing is given by Lawrence as:

$$w(x,y) = -\frac{1}{2\pi} \frac{\partial}{\partial y} \int_0^c \left\{ \int_{-s(\xi)}^{s(\xi)} \frac{u(\xi,\eta)}{y-\eta} \left[1 + \frac{\sqrt{(x-\xi)^2 + (y-\eta)^2}}{x-\xi} \right] d\eta \right\} d\xi \qquad (21)$$

which is just Eq. (20) after an integration by parts.

When the low-aspect ratio approximation

$$\sqrt{(x-\xi)^2 + (y-\eta)^2} \sim \sqrt{(x-\xi)^2 + (s(x))^2} \qquad (22)$$

is introduced, the equation may be rewritten, after evaluating some integrals, as:

$$K(x) = \frac{1}{2} g(x) + \frac{1}{4} \int_0^c g'(\xi) \left[1 + \frac{\sqrt{(x-\xi)^2 + (s(x))^2}}{x-\xi} \right] d\xi \qquad (23)$$

where

$$g'(x) = \int_{-s(x)}^{s(x)} u(x,\eta) d\eta = \frac{1}{2\rho_\infty U_\infty} \frac{dL}{dx} \qquad (24)$$

and

$$K(x) = -\int_{-s(x)}^{s(x)} w(x,y) \sqrt{(s(x))^2 - y^2} \; dy \qquad (25)$$

It is shown in Ref. 6 that this same integral equation (Eq. (23)) may be applied to a wing-body combination, provided $K(x)$ is re-defined as:

19

$$k(x) = \int_{-S(x)}^{S(x)} \left[\alpha(x,y) + \alpha_\beta f_1(y) \right] \sqrt{\overline{S(x)} - \overline{y}^2} \; dy \qquad (26)$$

where $\alpha(x,y)$ is an arbitrary angle of attack distribution of the wing with respect to the wing root chord, α_β is the angle of attack of the body, and $f_1(y)$ is a function relating the flow about the body in question to the flow about a vertical flat plate, defined as

$$f_1(y) = R.P.\left(\frac{d\bar{t}}{dt}\right) - 1 \qquad (27)$$

The variables are defined in the following sketch, illustrating the untransformed wing-body combination and the transformed equivalent wing and vertical line body.
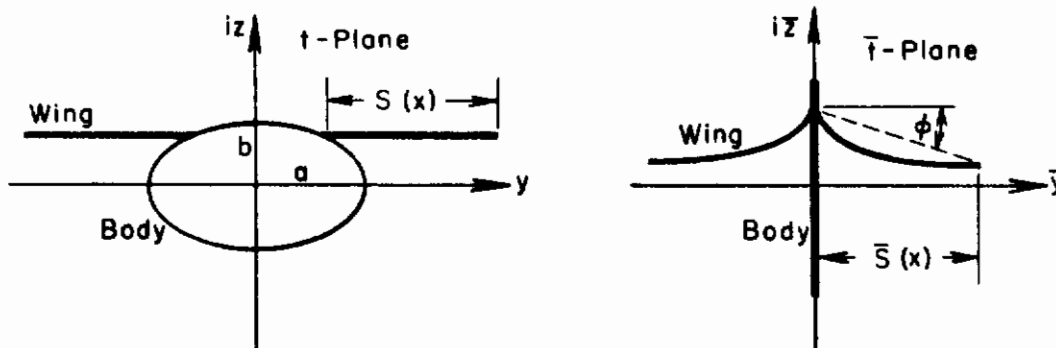
The numerical procedure used for solving Eq. (23) is outlined in Section III-D below. A FORTRAN program including this procedure was given in Appendix B of Ref. 1. In this program, $k(x)$ is input in the form

$$f(\theta) = \frac{4}{\pi} k(\theta) \Big/ \left(\frac{S(\theta)}{S}\right)^2 \qquad (28)$$

where the transformation

$$x = \frac{c}{2} (1 - \cos\theta) \qquad (29)$$

has been applied. The function $f(\theta)$ gives the distribution of effective angle of attack in the chordwise direction.

For solutions of Eq. (23) and $k(x)$ defined as in Eq. (26), it has been necessary to modify the existing program to correctly calculate $f(\theta)$ for use as input. It will be noted that as a value of $k(x)$ is to be calculated at each chordwise station, there is nothing to prevent replacement of α_β in Eq. (23) by $\alpha_\beta(x)$ to account for body camber, or of $f_1(y)$ by $f_1(x,y)$ to account for variations in the elliptical cross-section. These variations should be small to prevent serious violation of the boundary conditions of no flow through the body.

20

The following procedure is to be followed in calculating $f(\theta)$:

1. Divide the root chord of the wing into m spanwise strips whose centers lie at the stations $\theta_n = \frac{c}{2}\left(1 - \cos\frac{n\pi}{m+1}\right)$, $n = 1, 2, 3 \ldots m$

2. At each station, calculate

$$f(\theta_n) = \frac{4}{\pi}\frac{1}{(S(\theta_n)/S)^2}\int_{-\frac{S(\theta_n)}{S}}^{\frac{S(\theta_n)}{S}}\left[\alpha\left(\theta_n, \frac{y}{S}\right) + \alpha_\beta(\theta_n)f_1\left(\theta_n, \frac{y}{S}\right)\right]$$

$$\sqrt{\left(\frac{\overline{S}(\theta_n)^2}{S}\right)^2 - \left(\frac{\overline{y}}{S}\right)^2}\; dy \tag{30}$$

where

$$f_1\left(\theta_n, \frac{y}{S}\right) = R.P.\left(\frac{d\overline{t}(x)}{dt(x)}\right) - 1 \tag{31}$$

and

$$\overline{y} = R.P.\left(\overline{t}(x)\right) \tag{32}$$

It will be noted from the sketch above that if the wing is located above or below the mid-plane, the transformed wing segment may be one of varying dihedral. The approximation is made here that the lift on the transformed wing segment is the same as the lift on a horizontal wing segment with a span equal to the projected span of the transformed wing segment. It has been shown in Ref. 6 that the lift on a wing-body combination is the same as the lift on the isolated wing which is obtained by applying the appropriate conformal transformation to the wing body combination, i.e. that which collapses the body into a vertical straight line in the plane of symmetry. It is felt that this additional approximation is sufficiently accurate to predict the body carry-over lift.

It will also be noted that the transformation

$$\overline{t} = \overline{t}(t) \tag{33}$$

may be different at each of the n chordwise stations. The general form of this transformation is:

$$\overline{t} = \frac{(r^2 + k^2)(t^2 - 4k^2)^{1/2} - (r^2 - k^2)t}{2k^2} \tag{34}$$

where $r = \frac{1}{2}(a + b)$ and $k^2 = \frac{(a+b)(a-b)}{4}$ and a and b are defined in the sketch on page 20.

The foregoing procedure will be used to calculate the chordwise (axial) distribution of body carry-over lift only as far as the root of the trailing edge of the wing. This restriction has been prescribed so as to

21

include the inherent limitation in the Lawrence method that the trailing edges may not be swept more than a few degrees. Beyond the root of the trailing edge, the method given in the following section should be used. The following sketch compares the physical situation and the model for the present procedure.
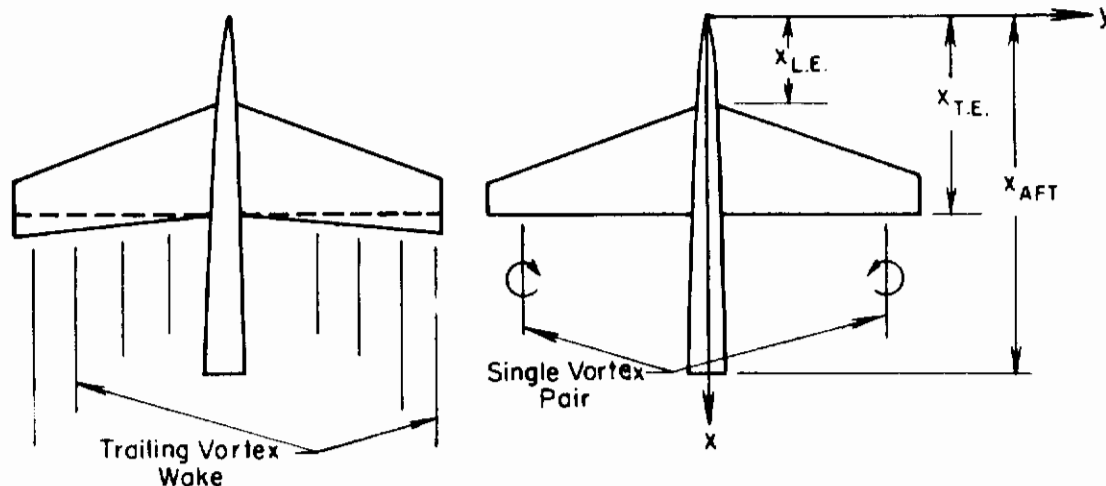
The approximation of removing the portion of the wing aft of the root of the trailing edge is not so drastic as it may seem, as the lift on this portion of the wing will be included in the strength of the trailing vortex pair.

3. Body Carry-Over Lift Due to Vortex Wake

The true spanwise lift distribution dL/dy on the wing may be calculated by any appropriate method. It is recommended that the effect of the body on the wing lift distribution be included. Section II-B of this report gives a method for including this effect when the wing-alone lift distribution is known.

This lift distribution should then be replaced by a single pair of trailing vortices (actually the tails of a single horseshoe vortex) of strength

$$\Gamma_o = \frac{1}{\rho U_\infty} \left(\frac{dL}{dy}\right)_{y=0} \tag{35}$$

and span such that the correct total lift is produced, i.e.

$$b' = vortex\ span = \frac{L}{(dL/dy)_{y=0}} \tag{36}$$

The following sketch illustrates the calculation of the vortex position. The top curve shows the actual spanwise loading, dL/dy. The second curve shows the derivative of this loading, $\left|d^2L/dy^2\right|$, which is proportional to the vorticity distribution $\Gamma'(y)$. The single trailing vortex is then located

22

at the centroid of this curve on the half wing. That is,

$$b' = \int_0^{\frac{b}{2}} y \left| \frac{d^2 L}{dy^2} \right| dy \Big/ \int_0^{\frac{b}{2}} \frac{d^2 L}{dy^2} \, dy$$

$$= L \Big/ \left(\frac{dL}{dy} \right)_{y=0} \tag{37}$$
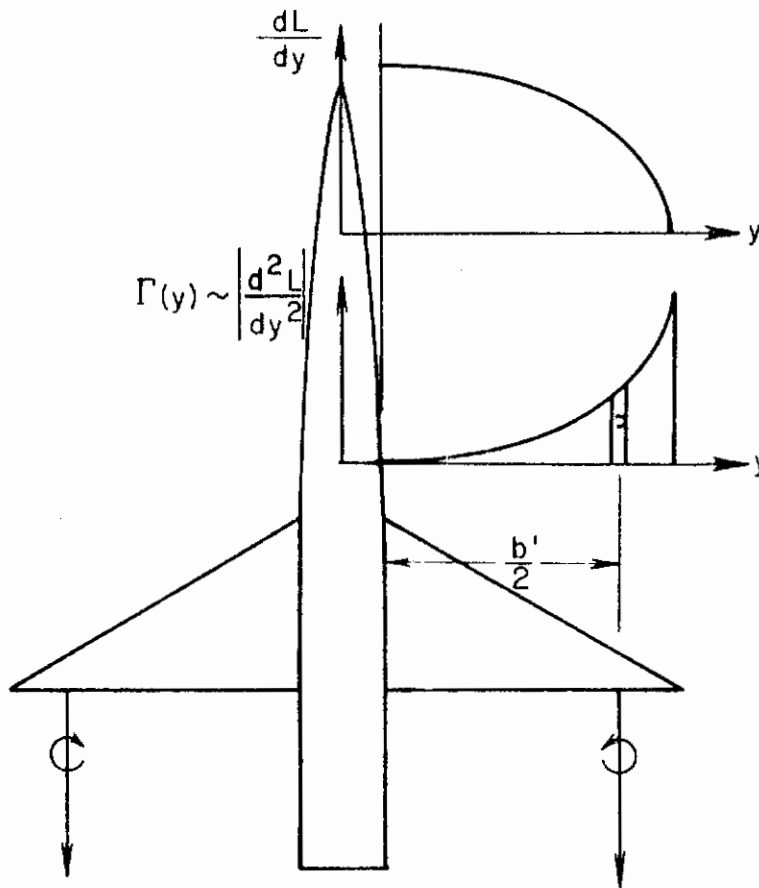
The distribution of lift on the aft portion of the body is given by Ref. 11 as:

$$\left(\frac{dL}{dx} \right)_{vortex} = \rho_\infty U_\infty \cos \alpha_o \Gamma_o \frac{d}{dx} \left[R.P. \left\{ \left(\frac{r^2 + k^2}{k^2} \right) \left(\xi_1^2 - 4k^2 \right)^{\frac{1}{2}} - \left(\frac{r^2 - k^2}{k^2} \right) t_1 \right\} \right] \tag{38}$$

where t_i is the position of the vortex, and α_o is the average angle of attack of the body. The vortex is assumed to trail back from the trailing edge of the wing in the streamwise direction. A slight nonlinearity with angle of attack is thus introduced into the method. The forces due to changes in vortex position are so small, however, that it is still felt justified that the theory be used as a linear one for computing lift-curve slopes.

D.   DESCRIPTION OF NUMERICAL METHODS

1.   Formulation for Aeroelastic Calculations

As discussed in Section III-A, it is desirable that the methods developed for calculating interference loads be readily adaptable for aeroelastic calculations. It was further decided that "box" methods were more desirable than "mode shape" methods for treating general configurations, and that methods should be chosen which allowed for aeroelastic treatment of the wing and body separately, as well as for treatment of the complete configuration. The numerical methods described here, then, are based on such a box-type representation of the vehicle.

The sketch below shows the scheme of grid divisions which has proven the most easily adaptable to the methods described above.
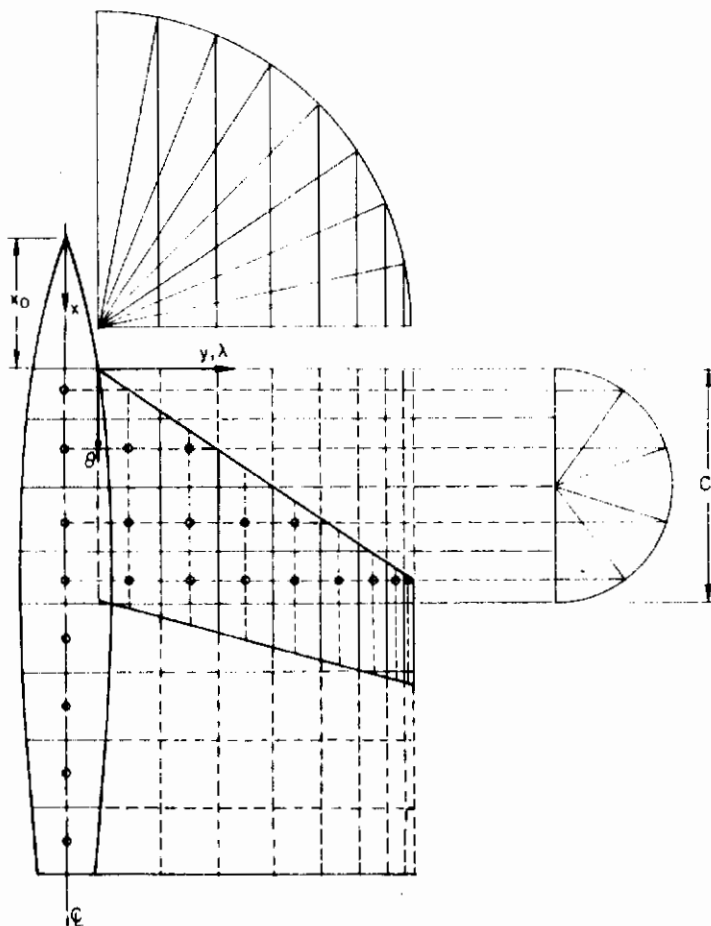
The wing is divided into chordwise and spanwise strips, forming a grid of rectangular boxes. The y-coordinates of the edges of the boxes are given by

$$y_i = \frac{b}{2} \cos\left(\frac{(i-1)}{m+1}\right); \quad i = 1, 2 \cdots \left(\frac{m+1}{2}\right)$$

(39)

where m is the number of stations on the full span of the exposed wing. This division is identical to that used in Weissinger's procedure, discussed below. The centers of these boxes lie at distances

$$\lambda_i = \frac{y_i + y_{i+1}}{2}; \quad i = 1, 2 \cdots \frac{m+1}{2} - 1$$

(40)

from the root chord.

The chordwise divisions are made such that the centers of the boxes lie at distances aft of the root of the leading edge

$$\theta_j = \frac{1}{2} c_r \left[1 - \cos\left(\frac{j\pi}{N+1}\right) \right]; \quad j = 1, 2 \cdots N$$

(40.1)

for boxes ahead of the root of the trailing edge. This division is the same as that used in the Lawrence procedure, discussed below.

The edges of these boxes then lie at distances

$$x_j = x_{j-1} + 2 \left(\theta_j + x_0 - x_{j-1}\right)$$

(40.2)

aft of the nose of the body, where x_0 is the location of the leading edge.

The body is divided, from the leading edge to trailing edge, into N segments, where the centers of the segments are located at distances aft of the leading edge given by Eq. (40.1).

The portions of the body aft of the root of the trailing edge is divided evenly into $N1$ segments, whose centers lie at a distance:

$$\theta_j = \frac{(x_j + x_{j-1})}{2} - x_0; \quad j = N+1, N+2, \cdots N1$$

(40.3)

where

$$x_j = x_N + j \left(\frac{l - x_N}{N1}\right); \quad j = N+1, N+2, \cdots N1$$

(40.4)

and where $x_0 \cdot x$-coordinate of the leading edge root, measured from the body nose

l- body length

$x_N = x_N$-coordinate of the trailing edge root.

The area of the wing aft of the trailing edge root is divided into the same segments in the x-direction as the aft portion of the body, and in the y-direction into the same segments as the area forward of the trailing edge root.

25

In the sketch, which shows a sample division of a typical configuration into wing boxes and body segments, $N = N_1 = 4$, and $m = 15$. In practice the number chosen would be much larger, but such choice would make the illustration difficult to interpret.

In the calculation of wing or wing-body interference load distributions, using an arbitrary angle of attack distribution, the "true" wing is replaced by an "effective" wing. The effective wing is made up of the rectangular boxes defined above. A box is included in the effective wing if its center would lie on the planform of the true wing, for those boxes ahead of the root of the trailing edge. Behind the root of trailing edge, only that portion of each box which equals the true wing area within the box is used. The following sketch illustrates the effective wing geometry for the sample divisions given above.
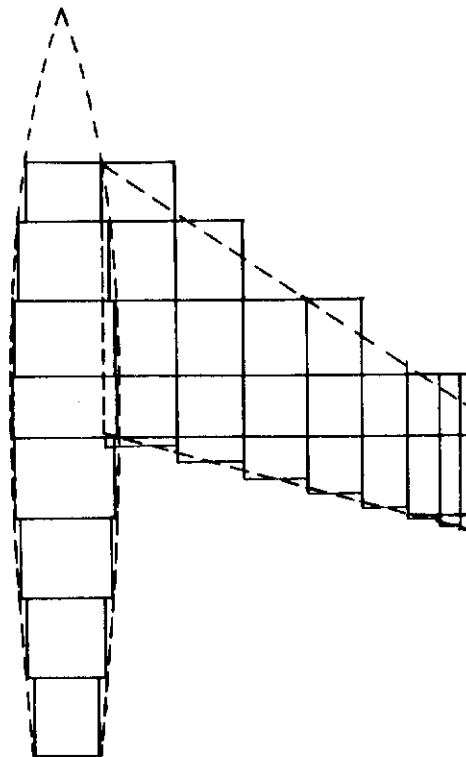
It has been necessary to represent the wing leading edge in such a manner so that the Lawrence procedure, which divided the wing into spanwise strips, could be used conveniently. Since this method is not used past the trailing edge of the root, a more accurate representation of a swept trailing edge could be used, as is seen in the above sketch.

2.   Effect of the Body on the Wing

This section describes the numerical procedures to be followed in using the modified Gray and Schenk method described above to calculate the lift distribution over a wing in the presence of an elliptical body. This procedure has been included in a computer program for calculating interference loads on wing-body combinations, which is described

in Appendix I of this report. The program is restricted to subsonic wings because a method which is limited to the subsonic Mach number range is used to calculate the original load on the wing alone. If supersonic interference loads are desired, linear wing theory should be used along with the modified Gray and Schenk method.

a. Modified Gray and Schenk Method

The numerical procedure may be outlined as follows:

1) Calculate the spanwise lift distribution $cc_\ell(y)$ for the exposed wing by Weissinger's procedure. Details of this method are given below. Values of $c(y)$, $c_\ell(y)$ and $x_{cp}(y)$ should be found at $m+1/2$ spanwise stations located at y_i, where:

$$y_i = \frac{b}{2} \cos\left(\frac{(i-1)\pi}{m+1}\right); \quad i = 1, 2, \cdots \left(\frac{m+1}{2} + 1\right) \tag{41}$$

as shown in the following sketch.
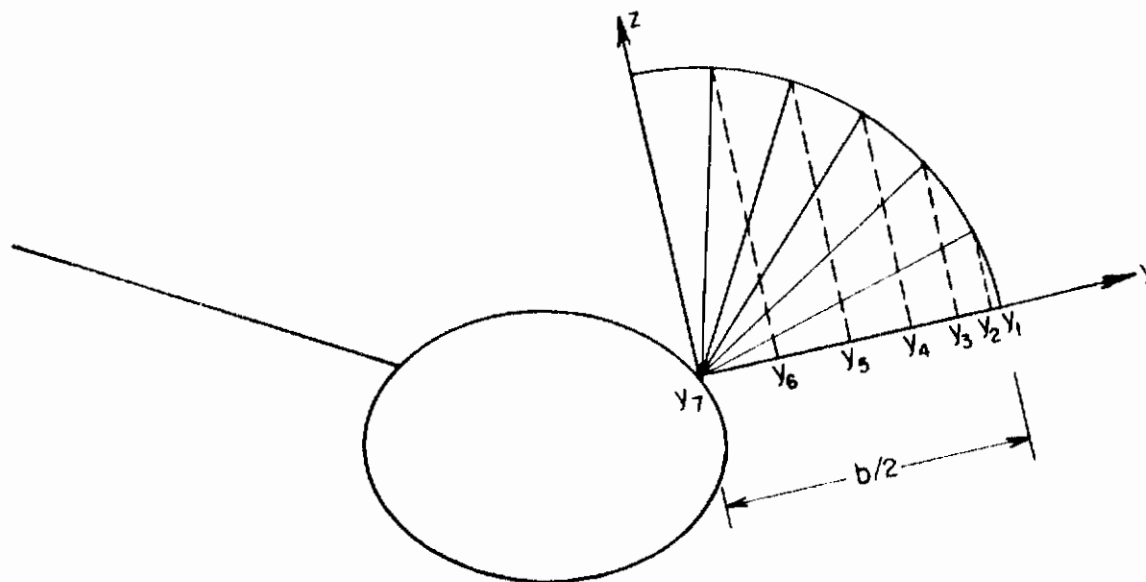
2) At each station y_i, replace the lift distribution by a horseshoe vortex of strength $\Gamma(y_i)$, composed of a bound vortex segment normal to the free stream direction, and two trailing vortices, located at y_i and y_{i+1}. The vortex strength is found by

$$\frac{\Gamma(y_i)}{U} = \frac{1}{4}\left[cc_\ell(y_i) + cc_\ell(y_{i+1})\right] \tag{42}$$

This is equivalent to the stepwise approximation shown in the sketch on page 13. Note that there are horseshoe vortices on both halves of the wing due to the symmetric loading condition.

27

3) From the value of the semi-major and semi-minor axes of the elliptical cross section of the body, calculate the elliptical parameter k^2 and the radius r of the equivalent circle:

$$k^2 = \frac{(a+b)(a-b)}{4} \tag{43}$$

$$r = \frac{1}{2}(a+b) \tag{44}$$

where a is one-half the horizontal axis of the ellipse, and b is one-half the vertical axis of the ellipse. Either may be the semi-major axis.

4) Using the center of the ellipse as the point $y = 0$, see if the positions y_0 of the trailing vortices located on the wing at y_i satisfy Eq. (6). Those trailing vortices which do not should be ignored, along with the bound vortex segments which connect them (see sketch below).

$$\zeta = \xi + i\eta$$

Ellipse: $\dfrac{\xi_0^2}{a^2} + \dfrac{\eta_0^2}{b^2} = 1$

Ellipse: $\dfrac{\xi_0^2}{\left(\dfrac{r^2}{|k|} + \dfrac{k^2}{r^2}|k|\right)^2} + \dfrac{\eta_0^2}{\left(\dfrac{r^2}{|k|} - \dfrac{k^2}{r^2}|k|\right)} = 1$

28
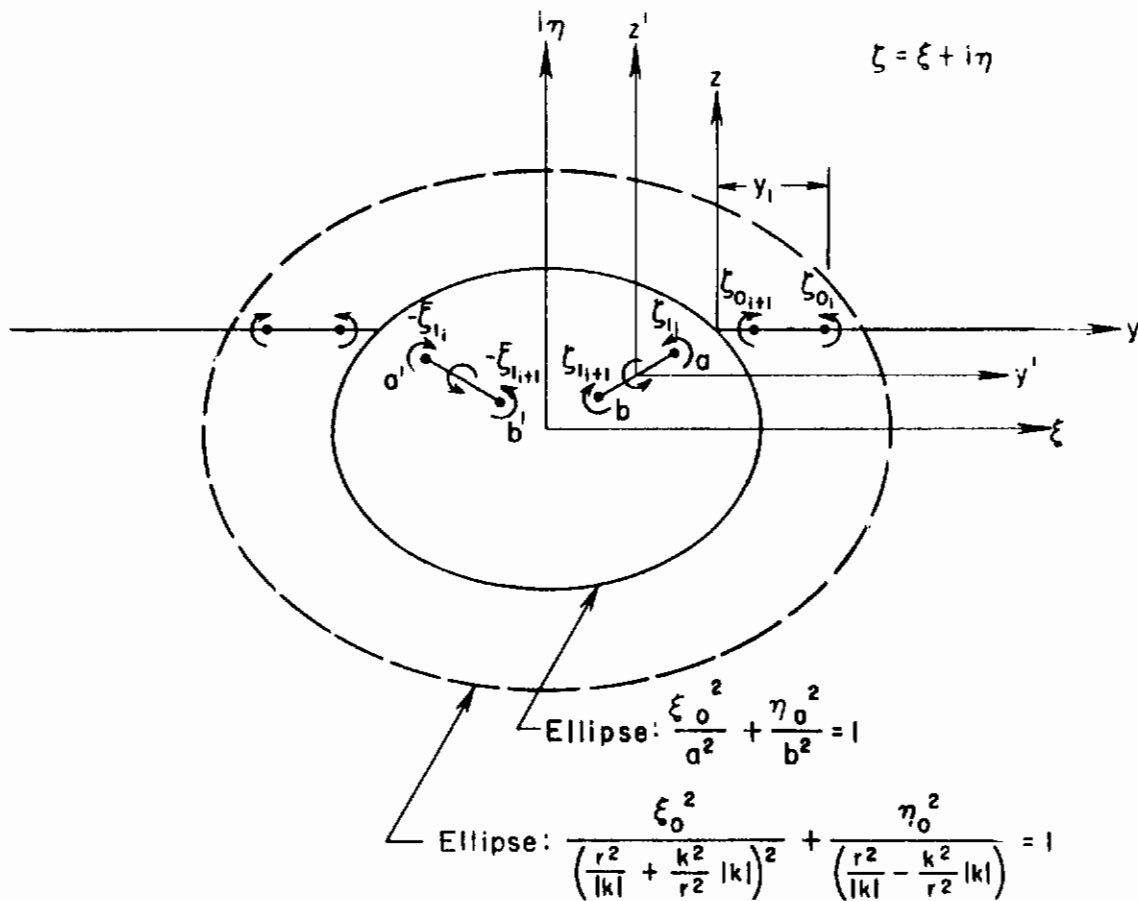
5) Find the positions of the image vortices $\mathcal{S}_i$ by Eq. (4).

6) At each spanwise station on the wing (control point), calculate the upwash due to all the elements of each symmetrically located pair of horseshoe vortices. The relations for calculating upwash are:

$$\frac{w_a}{U} = \frac{\Gamma_i/U}{4\pi A^2}\left(1 + \frac{x'}{\sqrt{x'^2 + A^2}}\right)\left(y'' - H_i \cos\gamma_i\right)$$

(45)

$$\frac{w_b}{U} = -\frac{\Gamma_i/U}{4\pi B^2}\left(1 + \frac{x'}{\sqrt{x'^2 + B^2}}\right)\left(y'' + H_i \cos\gamma_i\right)$$

(46)

$$\frac{w_{ab}}{U} = -\frac{\Gamma_i/U}{4\pi B^2}\left(\frac{x'}{f^2 + x'^2}\right)\left(\sqrt{\frac{B^2 - f^2}{B^2 + x'^2}} - \sqrt{\frac{A^2 - f^2}{A^2 + x'^2}}\right)\cos\gamma_i$$

(47)

$$\frac{w_a'}{U} = -\frac{\Gamma_i/U}{4\pi A'^2}\left(1 + \frac{x'}{\sqrt{x'^2 + A'^2}}\right)\left(y''^* + H_i \cos\gamma_i'\right)$$

(48)

$$\frac{w_b'}{U} = \frac{\Gamma_i/U}{4\pi B'^2}\left(1 - \frac{x'}{\sqrt{x'^2 + B'^2}}\right)\left(y''^* - H_i \cos\gamma_i'\right)$$

(49)

$$\frac{w_{ab}'}{U} = -\frac{\Gamma_i/U}{4\pi}\left(\frac{x'}{f'^2 + x'^2}\right)\left(\sqrt{\frac{A'^2 - f'^2}{A'^2 + x'^2}} - \sqrt{\frac{B'^2 - f'^2}{B'^2 + x'^2}}\right)\cos\gamma_i'$$

(50)

The symbols are defined in the two sketches on the following page.

7) The upwash due to the image vortices which are coincident with the wing root must be ignored, as these vortices are cancelled directly by the wing trailing vortices of equal and opposite strength at the same location.

8) After the upwash contributions from all the vortex elements are summed, add the upwash at each point due to body angle of attack. This is given by

$$\left(\frac{w}{U}\right)_{body} = R.P.\left\{\frac{4r^2}{\left(\mathcal{S}_0 + \sqrt{\mathcal{S}_0^2 - 4k^2}\right)^2}\right\}$$

(51)

where $\mathcal{S}_0$ is the location of the control point.

9) Add the induced angle of attack, w/U_{TOTAL} to the original angle of attack at each spanwise station, and recalculate the spanwise lift distribution by Weissinger's procedure.

29
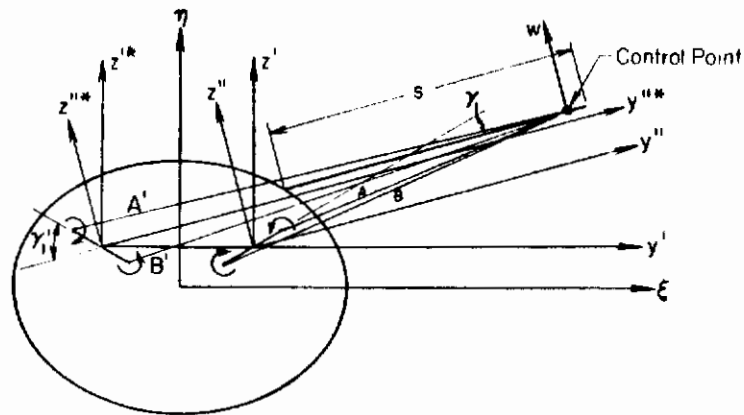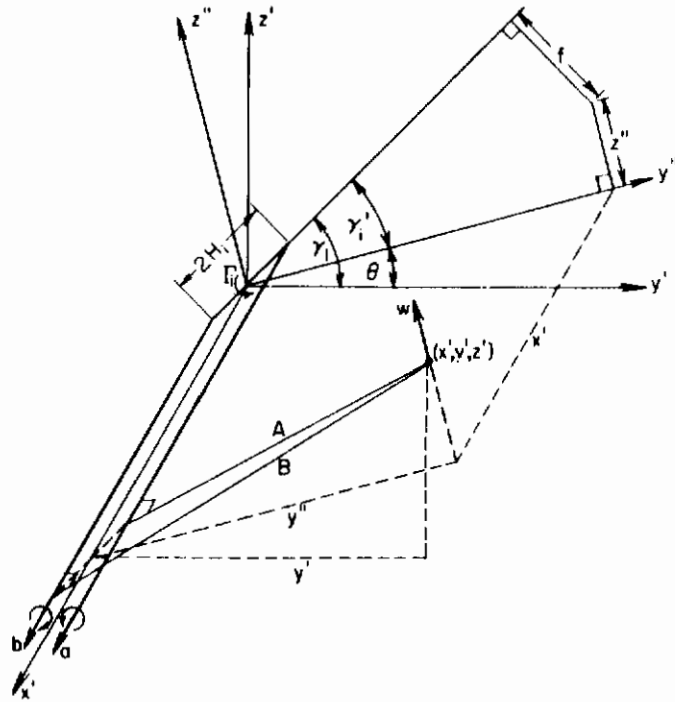
b. Weissinger's Method

Equation (17), relating the upwash velocity on a wing surface to a distribution of vorticity, forms the basis of most linear subsonic lifting theories. As has been previously mentioned, solutions of the two-dimensional integral equation are exceedingly complex. Weissinger, in Ref. 11, reduces the equation to a one-dimensional one by prescribing the chordwise variation of vorticity, and solves the resulting integral equation for the spanwise variation. The numerical procedures for its solution, given below in condensed form and in Ref. 14 in full detail, are included in the computer program described in Appendix I.

30

Weissinger's "L" method assumes that the vorticity distributed across the chord at each spanwise station is all collected into a concentrated vortex at the quarter-chord. Then when the boundary condition of no flow through the wing

$$\alpha\,(x,y) = -\frac{w\,(x,y)}{U} \tag{52}$$

is applied at the three-quarter-chord the two-dimensional (infinite aspect ratio) boundary condition is satisfied if the wing is flat. Thus, Weissinger's method may be expected to give best results for high aspect ratio wings. The limit of zero aspect ratio gives the correct result of zero lift, however.

If the wing is not flat, but has an arbitrary variation of slope in the chordwise direction, the two-dimensional boundary condition is no longer satisfied. It is necessary, therefore, to define an "effective angle of attack" which is then treated as before. The process of finding this effective angle is treated below in Section c.

The geometry of the problem is shown in the following sketch, where a concentrated vortex is placed on the quarter-chord line which has a sweep-back angle $\Lambda_{c/4}$.

31
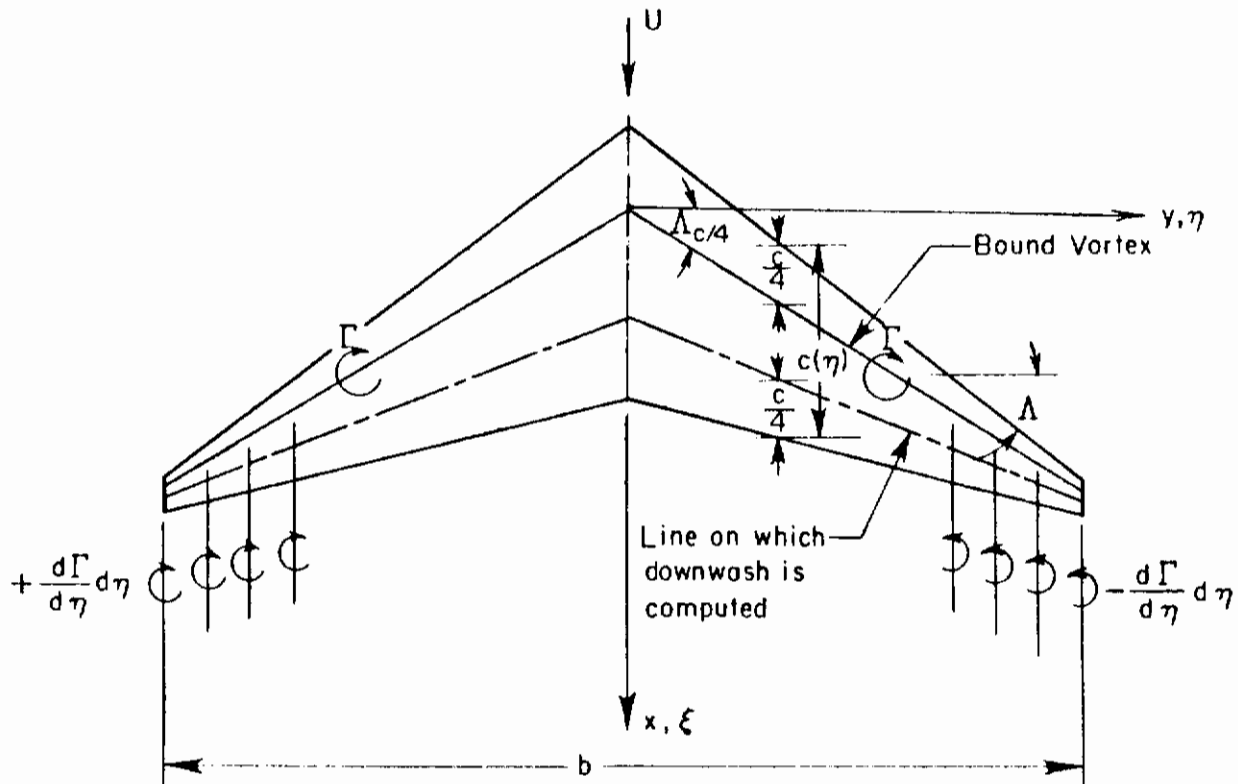
The strength of the bound vortex $\Gamma(y)$ varies in an unknown manner along its length starting at zero at the right wing tip. Then at every point it is joined by an infinitesimal trailing vortex which increases the strength of the bound vortex by $d\Gamma$, to a maximum of Γ_o at the center, after which departing vortices reduce the strength to zero at the left wing tip. Since the general distribution of vorticity $\gamma(x,y)$ is now to be replaced by a system of vortex elements, the total upwash must be calculated by considering separately all the elements of the system. Thus the integral equation for the vorticity distribution, Eq. (17), becomes, after some manipulations,

$$w(x,y) = +\frac{1}{4\pi}\int_{-\frac{b}{2}}^{\frac{b}{2}}\frac{\Gamma'(\eta)d\eta}{y-\eta} + \frac{1}{4\pi}\int_{-\frac{b}{2}}^{0}\left[\frac{\sqrt{(x+\eta\tan\Lambda_{c/4})^2+(y-\eta)^2}}{(x+y\tan\Lambda_{c/4})(y-\eta)}\right.$$

$$\left. -\frac{1}{y-\eta} + \frac{2\tan\Lambda_{c/4}\sqrt{x^2+y^2}}{x^2-y^2\tan^2\Lambda}\right]\Gamma'd\eta + \frac{1}{4\pi}\int_{0}^{\frac{b}{2}}\left[\frac{\sqrt{(x-y\tan\Lambda_{c/4})^2+(y-\eta)^2}}{(x-y\tan\Lambda)(y-\eta)}-\frac{1}{y-\eta}\right]\Gamma'(\eta)d\eta$$

$$(53)$$

Evaluating at the three-quarter-chord line, where

$$x = \frac{c}{2} + |y|\tan\Lambda_{c/4} \qquad (54)$$

the nondimensional equation for the upwash distribution becomes

$$\frac{w(y)}{U} = \frac{1}{\pi}\int_{-1}^{1}\frac{G'(\tau)d\tau}{t-\tau} + \frac{b}{2\pi}\int_{-1}^{1}L(t,\tau)G'(\tau)d\tau \qquad (55)$$

where

$$\tau = \frac{\eta}{b/2} \; ; \; t = \frac{y}{b/2} \; ; \; G = \frac{\Gamma}{bU_\infty}$$

On the right wing

$$L(t,\tau) = \frac{1}{\frac{b}{c}(t-\tau)}\left[\frac{\sqrt{\left[1+\frac{b}{c}(t+\tau)\tan\Lambda_{c/4}\right]^2+\left(\frac{b}{c}\right)^2(t-\tau)}}{1+2\frac{b}{c}t\tan\Lambda_{c/4}} - 1\right]$$

$$+\frac{2\tan\Lambda_{c/4}\sqrt{\left[1+\frac{b}{c}t\tan\Lambda_{c/4}\right]^2+\frac{b^2t^2}{c^2}}}{1+2\frac{b}{c}t\tan\Lambda_{c/4}} \; ; \; \tau \le 0$$

$$= \frac{1}{\frac{b}{c}(t-\tau)} \left[\sqrt{\left[1 + \frac{b}{c}(t-\tau)\tan\Lambda_{c/4}\right]^2 + \left(\frac{b}{c}\right)^2(t-\tau)^2} - 1 \right] \quad \tau \geq 0 \tag{56}$$

$\frac{w(y)}{U}$ on the left wing may be found by symmetry with the right wing.

Weissinger solves the integral equation for $G(\tau)$, Eq. (55), by replacing $G(\tau)$ by a Fourier series, using Multhopp's integration formula to express the unknown coefficients, and performing the integrals in Eq. (55) by trapezoidal integration. Thus the integral equation is transformed to the following set of simultaneous linear equations:

$$\left(\frac{w}{U}\right)_\nu = \sum_{n=1}^{\frac{m+1}{2}} a_{\nu n} G_n ; \quad \nu = 1, 2, 3, \cdots \frac{m+1}{2} \tag{57}$$

where

$$a_{\nu n} = 2b_{\nu\nu} + \frac{b}{c_\nu}\bar{g}_{\nu\nu} \quad \text{for } n = 0$$

$$= -2\beta_{\nu n} + \frac{b}{c_\nu}\bar{g}_{\nu n} \quad \text{for } n \neq \nu \tag{58}$$

and

$$\bar{g}_{\nu n} = \frac{-1}{2(M+1)} \sum_{\mu=0}^{\frac{M-1}{2}} f_{n\mu} L^*_{\nu\mu} \tag{59}$$

where

$$b_{\nu\nu} = \frac{m+1}{4\sin\phi_\nu} \tag{60}$$

$$\beta_{\nu n} = b_{\nu n} + b_{\nu, m+1-n} \quad \text{for } n \neq \frac{m+1}{2}$$

$$= b_{\nu n} \quad \text{for } n = \frac{m+1}{2} \tag{61}$$

33

where

$$b_{\nu n} = \frac{\sin \phi_n}{(\cos \phi_n - \cos \phi_\nu)^2} \left[\frac{1-(-1)^{n-\nu}}{2(m+1)} \right]$$

(62)

and

$$L^*_{\nu\mu} = \frac{1}{\frac{b}{c_\nu}(\tau_\nu - \bar{\tau}_\mu)} \left\{ \sqrt{\left[1+\frac{b}{c_\nu}(\tau_\nu - \bar{\tau}_\mu)\tan\Lambda_{c/4}\right]^2 + \left(\frac{b}{c_\nu}\right)^2 (\tau_\nu - \bar{\tau}_\mu)^2 } - 1 \right\}$$

$$- \frac{1}{\frac{b}{c_\nu}(\tau_\nu + \bar{\tau}_\mu)} \left\{ \frac{\sqrt{\left[1+\frac{b}{c_\nu}(\tau_\nu - \bar{\tau}_\mu)\tan\Lambda_{c/4}\right]^2 + \left(\frac{b}{c_\nu}\right)^2(\tau_\nu + \bar{\tau}_\mu)^2} - 1}{1 + 2\frac{b}{c_\nu}\tau_\nu \tan\Lambda_{c/4}} \right\}$$

$$- \frac{2\tan\Lambda_{c/4}\sqrt{\left[1+\frac{b}{c_\nu}\tau_\nu\tan\Lambda_{c/4}\right]^2 + \left(\frac{b}{c_\nu}\right)^2\tau_\nu^2}}{1 + 2\frac{b}{c_\nu}\tau_\nu\tan\Lambda_{c/4}}$$

(63)

where

$$\hat{\tau}_\nu = \cos\frac{\nu\pi}{m+1}$$

(64)

$$\tau_\mu = \cos\frac{\mu\pi}{M+1}$$

(65)

Also

$$f_{n\mu} = 2f_{n\mu} \text{ for } n \neq \frac{m+1}{2}, \mu \neq 0$$

$$= f_{n\mu} \text{ for } n = \frac{m+1}{2}, \mu \neq 0$$
$$\text{or } n \neq \frac{m+1}{2}, \mu = 0$$
$$= \frac{f_{n\mu}}{2} \text{ for } n = \frac{m+1}{2}, \mu = 0$$

(66)

where

$$f_{n\mu} = \frac{2}{m+1} \sum_{\mu = 1,3,5 \cdots odd}^{m} \mu_1 \sin \mu_1 \phi_n \cos \mu_1 \bar{\phi}_\mu$$

(67)

and

$$\phi_n = \frac{n\pi}{m+1}$$

(68)

$$\varphi_\mu = \frac{\mu\pi}{M+1}$$

(69)

The parameters m and M are the number of spanwise stations on the wing and the number of intervals in the trapezoidal integration. They must be different and odd.

Although the above relations may appear to be quite complicated, they may easily be programmed for machine computation. Solution of the set of simultaneous equations for G_n is accomplished by a simple matrix inversion procedure, when the effective spanwise angle of attack distribution, $-w(y)/U$, is known. The section lift coefficient, $C_\ell(y)$, is then given by

$$C_\ell(y) = 2 \frac{b}{c_v} G_n$$

(70)

Values of $C_\ell(y)$ may then be used in the procedure of Gray and Schenk to find a new effective spanwise angle of attack distribution which expresses the presence of the body, as outlined above.

It should be noted that the actual distribution of vorticity used in the Weissinger procedure is different from that used in the modified Gray and Schenk method. In the former, the bound vortex was assumed to lie in a straight line along the quarter-chord of the wing, while in the latter, portions of a bound vortex were assumed to be normal to the free stream direction in order to simplify the process of finding the image vortices within the body.

Although the Weissinger procedure was derived from the equations of incompressible flow, compressibility effects may be accounted for by a Prandtl-Glauert transformation. This subject is treated in Section d below.

c. Effective Angle of Attack

For a flat wing, or one which has an arbitrary angle of attack variation only in the spanwise direction, Eq. (57) may be solved directly. If the wing has a chordwise angle of attack distribution (camber) the boundary condition is not satisfied at the three-quarter-chord by the assumption that all the vorticity is collected into a concentrated vortex at the quarter-chord. If Weissinger's procedure is to be used, it will be necessary to find an effective angle of attack to be used for $-w(y)/U$ at each spanwise station.

35

Since the three-quarter-chord position for applying the boundary conditions arises from the two-dimensional or infinite aspect ratio approximation to the three-dimensional problem, the effective angle of attack will be determined by solving the two-dimensional thin lifting airfoil problem. The following sketch illustrates the situation when a vortex sheet of strength $\gamma(x) = \partial \Gamma / \partial x$ is assumed to lie in the plane of the wing.
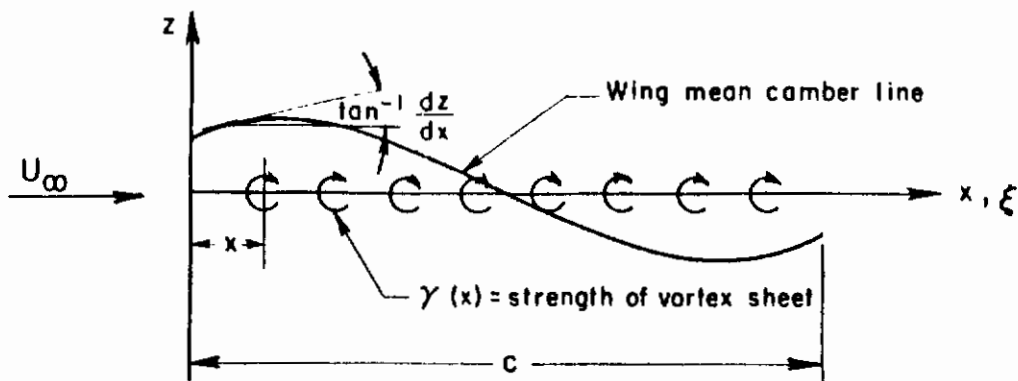
The flow angles induced by this vorticity are then equated to the local slope of the wing mean camber line. The vertical velocity induced by the distributed vorticity a $\xi = x$, $z = 0$ will be

$$w(x) = \frac{1}{2\pi} \int_0^c \frac{\gamma(\xi)d\xi}{\xi - x} \tag{71}$$

The boundary condition, applied in the $z = 0$ plane, then requires that for a local wing slope dz/dx

$$\frac{dz}{dx} = \frac{w(x)}{U_\infty} = \frac{1}{2\pi U_\infty} \int_0^c \frac{\gamma(\xi)d\xi}{\xi - x} \tag{72}$$

The singularity in the integrand at $\xi = x$ is to be evaluated by using the Cauchy principal value.

The general solution for this equation (Ref. 1) is:

$$\gamma(x) = \frac{2U_\infty}{\pi} \sqrt{\frac{c-x}{x}} \left[\int_0^c \frac{dz/d\xi}{x-\xi} \sqrt{\frac{\xi}{c-\xi}} \, d\xi + k \frac{c}{c-x} \right] \tag{73}$$

The constant of integration k must vanish since the vorticity is required by the Kutta condition to be zero at the wing trailing edge. The vorticity is equal to the streamwise velocity perturbation

$$\Delta u = u_{upper} - u_{lower} = \gamma(x) \tag{74}$$

36

and by linear theory

$$C_p = -\frac{2u}{U_\infty} \qquad (75)$$

The two-dimensional lifting pressure may then be written as

$$\Delta C_{p_{2\text{-dim}}} = \frac{2\,\gamma(x)}{U_\infty} = \frac{4}{\pi}\sqrt{\frac{c-x}{x}} \int_0^c \frac{dz/d\xi}{x-\xi} \sqrt{\frac{\xi}{c-\xi}}\, d\xi \qquad (76)$$

The spanwise loading is determined by integrating this expression across the wing

$$c c_{\ell_{2\text{-dim}}} = \int_{L.E.}^{T.E.} \Delta C_{p_{2\text{-dim}}}\, dx = \frac{1}{q}\frac{dL}{dy} \qquad (77)$$

where q is the dynamic pressure $\rho/2\, U_\infty^2$. From two-dimensional airfoil theory, the lift on a unit span of the wing is proportional to the circulation, and produces a section lift coefficient of $2\pi\alpha$. Thus the angle of attack is related to the spanwise lift distribution by

$$\frac{1}{q c}\frac{dL}{dy} = c_{\ell_{2\text{-dim}}} = 2\pi\alpha \qquad (78)$$

The effective angle of attack may be found from the two-dimensional solution as

$$\alpha(y)_{eff} = \frac{1}{2\pi c(y)} \int_{L.E.}^{T.E.} \Delta C_{p_{2\text{-dim}}}\, dx \qquad (79)$$

where $\Delta C_{p_{2\text{-dim}}}$ is given by Eq. (76).

It is possible to evaluate the above integrals numerically when the wing geometry and the chordwise slope distribution dz/dx are known. Since the integral in Eq. (76) must be evaluated by the Cauchy principal value technique, the numerical integration should contain as many intervals as possible, since the step when $x = \xi$ is omitted from the calculation. Results of this approximation are discussed in Appendix I.

In calculating the effective angle of attack, the chordwise slope distribution dz/dx is taken as constant over the area of each box on the wing. Thus the chord used is the local chord of the effective wing discussed above.

d. Compressibility Effects

Compressibility may be accounted for by application of the Prandtl-Glauert rule, as indicated in Ref. 14. The approximations and limitations of this rule are well-known and will not be discussed here.

The rule states that the flow over a wing at some subsonic Mach number is similar to the incompressible flow over a wing whose chordwise dimensions are stretched by an amount equal to $1/\sqrt{1-M_\infty^2}$, where M_∞ is the free-stream Mach number. The following procedure should be applied to calculate the lift distribution on subsonic wings:

1) Replace the wing by a transformed wing, with

$$AR' = \beta AR \qquad (80)$$

and

$$\Lambda' = \tan^{-1}\left(\frac{\tan\Lambda}{\beta}\right) \qquad (81)$$

where $\beta = \sqrt{1-M_\infty^2}$, and primes denote the parameters describing the transformed wing. Thus the coordinates of any point on the transformed wing, (x', y') , may be found as $(x/\beta, y)$.

2) Calculate the spanwise load distribution on the transformed wing by Weissinger's procedure.

3) Increase the values of C_L and $C_\ell(y)$ found for the transformed wing by multiplying by $1/\beta$ to get the values for the untransformed wing. This is necessary because the angle of attack distribution was reduced by a factor of β due to the stretching of the x -coordinate. The true lift on the untransformed wing may thus be recovered, because lift varies linearly with angle of attack.

3. Effect of the Wing on the Body

a. Modified Lawrence Method

The modified Lawrence method described in Section III-C above is used to calculate the effect of the presence of a wing on the axial distribution of lift on an elliptic body. The body may have small variations in cross-section and camber. The procedure may be outlined as follows:

1) Solve the integral Eq. (23) for $g'(x)$, with $K(x)$ defined by Eq. (26). The axial distribution of lift on the wing-body combination is given by

$$\frac{1}{q}\frac{dL}{dx} = 2g'(x)\cos\phi_0(x) \qquad (82)$$

where

$$\phi_0(x) = \tan^{-1}\left(\frac{\bar{z}_{root} - \bar{z}_{tip}}{\bar{y}_{tip} - \bar{y}_{root}}\right) \qquad (83)$$

and the other quantities are defined by the sketch on page 20.

2) Solve Eq. (23) for $g'(x)$ with $K(x)$ defined by Eq. (25). Then the axial distribution of lift on the wing alone is given by

$$\frac{1}{q}\frac{dL}{dx} = 2g'(x) \qquad (84)$$

38

3) Find the axial distribution of body carry-over lift by subtracting the result of 2) from that of 1).

    b.   Solution of the Integral Equation

       The integral equation relating streamwise velocity perturbation to upwash velocity was reduced by Lawrence to the following

$$k(x) = \frac{1}{2} g(x) + \frac{1}{4} \int_0^c g'(\xi) \left[1 + \frac{\sqrt{(x-\xi)^2 + (b/2(x))^2}}{x - \xi} \right] d\xi$$

(23)

This equation may be rewritten, after the transformations

$$X = \frac{c}{2}(1 - \cos\theta)$$

and

$$\xi = \frac{c}{2}(1 - \cos\tau)$$

(85)

as

$$4k(\theta) = 2g(\theta) + g(\pi) + \frac{b(\theta)}{c} \int_0^\pi \frac{g'(\tau) d\tau}{\cos\tau - \cos\theta} + \int_0^\pi g'(\tau) H(\theta,\tau) d\tau$$

(86)

where

$$H(\theta_n, \tau) = \frac{\sqrt{(\cos\tau - \cos\theta_n)^2 + \left(\frac{b^2(\theta_n)}{c^2}\right)} - \frac{b(\theta_n)}{c}}{\cos\tau - \cos\theta_n}$$

$$\theta_n = \frac{n\pi}{N+1}$$

(87)

If $g(\theta)$ is expanded in a Fourier series, and the coefficients for each harmonic are matched, the following set of simultaneous equations is obtained

$$\frac{4}{\pi} k_n = (F_{1n} - F_{0n}) A_0 + \sum_{r=1}^{N-2} (F_{r+1,n} - F_{r-1,n}) A_r \, ; \quad n = 1, 2 \cdots N-1$$

(88)

where

$$k_n = k\left(\frac{n\pi}{N}\right) \text{ and } F_{r,n} = F_r\left(\frac{n\tau}{N}\right)$$

and
$$F_0(\theta_n) = \frac{2\theta_n}{\pi} + H_0(\theta_n, b(\theta_n)) - 3$$

$$F_r(\theta_n) = \frac{2\sin r\theta}{\pi r} + \frac{b(\theta_n)\sin r\theta}{\sin\theta} + H_r(\theta_n, b(\theta)) \quad r = 1, 2 \cdots$$

$$(89)$$

where

$$H_r(\theta_n, b(\theta_n)) = \frac{1}{M}\left[\frac{H(\theta_n, 0) + (-1)^r H(\theta_n, \pi)}{2} + \sum_{m=1}^{M-1} \cos\frac{m\pi r}{M} H\left(\theta_n, \frac{m\pi}{M}\right)\right]$$

$$(90)$$

with $H(\theta_n, \tau)$ defined by Eq. (87). The parameters N and M are the number of stations on the root chord and the number of intervals in the trapezoidal integration, Eq. (90). The values of the semi-span, $b(\theta_n)$ are taken at the centers of N spanwise strips which lie at a distance

$$X_n = \frac{c}{2}\left(1 - \cos\frac{n\pi}{N+1}\right); \quad n = 1, 2, 3 \cdots N$$

$$(91)$$

from the leading edge of the root chord.

The set of simultaneous Eqs. (88) is solved by a matrix inversion procedure. Once the coefficient $g'(x)$ are obtained, the values of $g'(x)$ are found by

$$g'(x) = A_0 \tan(\theta/2) + 2\sum_{r=1}^{N-2} A_r \sin r\theta$$

$$(92)$$

where

$$X = \frac{c}{2}(1 - \cos\theta)$$

It should be noted that compressibility effects are handled by a Prandtl-Glauert transformation in the same manner as described above. If the chordwise distribution of lift is found on a transformed wing-body combination, it must be increased by a factor of $1/\beta$ to get the correct result.

c. Effect of Vortex Wake

The body carry-over lift may only be found by the modified Lawrence method up to the trailing edge of the root chord, as discussed in Section III-C above. On the aft portion of the body, the lift is given by

$$\frac{1}{q}\frac{dL}{dx} = \frac{\Gamma}{U_\infty}\cos\alpha_0 \frac{d}{dx}\left[R.P.\left\{\left(\frac{r^2+k^2}{k^2}\right)\left(t_1^2 - 4k^2\right)^{1/2} - \left(\frac{r^2-k^2}{k^2}\right)t_1\right\}\right]$$

$$(93)$$

40

The strength and position of the vortex are found by considering the lift distribution on the wing in the presence of the body, as discussed in Section III-C-3 above. The change in vortex position and/or body cross-section with X is found by dividing the portion of the body aft of the trailing edge into equal segments, calculating the vortex position at each segment, and differentiating linearly. This process is included in the computer program of Appendix I.

SECTION IV

NONLINEAR WING BODY INTERFERENCE

A. NONLINEAR FLOW PHENOMENA

The methods described in the preceding section are limited in the range of angle of attack over which they may be usefully applied. Above certain angles of attack various flow phenomena appear which cause non-linearities in the forces on wings, bodies, or wing-body combinations. The most common of these phenomena are stall and vortex separation.

Stall occurs most often on wings of moderate to high aspect ratio with slightly or moderately swept leading edges, at fairly high angles of attack. It is characterized by a separation of the flow from the trailing or leading edges or both, and is usually accompanied by a severe decrease in lift. The problem has, in the past, not proved amendable to analytic solution, and has been treated primarily by correlation of experimental data. Much work remains to be done in this area.

Vortex separation, on the other hand, may appear at very low angles of attack, and thus put severe limitations on the linear theories. This is especially true of highly swept slender wings and bodies. Since the effect is primarily one of an increase in lift, which may be desirable, the design operating condition of certain configurations may include vortex separation, whereas it is unlikely that a vehicle will be flown in a stalled condition for very long. Even at low flight angles of attack, vortex separation may be present due to the effective angle of attack as, for example, on a missile launched vertically in a cross wind.

Vortex separation on wing-body configurations will, therefore, be the principal nonlinear effect considered in this report. Further dis- cussion on nonlinear loads may be seen in Ref. 15.

B. FLOW MODELS

1. Description of the Models

Starting at moderate angles of attack, the flow separates from the lee side of lifting bodies, due to the inability of the cross-flow boundary layer to negotiate an adverse pressure gradient, and rolls up into a pair of trailing vortices. In a similar manner, the flow separates from the leading edges of slender wings. Both of these separated flow phenomena will be present for a wing-body combination, if the body extends far enough forward of the leading edge of the wing to allow the separated flow on the body to develop. This section describes a method to be used for taking account of these phenomena in calculating the forces on a wing-body combination.

Three models of the flow are examined. In the first, or "approximate" model, the strength and position of the vortices separating from the body are

43

calculated by the method of Ref. 13 up to the position of the wing leading edge. These are then held constant to the trailing edge of the wing, where changes in their strength and position are allowed to resume. The wing vortex strength and position are found by applying the method of Ref. 16 to the exposed wing alone.

Aft of the trailing edge of the wing, the separated wing vortices are included in the trailing vortices due to wing lift. The body vortices are considered to have no influence on the strength and position of the wing vortices, and vice versa.

In the second, or "exact" model of the flow, the two-dimensional cross flow about the wing-body combination with four separated vortices is considered at each station aft of the leading edge of the wing. The strengths and positions of the vortices are the unknowns. They may be found by slender body theory applying the appropriate boundary conditions and force equations; i. e., that the points where the feeding sheets leave the body and the wing are stagnation points, and that the total force on each vortex and its feeding sheet is zero.

In the third, or "quasi-exact" model, the assumption is made that, because of the blocking effect of the wing, there can be no separation on the body over the area of the wing body juncture. Thus the strength of the body vortex remains constant over this area, and both the vortex and its feeding sheet (which will be of zero strength) are force free. Interactions between wing and body vortices are permitted as in the "exact" model.

Once the strengths and positions of the vortices are known, from one of the above flow models, the forces on the wing-body combination are calculated. Reference 16 gives the nonlinear wing lift due to the wing vortices for uncambered delta wings. This method will be adapted to include the effect of the body vortices. The forces on the body may be found by the method of Ref. 13.

It will be noted that slender body theory is used throughout for calculating the vortex strengths and positions and the nonlinear forces which they induce. While it is anticipated that better methods would be used for calculating linear wing-body interference effects, it is felt that inclusion of the nonlinear results is a significant enough improvement to warrant use of the simplifying assumptions of slender body theory.

This method for calculating nonlinear forces is restricted to bodies with mid-plane wings only, but could be adapted to nonmid plane wings by the inclusion of the necessary conformal transformations. Extension to cambered wing-body combination could be accomplished by a method similar to that of Ref. 13.

2. Approximate Model

In the approximate model, the wing vortex system and the body vortex system are assumed to be independent. Both have an effect on the flow field, and thus on the forces on the wing-body combination, but neither vortex system has an effect on the strength and position of the other.

The following procedure will be applied:

1) Calculate the strength and position of the body vortex system up to the position of the wing leading edge, by the method of Ref. 13 (outlined below).

2) Calculate the strength and position of the vortex system on the wing alone, from the leading to trailing edges, by the method of Ref. 16.

3) Resume calculation of the body vortex strength and position, using the final values obtained at the leading edge as initial conditions, up to the end of the body. (If the end of the body occurs at the same axial station as the trailing edge of the wing, this step will be omitted).

4) Assuming that the strength and position of the body vortices remains constant over the wing-body juncture, and that the strengths and positions of the wing and body vortices vary as found in Steps 1) thru 3) above, calculate the loads on the wing-body combination. Part C of this section outlines methods for doing this.

a. Body Vortex Theory

Of various possible methods for taking account of the vortex separation on slender bodies (Refs. 17, 18, 19, 20), that proposed by Bryson (Ref. 20) seems to incorporate the main features of the flow in the simplest mathematical form. In this model, illustrated in the following sketch, the separated vortices are joined to the body by straight feeding sheets.
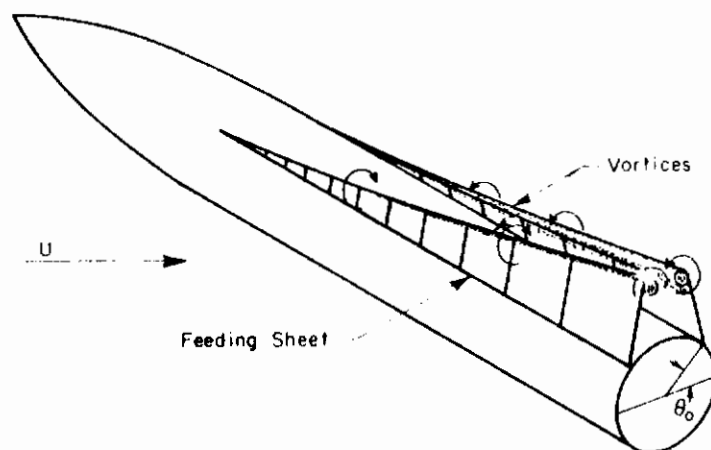
Bryson gives solutions for the vortex strength and position as a function of time (or distance along the body) and calculates the resulting body normal force for circular cones and cylinders. These solutions have been extended in Ref. 13 to bodies of elliptic cross section having arbitrary contour and camber distribution.

Bryson's treatment of a circular body may be summarized as follows:

1) According to slender body theory, the flow in a plane perpendicular to the body, at a distance x from the nose is analogous to the cross flow at $t = x/U_\infty \cos \alpha$ about a cylinder whose dimensions may be changing.

2) The force on each vortex is assumed to be balanced by an opposite force on its feeding sheet. Since each feeding sheet carries vorticity to its

45

main vortex at a rate $\frac{d\Gamma}{dt}$, it must support a force in the cross flow plane equal to

$$F = \rho \frac{d\Gamma}{dt} (\mathcal{S}_1 - \mathcal{S}_1') \tag{94}$$

where $\mathcal{S}_1$ is the position of the vortex, and $\mathcal{S}_1'$ is the base of the feeding sheet. The force on the main vortex is

$$F = \rho \Gamma \left(w_{\mathcal{S}_1} - \frac{d\mathcal{S}_1}{dt} + S_1 \right) \tag{95}$$

where $w_{\mathcal{S}_1}$ is the velocity at the vortex due to all elements of the flow except the vortex itself; S_1 is the velocity due to a source flow needed to account for the rate of growth of the body cross section; $\frac{d\mathcal{S}_1}{dt}$ is the relative velocity of the vortex. Equating the force makes

$$\frac{d\Gamma}{dt} (\mathcal{S}_1 - \mathcal{S}_1') = \Gamma \left(w_{\mathcal{S}_1} - \frac{d\mathcal{S}_1}{dt} + S_1 \right) \tag{96}$$

The velocity $w_{\mathcal{S}_1}$ at $\mathcal{S}_1$ is easily calculated by adding the velocity potential for a cylinder in a cross flow to the potentials for a vortex at $-\mathcal{S}_1$ and corresponding image vortices inside the circle which preserve the boundary condition on the surface.

3) This equation is then integrated numerically by a finite-difference approximation to give the vortex strength and position.

In Bryson's treatment of the development of a time-varying vortex wake behind a circular cylinder, two parameters appear which must be empirically prescribed. One such parameter is the point around the cylinder (determined by the angle θ_0) at which the feeding sheets depart from the surface of the body. The other parameter is the distance from either vortex to the body at the instant when the calculation begins. Bryson's potential flow theory predicts an exponential initial development of the vortex; that is, the rate of increase is proportional to the strength, hence it would never grow if it started with zero strength on the surface of the body. Analogous parameters appear in the three-dimensional theory. The assumption is made, however, that the potential flow analysis is not valid until the vortex has emerged from the boundary layer; while Bryson, on the other hand, imposed the additional restriction that the vortex must approach the body surface at a long time before the start of the problem.

Theoretical predictions of the location of separation of the feeding sheet and the initial strength of the emerging vortex would in principle, require an analysis of the viscous separation process. However, a preliminary investigation, reported in Ref. 21 indicated that the separation process would probably be more sensitive to the pressure gradients created by a viscous flow than to the viscous forces themselves. Consequently, "infinite Reynolds number" theories have been applied to the two-dimensional and three-dimensional separation problems. These theories, described in Ref. 13, were not successful, partly because the two-vortex model of the separated flow gives a distorted prediction of local surface pressure distribution.

46

Since analytic determination of the parameters was unsuccessful, they have been established empirically on the basis of experiments reported in Refs. 22 and 23. Comparisons of theoretical and experimental normal force and pitching moment in Ref. 13 show good agreement, which could have been improved by a better selection of the separation parameters. Selection of the separation points is discussed in Section D below.

b. Wing Vortex Theory

The wing vortex theory of Ref. 16 may be thought of as a special case of the general theory of Ref. 13, when the elliptic cross-section collapses to a flat plate. A conical body would thus approach a delta wing.

The separation points, however, are determined by applying a Kutta condition at the wing leading edge. In order that this be satisfied, the flow must leave the wing tangentially at this point.

3. "Exact" Flow Model

The "exact" flow model is one in which the strength and positions of the four separated vortices are calculated simultaneously, i.e., the approximation that the body vortices are constant in strength and position over the area of the wing is not made.

a. Velocity Potential

Consider, in the two-dimensional cross flow plane, the flow about two pairs of symmetrically placed vortex-feeding sheet systems, as shown in the following sketch.
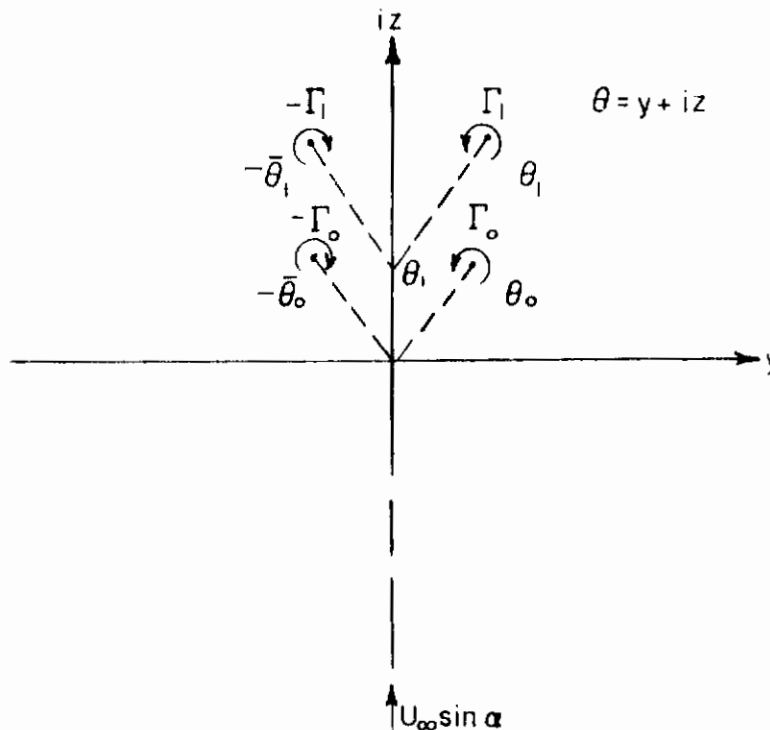
The complex potential function may be written

$$\bar{\phi}(\theta) = \frac{-i\Gamma_o}{2\pi} \ln\left(\frac{\theta - \theta_o}{\theta + \bar{\theta}_o}\right) - \frac{i\Gamma_i}{2\pi} \ln\left(\frac{\theta - \theta_i}{\theta + \bar{\theta}_i}\right) - iU_\infty \sin\alpha\,\theta \tag{97}$$

After applying the conformal transformation $\theta = \sqrt{\sigma^2 - s'^2}$, the potential function $\bar{\phi}(\sigma)$ will represent the cross flow about a flat plate of half-width s' and the vortex systems, as shown below
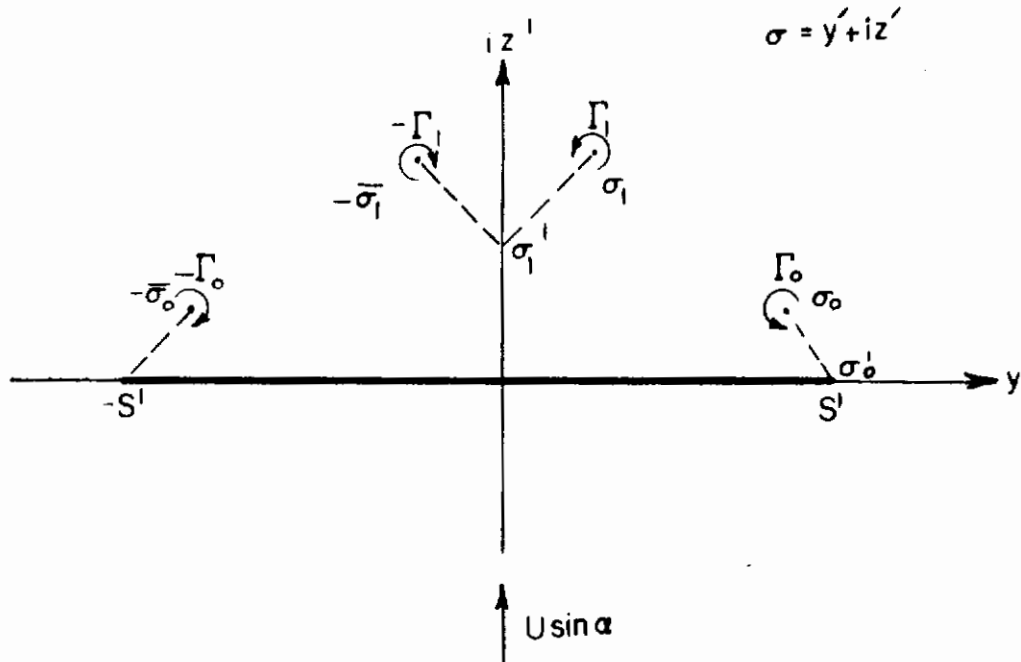
The complex potential function is:

$$\bar{\phi}(\sigma) = \frac{-i\Gamma_o}{2\pi} \ln\left(\frac{\sqrt{\sigma^2 - s'^2} - \sqrt{\sigma_o^2 - s'^2}}{\sqrt{\sigma^2 - s'^2} + \sqrt{\bar{\sigma}_o^2 - s'^2}}\right)$$

$$-\frac{i\Gamma_i}{2\pi} \ln\left(\frac{\sqrt{\sigma^2 - s'^2} - \sqrt{\sigma_i^2 - s_i'^2}}{\sqrt{\sigma^2 - s'^2} + \sqrt{\bar{\sigma}_i^2 - s'^2}}\right) - iU\sin\alpha \sqrt{\sigma^2 - s'^2} \tag{98}$$

By applying a further transformation to the $\mathcal{S}$-plane,

$$\sigma = \frac{(k^2 - r^2)\mathcal{S} + (k^2 + r^2)(\mathcal{S}^2 - 4k^2)^{\frac{1}{2}}}{2k^2} \tag{99}$$

where $k^2 = (a+b)(a-b)/4$ and $r = (a+b)/2$, the potential function can be made to represent the flow about an elliptical two-dimensional body with a mid-plane wing and the four vortex systems, as shown in the following sketch.
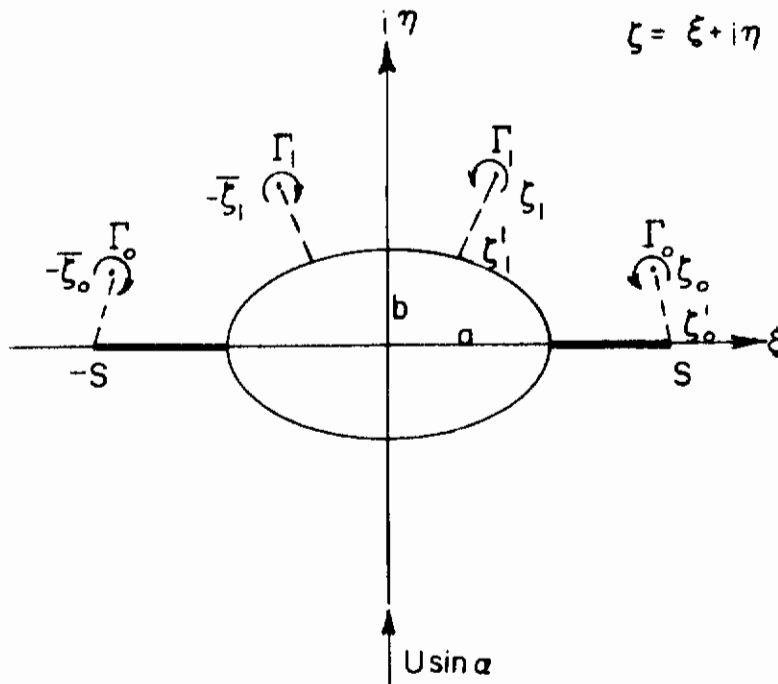
The potential function may then be written as:

$$\phi(\vartheta) = -\frac{i\Omega}{2\pi}R_m\left\{\sqrt{\frac{(k^2-\nu)^3\bar{J}^2+2(k^4-\nu^4)\bar{J}(\bar{J}^2-4k^2)^{1/2}+(k^2+\nu)^2(\bar{J}^2-4k^2)-S'^2}{4k^2}} - \sqrt{\frac{(k^2-\nu)^3\bar{J}_0^2+2(k^4-\nu^4)\bar{J}_0(\bar{J}_0^2-4k^2)^{1/2}+(k^2+\nu)^2(\bar{J}_0^2-4k^2)-S'^2}{4k^2}}\right\}$$

$$+\frac{i\Omega}{2\pi}R_m\left\{\sqrt{\frac{(k^2-\nu)^3\bar{J}^2+2(k^4-\nu^4)\bar{J}_1(\bar{J}_1^2-4k^2)^{1/2}+(k^2+\nu)^2(\bar{J}_1^2-4k^2)-S'^2}{4k^2}} - \sqrt{\frac{(k^2-\nu)^3\bar{J}_0^2+2(k^4-\nu^4)\bar{J}_1(\bar{J}_1^2-4k^2)^{1/2}+(k^2+\nu)^2(\bar{J}_1^2-4k^2)-S'^2}{4k^2}}\right\}$$

$$-iU_\alpha\sqrt{\frac{(k^2+\nu)^2\bar{J}^2+2(k^4-\nu)\bar{J}(\bar{J}^2-4k^2)^{1/2}+(k^2+\nu)^2(\bar{J}^2-4k^2)-S'^2}{4k^2}}$$

(100)

50

This function represents the two-dimensional cross-flow about a wing-body combination. In order to take account of the growth of the body in the X-direction, the complex velocity potential of a source within the body must be added. The strength of the source must be such that the outflow at the surface of the body just matches the growth rate of the body. In this way, the boundary condition of no flow through the body is satisfied in the X-direction. The assumption that a two-dimensional source in the cross flow plane may be applied is just the slender body approximation.

The complex velocity potential of a source satisfying the boundary conditions on an elliptic body may be found by transforming the complex potential which satisfies the boundary conditions on a circular body. This function may be written

$$\phi_s = k \ln X \tag{101}$$

The following sketch shows the circular body in the X-plane
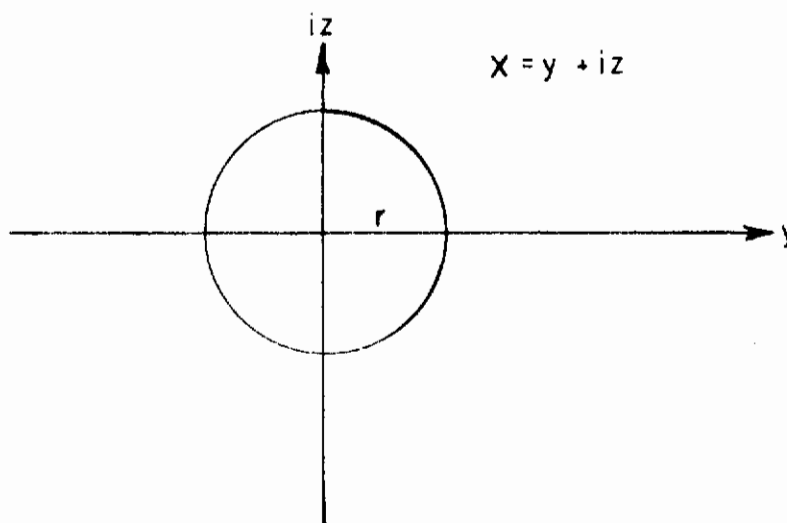
The circle in the X-plane may be transformed to an ellipse in the $\mathcal{Y}$-plane by the transformation

$$X = \frac{1}{2}\left(\mathcal{Y} + \sqrt{\mathcal{Y}^2 - 4k^2}\right) \tag{102}$$

The potential due to the source in the $\mathcal{Y}$-plane is

$$\phi_s(\mathcal{Y}) = k \ln\left[\frac{1}{2}\left(\mathcal{Y} + \sqrt{\mathcal{Y}^2 - 4k^2}\right)\right] \tag{103}$$

51

and the complex conjugate of the velocity is given by

$$\bar{S} = \frac{d\bar{\phi}(\mathcal{Y})}{d\mathcal{Y}} = \frac{K}{\sqrt{\mathcal{Y}^2 - 4k^2}} \tag{104}$$

The boundary condition of no flow through the surface requires that

$$\left.\frac{\bar{S}}{U_\infty \cos \alpha}\right|_{\mathcal{Y} = r + \frac{k^2}{r}} = \frac{d a}{d x} \tag{105}$$

Thus

$$K = U_\infty \cos \alpha \frac{d a}{d x}\left(r - \frac{k^2}{r}\right) \tag{106}$$

or finally

$$\bar{\phi}_s(\mathcal{Y}) = U_\infty \cos \alpha \frac{d a}{d x}\left(r - \frac{k^2}{r}\right) \ln\left[\frac{1}{2}\left(\mathcal{Y} + \sqrt{\mathcal{Y}^2 - 4k^2}\right)\right] \tag{107}$$

The complex potential for treating the three-dimensional wing-body combination by slender body techniques is thus

$$\bar{\phi}_{3-b}(\mathcal{Y}) = \bar{\phi}(\mathcal{Y}) + \bar{\phi}_s(\mathcal{Y}) \tag{108}$$

where $\bar{\phi}(\mathcal{Y})$ is given by Eq. (100).

b. Boundary Conditions

The four unknowns in the problem are the strengths of the vortices, $\mathcal{L}_o$ and $\mathcal{L}_1$, and their positions $\mathcal{Y}_o$ and $\mathcal{Y}_1$. The four specified conditions are:

1) The flow leaves tangentially at the edge of the wing, $\mathcal{Y} = \mathcal{Y}_o'$.

2) There is a stagnation point at the separation point of the body vortex feeding sheet, $\mathcal{Y}_1'$.

3) There is no net force on each wing vortex-feeding sheet system.

4) There is no net force on each body vortex-feeding sheet system.
These conditions may be arrived at as follows:

1) The boundary condition of tangential flow at the leading edge may be satisfied by requiring a stagnation point at the origin of the θ-plane, as the wing tip location maps to the origin when the transformations are applied. The flow in the θ-plane is represented by

$$\bar{\phi}(\theta) = -\frac{i\mathcal{L}_o}{2\pi} \ln\left(\frac{\theta - \theta_o}{\theta + \theta_o}\right) - \frac{i\mathcal{L}_1}{2\pi} \ln\left(\frac{\theta - \theta_1}{\theta + \theta_1}\right) - i U_\infty \sin \alpha \, \theta \tag{109}$$

52

Taking the derivative with respect to θ:

$$\frac{d\bar{\phi}(\theta)}{d\theta} = -\frac{i\Gamma_0}{2\pi}\left(\frac{\theta+\bar{\theta}_0}{\theta-\theta_0}\right)\left(\frac{\theta_0+\bar{\theta}_0}{(\theta+\bar{\theta}_0)^2}\right) - \frac{i\Gamma_1}{2\pi}\left(\frac{\theta+\bar{\theta}_1}{\theta-\theta_1}\right)\left(\frac{\theta_1+\bar{\theta}_1}{(\theta+\bar{\theta}_1)^2}\right) - iU_\infty \sin\alpha \tag{110}$$

Requiring a stagnation point at the origin dictates that

$$\left.\frac{d\bar{\phi}(\theta)}{d\theta}\right|_{\theta=0} = 0 \tag{111}$$

Thus:

$$\frac{\Gamma_0}{2\pi}\left(\frac{1}{\theta_0} + \frac{1}{\bar{\theta}_0}\right) + \frac{\Gamma_1}{2\pi}\left(\frac{1}{\theta_1} + \frac{1}{\bar{\theta}_1}\right) = -U_\infty \sin\alpha \tag{112}$$

2) In a similar manner, the boundary condition of the existence of a stagnation point at the base of the body vortex feeding sheet $(\mathscr{S}_1')$ may be satisfied by requiring a stagnation point at θ_1'. Thus

$$\left.\frac{d\bar{\phi}(\theta)}{d\theta}\right|_{\theta=\theta_1'} = 0 \tag{113}$$

which becomes

$$\frac{\Gamma_0}{2\pi}\left(\frac{\bar{\theta}_0+\theta_0}{(\theta_1'-\theta_0)(\theta_1'+\bar{\theta}_0)}\right) + \frac{\Gamma_1}{2\pi}\left(\frac{\bar{\theta}_1+\theta_1}{(\theta_1'-\theta_1)(\theta_1'+\bar{\theta}_1)}\right) = -U_\infty \sin\alpha \tag{114}$$

3) The condition of no net force on the wing vortex-feeding sheet structure may be satisfied by letting the force on an element of the vortex be just balanced by the force on an element of the feeding sheet.

The force on an element of the feeding sheet between X and $X+dx$ is:

$$dF_{f.s.} = i\rho U_\infty \cos\alpha \frac{d\Gamma_0}{dx}(\mathscr{S}_0 - s)\,dx \tag{115}$$

The force on an element of the concentrated vortex is

$$dF_v = i\rho V_{\mathscr{S}_0}^* \Gamma_0 \, dx \tag{116}$$

where $V_{\mathscr{S}_0}^*$ is the complex flow velocity at the position of the vortex, relative to the vortex itself. The force equation for the wing vortex system is thus

$$\rho U_\infty \cos\alpha \frac{d\Gamma_0}{dx}(\mathscr{S}_0 - s) - \rho V_{\mathscr{S}_0}^* \Gamma_0 = 0 \tag{117}$$

or

$$\frac{d\Gamma_0}{dx} - \frac{V_{\mathscr{S}_0}^*}{U_\infty \cos\alpha}\left(\frac{1}{\mathscr{S}_0 - s}\right)\Gamma_0 = 0 \tag{118}$$

53

Approved for Public Release

The complex velocity at the position of the vortex relative to the vortex, $V_{y_0}^*$, is made up of the velocity due to the complex velocity potential at the position of the vortex minus the complex velocity potential of the vortex itself, minus the velocity of the vortex in the cross flow plane.

The complex velocity potential at the position of the vortex minus the complex velocity potential of the vortex itself may be written

$$\phi_1 (y) = \phi_{(3-D)} (y) + \frac{i \Gamma_0}{2\pi} \ln (y - y_0) \tag{119}$$

where

$$\phi_{(3-D)} (y) = \phi (y) + \phi_s (y) \tag{120}$$

and $\phi_s (y)$ is the complex velocity potential of the source. It is given by

$$\phi_s = U_\infty \cos \alpha \, b \frac{d\alpha}{dx} \ln \left(\frac{1}{2} y + \frac{1}{2} \sqrt{y^2 - 4k^2} \right) \tag{121}$$

The complex potential $\phi_1 (y)$ contributes a velocity

$$(v + i w)_{y_0} = \overline{\left(\frac{d \phi_1 (y)}{dy} \right)}_{y = y_0} \tag{122}$$

The velocity of the vortex in the cross flow plane is

$$\frac{dy_0}{dt} = U_\infty \cos \alpha \frac{dy_0}{dx} \tag{123}$$

Since the velocity relative to the vortex is desired, this term must be subtracted.

The velocity $V_{y_0}^*$ may then be written

$$V_{y_0}^* = \overline{\left(\frac{d \phi_1}{dy} \right)}_{y = y_0} - U_\infty \cos \alpha \frac{dy_0}{dx} \tag{124}$$

It is possible to obtain an expression for $(d\phi_1 / dy)_{y=y_0}$ by differentiating Eq.(119) and evaluating at y_0 . This procedure is rather tedious, however, and a different approach is more desirable.

Equation (119) may be written in the θ-plane as:

$$\phi_1 (\theta) = - \frac{i \Gamma_0}{2\pi} \ln \left(\frac{\theta - \theta_0}{\theta + \theta_0} \right) - \frac{i \Gamma_1}{2\pi} \ln \left(\frac{\theta - \theta_1}{\theta + \theta_1} \right) - i U_\infty \sin \alpha \, \theta +$$

$$\phi_s (\theta) + \frac{i \Gamma_0}{2\pi} \ln (\theta - \theta_0) \tag{125}$$

54

Differentiating with respect to θ and evaluating at θ_0

$$\left. \frac{d\bar{\ell}_1(\theta)}{d\theta} \right|_{\theta=\theta_0} = \frac{i\ell_0}{2\pi}\left(\frac{1}{\theta_0+\bar{\theta}_0}\right) - \frac{i\ell_1}{2\pi}\frac{\bar{\theta}_1+\theta_1}{(\theta_0-\theta_1)(\theta_0+\bar{\theta}_1)} - iU_\infty \sin\alpha + \left. \frac{d\bar{\ell}_s(\theta)}{d\theta}\right|_{\theta=\theta_0} \tag{126}$$

The final term, $d\bar{\ell}_s/d\theta$ may be easily seen as

$$\frac{d\bar{\ell}_s}{d\theta} = \frac{d\bar{\ell}_s}{d\mathcal{S}}\frac{d\mathcal{S}}{d\theta} \tag{127}$$

$$= U_\infty \cos\alpha \; b\frac{da}{dx}\left(1/\sqrt{\mathcal{S}^2-4k^2}\right)\left.\frac{d\mathcal{S}}{d\theta}\right|_{\theta=\theta_0} \tag{128}$$

where

$$\mathcal{S} = \frac{(k^2+\ell^2)(\sqrt{\theta^2+s'^2+4r^2})-(k^2-r^2)(\sqrt{\theta^2+s'^2})}{2r^2} \tag{129}$$

which may be found from the inverse of the transformations $\sigma = \sigma(\mathcal{S})$ and $\theta = \theta(\sigma)$ given above.

Taking the derivative of Eq.(129):

$$\frac{d\mathcal{S}}{d\theta} = \left(\frac{k^2+r^2}{2r^2}\right)\left(\frac{\theta}{\sqrt{\theta^2+s'^2+4r^2}}\right) - \left(\frac{k^2-r^2}{2r^2}\right)\left(\frac{\theta}{\sqrt{\theta^2+s'^2}}\right) \tag{130}$$

By substituting the expressions for $\mathcal{S}$ (from Eq. 129) and $d\mathcal{S}/d\theta$ (from Eq. 130), an expression in terms of θ only maybe derived for $d\bar{\ell}_s/d\theta$.

4) The condition of no force on the body vortex-feeding sheet structure may be found in a completely analogous manner as

$$\frac{d\mathcal{L}_1}{dx} - \frac{V_{\mathcal{S}_1}^*}{U_\infty \cos\alpha}\left(\frac{1}{\mathcal{S}_1-\mathcal{S}_1'}\right)\mathcal{L}_1 = 0 \tag{131}$$

where the complex velocity V_1^* is now to be evaluated at the position of the body vortex $\mathcal{S}_1$, and where $\mathcal{S}_1'$ is the prescribed separation point of the feeding sheet.

    c.   Solution of Equations

The system of four simultaneous equations to be solved for the four unknown $\mathcal{L}_0$, $\mathcal{L}_1$, $\mathcal{S}_0$, $\mathcal{S}_1$, may now be written as:

$$\frac{d\mathcal{L}_o}{dx} - \frac{V_{S_o}^*}{U_\infty \cos\alpha}\left(\frac{1}{S_o - S}\right)\mathcal{L}_o = 0 \qquad (132a)$$

$$\frac{d\mathcal{L}_1}{dx} - \frac{V_{S_1}^*}{U_\infty \cos\alpha}\left(\frac{1}{S_1 - S_1'}\right)\mathcal{L}_1 = 0 \qquad (132b)$$

$$\frac{\mathcal{L}_o}{2\pi}\left(\frac{1}{\theta_o} + \frac{1}{\bar{\theta}_o}\right) + \frac{\mathcal{L}_1}{2\pi}\left(\frac{1}{\theta_1} + \frac{1}{\bar{\theta}_1}\right) = -U_\infty \sin\alpha \qquad (132c)$$

$$\frac{\mathcal{L}_o}{2\pi}\frac{\bar{\theta}_o - \theta_o}{(\theta_1' - \theta_o)(\theta_1' + \bar{\theta}_o)} + \frac{\mathcal{L}_1}{2\pi}\frac{\bar{\theta}_1 + \theta_1}{(\theta_1' - \theta_1)(\theta_1' + \bar{\theta}_1)} = -U_\infty \sin\alpha \qquad (132d)$$

when the appropriate substitutions for θ_o, $\bar{\theta}_o$, θ_1 and θ_1' are made in terms of S_o, $\bar{S}_o$, S_1, $\bar{S}_1$ and S_1'.

It is obvious that solution of the above set of equations should be accomplished numerically, in order to obtain meaningful solutions with a reasonable amount of effort. Such a solution would be in the form of a simultaneous numerical integration in the X -direction of the force equations, (132a) and (132b), subject to the boundary conditions (132c) and (132d). The solution may then be started at any axial station X, provided the initial values of $\mathcal{L}_o$, $\mathcal{L}_1$, S_o and S_1 are known. The separation point S_1', the body cross section, given by a and b, and the total span S must all be prescribed explicitly as functions of X.

The numerical solution may be carried out by starting the integrations a short distance back from the nose of the body. A discussion of the starting problem will be found in Section D below and in Ref. 13 Since at these forward stations the exposed wing span is zero, only the body vortex system would be present. The wing vortex system would begin when the leading edge of the wing was reached. It would thus be possible to compare solutions by this method with those for the body vortex strength and position by the method of Ref. 13. This would be desirable in order to assure that the inclusion of the wing vortex terms introduces no unforeseen numerical difficulties.

A direct check on the approximate model would also be provided. The assumptions that the body vortex is constant over the wing, and that there is no mutual interaction between the wing and body vortex systems would also be tested.

4. "Quasi-Exact" Model

Although a solution to the above "exact" model would give (within the limitations of the original vortex feeding sheet model of the separated flow) the correct nonlinear load on wing-body combinations, the numerical procedures involved are quite lengthy. If certain physical assumptions are made (not quite so restrictive as those of the "approximate" model), the solution may be greatly simplified, without losing any of the essential features of the exact model. This section describes the resulting "quasi-exact" model of the flow.

56

a. Physical Considerations

In Section 3, the existence of two separate vortex feeding sheet systems, one on the wing and one on the body, is assumed. In order to solve the resulting equations, the separation points of both feeding sheets must be specified. By applying a Kutta condition to the wing, it is determined that the flow must leave the wing tangentially at the leading edge. The separation point on the body is not so easily determined. For the portion of the body ahead of and behind the wing, the methods of Ref.13 may be applied. Between the leading and trailing edges, however, it is likely that the blocking effect of the wing prohibits any further separation of the flow from the lee side of the body, except secondary separation which will not be considered here. Thus the strength of the body vortex would remain constant over the wing. In light of this physical consideration, then, it seems more plausible to specify the strength of the body vortex as constant over the wing, rather than specifying the position of the separation point and allowing the strength to vary as in the exact model. Thus the feeding sheet disappears and the vortex becomes force-free. In general, at low angles of attack a stagnation point will appear on the top surface of the wing and another behind the lee side of the body as shown below on the left. At higher angles, the two reverse flow regions may merge as shown on the right.


```
BODY VORTEX
ZERO STREAMLINE

WING VORTEX
ZERO STREAMLINE

COMBINED ZERO
STREAMLINE
```

$U_\infty \sin \alpha$ $U_\infty \sin \alpha$

x - STAGNATION POINTS
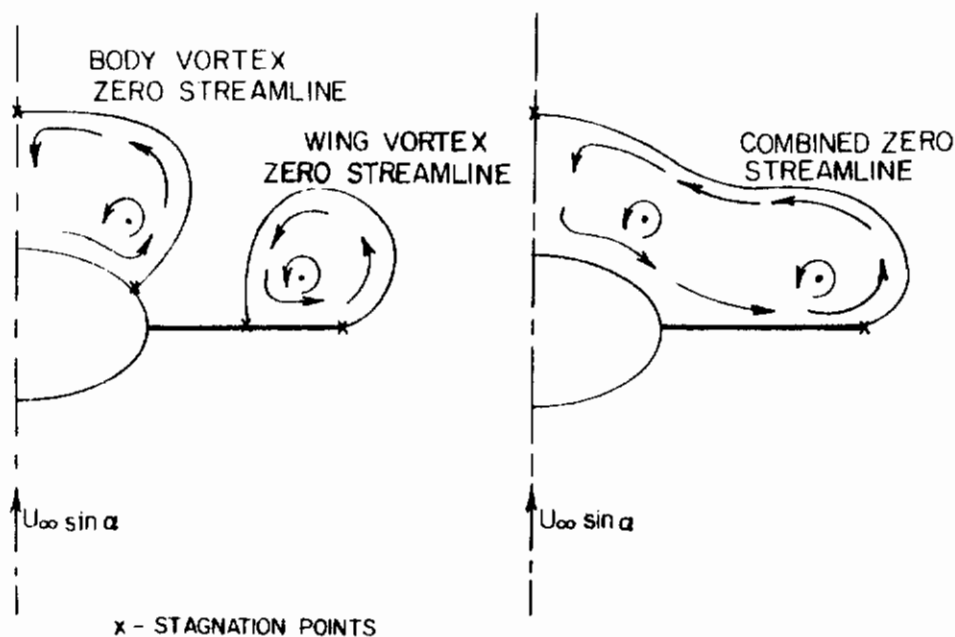
The situation depicted on the left is especially likely to be encountered on not-so-slender configurations at low angles of attack $(\alpha/\epsilon < \approx 1)$. Brown and Michael (Ref. 16) show that for a conical wing alone the stagnation point occurs just at the wing centerline when $\alpha/\epsilon \approx 1$.

In the case illustrated on the left, the assumption of the nonexistence of a feeding sheet for the body vortex may not be valid. In such cases, therefore, the "exact" model might give better results if the appropriate separation point location can be specified.

57

In the present simplified model the boundary conditions tend to make the mathematical description of the physical situation more tractable than for the "exact" model. It is felt that the assumptions made are logical ones, based on the physical nature of the problem, and that no essential features of the exact model are destroyed by them, within the above mentioned limitations on angle of attack and slenderness.

b. Mathematical Description

The derivation of the two-dimensional complex potential for a wing-body combination given in Section 3 is still valid, since only the presence of the vortices is assumed, and not any changes in their strengths. The sketches should be modified so that the body vortex feeding sheet is replaced by a "branch cut". The set of boundary conditions listed in Section 3-b as uniform over the entire length of the body, should be replaced by the following sets over the appropriate portions of the body:

a) For $0 < X \leq X_{LE}$ (body nose to wing leading edge)
   1) The body separation point y_1' is a stagnation point.
   2) There is no net force on each body vortex-feeding sheet system.

b) For $X_{LE} < X \leq X_{TE}$ (leading edge to trailing edge)
   1) The flow leaves tangentially at the edge of the wing y_0'.
   2) There is no net force on the wing vortex-feeding sheet system.
   3) There is no force on the body vortex.

c) For $X_{TE} < X \leq \ell$ (trailing edge to aft end of body)
   1) The body separation point is a stagnation point.
   2) There is no net force on the body vortex-feeding sheet system.
   3) There is no force on the wing vortex.

One other physical feature of the flow must be considered in setting up the mathematical model. Free vortices rotating in the same direction in close proximity will tend to roll up together. This may be seen in the rolling up of the trailing vortex sheet behind a wing into two strong tip vortices. It is possible, with the proposed exact model, that the interaction between the wing and body vortices might be such as to cause the rolling-up of these two vortices, in which case the body vortex would pass through the wing vortex feeding sheet. It is felt, however, that this tendency would not be serious enough to invalidate the proposed model because: 1) a complete rolling-up in the manner described would probably occur, except in rare circumstances, only at locations far downstream of the leading edge, due to the weakness of the vortex at forward stations; and 2) the concept of a straight feeding sheet is merely an idealization of the complicated nature of flow separation at the leading edge, and the crossing of the supposed location of the feeding sheet by the body vortex would in reality have no physical significance.

c. Boundary Conditions

The boundary conditions stated above may be expressed over the three portions of the wing-body combination as follows:

a) $0 < X \leq X_{L_{\scriptsize{\theta}}}$

1) The boundary condition of a stagnation point at the base of the body vortex feeding sheet $(\mathcal{T}_{1}')$ may be satisfied by requiring a stagnation point at θ_{1}' in the θ-plane, which is the location of the prescribed body separation point under the transformations given above.

The flow in the θ-plane, due to the body vortex and the free stream is given by

$$\bar{\phi}(\theta) = - \frac{i \Gamma_{1}}{2\pi} \ln\left(\frac{\theta - \theta_{1}}{\theta + \bar{\theta}_{1}}\right) - i U_{\infty} \sin \alpha \; \theta \tag{133}$$

Requiring a stagnation point at the body separation point dictates that:

$$\frac{d\bar{\phi}(\theta)}{d\theta}\bigg|_{\theta = \theta_{1}'} = 0 \tag{134}$$

Thus:

$$\frac{\Gamma_{1}}{2\pi}\left(\frac{\bar{\theta}_{1} + \theta_{1}}{(\theta_{1}' - \theta_{1})(\theta_{1}' + \bar{\theta}_{1})}\right) = -U_{\infty} \sin \alpha \tag{135}$$

2) The condition of no net force on the body vortex-feeding sheet structure may be satisfied by letting the force on an element of the vortex just be balanced by the force on an element of the feeding sheet.

The force on an element of the feeding sheet between X and $X + dX$ is

$$dF_{f.s.} = - i \rho V_{\mathcal{T}_{1}}^{*} \Gamma_{1} dX \tag{136}$$

The force on an element of the concentrated vortex is

$$dF_{v} = i \rho V_{\mathcal{T}_{1}}^{*} \Gamma_{1} dX \tag{137}$$

where $V_{\mathcal{T}_{1}}^{*}$ is the complex flow velocity at the position of the vortex, relative to the vortex itself. The force equation for the body vortex system is thus

$$\rho U_{\infty} \cos \alpha \frac{d\Gamma_{1}}{dX}\left(\mathcal{T}_{1} - \mathcal{T}_{1}'\right) - \rho V_{\mathcal{T}_{1}}^{*} \Gamma_{1} = 0 \tag{138}$$

59

or:

$$\frac{d\Gamma_1}{dx} - \frac{V_{\mathcal{Y}_1}^*}{U_\infty \cos\alpha}\left(\frac{1}{\mathcal{Y}_1 - \mathcal{Y}_1'}\right)\Gamma_1 = 0 \qquad (139)$$

as before.

b) $X_{LE} < X \leq X_{TE}$

1) The boundary condition that the flow leaves tangentially at the edge of the wing $(\mathcal{Y}_0)$ may be satisfied by requiring a stagnation point at the origin of the θ -plane, since the wing tip location maps to the origin when the transformations are applied.

The flow in the θ -plane now includes the wing vortex, and is given by

$$\bar{\phi}(\theta) = -\frac{i\Gamma_1}{2\pi}\ln\left(\frac{\theta - \theta_1}{\theta + \bar\theta_1}\right) - \frac{i\Gamma_0}{2\pi}\ln\left(\frac{\theta - \theta_0}{\theta + \bar\theta_1}\right) - iU_\infty \sin\alpha\,\theta \qquad (140)$$

Requiring a stagnation point at the origin:

$$\left.\frac{d\bar{\phi}(\theta)}{d\theta}\right|_{\theta=0} = 0 \qquad (141)$$

Thus:

$$\frac{\Gamma_0}{2\pi}\left(\frac{1}{\theta_0} + \frac{1}{\bar\theta_0}\right) + \frac{\Gamma_0}{2\pi}\left(\frac{1}{\theta_1} + \frac{1}{\bar\theta_1}\right) = -U_\infty \sin\alpha \qquad (142)$$

2) The boundary condition that there is no net force on the wing vortex-feeding sheet system is satisfied by letting the forces on the vortex and the feeding sheet cancel as shown in a-2) above for the body vortex.

Thus:

$$\frac{d\Gamma_0}{dx} - \frac{V_{\mathcal{Y}_0}^*}{U_\infty \cos\alpha}\left(\frac{1}{\mathcal{Y}_0 - s}\right)\Gamma_0 = 0 \qquad (143)$$

3) The condition that the body vortex is force free is satisfied by letting the flow velocity at the position of the vortex relative to the vortex be zero.

That is:

$$V_{\mathcal{Y}_1}^* = 0 \qquad (144)$$

60

Or, from Eq. (124):

$$U_\infty \cos \alpha \, \frac{d\mathcal{S}_1}{dx} = \overline{\left(\frac{d\bar{\Phi}_1}{d\mathcal{S}}\right)}_{\mathcal{S}=\mathcal{S}_1} \tag{145}$$

where $\Phi_1(\mathcal{S})$ is the complex potential of the flow without the inclusion of the vortex in question, located at $\mathcal{S}_1$, but includes the flow due to a source, as discussed in Section IV-B-3 above.

    c) $X_{TE} < X \leq \mathcal{L}$

        1) The condition of a stagnation point at the body separation point is identical to that given in Eq. (134) above except that $\Phi(\theta)$ must now include the wing vortices.

Thus:

$$\frac{\mathcal{L}_0}{2\pi}\left(\frac{\bar{\theta}_0 + \theta_0}{(\theta' - \theta_0)(\theta' + \theta_0)}\right) + \frac{\mathcal{L}_1}{2\pi}\left(\frac{\bar{\theta}_1 + \theta_1}{(\theta' - \theta_1)(\theta' + \bar{\theta}_1)}\right) = -U_\infty \sin \alpha \tag{146}$$

        2) The force-free condition on the body vortex-feeding sheet system is the same as that of Eq. (139) above, except that now $V_{\mathcal{S}_1}^*$ includes the velocity due to the wing vortices.

$$\frac{d\mathcal{L}_1}{dx} - \frac{V_{\mathcal{S}_1}^*}{U_\infty \cos \alpha}\left(\frac{1}{\mathcal{S}_1 - \mathcal{S}_1'}\right)\mathcal{L}_1 = 0 \tag{147}$$

        3) The force-free condition of the wing vortex is similar to that of Eq. (145) above, but the velocity is calculated relative to the wing vortex.

Thus:

$$U_\infty \cos \alpha \, \frac{d\mathcal{S}_0}{dx} = \overline{\left(\frac{d\bar{\Phi}_1}{d\mathcal{S}}\right)}_{\mathcal{S}=\mathcal{S}_0} \tag{148}$$

where now $\Phi_1(\mathcal{S})$ does not include the vortex at $\mathcal{S}_0$.

    Here the physical nature of the situation must be again considered. The developed mathematical model must be used with caution, due to possible interactions between the body vortex, the wing vortex, and the trailing vortex sheet behind the wing which was generated by the linear component of lift on the wing. Since the determination of this component, and the strength of the resulting trailing vortex sheet or rolled-up vortex, was described in Section III above, no attempt will be made here to include it in the nonlinear model. It should suffice to say, rather, that the model must be used with caution behind the trailing edge of the wing, especially for configurations with long afterbodies at lower angles of attack, and that further investigations in this area might be desirable.

d. Solution of Equations

The method outlined in Section 3 for finding the strength and position of the separated vortices remains essentially unchanged, except that now there is only one complex differential equation to be integrated numerically at any particular axial station, subject to one or two boundary conditions. The resulting numerical procedures, discussed below, are much less cumbersome than for the exact model.

C. NONLINEAR FORCES ON WING-BODY COMBINATIONS

Once the unknown strengths and positions of the separated vortices are found, the resulting lift distributions on the wing and body may be determined. The spanwise lift distribution on the wing is found by chordwise integration of the pressure distribution. The axial distribution of lift on the body is found by momentum considerations.

An expression for the pressure coefficient is given in Ref. 16 as:

$$\frac{\Delta P}{q} = \left(-2\, \frac{\phi_x(x,z)}{U} + \alpha^2 - \frac{\phi_z^2(x,z)}{U^2} \right)_{z=0} \tag{149}$$

where $\phi =$ velocity potential $= R.P.(\bar{\phi}(\varsigma))$, since $\bar{\phi}(\varsigma)$ may be written as

$$\bar{\phi}(\varsigma) = \phi + i\, \psi \tag{150}$$

The derivatives of the velocity potential are then:

$$\phi_x = \frac{\partial \phi}{\partial x} = \frac{\partial}{\partial x}\, R.P.\, (\bar{\phi}(\varsigma)) \tag{151}$$

and

$$\phi_z = R.P.\left(\frac{d\bar{\phi}(\varsigma)}{d\varsigma} \right) \tag{152}$$

The complex potential may be written

$$\bar{\phi}(\varsigma) = \bar{\phi}_{vortices} + \bar{\phi}_{free-stream} + \bar{\phi}_{source} \tag{153}$$

and is given as $\bar{\phi}_{(3-0)}(\varsigma)$ in Eq.(108). The derivative of the real part of the complex potential with respect to x will be evaluated numerically at several points in the spanwise direction for each chordwise station on the wing, to give $\phi_x(x,\varsigma)$. Similarly, $d\bar{\phi}(\varsigma)/d\varsigma$ is found as before. The real part will also be evaluated numerically at several points in the spanwise direction for each chordwise station on the wing, to give $\phi_z(x,z)$. The complete pressure distribution on the wing may then be found by Eq.(149) above. The pressure distribution may then be integrated to give

62

the total lift and/or center of pressure of the wing and the spanwise lift distribution. Predicted spanwise pressure distributions are not very good, however, due to the negative pressure peaks that will generally appear under the vortices. Further discussion of the limitations of the two-vortex model for predicting loads and pressure distributions on wings will be found in Ref. 15.

The axial distribution of force on the body may be found by momentum considerations. The total force on the wing-body combination, up to station X, may be computed by calculating the change in downward momentum imparted to a cylinder of air enclosing the wing-body combination up to the station X, as shown in the sketch below.
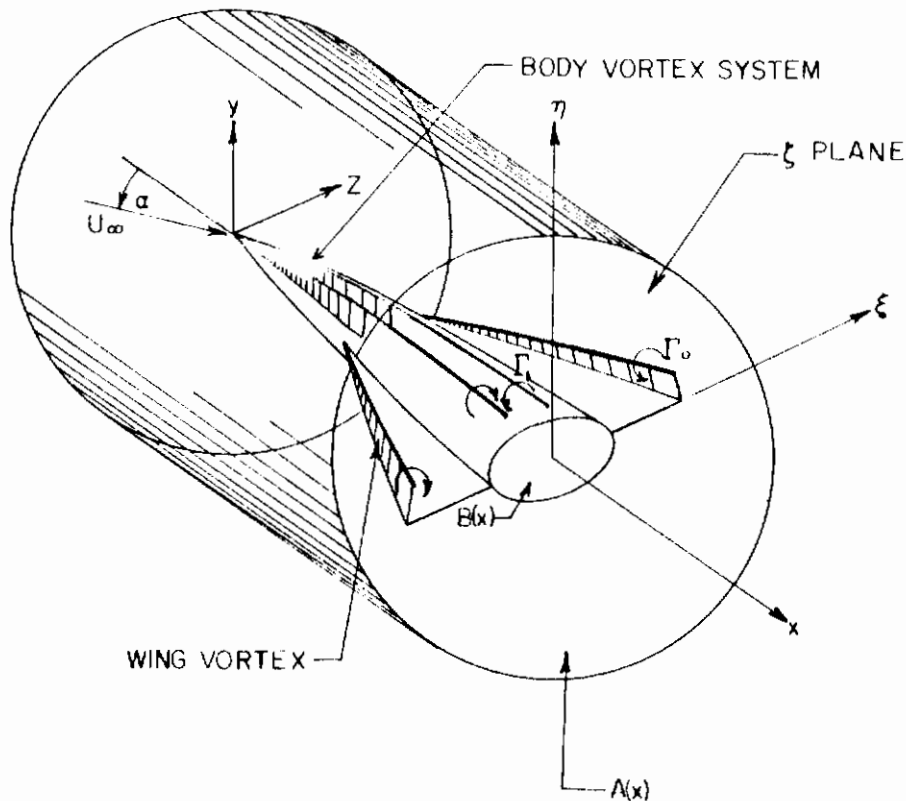
The total normal force up to station X is equal to the rate of downward momentum emerging from the ζ-plane:

$$ N(x) = -\rho U_\infty \cos\alpha \iint_{A(x)} \left[W\eta - U_\infty \sin\alpha \right] d\xi \, d\eta \tag{154} $$

where $A(x)$ is the entire area of the ζ-plane outside the wing-body combination. That is,

$$N(x) = -\rho U_\infty \cos\alpha \left\{ \int\int_{-\infty}^{\infty} \left[W\eta - U_\infty \sin\alpha \right] d\xi \, d\eta - \int\int_{B(x)} \left[W\eta - U_\infty \sin\alpha \right] d\xi \, d\eta \right\}$$

(155)

Integration with respect to η produces contour integrals of the velocity potential:

$$N(x) = -\rho U_\infty \cos\alpha \left\{ \oint_\infty \left[\phi - U_\infty \sin\alpha\, \eta \right] d\xi + \oint_{B(x)} \left[\phi - U_\infty \sin\alpha\, \eta \right] d\xi \right\}$$
(156)

The first integral vanishes, because there is no vertical momentum change at the cylindrical surface as the radius becomes infinite. Also since there is no net force on the vortex-feeding sheet system, the vortices may be included in the integration around $B(x)$ without affecting the normal force. Thus

$$N(x) = -\rho U_\infty \cos\alpha \oint_{B(x)} \left[\phi - U_\infty \sin\alpha\, \eta \right] d\xi$$
(157)

The contour of integration is shown in the following sketch.

Since

$$\overline{\phi}(\mathfrak{z}) = \phi + i\psi, \text{ and } d\mathfrak{z} = d\xi + i\, d\eta$$
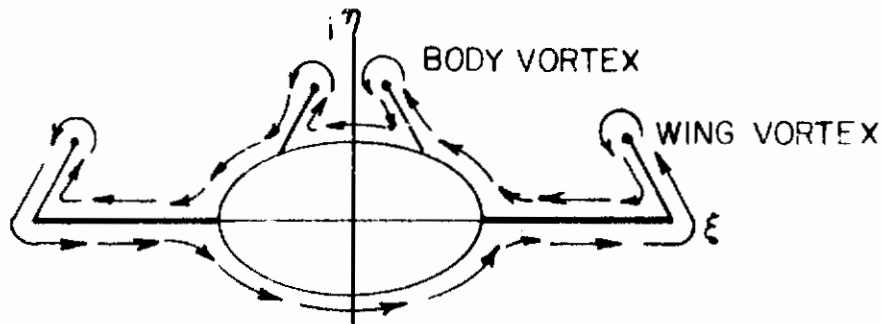
$$\oint_{B(x)} \phi \, d\xi = R.P. \oint_{B(x)} \overline{\phi} \, d\mathfrak{z} + \oint_{B(x)} \psi \, d\eta$$
(158)

The last term is zero, since $\psi = 0$ on the body and is single valued on the vortices and feeding sheets. The source term, which is axisymmetric and thus produces no downward momentum, need not be included here.

Thus

$$N(x) = -\rho U_\infty \cos\alpha \left\{ R.P. \oint_{B(x)} \bar\phi(\mathcal{S})\, d\mathcal{S} - \oint_{B(x)} U_\infty \sin\alpha\, \eta\, d\xi \right\}$$

(159)

where $\bar\phi(\mathcal{S})$ is given by Eq. (108).

The free stream term (last integral) may be evaluated directly, giving

$$\oint_{B(x)} U_\infty \sin\alpha\, \eta\, d\xi = -U_\infty \sin\alpha \left(r - \frac{k^2}{r} \right)\left(r + \frac{k^2}{r} \right)\pi$$

(160)

The integral of the complex velocity potential is most easily evaluated in the θ-plane. The transformed potential function $\bar\phi(\theta)$ is given by Eq. (109). Since

$$d\mathcal{S} = \frac{d\mathcal{S}}{d\theta}\, d\theta$$

(161)

the integral may be written

$$\oint_{B(x)} \bar\phi(\mathcal{S})\, d\mathcal{S} = \oint_{B(x)} \bar\phi(\theta)\, \frac{d\mathcal{S}}{d\theta}\, d\theta$$

(162)

where $d\mathcal{S}/d\theta$ is given by Eq.(130). Thus:

$$\oint_{B(x)} \bar\phi(\theta)\, \frac{d\mathcal{S}}{d\theta}\, d\theta = \int_{B(x)} \left\{ -\frac{i\Omega_o}{2\pi} \ln\left(\frac{\theta-\theta_o}{\theta+\bar\theta_o}\right) - \frac{i\Omega_1}{2\pi} \ln\left(\frac{\theta-\theta_1}{\theta+\bar\theta_1}\right) - i U_\infty \sin\alpha\, \theta \right\}$$
$$\times \left\{ \left(\frac{k^2+r^2}{2r^2}\right)\left(\frac{\theta}{\sqrt{\theta^2+s'^2+4r^2}}\right) - \left(\frac{k^2-r^2}{2r^2}\right)\left(\frac{\theta}{\sqrt{\theta^2+s'^2}}\right) \right\} d\theta$$

(163)

Details of evaluation of the contour integral in Eq.(162) may be seen in Appendix C. The result will be stated here

$$\oint_{B(x)} \bar\phi(\mathcal{S})\, d\mathcal{S} = -\Omega_o(\theta_o+\bar\theta_o) - \Omega_1(\theta_1+\bar\theta_1) - U_\infty \sin\alpha \left\{ \left(\frac{k^2+r^2}{2r^2}\right)(s'^2+4r^2)\pi \right.$$
$$\left. -\left(\frac{k^2-r^2}{2r^2}\right)s'^2\pi \right\}$$

(164)

65

where

$$\theta = \frac{(k^2 - r^2)^2 s^2 + 2(k^2 + r^2) s (s^2 - 4t^2)^{1/2} + (k^2 + r^2)^2 (s^2 - 4t^2)}{4t^4} - s'^2$$

(165)

and

$$S' = \frac{(k^2 - r^2) s + (k^2 + r^2)(s^2 - 4t^2)^{1/2}}{2t^2}$$

(166)

The load on the wing-body combination up to a station X is then given by

$$N(x) = \rho U_\infty \cos \alpha \; R.P. \left[\mathcal{L}_o (\theta_o + \bar{\theta}_o) + \mathcal{L}_1 (\theta_1 + \bar{\theta}_1) \right]$$

$$- \rho U_\infty^2 \sin \alpha \cos \alpha \left(r - \frac{k^2}{r} \right) \left(r + \frac{k^2}{r} \right) \pi$$

$$+ \rho U_\infty^2 \sin \alpha \cos \alpha \left\{ \left(\frac{k^2 + r^2}{2r^2} \right) (s'^2 + 4r^2) \pi - \left(\frac{k^2 - r^2}{2r^2} \right) s'^2 \pi \right\}$$

(167)

The axial distribution of force may be found by numerically differentiating the above expression with respect to X .

Once the axial distribution of force on the wing·body combination is found by the above method, it is possible to find the body alone load, if desired, by subtracting the load on the wing calculated by integration of the pressure distribution. It is also possible to determine the nonlinear load due to the vortices alone by considering only the terms containing vortex strength. Then the linear lift, computed by more accurate methods, can be added.

D.   DESCRIPTION OF NUMERICAL METHODS

1.   Selection of Separation Points

The point of flow separation on a highly swept wing is defined by a Kutta condition to be at the leading edge. No such condition exists, however, for the separation points on bodies or on wing-body combinations. The exact position of separation is the result of a complicated interaction between the viscous flow around the body and the flow in the separated region. Short of a complete solution of the viscous flow problem, which has proven exceedingly difficult, the most practical method of predicting separation points seems to be a semi-empirical one. Certain simplified analytic attempts at a solution, reported in Ref. 13, have been unsuccessful.

The separation point on a wing-body combination (over the wing-body juncture) is defined in both the "approximate" and "exact" models described above to be just that which would occur on the body alone at angle

66

of attack. For the "quasi-exact" model, there is no separation on the body in this region. Ahead of the wing leading edge and aft of the trailing edge the separation point is just that for the body alone in all three flow models.

Two-dimensional time-varying flow studies on elliptic cylinders (Ref. 22) have indicated that the points at which the major part of the vorticity seems to leave the cylinder starts near the rear stagnation point $(\theta_0 = 90°)$ and moves rapidly around to some steady position $(\theta_0 = \theta_\infty)$ where it remains throughout the development of the two-vortex flow pattern. For a three-dimensional body, this "equilibrium separation angle", θ_∞, has been seen to be a function of the local body slope, angle of attack, axis ratio, and the state of the axial boundary layer (laminar or turbulent). This equilibrium angle is assumed to be that for the appropriate tangent cone for a body with changing slope, such as one with an ogival nose or a cone-cylinder. On such a body, however, the true separation angle lags the equilibrium angle, as the separation angle cannot immediately adjust to a change in slope.

The experimentally determined equilibrium separation angle for a circular cone in laminar flow is given in Ref. 23 as

$$\theta_{\infty_{cir}} = (13.12 + \delta)(3.13 - \sqrt{.116\,\alpha - 1.16}) \qquad \begin{array}{l} 10° \le \alpha \le 40° \\ 0° < \delta \le 20° \end{array}$$

$$\theta_{\infty_{cir}} = 3.13\,(13.12 + \delta) \qquad \begin{array}{l} 0° < \alpha \le 10° \\ 0° < \delta \le 20° \end{array}$$

(168)

where $\tan \delta$ is the slope of the body.

The separation on elliptic cones may be found by assuming that the separation angle is a function of the angle through which the flow turns as it separates from the body. Then

$$\theta_\infty = 90° - \tan^{-1}\left[\frac{a^2}{b^2}\tan\left(90° - \theta_{\infty_{cir}}\right)\right]$$

(169)

where $\theta_{\infty_{cir}}$ is obtained from Eq.(168) by defining an average slope of an elliptic body to be

$$\tan \delta = \sqrt{\frac{b}{a}}\,\frac{da}{dx}$$

(170)

This conclusion is verified by comparison with experimental data. For a body with varying slope, the rate of change of separation angle is assumed to be of the form

$$\frac{d\theta_0}{dx} = K\,\frac{\tan\alpha}{2b}\,(\theta_\infty - \theta_0)$$

(171)

where in Ref. 22 a good value for the constant is found to be $K = .7$ with the angles in degrees.

No such experimental correlation is available for turbulent flow. From comparison of incremental force data on turbulent cones with the

results of predicted loads a value of $\theta_{\infty_{cir}} = 53°$ is prescribed for the turbulent case in Ref. 13. The separation angle θ_0 on elliptic bodies is found as before (from Eq. 169).

2. Discussion of the Starting Problem

For bodies at low angles of attack, the growth of the body may be sufficient to prevent the departure of vortices from the surface. This is reflected by the lack of a solution to the equations for vortex strength and position for the appropriate tangent cone. On a nonconical body, however, the decreasing slope may permit departure of the vortices at some point aft of the nose. If separation is assumed just at the point where a solution is first obtained, an incorrect result will be found for the vortex strength and position. It is necessary, on such a body, to continue the "tangent cone" solutions back along the body until the nondimensional vortex strength λ is greater than an experimentally determined value of a parameter, λ_{sep}, which measures the strength of the vortices as they break out of the boundary layer and separate from the body. A full discussion of this process will be found in Ref. 13.

Provisions have been made for this case in the numerical procedure described below. Unfortunately, values of λ_{sep} have been measured only for a circular body. They are:

$$\lambda_{sep} = .225 \text{ -- laminar boundary layer}$$
$$\lambda_{sep} = .295 \text{ -- turbulent boundary layer}$$

(172)

Since it is expected that measurements of this parameter will be made in the future for bodies of elliptic cross-section, the numerical methods have been developed for use with elliptical or circular bodies. Actual calculations have been made only for circular bodies, however.

3. Procedure for Approximate Model

In the "approximate" model, there is no interaction between wing and body vortices, and the strength and position of the body vortices remains constant over the wing-body juncture. Calculation of vortex trajectories may therefore be made in two separate steps:
1. Calculate the strength and position of the vortices on a body consisting of only the sections fore and aft of the wing-body juncture.
2. Calculate the strength and position of the vortices on the wing alone.

Once the vortex trajectories and strengths are known (the wing vortices are assumed constant aft of the trailing edge), the resultant distribution of nonlinear normal force on the wing body combination is just given by

$$\frac{dN(x)}{dx} = \rho U_\infty \cos \alpha \frac{d}{dx}\left[\Gamma_0 (\theta_0 + \bar{\theta}_0) + \Gamma_1 (\theta_1 + \bar{\theta}_1) \right]$$

(173)

A complete numerical procedure for calculating nonlinear loads on elliptic cones and circular tangent ogive bodies is presented in Ref. 13, and this has been adapted for calculating loads on wings in Ref. 15. Comparisons of this method with experimental data are given in Section V. Agreement is not considered adequate, primarily due to the failure of the two-vortex theory to correctly estimate loads on the wing alone. (Comparisons of the wing alone theory with experiment may be seen in Ref. 15).

4. Procedure for Quasi-Exact Model

The "quasi-exact" model, which permits interactions between the wing and body vortices, but not separation on the body, over the wing-body juncture, is solved in three steps:

1. Calculate the strength and positions of the vortices on the portion of the body ahead of the wing leading edge using Eqs. (135) and (139).

2. Calculate, simultaneously, the strength and trajectories of the wing and body vortices over the wing-body juncture using Eqs. (142), (143), and (145).

3. Calculate the strength and trajectories of the wing and body vortices over the aft portion of the body, using Eqs. (146), (147), and (148).

The initial conditions for integrating the appropriate differential equations are found by considering the solutions for a) a tangent cone at or near the body nose, to start Step 1, and b) a delta wing at the wing leading edge, to start Step 2. No starting procedure is needed for Step 3, as both wing and body vortices have finite strength and position at the wing trailing edge.

A complete numerical procedure for the quasi-exact model has not been developed. It is felt that, due to the apparent failure of the wing-alone theory, the necessary expenditure of effort would result in only slight improvement in the agreement with experiment, and would not be justified in the present program. If a better theory for the wing alone could be devised (see Section VI), an empirical correction of the form

$$\Delta C_{N_{nonlinear}} = \Delta C_{N_{quasi-exact}} - \Delta C_{N_{wing\ alone\ two-vortex}} + \Delta C_{N_{wing\ alone\ improved}} \tag{174}$$

might considerably improve the chances for agreement with experiment. In light of this possibility, the proposed numerical procedure for the quasi exact model is outlined as follows:

a) For $0 < x \leq x_{LE}$

Eq. (139) may be written as:

$$\frac{d\mathcal{Y}_1}{dx} = F(x, \mathcal{Y}_1) \tag{175}$$

where

$$F(x, \mathcal{Y}_1) = \frac{w_1}{U_\infty \cos \alpha} - \frac{d(a\lambda_1)}{dx}\left[\frac{\mathcal{Y}_1 - \mathcal{Y}_1'}{(a\lambda_1)}\right] \tag{176}$$

69

and

$$\frac{W_1}{U_\infty \cos\alpha} = \frac{\overline{\left\{-i\left[\frac{a\lambda_1 \tan\alpha}{(\theta_1 + \bar\theta_1)} + \tan\alpha\right] + \left[b\frac{d\alpha}{dx}\left(\frac{1}{\sqrt{\mathscr{S}_1^2 - 4t^2}}\right)\frac{d\mathscr{S}_1}{d\theta}\right]\right\}}}{\overline{\left\{\frac{d\mathscr{S}_1}{d\theta}\right\}}} \tag{177}$$

where bars denote the complex conjugates of quantities. Also:

$$(a\lambda_1) = \frac{\mathscr{L}_1}{2\pi U_\infty \sin\alpha}$$

$$= -\left[\frac{(\theta_1' - \theta_1)(\theta_1' + \bar\theta_1)}{\theta_1 + \bar\theta_1}\right] \tag{178}$$

from Eq. (135). Equation (175) is integrated numerically by a four point Runge-Kutta scheme up to $x = x_{LE}$. That is:

$$\Delta\mathscr{S}_1 = \frac{1}{6}\left(k_1 + 2k_2 + 2k_3 + k_4\right) \tag{179}$$

where

$$k_1 = F(x, \mathscr{S}_1)\Delta x$$

$$k_2 = F(x + \Delta x/2, \mathscr{S}_1 + k_1/2)\Delta x$$

$$k_3 = F(x + \Delta x/2, \mathscr{S}_1 + k_2/2)\Delta x$$

$$k_4 = F(x + \Delta x, \mathscr{S}_1 + k_3)\Delta x$$

The initial values of x, $\mathscr{S}_1$, and $a\lambda_1$, for starting the integration are found from solutions to the equations for an elliptic cone:

$$2\varphi_i - \varphi_i' - \frac{ab}{\sqrt{\bar{\varphi}_i^2 - 4\ell^2}} = i\tan\alpha \left\{ -a\lambda_i \left[\frac{\bar{\varphi}_i \frac{r^2+\ell^2}{(\bar{\varphi}_i^2-4\ell^2)^{1/2}} - (r^2-\ell^2)}{(r^2+\ell^2)\left[(\varphi_i^2-4\ell^2)^{1/2}+(\bar{\varphi}_i^2-4\ell^2)^{1/2}\right] - (r^2-\ell^2)(\varphi_i+\bar{\varphi}_i)} \right] \right.$$

$$\left. + \frac{2\ell^2(r^2+\ell^2)}{\bar{\varphi}_i(r^2+\ell^2)(\bar{\varphi}_i^2-4\ell^2)-(r^2-\ell^2)(\bar{\varphi}_i^2-4\ell^2)^{3/2}} + \frac{1}{2\ell^2}\left[\bar{\varphi}_i \frac{r^2+\ell^2}{(\bar{\varphi}_i^2-4\ell^2)^{1/2}} - (r^2-\ell^2) \right] \right\}$$

(180)

and

$$a\lambda_i = \frac{1}{2\ell^2} \frac{\left\{(r^2+\ell^2)\left[(\varphi_i^2-4\ell^2)^{1/2}+(\bar{\varphi}_i^2-4\ell^2)^{1/2}\right] - (r^2-\ell^2)(\varphi_i'+\bar{\varphi}_i)\right\}}{}$$

$$\frac{\left\{(r^2+\ell^2)\left[(\varphi_i^2-4\ell^2)^{1/2}-(\varphi_i^2-4\ell^2)^{1/2}\right] - (r^2-\ell^2)(\varphi_i'-\varphi_i)\right\}}{(r^2-\ell^2)(\varphi_i+\bar{\varphi}_i)-(r^2+\ell^2)\left[(\varphi_i^2-4\ell^2)^{1/2}+(\bar{\varphi}_i^2-4\ell^2)^{1/2}\right]}$$

(181)

These equations may be solved simultaneously for the strength and position of the vortex by a logarithmic search procedure. At low angles of attack, or for cones with wide semi-vertex angles (δ) these equations may not have a solution. (The semi-vertex angle is related to the position of the separation point, for laminar flow, by Eqs. (168)-(170)). Physically, this indicates that the expansion of the body prevents the separation of vortices. For a body with varying slope $da/dx = \tan\delta$, such as a tangent-ogive cylinder, separation may take place at some position aft of the nose. A similar situation may exist for cone-cylinder bodies where separation may begin at the shoulder of the body. This axial separation point is found by attempting to solve the cone equations for cones of decreasing semi-vertex angle. An additional restriction on the axial separation point is that the vortex strength λ, which may be found from Eq. (181), must be greater than λ_{sep}, as discussed above.

b) $X_{LE} < X \leq X_{TE}$

The governing equations, (143) and (145), may be written

$$\frac{d\varphi_o}{dx} = \mathcal{G}_o(X, \varphi_o, \varphi_i)$$

(182)

71

and

$$\frac{d\mathcal{G}_1}{dx} = G_1(x, \mathcal{G}_0, \mathcal{G}_1) \tag{183}$$

where

$$G_0(x, \mathcal{G}_0) = \frac{w_0}{U_\infty \cos\alpha} - \frac{d(a\lambda_0)}{dx}\left[\frac{\mathcal{G}_0 - \mathcal{G}}{(a\lambda_0)}\right] \tag{184}$$

where

$$\frac{w_0}{U_\infty \cos\alpha} = \frac{\left\{-i\left[\frac{(a\lambda_0)\tan\alpha}{(\theta_0 + \bar{\theta}_0)} + \frac{(a\lambda_1)\tan\alpha(\theta_1 + \bar{\theta}_1)}{(\theta_0 - \theta_1)(\theta_0 + \bar{\theta})} + \tan\alpha\right] + \left[b\frac{da}{dx}\left(\frac{1}{\sqrt{\mathcal{G}_0^2 - 4L^2}}\right)\frac{d\mathcal{G}_0}{d\theta}\right]\right\}}{\left\{\frac{d\mathcal{G}_0}{d\theta}\right\}} \tag{185}$$

and

$$G_1(x, \mathcal{G}_1) = \frac{\left\{-i\left[\frac{(a\lambda_1)\tan\alpha}{(\theta_1 + \bar{\theta}_1)} + \frac{(a\lambda_0)\tan\alpha(\theta_0 + \bar{\theta}_0)}{(\theta_1 - \theta_0)(\theta_1 + \bar{\theta}_1)} + \tan\alpha\right] + \left[b\frac{da}{dx}\left(\frac{1}{\sqrt{\mathcal{G}_1^2 - 4L^2}}\right)\frac{d\mathcal{G}_1}{d\theta}\right]\right\}}{\left\{\frac{d\mathcal{G}_1}{d\theta}\right\}} \tag{186}$$

Also

$$a\lambda_0 = \frac{\mathcal{L}_0}{2\pi U_\infty \sin\alpha}$$

$$= -\left[1 + (a\lambda_1)\left(\frac{1}{\theta_1} + \frac{1}{\bar{\theta}_1}\right)\right]\bigg/\left[\frac{1}{\theta_0} + \frac{1}{\bar{\theta}_0}\right] \tag{187}$$

and

$$a\lambda_1 = a\lambda_1 \text{ at } X_{LE} = \text{constant} \tag{188}$$

72

Equations (182) and (183) are integrated simultaneously up to X_{TE} using the Runge-Kutta technique. That is:

$$\Delta \mathcal{S}_0 = \frac{1}{6} (k_1 + 2k_2 + 2k_3 + k_4) \tag{189}$$

$$\Delta \mathcal{S}_1 = \frac{1}{6} (\ell_1 + 2\ell_2 + 2\ell_3 + \ell_4) \tag{190}$$

where

$$k_1 = G_0(X, \mathcal{S}_0, \mathcal{S}_1) \Delta X$$

$$\ell_1 = G_1(X, \mathcal{S}_0, \mathcal{S}_1) \Delta X$$

$$k_2 = G_0(X + \Delta X/2, \mathcal{S}_0 + k_1/2, \mathcal{S}_1 + \ell_1/2) \Delta X$$

$$\ell_2 = G_1(X + \Delta X/2, \mathcal{S}_0 + k_1/2, \mathcal{S}_1 + \ell_1/2) \Delta X$$

$$k_3 = G_0(X + \Delta X/2, \mathcal{S}_0 + k_2/2, \mathcal{S}_1 + \ell_2/2) \Delta X$$

$$\ell_3 = G_1(X + \Delta X/2, \mathcal{S}_0 + k_2/2, \mathcal{S}_1 + \ell_2/2) \Delta X$$

$$k_4 = G_0(X + \Delta X, \mathcal{S}_0 + k_3, \mathcal{S}_1 + \ell_3) \Delta X$$

$$\ell_4 = G_1(X + \Delta X, \mathcal{S}_0 + k_3, \mathcal{S}_1 + \ell_3) \Delta X$$

The initial values of $\mathcal{S}_0$ and $\alpha \lambda_0$ are found from the solutions to the cone equations ((180) and (181)) for a flat wing. Since for this case the equations will always have a solution, no starting procedure such as that described above is necessary. The values of $\mathcal{S}_1$ and $\alpha \lambda_1$ are those found at the leading edge as the last step of a) above.

c) $X_{TE} < X < \ell$

Equations (147) and (148) may be written as

$$\frac{d \mathcal{S}_1}{dX} = H_1(X, \mathcal{S}_0, \mathcal{S}_1) \tag{191}$$

and

$$\frac{d \mathcal{S}_0}{dX} = H_0(X, \mathcal{S}_0, \mathcal{S}_1) \tag{192}$$

where

$$H_1(X, \mathcal{S}_0, \mathcal{S}_1) = \frac{W_1}{U_\infty \cos \alpha} - \frac{d(\alpha \lambda)}{dX} \left[\frac{\mathcal{S}_1 - \mathcal{S}_1'}{(\alpha \lambda_1)} \right] \tag{193}$$

73

where

$$\frac{W_1}{U_\infty \cos\alpha} = \frac{\left\{-i\left[\frac{(a\lambda_0)\tan\alpha\,(\theta_0+\bar{\theta}_0)}{(\theta_1-\theta_0)(\theta_1+\bar{\theta}_0)} + \frac{(a\lambda_1)\tan\alpha}{(\theta_1+\bar{\theta}_1)} + \tan\alpha\right] + \left[b\frac{da}{dx}\left(\frac{1}{\sqrt{\varphi_1^2-4L^2}}\right)\left(\frac{d\varphi_1}{d\theta}\right)\right]\right\}}{\left\{\frac{d\varphi_0}{d\theta}\right\}}$$

(194)

and

$$H_0(x,\varphi_0,\varphi_1) = \frac{\left\{-i\left[\frac{(a\lambda_0)\tan\alpha}{(\theta_0+\bar{\theta}_0)} + \frac{(a\lambda_1)\tan\alpha\,(\theta_1+\bar{\theta}_1)}{(\theta_0-\theta_1)(\theta_0+\bar{\theta}_1)} + \tan\alpha\right]\left[b\frac{da}{dx}\left(\frac{1}{\sqrt{\varphi_0^2-4L^2}}\right)\left(\frac{d\varphi_0}{d\theta}\right)\right]\right\}}{\left\{\frac{d\varphi_0}{d\theta}\right\}}$$

(195)

Also

$$a\lambda_1 = -\frac{\left[1+(a\lambda_0)\left(\frac{\theta_0+\bar{\theta}_0}{(\theta_1'-\theta_0)(\theta_1'+\bar{\theta}_0)}\right)\right]}{\left[\frac{\theta_1+\bar{\theta}_1}{(\theta_1'-\theta_1)(\theta_1'+\bar{\theta}_1)}\right]}$$

(196)

and

$$a\lambda_0' = a\lambda_0 \quad \text{at} \quad x_{TE} = constant$$

(197)

The equations are solved simultaneously by the Runge-Kutta technique as in Eqs. (189) and (190). The initial values of φ_1 and $a\lambda_1$, are those found at the trailing edge as the last step of b) above. As all the quantities have finite values, the integration may be begun immediately after the trailing edge.

Once the strengths and positions of the four vortices are found, the axial load distribution is found from Eq. (173) as before.

74

5. Discussion of Exact Model

    The limitations mentioned above for the quasi-exact model apply also to the "exact" model. Furthermore, the simultaneous solution of the two complex algebraic and two complex differential equations is exceedingly difficult, requiring a double logarithmic search procedure more complicated than that mentioned for solutions to the cone equations. The resultant machine programs would be exceedingly expensive in terms of computation time. Also, due to the physical considerations discussed above, it is not felt that, for most configurations of interest, the exact model represents a significant practical improvement over the quasi-exact model, although the arbitrarily imposed condition that there is no flow separation on the body need not be imposed.

SECTION V

COMPARISON OF THEORY AND EXPERIMENT

A.   LINEAR INTERFERENCE LOADS

Comparisons with experimental data of wing body interference effects calculated by the methods discussed in this report are severely limited by the rarity of systematic experiments on wing-body combinations at subsonic speeds. Although a wealth of data exists on various airplane-type configurations, this is relatively useless when trying to determine the range of validity of the theories or the effect on load distributions of systematic variations in some geometric or flight parameter. Furthermore, in model force tests, it is not usually possible to separate the interference load on the body due to the presence of the wing, from that on the wing due to the presence of the body. Some information of this nature may be obtained from pressure measurements, however.

Figure 3 shows one member of a family of wing-body combinations, tested at several high subsonic Mach numbers. The data, from force measurements, are reported in Ref. 24. Three high aspect ratio swept wings, with quarter-chord sweep angles of 40°, 45°, and 50°, were used. Figures 4, 6, and 8 show the theoretical and experimental reduced lift curve slopes at zero angle of attack (βC_{L_α}, where $\beta = \sqrt{1-M_\infty^2}$) plotted against reduced aspect ratio (βAR) for the three swept wing-straight body configurations. A contoured body was also tested, but provided negligible difference in the data.

Use of these reduced coordinates provides correlation of data taken at different Mach numbers. The various dashed lines show the contributions of the wing and body without the interference loads. The body-alone lift was determined by the slender body theory method given in Ref. 2. The solid lines show the theoretically determined total lift. Violations of the slender body approximations used to determine the lift on the aft portion of the body due to wing-lift gives rise to a larger load in this region than actually exists for these high aspect ratio configurations. That the disagreement between theory and experiment is due to this effect may be seen by considering the sum of the load on the wing in the presence of the body and the load on the body alone, also shown in Figs. 4, 6, and 8. Other portions of the interference theory developed here may be seen to compare favorably with experiment. Further investigation of this difficulty, including systematic experiments, might be desirable. In lieu of this, however, it is recommended that the lift due to the trailing vortex system on the aft portion of the body not be included for high reduced aspect ratio configurations $(\beta AR > \sim 4)$.

77

Figures 5, 7, and 9 show the theoretical and experimental centers of pressure (x_{cp}/c_{root}, measured from the leading edge root) plotted against reduced aspect ratio for these configurations. The effect of the trailing vortex system is again not included. Agreement is generally satisfactory. The discrepancies may be due to the inaccuracies of the slender body theory.

Figure 10 shows a configuration with a medium aspect ratio swept wing, tested at high subsonic Mach numbers with a basic and indented body. The data, in the form of integrated pressure distributions, are from Ref. 25. Figures 11 and 12 give the experimental and calculated reduced lift curve slopes on the wing-basic body combination, and on the wing in the presence of the basic body. Figures 13 and 14 give the same information for the indented body. The lifts on the body alone are experimental values from pressure distributions, with the theoretically determined body carry-over lift subtracted out. Agreement of the lift with experimental values is good, both for the wing in the presence of the body, and for the total configuration. Here the lift due to the trailing vortex system has been included.

Figures 15 and 17 give centers of pressure on the wing-basic body combination and wing-indented body combinations. The centers of pressure for the wing in the presence of these two bodies are given in Figs. 16 and 18. It may be seen that the discrepancy between theory and experiment for both combinations is essentially due entirely to the wing. This disagreement is a consequence of the assumption that the wing lift is concentrated along the quarter-chord line. For high aspect ratio wings, such as that shown in Fig. 3, this assumption gives good agreement with experiment (see Figs. 4, 7, 9). For medium-to-low aspect ratio wings, however, the center of pressure appears further back on the wing. (The Lawrence method cannot be used to predict centers of pressure on wings which have a fore or aft swept trailing edge, and has only been used for calculating the body carry over lift). A lifting surface theory would give considerably better agreement.

A similar configuration, from Ref. 26, is shown in Fig. 19. The basic body is identical to that of Fig. 10, but the wing is less severly swept. This wing was also tested with two bodies, basic and elliptical, at high subsonic Mach numbers. The major axis of the elliptic cross section was oriented normal to the plane of the wing. Figures 20 through 27 give comparison of wing, body, and total lifts, and center of pressure locations for both the basic and elliptic configurations. The lift on the wing in the presence of the body is slightly underestimated in both cases, probably due to the inaccuracy of Weissinger's procedure for such a low aspect ratio. Center of pressure agreement is better. Agreement is about the same for both basic and elliptic configurations.

B. NONLINEAR INTERFERENCE LOADS

The method of Section IV, using the approximate model, for calculating nonlinear loads on wing-body combinations has been compared with experimental data only in a limited manner. A configuration was chosen which should minimize the effects of the limitations of the theory. Agreement was found to be less than satisfactory.

Tests were made (Ref. 27) on a tangent ogive cylinder in combination with several delta wings. For comparison with theory, a wing was chosen which would be wide enough to contribute substantially to the lift, but not violate the assumptions of the slender body approximations. The model is shown in Fig. 28. Data was taken at a Mach number of 1.50. The experimental lift coefficient is plotted against angle of attack in Fig. 29, and the experimental pitching moment is plotted in Fig. 30. The theoretical curves were determined by adding the calculated nonlinear incremental lift and pitching moment to a linear value which was empirically determined by considering the experimental lift and pitching moment slopes at zero angle of attack. In this way, any effects due to the inaccuracy of the linear slender body theory are eliminated. It may be seen that both the lift and pitching moment are both seriously overestimated by the theory, even at very low angles of attack. This is due primarily to the failure of the two-vortex model to correctly predict the loads on the wing alone. Agreement is good with predicted loads on the body alone. Suggestions for further improvement of the analysis are made in Section VI. It is also possible than an effect due to compressibility is present. The theory, being based on the slender body approximation, is independent of Mach number.

SECTION VI

RECOMMENDATIONS FOR FURTHER STUDY

A. LINEAR WING-BODY INTERFERENCE EFFECTS

This report has presented some possible improvements to current wing-body interference theory. Much work remains to be done in this field, however. The studies contained herein suggest certain areas for further investigation. One straightforward, but very complicated, improvement to the calculation of the effect of an elliptic body on a wing would be to include the terms in Eq. (8) representing distributed vorticity in the calculation of downwash. This would be especially worthwhile for elliptical bodies of high eccentricity. A more difficult, but potentially more fruitful, approach to the problem would be the derivation and solution of an integral equation representing the distribution of vorticity on a body of generally-shaped cross section.

Another difficult but possibly worthwhile approach would be the development of an "image vortex" theory which would use a lifting-surface representation of the wing lift distribution (such as that found in Ref. 10) rather than the horse-shoe vortex representation of Ref. 5. Such a theory, in combination with the "exact" distribution of vorticity on the body mentioned above, would seem to represent the maximum possible improvement in this method of calculating interference effects.

One further area should be mentioned in connection with complete calculations on wing-body combinations. That is the need for an improved subsonic theory for load distributions on bodies alone. The slender body theory gives adequate results for smooth bodies of medium fineness ratio at low angles of attack. Effects of nose bluntness, boundary layer growth, vortex separation, and not-so-slender body shapes can cause serious errors in calculation of body load, which can minimize the usefulness of improvements to wing-body interference theory unless they are accounted for, or unless data becomes available with which the accuracy of interference theories can be systematically determined.

B. NONLINEAR WING-BODY INTERFERENCE EFFECTS

The theory for determining nonlinear interference loads is in considerably more of a primitive state than that for linear loads. Investigation should be made to determine what improvements to the theory would be worthwhile. Among possible topics for examination are:

a) Improvements to the vortex model. The work of Maskell and Smith on a delta wing (Refs. 28 and 29) has shown that representation of the vorticity in the flow as a rolled-up vortex sheet rather than as a concentrated vortex can greatly improve the prediction of the vortex core location.

81

Presumably, improvements in predicted force and pressure distribution would follow. Furthermore, the question of whether the wing and body vortices mutually affect each other's boundary conditions, whether there is separation on the body, and whether the vortices tend to roll up, over the wing-body juncture, is still open. These questions cannot be examined with the present flow models.

b) Better specification of separation points. Current specification is dependent on experimental data. A viscous flow analysis of the wing-body combination, although difficult, would settle this question, and possibly that of corrections to the flow model. Other approaches, such as that discussed in Ref. 21, might be possible.

c) Better potential flow theory. The current theory contains all of the drawbacks of the slender body theory discussed above. Some improvement might possibly be gained by use of a three-dimensional potential flow theory (Ref. 30), or a three-dimensional method of characteristics procedure for the supersonic range (Ref. 31).

d) Effect of secondary separation. Separation of the reverse flow region has been observed on elliptic cones at high angles of attack by Friberg (Ref. 23). Pershing (Ref. 32) has shown that when the vortex is placed in its observed position, the force is determined more accurately than by the Brown and Michael model (Ref. 16), and the separation points are similar to those that would exist if secondary separation occurred. A solution of the secondary separation problem was not attempted, and the work of Maskell and Smith places the vortex in its correct location without such simulation of boundary conditions. Secondary separation has not been ruled out as a possible factor, however.

e) Treatment of more general configurations. The present theory is limited to wing-body combinations with circular or elliptic bodies, and flat, mid-plane wings. With other conformal transformations, more general configurations (such as non-mid-plane wings or nonelliptical bodies) might be treated. More promising, perhaps, would be the treatment of a wing-body combination with a generally twisted and cambered wing, even though separation on such a wing is a difficult problem in itself.

Finally, more experimental data is needed on the nonlinear effects on wings, bodies, and wing-body combinations. Of primary interest would be flow visualization studies by, for example, the vapor screen technique, in conjunction with model force tests. This would not only improve or extend to more general shapes the present analysis, by better determination of the experimental parameters, but would eliminate a great deal of uncertainty present in the specification of the flow model to be used.

APPENDIX I

DESCRIPTION OF LINEAR LOADS COMPUTER PROGRAM

The methods for calculating linear wing-body interference loads discussed in Section III above have been included in a computer program. This program consists of a MAIN program and 27 subroutines written in FORTRAN II, plus a general purpose subroutine for doing complex arithmetic written in the FAP language. It has been compiled and run on the IBM 7094 at the M.I.T. Computation Center, which is equipped with a 32K memory; a library tape containing the trigonometric functions sin, cos, tan, and arctan, and a modified version of the IBM Fortran Monitor System (FMS). A schematic diagram of the execution of the program is given in Fig.31 . Descriptions of the required input and the resultant output are given below. Listings of the input and output of one sample case follows the listings of the program, which will be found at the end of this Appendix.

The computer program may be used to find the interference loads at subsonic Mach numbers on a configuration consisting of (1)a body of any varying elliptic cross section and camber distribution, and (2) a wing with straight leading and trailing edges of any sweep angle, aspect ratio, taper ratio, dihedral angle, incidence angle, twist distribution, and camber distribution. The restriction is made that the angles defining the twist and camber distributions be small. With some modifications, the program could be used to treat more general planforms (such as ogee wings) or configurations at supersonic Mach numbers. Treatment of a body with elliptic cross sections is an inherent part of the method. More general bodies may be treated by considering the cross section to be approximately defined by an equivalent ellipse. The generality of the twist and camber distribution of the wing is limited only by the number of boxes used, as the wing is treated as a flat wing at angle of attack over the area of each box. The generality of the cross section or camber distribution of the body is similarly limited, as the body is treated as an elliptic cylinder at angle of attack, which is assumed constant within the length of each body segment.

a. Description of Subroutines

The following is a description of the functions of the main program and the various subroutines.
(a) (MAIN)
This executive program calls, in turn, INPUT, SETUP, LABEL, COMPRS, PART1, and PART2.
(b) INPUT
This subroutine receives as input data parameters M , η , m_1, m_2, and m_3 , (defined below) and parameters describing wing and body geometry.
(c) SETUP
This subroutine establishes the coordinates of the edges and centers of the boxes into which the wing and body are divided. The rectangular

area bounded by (1) the chordwise locations of the leading and trailing edges of the wing root, and (2) the spanwise locations of the root and tip of the leading edge, is divided into n boxes in the spanwise (y) direction and m boxes in the chordwise (x) direction.

The coordinates of the edges and centers of these boxes are given by Eqs. (39) and (40) in Section III above.

In the subroutine INPUT, a separate constant angle of attack is read in for each box (unless the wing is flat), whether the box is partially or entirely located on the wing or not, (the angle of attack of boxes not on the wing is ignored in later calculations). In this way, a general distribution of twist and camber may be specified. The angle of attack of each body segment, with respect to the average wing angle of attack, is similarly received.

(d) LABEL

This subroutine produces that portion of the output shown on pages 136 to 151, giving the numerical, geometrical, and flight conditions received as input, and listing the angle of attack distributions of the wing and the body together with the coordinates of the centers of the appropriate wing boxes or body segments, with respect to the leading edge root.

(e) COMPRS

This subroutine performs a Prandtl-Glauert transformation on the configuration by replacing all chordwise positions x by their transformed equivalents $x/\sqrt{1-M^2}$. The remainder of the calculations are then performed on the transformed configuration. The inverse transformation is performed upon output.

(f) PART1

This subroutine performs the calculation of the chordwise distribution of body carry-over lift by the modified Lawrence method described above, over the portion of the body between the leading and trailing edges.

(g) FUNC

This subroutine calculates $f(\theta)$ for the wing-body combination (see Eq. (30)).

(h) TRANS, DTBRDT

These subroutines, used by FUNC, calculate $\bar{t}$ and $d\bar{t}/dt$ (see Eq. (34)).

(i) FUNC2

This subroutine calculates $f(\theta)$ for the wing alone (see Appendix B of Ref. 1).

(j) PART2

This subroutine calls ALPEFF, WEISS, ELIPWB, BCOLFT, and output routines.

(k) ALPEFF

This subroutine calculates an effective spanwise angle of attack distribution from the complete distribution of twist and camber, for use in the Weissinger procedure. At any spanwise station λ_i the effective angle of attack is given by:

$$\alpha(\lambda) = \frac{1}{2\pi c(\lambda)} \int_{L.E.}^{T.E.} \Delta C_{p_{2-dim}} \, dx \qquad (I-1)$$

84

where

$$\Delta C_{p_{2\text{-}dim}} = \frac{4}{\pi} \sqrt{\frac{c(\lambda)-x}{x}} \int_0^{c(\lambda)} \frac{dz/d\xi}{x-\xi} \sqrt{\frac{\xi}{c(\lambda)-\xi}} \, d\xi \qquad (I-2)$$

where $dz/d\xi = -\alpha_{ij}$ is constant over the area of a box on the wing. The effective chord $c(\lambda)$ is found by considering an effective wing made up of chordwise strips of rectangular boxes. The geometry of the effective wing is discussed in Section III-D.

In order to test the accuracy of the approximation to the Cauchy Principle Value integral of treating the slope $dz/d\xi$ as constant over the area of each box, and ignoring the box where $x = \xi$ when performing the required summation, calculations of effective angle of attack have been made for a flat rectangular wing with the number of boxes on the chord varying from 4 to 24. The results are shown in Fig. 32. It may be seen that a large number of boxes is required in order to accurately represent the true angle of attack. Therefore, the computer program will use this procedure only when necessary, i.e., for a wing which is not flat. For a flat wing, the angle of attack used is that given as input data.

(1) WEISS

This subroutine, which uses AMAT, B, GBAR, FBAR. ELSTAR, and MATINV, is used to calculate the spanwise load distributions (with and without body effect) on the actual wing.

(m) AMAT

This subroutine generates the quantities a_{ij} of Eq. (58), which may be treated as the elements of a square matrix.

(n) B

This FORTRAN function generates the value of $b\upsilon_n$ for use in AMAT, from Eq. (62).

(o) GBAR

This FORTRAN function generates the value of $\bar{g}_{\upsilon\eta}$ for use in AMAT, from Eq. (59).

(p) FBAR

This FORTRAN function generates the value of $\bar{f}_{n\mu}$ for use in GBAR, from Eq. (66).

(q) ELSTAR

This FORTRAN function generates the value of $\mathcal{L}_{\upsilon\mu}^{*}$ for use in GBAR, from Eq. (63).

(r) MATINV

This subroutine solves the matrix equation set up by WEISS. It is a modified version of IBM Share routine No. 664, and is also used by PART I.

(s) ELIPWB

This subroutine calculates the effect of an elliptic body on a wing, by finding an effective spanwise angle of attack distribution due to the image vortices and the body upwash, as discussed in Section III.

85

(t) IMAGE

This subroutine is called by ELIPWB to calculate the positions of the image vortices by Eq. (4).

(u) UPWASH

This subroutine is called by ELIPWB to calculate the upwash due to body angle of attack given by Eq. (51).

(w) BCOLFT

This subroutine calculates the body carry-over lift on that portion of the body aft of the root of the trailing edge, by considering the change with X of the total force on the body up to X due to the presence of the two free vortices. The strength and position of the vortices are determined from the load distributions on the wing. The vortices are considered to extend backwards from the trailing edge of the wing in the streamwise direction.

(x) OP1, OP2, OP3, OP4, OP5

These subroutines perform the necessary inverse Prandtl-Glauert transformations and generate the output shown on pages 152 to 158.

(q) COMPLX

This general purpose subroutine is actually a collection of FAP routines, and is used for doing complex arithmetic in FORTRAN II. Available operations are addition, subtraction, multiplication, division, square, cube, and square root.

As an illustration of the use of COMPLX, the FORTRAN coding for the following complex equation will be generated:

$$z = \left[(a+b)^2/(c-d) \right] e \qquad (I-3)$$

where a, b, c, d, e, and z are all complex numbers.

The FORTRAN statements may be written

```
R1 = RCP (AR, AI, BR, BI)
E1 = EICP (AR, AI, BR, BI)
R2 = RCS (R1, E1)
E2 = EICS (R1, E1)
R3 = RCM (CR, CI, DR, DI)
E3 = EICM (CR, CI, DR, DI)
R4 = RCD (R2, E2, R3, E3)
E4 = EICD (R2, E2, R3, E3)
ZR = RCMT (R4, E4, ER, EI)
ZI = EICMT (R4, E4, ER, EI)
```

The real parts of a, b, c, d, e, and z may be found in AR, BR, CR, DR, Er, and ZR, respectively. The imaginary parts are similarly stored. The following table of entry points to the subroutine COMPLX lists the operational elements of the above statements.

RCP	Real part of Complex "plus"
EICP	Imaginary part of Complex "plus"
RCM	Real part of Complex "minus"
EICM	Imaginary part of Complex "minus"
RCS	Real part of Complex "square"
EICS	Imaginary part of Complex "square"

RCMT	Real part of Complex "multiply"
EICMT	Imaginary part of Complex "multiply"
RCD	Real part of Complex "divide"
EICD	Imaginary part of Complex "divide"
RCSR	Real part of Complex "square root"
EICSR	Imaginary part of Complex "square root"
RCC	Real part of Complex "cube"
EICC	Imaginary part of Complex "cube"

Note that both the real and imaginary parts of a variable must be referred to explictly, and must be calculated separately, but that they are included together in the complex arithmetic operations. Also, it is possible to nest the above operations to any depth desired, by referring to a function instead of a variable name. However, this demands a large amout of repetitive coding. For example, the equation

$$z = a(b+c)$$

$(I-4)$

may be coded in two statements as

ZR = RCMT (AR, AI, RCP (BR, BI, CR, CI), EICP (BR, BI, CR, CI))

ZI = EICMT (AR, AI, RCP (BR, BI, CR, CI), EICP (BR, BI, CR, CI))

It should be noted that care must be taken in the use of the square root portions of this subroutine, lest the wrong square root be taken of a complex quantity which has an argument of greater than 2π. If the quantity has an argument of between 2π and 4π, or between 6π and 8π, etc., the correct results will be obtained by applying the square root subroutines to the negative of the quantity.

b. Description of Input

The following table defines the necessary input parameters in terms of their usual symbol, program variable name, and meaning.

Symbol	Variable	Meaning
Λ	ALAM	Leading edge sweep angle, in degrees
AR	AR	Aspect Ratio
λ	TR	Taper Ratio
s	S	Exposed wing semi-span
α	ALPHA	Average wing angle of attack, in degrees
θ	THETA	Dihedral angle, in degrees
M	MACH	Mach number
m	M	Number of chordwise boxes at the wing root
$m1$	M1	Number of segments on aft portion of the body
$m2$	M2	Parameter used in the numerical integration in the Lawrence method
$m3$	M3	Parameter used in the numerical integration in the Weissinger method
n	N	Number of spanwise boxes on the wing

87

Symbol	Variable	Meaning
—	KEY	Parameter defining a flat wing if KEY $\neq$ 0, or a twisted and/or cambered wing if KEY $\neq$ 0
$\alpha_{i,j}$	ALPH(I, J)	Angle of attack, in degrees, of an individual wing box
X_w	XW	Location of the wing leading edge root aft of the nose
Z_w	ZW	Height of the midpoint of the root chord above the body center line
ℓ	L	Body length
a_j	A(J)	Semi-major axis of body segment
c_j	C(J)	Semi-minor axis of body segment
α_{b_j}	ALPHB(J)	Angle of attack, in degrees, of an individual body segment, with respect to the body centerline at the midpoint of the wing root chord

Values of these parameters must be given as input, for each configuration to be analyzed, in the following order (expressions in parenthesis refer to appropriate format):

Card 1: ALAM, AR, TR, S, ALPHA, THETA, MACH   (7F10.4)

Card 2: M, M1, M2, M3, N, KEY   (6I5)

       If KEY $\neq$ 0

Card 3 thru card $(\dfrac{N \times (M + M1)}{5} + 3)$

       ALPH (I, J)   (5(F5.3, 5X))

(Continue as below for KEY = 0)

       If KEY = 0

Card 3: XW, ZW, L   (3F10.4)

Card 4 thru card (4 + M + M1):

       A(J), C(J), ALPHB(J)   (3F10.4)

For another case, repeat entire data deck with new parameters.

The following values of the required numerical parameters have been used for comparison of theory and experiment:

$$m = 24$$
$$m1 = 12$$
$$m2 = 13$$
$$m3 = 13$$
$$n = 20$$

The solutions have proven relatively insensitive to changes in the numerical parameters above these values, except for the effective angle of attack calculation for a cambered wing, as noted above. Note that m must be different from m_2 as must n from m_3, and that m_2 and m_3 must be odd numbers. Within these restrictions the maximum values of all these parameters is 50.

With the above values, the program requires approximately 3.25 minutes of computation time on the 7094 to perform the entire calculation for one case.

    c.   Use of Output

The total lift on a given wing-body configuration may be found by using the values obtained from the computer program as follows:

$$C_{L_{total}} = C_{L_{W(B)}} + C_{L_{B(W)}} \qquad (I-5)$$

where

$$C_{L_{W(B)}} = \text{lift coefficient of the wing in the presence of the body (p. 157).}$$

and

$$C_{L_{B(W)}} = \text{lift coefficient of the body in the presence of the wing.}$$

$$= C_{L_B} + C_{L_{BCO}} \qquad (I-6)$$

where

$$C_{L_B} = \text{lift coefficient of the body alone}$$

$$C_{L_{BCO}} = \text{coefficient of total body carry-over lift (p. 158).}$$

All coefficients are based on wing area. The lift on the body alone may be found by use of any suitable method, such as the slender body theory. More accurate results will be obtained, however, if experimental data is used for the body lift due to the inadequacy of the theory for most configurations.

The total pitching moment about the root of the leading edge may be found similarly:

$$C_{m_{total}} = C_{m_{W(B)}} + C_{m_B} + C_{m_{BCO}} \qquad (I-7)$$

$$= x_{cp_{W(B)}} C_{L_{W(B)}} + C_{m_B} + x_{cp_{BCO}} C_{L_{BCO}} \qquad (I-8)$$

where

$$x_{cp_{W(B)}} = \frac{C_{root}}{4} + \frac{y_{cp_{W(B)}}}{s} \tan \Lambda_{c/4} \, s \qquad (I-9)$$

where

$$\frac{y_{cp_{W(B)}}}{s} = \text{spanwise center of pressure of the wing in the presence of the body (p. 157).}$$

and

$$x_{cp_{BCO}} = \text{center of pressure of body carry over lift (p. 158).}$$

The above remarks on the **body-alone** lift also apply to the body alone moment coefficient, C_{m_B}. If experimental data is used, care should be taken to see that the coefficients are properly defined.

If the center of pressure of the complete configuration is desired:

$$x_{CP_{total}} = C_{m_{total}} \Big/ C_{L_{total}} \qquad (I\text{-}10)$$

The total bending moment about the wing root is simply:

$$C_{m_{B_{total}}} = \frac{y_{CP}}{s} {}_{W(B)} C_{L_{W(B)}} s \qquad (I\text{-}11)$$

since the body carry-over lift makes no contribution. The strength and position of the rolled-up wing vortex is included in order that effects such as wing-tail interference may be calculated by suitable methods, such as those in Ref. 33.

PROGRAM LISTING

```
C          LINEAR AERO LOADS-WING BODY INTERFERENCE
C          MAIN CONTROL PROGRAM- SUBSONIC
   COMMON CF,A,ELAMB,ALPH,X,Y,CL1EV,ALPHEV,ALPHB,C,THETB,TAU,TAUBAR,
  1 THETBR,BOC,BCO,THET1,THET,XB,CEFV,ALPHWB,OUTPUT,  BETA,PI,AR,TR,
  2 S,M,M1,M2,M3,N,ALPHA,CLTOT,MM1,XW,ZW,ELB,THETA,XWB,EMACH,ALAM,
  3 ALAMOC ,ALAMB ,BAR
   DIMENSION CF(50,50),ELAMB(50),ALPH(100,50),X(101),Y(101),CL1EV(50)
  1 ,ALPHEV(50),ALPHB(100),A(100),C(100),THETB(101),TAU(50),BOC(50),
  2 TAUBAR(50),THETBR(50),BCO(50),THET1(99),THET(101),XB(101),
  3 CEFV(50),ALPHWB(50),OUTPUT(50)
1  CALL   INPUT  (EL,KEY)
   CALL   SETUP  (EL,CREF)
   CALL   LABEL  (EL)
   CALL   COMPRS (EL)
   CALL   PART1  (CREF)
   CALL   PART2  (KEY)
   GO TO 1
   END
```

```
      SUBROUTINE   INPUT  (EL,KEY)
C          INPUT DATA
      COMMON CF,A,ELAMB,ALPH,X,Y,CLIEV,ALPHEV,ALPHB,C,THETB,TAU,TAUBAR,
     1 THETBR,BOC,BCO,THET1,THET,XB,CEFV,ALPHWB,OUTPUT,  BETA,PI,AR,TR,
     2 S,M,M1,M2,M3,N,ALPHA,CLIOT,MM1,XW,ZW,ELB,THETA,XWB,EMACH,ALAM,
     3 ALAMOC  ,ALAMB
      DIMENSION CF(50,50),ELAMB(50),ALPH(100,50),X(101),Y(101),CLIEV(50)
     1 ,ALPHEV(50),ALPHB(100),A(100),C(100),THETB(101),TAU(50),BOC(50),
     2 TAUBAR(50),THETBR(50),BCO(50),THET1(99),THET(1 1),XB(101),
     3 CEFV(50),ALPHWB(50),OUTPUT(50)
      READ 1000,ALAM,AR,TR,S,ALPHA,THETA,EMACH
1000  FORMAT (7F10.4)
      READ 1001,M,M1,M2,M3,N,KEY
1001  FORMAT (6I5)
      MM1=M+M1
      IF (KEY) 2,1,2
1     DO 10 I=1,MM1,1
      DO 10 J=1,N
10    ALPH(I,J)=ALPHA
      GO TO 3
2     DO 20 I=1,MM1
      READ 1002,(ALPH(I,J),J=1,N)
20    CONTINUE
1002  FORMAT (5F10.7)
3     READ 1003,XW,ZW,EL
      READ 1003,(A(J),C(J),ALPHB(J),J=1,MM1)
1003 FORMAT (3F10.4)
      RETURN
      END
```

93

```
      SUBROUTINE   SETUP  (EL,CREF)
C     SET UP BODY AND WING COORDINATES
      COMMON CF,A,ELAMB,ALPH,X,Y,CL1EV,ALPHEV,ALPHB,C,THETB,TAU,TAUBAR,
     1 THETBR,BOC,BCO,THET1,THET,XB,CEFV,ALPHWB,OUTPUT,  BETA,PI,AR,TR,
     2 S,M,M1,M2,M3,N,ALPHA,CLTOT,MM1,XW,ZW,ELB,THETA,XWB,EMACH,ALAM,
     3 ALAMQC  ,ALAMB
      DIMENSION CF(50,50),ELAMB(50),ALPH(100,50),X(101),Y(101),CL1EV(50)
     1 ,ALPHEV(50),ALPHB(100),A(100),C(100),THETB(101),TAU(50),BOC(50),
     2 TAUBAR(50),THETBR(50),BCO(50),THET1(99),THET(101),XB(101),
     3 CEFV(50),ALPHWB(50),OUTPUT(50)
       PI=3.14159265
      FN=N
      MM2=M+M1+1
      FM=M
      FM1=M1
      X(1)=XW/S
       CR=(4./(AR*(1.+TR)))
      Y(1)=1.
      MP=M+1
       TNLAM=TANF(ALAM/57.2957795)
       IF (TNLAM-CR*(1.-TR)) 4,5,5
5      CREF=CR
       GO TO 6
4      CREF=TNLAM+CR*TR
6      DO 1 J=2,MP
      FJ=J-1
       THET(J-1)=(CREF/2.)*(1.-COSF(EJ*PI/(EM+1.)))
1      X(J)=X(J-1)+2.*(THET(J-1)+X(1)-X(J-1))
      MP1=MP+1
      DO 2 J=MP1,MM2
      EJ=J-1
       X(J)=X(MP)+(EJ-EM)*(EL/S-X(MP))/EM1
2      THET(J-1)=(X(J)+X(J-1))/2.-X(1)
      NP=N+1
      DO 3 J=2,NP
      EJ=J-1
      Y(J)=COSF(EJ*PI/(2.*EN))
3      ELAMB(J-1)=(Y(J)+Y(J-1))/2.
      RETURN
      END
```

```
      SUBROUTINE   LABEL  (EL)
C     INPUT DATA - LABELS AND LISTINGS
      COMMON CF,A,ELAMB,ALPH,X,Y,CL1EV,ALPHEV,ALPHB,C,THETB,TAU,TAUBAR,
     1 THETBR,BOC,BCO,THET1,THET,XB,CEFV,ALPHWB,OUTPUT,  BETA,PI,AR,TR,
     2 S,M,M1,M2,M3,N,ALPHA,CLTOT,MM1,XW,ZW,ELB,THETA,XWB,EMACH,ALAM,
     3 ALAMQC  ,ALAMB
      DIMENSION CF(50,50),ELAMB(50),ALPH(100,50),X(101),Y(101),CL1EV(50)
     1 ,ALPHEV(50),ALPHB(100),A(100),C(100),THETB(101),TAU(50),BOC(50),
     2 TAUBAR(50),THETBR(50),BCO(50),THET1(99),THET(101),XB(101),
     3 CEFV(50),ALPHWB(50),OUTPUT(50)
 1001 FORMAT (1H1/////1H 25X32HLINEAR AERODYNAMIC LOADS PROGRAM/1H0///
     1 20X50HLINEAR AERODYNAMIC LOAD DISTRIBUTIONS, INCLUDING  /1H020X
     2 50HTHE EFFECTS OF WING-BODY INTERFERENCE HAVE BEEN   /1H020X
     3 47HCALCULATED ON THE FOLLOWING CONFIGURATION AT   /1H020X16H5UBSO
     4NIC SPEEDS./////1H020X13HWING GEOMETRY)
 1002 FORMAT (1H025X15HASPECT RATIO = F6.3//1H 25X15HTAPER RATIO  = F6.
     13//1H 25X27HLEADING EDGE SWEEP ANGLE = F6.3,8H DEGREES//1H 25X
     2 17HDIHEDRAL ANGLE = F6.3,8H DEGREES//1H 25X25HEXPOSED WING SEMI-S
     3PAN = F6.3)
 1003 FORMAT (1H025X33HWING ANGLE OF ATTACK DISTRIBUTION//1H 20X
     1 35H(ORIGIN IS AT ROOT OF LEADING EDGE)///1H 28X3HX/512X3HY/510X5H
     2ALPHA//)
 1004 FORMAT (20X3F15.5)
 1005 FORMAT (1H1//////1H 10X13HBODY GEOMETRY //1H 25X14HBODY LENGTH =
     1 F7.3//1H 20X25HELLIPTICAL CROSS SECTIONS///1H 12X11HX (DISTANCE
     2 9X10HHORIZONTAL6X8HVERTICAL11X8HANGLE OF/1H 12X10HFROM NOSE)10X4H
     3AXIS12X4HAXIS15X6HATTACK//)
 1006 FORMAT (1H F22.5,F19.5,F16.5,F18.5)
 1007 FORMAT (1H1//////1H 10X30HWING-BODY COMBINATION GEOMETRY//1H 20X
     1 21HWING LOCATION ON BODY//1H 25X34HLEADING EDGE DISTANCE FROM NOS
     2E = F7.3//1H 25X45HHEIGHT OF ROOT CHORD ABOVE BODY CENTERLINE =
     3 F6.3/1H210X17HFLIGHT CONDITIONS//1H 25X18HANGLE OF ATTACK = F7.4,
     4 8H DEGREES//1H 25X14HMACH NUMBER = F6.3)
 1008 FORMAT (1H1/////1H 10X69HTHE FOLLOWING NUMERICAL PARAMETERS HAVE
     1BEEN USED IN THE CALCULATIONS///1H 15X9HPARAMETER15X5HUSE1/X5HVALU
     2E//1H017X1HM7X30HNUMBER OF STATIONS ON BODY    5X12/26X30HBETWEEN
     3WING LEADING AND    /26X14HTRAILING EDGES//1H 17X2HM1,6X30HNUMBE
     4R OF STATIONS ON BODY    5X12/26X30HBETWEEN WING TRAILING EDGE
     5 /26X19HAND AFT END OF BODY//)
 1009 FORMAT (1H 17X2HM26X30HNUMBER OF INTERVALS USED IN    5X12/26X
     1 30HTHE NUMERICAL INTEGRATIONS    /26X34HEMPLOYED IN THE LAWRENCE
     2PROCEDURE//1H 17X2HM36X30HNUMBER OF INTERVALS USED IN   5X12/26X
     3 30HTHE NUMERICAL INTEGRATIONS    /26X30HEMPLOYED IN THE WEISSINGE
     4R    /26X9HPROCEDURE//1H 17X1HN7X30HNUMBER OF STATIONS ON THE WING
     5 5X12/26X9HSEMI-SPAN//)
      PRINT 1001
      PRINT 1002,AR,TR,ALAM,THETA,S
      PRINT 1003
      PRINT 1004,((THET(I),ELAMB(J),ALPH(I,J),J=1,N),I=1,MM1)
      PRINT 1005,EL
      DO 1 J=1,MM1
      XS=X(J+1)*S
      PRINT 1006,XS,A(J),C(J),ALPHB(J)
      PRINT 1007,XW,ZW,ALPHA,EMACH
      PRINT 1008,M,M1
```

```
PRINT 1009,M2,M3,N
RETURN
END
```

```
      SUBROUTINE   COMPRS  (EL)
C     COMPRESSIBILTY CORRECTIONS -  SUBSONIC
      COMMON CF,A,ELAMB,ALPH,X,Y,CL1EV,ALPHEV,ALPHB,C,THETB,TAU,TAUBAR,
     1 THETBR,BOC,BCO,THET1,THET,XB,CEFV,ALPHWB,OUTPUT,  BETA,PI,AR,TR,
     2 S,M,M1,M2,M3,N,ALPHA,CL1EV,MM1,XW,ZW,FLB,THETA,XWB,EMACH,ALAM,
     3 ALAMQC  ,ALAMB   ,BAR
      DIMENSION CF(50,50),ELAMB(50),ALPH(100,50),X(101),Y(101),CL1EV(50)
     1 ,ALPHEV(50),ALPHB(100),A(100),C(100),THETB(101),TAU(50),BOC(50),
     2 TAUBAR(50),THETBR(50),BCO(50),THET1(99),THET(101),XB(101),
     3 CEFV(50),ALPHWB(50),OUTPUT(50)
      BETA = SQRTF(1.-EMACH*EMACH)
      ALAM1=ALAM/57.295779
      ALAMB=ATANF(TANF(ALAM1)/BETA)
      XWB=XW/BETA
      FLB=FL/BETA
      BAR=BETA*AR
      DO 1 J=1,MM1
      XB(J)=X(J)/BETA
    1 THETB(J)=THET(J)/BETA
      XB(MM1+1)=X(MM1+1)/BETA
      RETURN
      END
```

97

```
      SUBROUTINE   PART1 (CR)
C     PART1 - X LESS THAN XTE
      COMMON CF,A,ELAMB,ALPH,X,Y,CL1EV,ALPHEV,ALPHB,C,THETB,TAU,TAUBAR,
     1 THETBR,BOC,BCO,THET1,THET,XB,CEFV,ALPHWB,OUTPUT,  BETA,PI,AR,TR,
     2 S,M,M1,M2,M3,N,ALPHA,CLTOT,MM1,XW,ZW,ELB,THETA,XWB,EMACH,ALAM,
     3 ALAMQC,ALAMB,BAR,CL,CLWB,XCP
      DIMENSION CF(50,50),ELAMB(50),ALPH(100,50),X(101),Y(101),CL1EV(50)
     1 ,ALPHEV(50),ALPHB(100),A(100),C(100),THETB(101),TAU(50),BOC(50),
     2 TAUBAR(50),THETBR(50),BCO(50),THET1(99),THET(101),XB(101),
     3 CEFV(50),ALPHWB(50),OUT: (50)
      DIMENSION F(50),B(50),FB(50),HO(50),FO(50),B1(50,1),PHI(50),WB(50)
     1 ,A1(51),DGDX(50),DGDXX(50)
      GARBF(X) = ((SQRTF((COSF(X)-COSF(EJ*PI/(EM+1.)))**2+(BJNS**2))-
     1 BJNS)/(COSF(X)-COSF(EJ*PI/(EM+1.))))
      ALPHA=ALPHA/57.295779
      KEY=1
       PI=3.14159265
70    IF (KEY-2) 1,2,3
1     CALL FUNC(F,B,PHI)
      GO TO 4
2     CALL FUNC2(F,B)
4     LIM=M2-1
      EM=M
      FM2=M2
      DO 40 I=1,50
      DO 40 J=1,50
40    CF(I,J)=0.
      DO 50 J=1,M
       MJ1=M-J+1
       BJNS=B(MJ1)*BETA*2./CR
      EJ=J
      SUM=0.
      DO 51 K=1,LIM
      FK=K
      TERM=GARBF((EK*PI)/EM2)
51    SUM=SUM+TERM
      HO(J)=(1./EM2)*(((GARBF(0.)+GARBF(PI))/2.)+SUM)
      FO(J)=(2.*EJ/(EM+1.))+HO(J)-3.
       B1(J,1)=B(MJ1)*B(MJ1)*F(MJ1)
      DO 52 L=1,M
      FL=L
      SUM=0.
      DO 53 K=1,LIM
      FK=K
      TERM=COSF((EK*PI*EL)/EM2)*GARBF((EK*PI)/EM2)
53    SUM=SUM+TERM
      H=(1./EM2)*(((GARBF(0.)+((-1.)**L)*GARBF(PI))/2.)+SUM)
52    FB(L)=(2.*SINF(EL*EJ*PI/(EM+1.))/(EL*PI))+(BJNS*SINF(EL*EJ*PI/(EM+
     1 1.))/(SINF(EJ*PI/(EM+1.))))+H
      CF(J,1)=FB(1)-FO(J)
      CF(J,2)=FB(2)-FO(J)
      DO 6 I=3,M
6     CF(J,I)=FB(I)-FB(I-2)
```

```
50      CONTINUE
        CALL MATINV(M,B1,1,DET)
        DO 8 I=1,M
8       A1(I)=B1(I,1)
        A1(M+1)=0.
        DO 9 J=1,M
        FJ=J
        SUM=0.
        DO 10 L=2,M
        FL=L
        TERM=A1(L)*SINF((EL-1.)*EJ*PI/(EM+1.))
10      SUM=SUM+TERM
        MJ1=M-J+1
9       DGDX(MJ1)=(A1(1)*TANF(EJ*PI/((EM+1.)*2.))+2.*SUM)/BETA
        CL    =(2.*PI*BAR*(A1(1)+A1(2)))/BETA
        XCP=.5-(.25*((A1(1)-A1(3))/(A1(1)+A1(2))))
        DO 11 J=1,M
11      OUTPUT(J)=4.*DGDX(J)*COSF(PHI(J))
        IF (KEY-1) 61,60,61
60       CALL OP1 (B)
         CMWB=XCP*CL
        CLWB=CL
        DO 12 J=1,M
12      WB(J)=OUTPUT(J)
61      KEY=KEY+1
         CMW=XCP*CL
        GO TO 70
3       DO 13 J=1,M
13      BCO(J)=WB(J)-OUTPUT(J)
         CALL OP2
         CMBCO=CMWB-CMW
         CLBCO=CLWB-CL
         XCP=CMBCO/CLBCO
        RETURN
        END
```

99

```
      SUBROUTINE   FUNC (F,B,PHI)
C     CALCULATE F(THETA) - WING AND BODY
      COMMON CF,A,ELAMB,ALPH,X,Y,CL1EV,ALPHEV,ALPHB,C,THETB,TAU,TAUBAR,
     1 THETBR,BOC,BCO,THET1,THET,XB,CEFV,ALPHWB,OUTPUT,  BETA,PI,AR,TR,
     2 S,M,M1,M2,M3,N,ALPHA,CLTOT,MM1,XW,ZW,ELB,THETA,XWB,EMACH,ALAM,
     3 ALAMOC  ,ALAMB   ,BAR
      DIMENSION CF(50,50),ELAMB(50),ALPH(100,50),X(101),Y(101),CL1EV(50)
     1 ,ALPHEV(50),ALPHB(100),A(100),C(100),THETB(101),TAU(50),BOC(50),
     2 TAUBAR(50),THETBR(50),BCO(50),THET1(99),THET(101),XB(101),
     3 CEFV(50),ALPHWB(50),OUTPUT(50)
      DIMENSION R(50),EK2(50),B(50),F2(50),PHI(50),F(50)
      THETA=THETA/57.295779
      DO 1 I=1,MM1
      DO 2 J=1,N
2     ALPH(I,J)=ALPH(I,J)/57.295779
1     ALPHB(I)=ALPHB(I)/57.295779
      DO 10 J=1,M
      R(J)=.5*((A(J)/S)+(C(J)/S))
      EK2(J)=.25*((A(J)/S)+(C(J)/S))*((A(J)/S)-(C(J)/S))
       IF(THETB(J)-TANF(ALAMB)) 20,11,11
11    IF (THETB(J)-4./(BAR*(1.+TR))) 12,13,13
12    B(J)=1.0
       LIM=0
      GO TO 40
13    B(J)=0.
      GO TO 40
20    YLE=(THETB(J))/TANF(ALAMB)
      L=N+1
21    L=L-1
      IF (YLE-Y(L+1)) 30,30,21
30    IF (YLE-ELAMB(L+1)) 31,32,32
31    R(J)=Y(L+2)
      LIM=L+1
      GO TO 40
32    R(J)=Y(L+1)
      LIM=L
40    RT=R(J)
      EK2T=EK2(J)
      BRL=B(J)+A(J)*SQRTF(1.-(ZW/C(J))**2)/S
      BSRL=1.0+A(M)*SQRTF(1.-(ZW/C(M))**2)/S
      BIM=0.
      BSIM=0.
      SUM=0.
      CALL TRNS(BRL,BIM,BBRRL,BBRIM,RT,EK2T)
      CALL TRNS(BSRL,BSIM,BSBRRL,BSBRIM,RT,EK2T)
       LIMP=LIM+1
       DO 41 I=LIMP,N
       TRL=ELAMB(I)+A(J)*SQRTF(1.-(ZW/C(J))**2)/S
       TIM=ZW/S+ELAMB(I)*TANF(THETA)
      CALL TRNS(TRL,TIM,TBRRL,TBRIM,RT,EK2T)
      TERM1=SQRTF((BBRRL/BSBRRL)**2-(TBRRL/BSBRRL)**2)
      IF (I-LIM) 45,42,45
42    TOR=TBRRL
      TOI=TBRIM
      GO TO 43
```

100

```
45      IF (I-N) 43,44,43
44      T1R=TBRRL
        T1I=TBRIM
43      CALL DTBRDT(TRL,TIM,DTBRRL,DTRIM,RT,EK2T)
        F1=DTBRRL-1.
        TERM2=.5*(ALPH(J,I)+(ALPHB(J)+ALPHA)*F1)
41      F2(I)=TERM1*TERM2
        PHI(J)=ATANF((T1I-TOI)/(TOR-T1R))
         DO 46 I=LIMP,N
         TERM=(Y(I)-Y(I+1))*F2(I)
46      SUM=SUM+TERM
10      F(J)=(8./PI)*(1./(BRL/BSRL)**2)*SUM
        RETURN
        END
```

```
        SUBROUTINE TRNS(ZETAR,ZETAI,SIGMAR,SIGMAI,R,EK2)
C       ELLIPTICAL TRANSFORMATION
        IF (EK2) 1,2,1
1       R1=RCS (ZETAR,ZETAI)
        C1=EICS (ZETAR,ZETAI)
        R2=RCM (R1,C1,4.*EK2,0.)
        C2=EICM (R1,C1,4.*EK2,0.)
        R3=RCSR (R2,C2)
        C3=EICSR (R2,C2)
        R4=RCMT (R*R+EK2,0.,R3,C3)
        C4=EICMT (R*R+EK2,0.,R3,C3)
        R5 = RCMT (R*R-EK2,0.,ZETAR,ZETAI)
        C5 =EICMT (R*R-EK2,0.,ZETAR,ZETAI)
        R6=R4-R5
        C6=C4-C5
        SIGMAR=R6/(2.*EK2)
        SIGMAI=C6/(2.*EK2)
        RETURN
2       R1 = RCD(R*R,0.,ZETAR,ZETAI)
        C1 =EICD(R*R,0.,ZETAR,ZETAI)
         SIGMAR=ZETAR-R1
         SIGMAI=ZETAI-C1
        RETURN
        END
```

```
      SUBROUTINE DTBRDT(TRL,TIM,DTBRRL,DTBRIM,RT,EK2T)
C     DTBAR(X)/DT(X)
      IF (EK2T) 1,2,1
1     R1 = RCS (TRL,TIM)
      C1 =EICS (TRL,TIM)
      R2 = RCM (R1,C1,4.*EK2T,0.)
      C2 =EICM (R1,C1,4.*EK2T,0.)
      R3 = RCSR (R2,C2)
      C3 =EICSR (R2,C2)
      R4 = RCD (TRL,TIM,R3,C3)
      C4 =EICD (TRL,TIM,R3,C3)
      CC1 = (RT**2+EK2T)/(2.*EK2T)
      CC2 = (RT**2-EK2T)/(2.*EK2T)
      DTBRRL = CC1*R4-CC2
      DTBRIM = CC1*C4
      RETURN
2     R1 = RCS (TRL,TIM)
      C1 =EICS (TRL,TIM)
      R2 = RCD (RT*RT,0.,R1,C1)
      C2 =EICD (RT*RT,0.,R1,C1)
      DTBRRL=1.+R2
      DTBRIM= -C2
      RETURN
      END
```

103

```
      SUBROUTINE    FUNC2   (F,B)
C     CALCULATE F(THETA)   WING ALONE
      COMMON CF,A,ELAMB,ALPH,X,Y,CL1EV,ALPHEV,ALPHB,C,THETB,TAU,TAUBAR,
     1 THETBR,BOC,BCO,THET1,THET,XB,CEFV,ALPHWB,OUTPUT,   BETA,PI,AR,TR,
     2 S,M,M1,M2,M3,N,ALPHA,CLTOT,MM1,XW,ZW,ELB,THETA,XWB,EMACH,ALAM,
     3 ALAMQC   ,ALAMB
      DIMENSION CF(50,50),ELAMB(50),ALPH(100,50),X(101),Y(101),CL1EV(50)
     1 ,ALPHEV(50),ALPHB(100),A(100),C(100),THETB(101),TAU(50),BOC(50),
     2 TAUBAR(50),THETBR(50),BCO(50),THET1(99),THET(101),XB(101),
     3 CEFV(50),ALPHWB(50),OUTPUT(50)
      DIMENSION B(50),F2(50),F(50)
      DO 10 J=1,M
       IF (THETB(J)-TANF(ALAMB)) 1,3,3
3     B(J)=1.0
       LIM=0
      GO TO 11
1     YLE=THETB(J)/TANF(ALAMB)
      L=N+1
4     L=L-1
      IF (YLE-Y(L+1)) 6,6,4
6     IF (YLE-ELAMB(L+1)) 7,8,8
7     B(J)=Y(L+2)
      LIM=L+1
      GO TO 11
8     B(J)=Y(L+1)
      LIM=L
11    SUM=0.
       LIMP=LIM+1
       DO 13 I=LIMP,N
       TERM1=SQRTF(B(J)**2-(ELAMB(I))**2)
      TERM2=.5*ALPH(J,I)
13    F2(I)=TERM1*TERM2
       DO 14 I=LIMP,N
       TERM=(Y(I)-Y(I+1))*F2(I)
14    SUM=SUM+TERM
10    F(J)=(8./PI)*(1./B(J)**2)*SUM
      RETURN
      END
```

```
      SUBROUTINE    PART2    (KEY)
C     PART2 - X GREATER THAN XTE
      COMMON CF,A,ELAMB,ALPH,X,Y,CL1EV,ALPHEV,ALPHB,C,THETB,TAU,TAUBAR,
     1 THETBR,BOC,BCO,THET1,THET,XB,CEFV,ALPHWB,OUTPUT,  BETA,PI,AR,TR,
     2 S,M,M1,M2,M3,N,ALPHA,CLTOT,MM1,XW,ZW,ELB,THETA,XWB,EMACH,ALAM,
     3 ALAMQC  ,ALAMB   ,BAR
      DIMENSION CF(50,50),ELAMB(50),ALPH(100,50),X(101),Y(101),CL1EV(50)
     1 ,ALPHEV(50),ALPHB(100),A(100),C(100),THETB(101),TAU(50),BOC(50),
     2 TAUBAR(50),THETBR(50),BCO(50),THET1(99),THET(101),XB(101),
     3 CEFV(50),ALPHWB(50),OUTPUT(50)
      DIMENSION CL(50),DLDX(50),RT1(50),EIT1(50),CPX(50)
      CALL    ALPEFV   (KEY)
      CALL    WEISS  (CL,CPX,YCP)
      KEYOP4=1
      CALL OP4 (CL,YCP,KEYOP4)
      CALL    FLIPWB  (CPX)
      CALL    WEISS  (CL,CPX,YCP)
      KEYOP4=2
      CALL OP4 (CL,YCP,KEYOP4)
      CALL BCOLFT(DLDX,GAM,RT1,EIT1,ALPHO,CL1,CL2,CL3,XCP1,XCP2,XCP3)
      CALL   OP5  (DLDX,GAM,RT1,EIT1,ALPHO,CL1,CL2,CL3,XCP1,XCP2,XCP3)
      RETURN
      END
```

```
       SUBROUTINE   ALPEFV  (KEY)
C      EFFECTIVE ALPHA
       COMMON CF,A,ELAMB,ALPH,X,Y,CL1EV,ALPHEV,ALPHB,C,THETB,TAU,TAUBAR,
     1 THETBR,BOC,BCO,THET1,THET,XB,CEFV,ALPHWB,OUTPUT,  BETA,PI,AR,TR,
     2 S,M,M1,M2,M3,N,ALPHA,CLTOT,MM1,XW,ZW,ELB,THETA,XWB,EMACH,ALAM,
     3 ALAMQC  ,ALAMB  ,BAR
       DIMENSION CF(50,50),ELAMB(50),ALPH(100,50),X(101),Y(101),CL1EV(50)
     1 ,ALPHEV(50),ALPHB(100),A(100),C(100),THETB(101),TAU(50),BOC(50),
     2 TAUBAR(50),THETBR(50),BCO(50),THET1(99),THET(101),XB(101),
     3 CEFV(50),ALPHWB(50),OUTPUT(50)
       DIMENSION XTEEFV(50),XLE(50),XLEEFV(50),DXEFV(100),XEFV(100)
       TANLTE=TANF(ALAMB)-(4.*(1.-TR)/(BAR*(1.+TR)))
       DO 1 J=1,N
        XTEEFV(J)=4./(BAR*(1.+TR))+ELAMB(J)*TANLTE
       XLE(J)=TANF(ALAMB)*ELAMB(J)
       I=1
2      IF (THETB(I)-XLE(J)) 10,10,11
10     I=I+1
       GO TO 2
11     XLEEFV(J)=XB(I)-XB(1)
       IMIN=I
3      I=1
4      IF ((XB(I+1)-XB(1))-XTEEFV(J)) 12,12,13
12     I=I+1
       GO TO 4
13     IMAX=I
5      CEFV(J)=XTEEFV(J)-XLEEFV(J)
        IF(KEY) 22,23,22
23      ALPHEV(J)=ALPH(1,1)
        GO TO 1
22      DO 6 I=IMIN,IMAX
       IF (I-IMAX) 14,15,15
14     DXEFV(I)=XB(I+1)-XB(I)
       GO TO 20
15     DXEFV(I)=XTEEFV(J)-(XB(I)   -XB(1))
20     IF (I-M) 16,16,17
16     XEFV(I)=THETB(I)-XLEEFV(J)
       GO TO 6
17     IF (XTEEFV(J)-(XB(I+1)-XB(1))) 18,19,19
19      XEFV(I)=THETB(I)-XLEEFV(J)
       GO TO 6
18      XEFV(I)=XTEEFV(J)-(XTEEFV(J)-(XB(I)-XB(1)))/2.-XLEEFV(J)
6      CONTINUE
       SUM=0.
       DO 7 I=IMIN,IMAX
       TERM1=(4./PI)*SQRTF((CEFV(J)-XEFV(I))/XEFV(I))
       SUM2=0.
       DO 8 K=IMIN,IMAX
       IF (K-I) 21,8,21
21     TERM2=(-ALPH(K,J)/(XEFV(I)-XEFV(K)))*SQRTF(XEFV(K)/(CEFV(J)-
     1 XEFV(K)))*DXEFV(K)
       SUM2=SUM2+TERM2
8      CONTINUE
```

```
        TERM=TERM1*SUM2*DXEFV(I)
7       SUM=SUM+TERM
        ALPHEV(J)=SUM/(2.*PI*CEFV(J))
1       CONTINUE
        CALL OP3(XLEEFV,XTEEFV)
        RETURN
        END
```

```
        SUBROUTINE   WEISS  (CL,CPX,YCP)
C       WEISS
        COMMON A, O,ELAMB,ALPH,X,Y,CL1EV,ALPHEV,ALPHB,C,THETB,TAU,TAUBAR,
      1 THETBR,BOC,BCO,THET1,THET,XB,CEFV,ALPHWB,OUTPUT,  BETA,PI,AR,TR,
      2 S,M,M1,M2,M3,N,ALPHA,CLTOT,MM1,XW,ZW,ELB,THETA,XWB,FMACH,ALAM,
      3 ALAMQC,ALAMB,BAR,DUM,CLWB,XCP,CLPN,CR
        DIMENSION  A(50,50),ELAMB(50),ALPH(100,50),X(101),Y(101),CL1EV(50)
      1 ,ALPHEV(50),ALPHB(100),O(100),C(100),THETB(101),TAU(50),BOC(50),
      2 TAUBAR(50),THETBR(50),BCO(50),THET1(99),THET(101),XB(101),
      3 CEFV(50),ALPHWB(50),OUTPUT(50)
        DIMENSION G(50),CLP(50),ALPHA1(50,1),CPX(50),CL(50)
        CR=4./(BAR*(1.+TR))
        EM3=M3
        EN=N
        N2=N*2
        DO 6 J=1,N2
        EJ=J
6       THET1(J)=(EJ*PI)/(2.*EN)
        DO 1 J=1,N
        TAU(J)=COSF(THET1(J))
        ALPHA1(J,1)=ALPHEV(J)
1       BOC(J)=2./(CR*(1.-Y(J)*(1.-TR)))
        BOC(N+1)=2./CR
        DO 2 J=1,M3
        EJ=J
        THETBR(J)=(EJ*PI)/(2.*EM3)
2       TAUBAR(J)=COSF(THETBR(J))
        ALAMQC=ATANF(TANF(ALAMB)-(1.-TR)/(BAR*(1.+TR)))
        DO 7 I=1,50
        DO 7 J=1,50
7       A(I,J)=0.
        CALL AMAT
        L=1
        CALL MATINV(N,ALPHA1,L,DET)
        NP=N+1
        DO 3 J=2,NP
        G(J)=ALPHA1(J-1,1)
3       CLP(J)=2.*G(J)*BOC(J)
        CLPN=CLP(NP)
        CLP(1)=0.
        DO 4 J=1,N
        CL(J)=(CLP(J)+CLP(J+1))/2.
        BOCAV=(BOC(J)+BOC(J+1))/2.
        CL1EV(J)=CL(J)*BAR/BOCAV
4       CPX(J)=.25*CR+ELAMB(J)*TANF(ALAMQC)
        SUM=0.
        SUM1=0.
        DO 5 J=1,N
        TERM=CL1EV(J)*(Y(J)-Y(J+1))
        TERM1=TERM*ELAMB(J)
        SUM=SUM+TERM
5       SUM1=SUM1+TERM1
        CLTOT=SUM
```

```
YCP=SUM1/SUM
RETURN
END
```

```
      SUBROUTINE   AMAT
C     AMAT
      COMMON A, O,ELAMB,ALPH,X,Y,CL1EV,ALPHEV,ALPHB,C,THETB,TAU,TAUBAR,
     1 THETBR,BOC,BCO,THET1,THET,XB,CEEV,ALPHWB,OUTPUT,  BETA,PI,AR,TR,
     2 S,M,M1,M2,M3,N,ALPHA,CLTOT,""",XW,ZW,ELB,THETA,XWB,EMACH,ALAM,
     3 ALAMOC  ,ALAMB
      DIMENSION  A(30,50),ELAMB(50),ALPH(100,50),X(101),Y(101),CL1EV(50)
     1 ,ALPHEV(50),ALPHB(100),O(100),C(100),THETB(101),TAU(50),BOC(50),
     2 TAUBAR(50),THETBR(50),BCO(50),THET1(99),THET(101),XB(101),
     3 CEEV(50),ALPHWB(50),OUTPUT(50)
      DO 1 J=1,N
      DO 2 I=1,N
      IF (J-I) 3,4,3
3     IF (I-N) 5,6,5
5      IARG2=2*N-I
      BIGB=B(J,I)              +B(J,IARG2)
      GO TO 7
6      BIGB=B(J,I)
      GO TO 7
4      A(J,I)=2.*B(J,J)+BOC(J+1)*GBAR(J,J)
      GO TO 2
7      A(J,I)=-2.*BIGB+BOC(J+1)*GBAR(J,I)
2     CONTINUE
1     CONTINUE
      RETURN
      END
```

110

```
      FUNCTION    B( J,I )
C     B
      COMMON A, O,ELAMB,ALPH,X,Y,CL1EV,ALPHEV,ALPHB,C,THETB,TAU,TAUBAR,
     1 THETBR,BOC,BCO,THET1,THET,XB,CEFV,ALPHWB,OUTPUT,  BETA,PI,AR,TR,
     2 S,M,M1,M2,M3,N,ALPHA,CLTOT,MM1,XW,ZW,ELB,THETA,XWB,EMACH,ALAM,
     3 ALAMQC  ,ALAMB
      DIMENSION  A(50,50),ELAMB(50),ALPH(100,50),X(101),Y(101),CL1EV(50)
     1 ,ALPHEV(50),ALPHB(100),O(100),C(100),THETB(101),TAU(50),BOC(50),
     2 TAUBAR(50),THETBR(50),BCO(50),THET1(99),THET(101),XB(101),
     3 CEFV(50),ALPHWB(50),OUTPUT(50)
      FN=N
      IF (I-J) 1,2,1
2     B = ((2.*EN)/(4.*SINF(THET1(J))))
      RETURN
1     B = (SINF(THET1(I))/((COSF(THET1(I))-COSF(THET1(J)))**2))*
     1 (1.-(-1.)**(I-J))/(4.*EN)
      RETURN
      END
```

```
      FUNCTION    GBAR  (J,I)
C     GBAR
      COMMON A, O,ELAMB,ALPH,X,Y,CL1EV,ALPHEV,ALPHB,C,THETB,TAU,TAUBAR,
     1 THETBR,BOC,BCO,THET1,THET,XB,CEFV,ALPHWB,OUTPUT,  BETA,PI,AR,TR,
     2 S,M,M1,M2,M3,N,ALPHA,CLTOT,MM1,XW,ZW,ELB,THETA,XWB,EMACH,ALAM,
     3 ALAMQC  ,ALAMB
      DIMENSION   A(50,50),ELAMB(50),ALPH(100,50),X(101),Y(101),CL1EV(50)
     1 ,ALPHEV(50),ALPHB(100),O(100),C(100),THETB(101),TAU(5)),BOC(50),
     2 TAUBAR(50),THETBR(50),BCO(50),THET1(99),THET(101),XB(101),
     3 CEFV(50),ALPHWB(50),OUTPUT(50)
      TM3=2*M3
      SUM=0.
      DO 1 L=1,M3
      LM=L-1
      TERM=FBAR (I,LM)      *ELSTAR (J,LM)
    1 SUM=SUM+TERM
      GBAR=((-1.)/(2.*TM3))*SUM
      RETURN
      END
```

```
      FUNCTION    FBAR   (I,LM)
C     FBAR
      COMMON A, O,ELAMB,ALPH,X,Y,CL1EV,ALPHEV,ALPHB,C,THETB,TAU,TAUBAR,
     1 THETBR,BOC,BCO,THET1,THET,XB,CEFV,ALPHWB,OUTPUT,  BETA,PI,AR,TR,
     2 S,M,M1,M2,M3,N,ALPHA,CLTOT,MM1,XW,ZW,ELB,THETA,XWB,EMACH,ALAM,
     3 ALAMQC   ,ALAMB
      DIMENSION   A(50,50),FLAMB(50),ALPH(100,50),X(101),Y(101),CL1EV(50)
     1 ,ALPHEV(50),ALPHB(100),O(100),C(100),THETB(101),TAU(50),BOC(50),
     2 TAUBAR(50),THETBR(50),BCO(50),THET1(99),THET(101),XB(101),
     3 CEFV(50),ALPHWB(50),OUTPUT(50)
      EN=N
      SUM=0.
      MU2=2*N-1
      DO 1 MU1=1,MU2,2
      EMU=MU1
      IF (LM) 2,3,2
3     TERM=FMU*SINF(EMU*THET1(I))
      GO TO 1
2     TERM=EMU*SINF(EMU*THET1(I))*COSF(EMU*THETBR(LM))
1     SUM=SUM + TERM
      F  = SUM/EN
      IF (I-N) 5,6,5
5     IF (LM) 7,8,7
6     IF (LM) 8,10,8
7     FBAR=2.*F
      RETURN
8     FBAR=F
      RETURN
10    FBAR=F/2.
      RETURN
      END
```

```
      FUNCTION    ELSTAR  (J,LM)
C     ELSTAR
      COMMON A, O,ELAMB,ALPH,X,Y,CL1EV,ALPHEV,ALPHB,C,THETB,TAU,TAUBAR,
     1 THETBR,BOC,BCO,THET1,THET,XB,CEFV,ALPHWB,OUTPUT,  BETA,PI,AR,TR,
     2 S,M,M1,M2,M3,N,ALPHA,CLTOT,MM1,XW,ZW,ELB,THETA,XWB,EMACH,ALAM,
     3 ALAMQC  ,ALAMB
      DIMENSION  A(50,50),ELAMB(50),ALPH(100,50),X(101),Y(101),CL1EV(50)
     1 ,ALPHEV(50),ALPHB(100),O(100),C(100),THETB(101),TAU(50),BOC(50),
     2 TAUBAR(50),THETBR(50),BCO(50),THET1(99),THET(101),XB(101),
     3 CEFV(50),ALPHWB(50),OUTPUT(50)
      IF (LM) 1,2,1
2     ETAMU=1.
      GO TO 6
1     ETAMU=TAUBAR(LM)
6     ETANU=TAU(J)
      DIF=ETANU-ETAMU
      SUM=ETANU+ETAMU
      BOCN=BOC(J+1)
      TERM1=(1./(BOCN*DIF))*(SQRTF(((1.+BOCN*DIF*TANF(ALAMQC))**2)+
     1 ((BOCN*DIF)**2))-1.)
      TERM2 = (1./(BOCN*SUM))*((SQRTF(((1.+BOCN*DIF*TANF(ALAMQC))**2)+
     1 ((BOCN*SUM)**2)))/(1.+2.*BOCN*ETANU*TANF(ALAMQC)) 1.)
      TERM3=(2.*TANF(ALAMQC)*SQRTF(((1.+BOCN*ETANU*TANF(ALAMQC))**2)+
     1 ((BOCN*ETANU)**2)))/(1.+2.*BOCN*ETANU*TANF(ALAMQC))
      ELSTAR=TERM1-TERM2-TERM3
      RETURN
      END
```

114

```
      SUBROUTINE  ELIPWB  (  X)
C     ELIPTICAL BODY - WING
      COMMON CF,A,ELAMB,ALPH,X,Y,CL1EV,ALPHEV,ALPHB,C,THETB,TAU,TAUBAR,
     1 THETBR,BOC,BCO,THET1,THET,XB,CEFV,ALPHWB,OUTPUT,   BETA,PI,AR,TR,
     2 S,M,M1,M2,M3,N,ALPHA,CLTOT,MM1,XW,ZW,ELB,THETA,XWB,EMACH,ALAM,
     3 ALAMOC  ,ALAMB   ,BAR
      DIMENSION CF(50,50),ELAMB(50),ALPH(100,50),X(101),Y(101),CL1EV(50)
     1 ,ALPHEV(50),ALPHB(100),A(100),C(100),THETB(101),TAU(50),BOC(50),
     2 TAUBAR(50),THETBR(50),BCO(50),THET1(99),THET(101),XB(101),
     3 CEFV(50),ALPHWB(50),OUTPUT(50)
      DIMENSION Z(50),XI(50),ETA(50),XI1(50),ETA1(50),H(50),XIO(50),
     1 ETAO(50),GAM1(50),GAM1P(50),BIGGAM(50),WIM(50),WBUP(50),WTIM(50),
     2 CPX(50)
      XIW= A(1)*SQRTF(1.-(ZW/C(1))**2)/S
      ETAW=ZW/S
      THETA2=THETA
      AOS=A(1)/S
      BOS=C(1)/S
      NP=N+1
      DO 1 I=1,NP
      Z(I)=Y(I)*TANF(THETA2)
      XI(I)=XIW+Y(I)
1     ETA(I)=ETAW+Z(I)
      DO 2 I=1,N
2      BIGGAM(I)=CL1EV(I)/BAR
      R=(AOS+BOS)/2.
      EK2=(AOS+BOS)*(AOS-BOS)/4.
      EK=SQRTF(SQRTF(EK2*EK2))
      IF (EK) 10,11,10
10    TERM1=(R*R)/EK
      TERM2=EK2*EK/(R*R)
      ALIM=TERM1+TERM2
      BLIM=TERM1-TERM2
      DO 3 I=1,NP
      IF (((XI(I)/ALIM)**2+(ETA(I)/BLIM)**2)-1.) 12,12,3
12    IMIN=I
      GO TO 20
3     CONTINUE
11    IMIN=1
20    DO 4 I=IMIN,NP
      ZOR=XI(I)
      ZOI=ETA(I)
      CALL IMAGE(R,EK2,ZOR,ZOI,Z1R,Z1I)
      XI1(I)=Z1R
4     ETA1(I)=Z1I
      DO 5 I=IMIN,N
      H(I)=.5*SQRTF((XI1(I+1)-XI1(I))**2+(ETA1(I+1)-ETA(I))**2)
      GAM=ATANF((ETA1(I+1)-ETA1(I))/(XI1(I+1)-XI1(I)))
      XIO(I)=(XI1(I)+XI1(I+1))/2.
      ETAO(I)=(ETA1(I)+ETA1(I+1))/2.
      GAM1(I)=GAM-THETA2
5     GAM1P(I)=GAM+THETA2
      DO 14 J=1,N
```

115

```
      DO 6 I=IMIN,N
      YPM=ELAMB(J)+XIW-XIO(I)
      ZPM=ELAMB(J)*TANF(THETA2)+ETAW-ETAO(I)
      X1=ZPM-YPM*SINF(THETA2)
      YDPM=(YPM/COSF(THETA2))+X1*SINF(THETA2)
      ZDPM=X1*COSF(THETA2)
      Q=SQRTF((YDPM-H(I)*COSF(GAM1(I)))**2+(ZDPM-H(I)*SINF(GAM1(I)))**2)
      B=SQRTF((YDPM+H(I)*COSF(GAM1(I)))**2+(ZDPM+H(I)*SINF(GAM1(I)))**2)
      F=YPM*SINF(GAM1(I))-ZPM*COSF(GAM1(I))
      YDPST=YDPM+2.*XIO(I)*COSF(THETA2)
      ZDPST=ZDPM-2.*XIO(I)*SINF(THETA2)
      AP=SQRTF((ZDPST-H(I)*SINF(GAM1P(I)))**2+(YDPST+H(I)*COSF(
     1 GAM1P(I)))**2)
      BP=SQRTF((ZDPST+H(I)*SINF(GAM1P(I)))**2+(YDPST-H(I)*COSF(
     1 GAM1P(I)))**2)
      FP=YDPST*(SINF(GAM1P(I)))+ZDPST*(COSF(GAM1P(I)))
      XPM=CPX(J)+4./(BOC(J)+BOC(J+1))-CPX(I)
      SQA=SQRTF(XPM*XPM+Q*Q)
      SQB=SQRTF(XPM*XPM+B*B)
      SQAP=SQRTF(XPM*XPM+AP*AP)
      SQBP=SQRTF(XPM*XPM+BP*BP)
      COEFT=BIGGAM(I)/(4.*PI)
      WA = (COEFT/(Q*Q))*(1.+XPM/SQA)*(YDPM-H(I)*COSF(GAM1(I)))
      WB =-(COEFT/(B*B))*(1.+XPM/SQB)*(YDPM+H(I)*COSF(GAM1(I)))
      WAB=-(COEFT*(XPM/(F*F+XPM*XPM)))*((SQRTF(B*B-F*F)/SQB)-
     1 (SQRTF(Q*Q-F*F)/SQA))*COSF(GAM1(I))
      WAP=-(COEFT/(AP*AP))*(1.+XPM/SQAP)*(YDPST+H(I)*COSF(GAM1P(I)))
      WBP= (COEFT/(BP*BP))*(1.+XPM/SQBP)*(YDPST-H(I)*COSF(GAM1P(I)))
      WABP=-(COEFT*(XPM/(FP*FP+XPM*XPM)))*((SQRTF(AP*AP-FP*FP)/SQAP)-
     1 (SQRTF(BP*BP-FP*FP)/SQBP))*COSF(GAM1P(I))
      IF (I-N)       6,22,6
   22 WA=0.
      WAP=0.
    6 WIM(I)=WA+WB+WAB+WAP+WBP+WABP
      ZOR=ELAMB(J)+XIW
      ZOI=ELAMB(J)*TANF(THETA2)+ETAW
      CALL UPWASH(ZOR,ZOI,R,EK2,WUP)
      ALPT=ALPHA+ALPHP(1)
      WBUP(J)=-WUP*ALPT
      SUM=0.
      DO 7 I=IMIN,N
    7 SUM=SUM+WIM(I)
   14 ALPHEV(J)=ALPHEV(J)+SUM+WBUP(J)
      RETURN
      END
```

```
      SUBROUTINE IMAGE(R,EK2,ZOR,ZOI,ZIR,ZII)
C     IMAGE
      ZOI=-ZOI
      IF (EK2) 1,2,1
1     R1 = RCM (RCS (ZOR,ZOI),EICS (ZOR,ZOI),4.*EK2,0.)
      C1 =EICM (RCS (ZOR,ZOI),EICS (ZOR,ZOI),4.*EK2,0.)
      R2 = RCSR (R1,C1)
      C2 =EICSR (R1,C1)
      RTERM1 = RCM (ZOR,ZOI,R2,C2)
      ETERM1 =EICM (ZOR,ZOI,R2,C2)
      RTERM2= RCMT (.25*EK2,0.,RCS (RTERM1,ETERM1),EICS (RTERM1,ETERM1))
      ETERM2=EICMT (.25*EK2,0.,RCS (RTERM1,ETERM1),EICS (RTERM1,ETERM1))
      RNUM = RCP (R**4.,0.,RTERM2,ETERM2)
      ENUM =EICP (R**4.,0.,RTERM2,ETERM2)
      RDEN = RCMT (.5*R*R,0.,RTERM1,ETERM1)
      EDEN =EICMT (.5*R*R,0.,RTERM1,ETERM1)
      ZIR = RCD (RNUM,ENUM,RDEN,EDEN)
      ZII =EICD (RNUM,ENUM,RDEN,EDEN)
      ZOI=-ZOI
      RETURN
2     ZIR = RCD (R*R,0.,ZOR,ZOI)
      ZII =EICD (R*R,0.,ZOR,ZOI)
      ZOI=-ZOI
      RETURN
      END
```

117

```
      SUBROUTINE UPWASH(ZOR,ZOI,R,EK2,WUP)
C     UPWASH
      IF (EK2) 1,2,1
1     R1 = RCS (ZOR,ZOI)
      C1 =EICS (ZOR,ZOI)
      R2 = RCM (R1,C1,4.*EK2,0.)
      C2 =EICM (R1,C1,4.*EK2,0.)
      R3 = RCSR (R2,C2)
      C3 =EICSR (R2,C2)
      R4 = RCP (ZOR,ZOI,R3,C3)
      C4 =EICP (ZOR,ZOI,R3,C3)
      R5 = RCS (R4,C4)
      C5 =EICS (R4,C4)
      R6 = RCD (4.*R*R,0.,R5,C5)
      WUP= -R6
      RETURN
2      R1=RCS(ZOR,ZOI)
       C1=EICS(ZOR,ZOI)
       R2=RCD(R*R,0.,R1,C1)
       WUP=-R2
      RETURN
      END
```

```
      SUBROUTINE BCOLFT(DLDX,GAM,RT1,EIT1,ALPHO,CL1,CL2,CL3,XCP1,XCP2,
     1 XCP3)
C     BODY CARRY-OVER AFT
      COMMON CF,A,ELAMB,ALPH,X,Y,CL1EV,ALPHEV,ALPHB,C,THETB,TAU,TAUBAR,
     1 THETBR,BOC,BCO,THET1,THET,XB,CEFV,ALPHWB,OUTPUT,  BETA,PI,AR,TR,
     2 S,M,M1,M2,M3,N,ALPHA,CLTOT,MM1,XW,ZW,ELB,THETA,XWB,EMACH,ALAM,
     3 ALAMQC,ALAMB,BAR,CL,CLWB,XCP,CLPN,CR
      DIMENSION CF(50,50),ELAMB(50),ALPH(100,50),X(101),Y(101),CL1EV(50)
     1 ,ALPHEV(50),ALPHB(100),A(100),C(100),THETB(101),TAU(50),BOC(50),
     2 TAUBAR(50),THETBR(50),BCO(50),THET1(99),THET(1 1),XB(101),
     3 CEFV(50),ALPHWB(50),OUTPUT(50)
      DIMENSION DLDX(50),RT1(50),EIT1(50),TERM3(100)
       GAM=CLPN*CR/2.
       BP=2.*CLTOT/CL1EV(N)
      XW=A(1)*SQRTF(1.-(ZW/C(1))**2)
      SUM=0.
       SUM2=0.
      MP1=M+1
      DO 1 J=MP1,MM1
      RT1(J)=BP/2.*COSF(THETA)+XW/S
       TERM=(ALPHA+ALPHB(J))  *(XB(J+1)-XB(J))*BETA
      SUM=SUM+TERM
      EIT1(J)=SUM+ZW/S+(BP/2.)*SINF(THETA)
       TERM2=(XB(J+1)-XB(J))*BETA
1     SUM2=SUM2+TERM2
      ALPHO=SUM/SUM2
      DO 2 J=MP1,MM1
      EK2=((A(J)/S)**2-(C(J)/S)**2)/4.
      R2=(((A(J)/S)+(C(J)/S))**2)/4.
      IF (EK2) 6,7,6
6     CC1=(R2+EK2)/EK2
      CC2=(R2-EK2)/EK2
      RT1P=RT1(J)
      ET1P=EIT1(J)
      R1=RCS (RT1P,ET1P)
      C1=EICS(RT1P,ET1P)
      R21=R1-4.*EK2
      C21=C1
      R3=RCSR (R21,C21)
      R4=CC1*R3
      R5=CC2*RT1P
      R6=R4-R5
      GO TO 2
7     R1=RCD (R2,0.,RT1(J),EIT1(J))
       R5=RT1(J)-R1
      R6=2.*R5
2     TERM3(J)=R6
      MMM1=M+M1-1
      DO 3 J=MP1,MMM1
      DTDX=(TERM3(J+1)-TERM3(J))/(THETB(J+1)-THETB(J))
3     DLDX(J)=GAM*COSF(ALPHO)*DTDX
      DLDX(MM1)=DLDX(MMM1)+(DLDX(MMM1)-DLDX(MMM1-1))
       CL1=CLWB-CL
```

119

```
      XCP1=XCP
     SUM=0.
     SUM1=0.
     DO 5 J=MP1,MM1
     DX=(XB(J+1)-XB(J))*BETA*S
     TERM=DLDX(J)*DX
      TERM1=DLDX(J)*THETB(J)*DX*BETA
     SUM=SUM+TERM
     SUM1=SUM1+TERM1
5    CONTINUE
     CL2=SUM*BAR/4.
     XCP2=SUM1/SUM
     CL3=CL1+CL2
     XCP3=(CL1*XCP1+CL2*XCP2)/(CL1+CL2)
     RETURN
     END
```

```
      SUBROUTINE OP1(B)
C     OUTPUT-WING-BODY
      COMMON CF,A,ELAMB,ALPH,X,Y,CL1EV,ALPHEV,ALPHB,C,THETB,TAU,TAUBAR,
     1 THETBR,BOC,BCO,THET1,THET,XB,CEFV,ALPHWB,OUTPUT,  BETA,PI,AR,TR,
     2 S,M,M1,M2,M3,N,ALPHA,CLTOT,MM1,XW,ZW,ELB,THETA,XWB,EMACH,ALAM,
     3 ALAMQC,ALAMB,.AR,CL,CLWB,XCP
      DIMENSION CF(50,50),ELAMB(50),ALPH(100,50),X(101),Y(101),CL1EV(50)
     1 ,ALPHEV(50),ALPHB(100),A(100),C(100),THETB(101),TAU(50),BOC(50),
     2 TAUBAR(50),THETBR(50),BCO(50),THET1(99),THET(101),XB(101),
     3 CEFV(50),ALPHWB(50),OUTPUT(50)
      DIMENSION B(50)
1010  FORMAT (1H1,25X,29HLIFT ON WING-BODY COMBINATION///1H ,20X,50HCHOR
     1DWISE LIFT DISTRIBUTION ON THE BODY, INCLUDING//1H ,20X,55HTHE LIF
     2T OF THE WING.   THE FOLLOWING DEFINITIONS APPLY.///1H ,20X,1HX,9X,
     334HDISTANCE FROM ROOT OF LEADING EDGE/1H ,30X,27HTO CENTER OF SPAN
     4WISE STRIP//1H ,20X,1HB,9X,28HEFFECTIVE SEMI-SPAN OF STRIP//1H ,20
     5X,2HDX,8X,23HWIDTH OF SPANWISE STRIP//1H ,20X,1HQ,9X,16HDYNAMIC PR
     6ESSURE/////1H ,18X,1HX,14X,1HB,14X,2HDX,9X,10H(1/Q)DL/DX//)
1011  FORMAT (1H ,8X,4F15.4)
1012  FORMAT (1H0//1H ,20X,43HLIFT COEFFICIENT (WING-BODY COMBINATION) =
     1 ,F10.4//1H ,20X,31HCHORDWISE CENTER OF PRESSURE = ,F10.4/1H ,20X,
     223H(PERCENT OF ROOT CHORD))
      PRINT 1010
      XW=XWB*BETA
      DO 4 J=1,M
      THEA=THETB(J)*BETA*S
      XJ =XB(J+1)*BETA*S
      XJM=XB(J)*BETA*S
      DX=XJ-XJM
      B1=B(J)*S
4     PRINT 1011, THEA, B1, DX, OUTPUT(J)
      PRINT 1012, CL, XCP
      RETURN
      END
```

```
      SUBROUTINE OP2
C     OUTPUT - WING ALONE AND BODY CARRY-OVER
      COMMON CF,A,ELAMB,ALPH,X,Y,CL1EV,ALPHEV,ALPHB,C,THETB,TAU,TAUBAR,
     1 THETBR,BOC,BCO,THET1,THET,XB,CEFV,ALPHWB,OUTPUT,  BETA,PI,AR,TR,
     2 S,M,M1,M2,M3,N,ALPHA,CLTOT,MM1,XW,ZW,ELB,THETA,XWB,EMACH,ALAM,
     3 ALAMQC,ALAMB,BAR,CL,CLWB,XCP
      DIMENSION CF(50,50),ELAMB(50),ALPH(100,50),X(101),Y(101),CL1EV(50)
     1 ,ALPHEV(50),ALPHB(100),A(100),C(100),THETB(101),TAU(50),BOC(50),
     2 TAUBAR(50),THETBR(50),BCO(50),THET1(99),THET(101),XB(101),
     3 CEFV(50),ALPHWB(50),OUTPUT(50)
 1013 FORMAT (1H1,20X,45HCHORDWISE LIFT DISTRIBUTION ON THE WING ALONE//
     1//1H ,29X,1HX,20X,10H(1/Q)DL/DX//)
 1014 FORMAT (1H ,19X,F15.4,F25.4)
 1015 FORMAT (1H0//1H ,20X,32HLIFT COEFFICIENT (WING ALONE) = ,F10.4//1H
     1 ,20X,32HCHORDWISE CENTER OF PRESSURE =  F10.4)
 1016 FORMAT (1H2,20X,46HCHORDWISE DISTRIBUTION OF BODY CARRY-OVER LIFT/
     1/1H ,29X,1HX,20X,10H(1/Q)DL/DX//)
 1017 FORMAT (1H0//1H ,20X,37HLIFT COEFFICIENT (BODY CARRY-OVER) = ,F10.
     14)
      PRINT 1013
      DO 6 J=1,M
      THEA=THETB(J)*BETA*S
 6    PRINT 1014, THEA, OUTPUT(J)
      PRINT 1015, CL, XCP
      PRINT 1016
      DO 7 J=1,M
      THEA=THETB(J)*BETA*S
 7    PRINT 1014, THEA, BCO(J)
      CLBCO=CLWB-CL
      PRINT 1017, CLBCO
      RETURN
      END
```

122

122

```
      SUBROUTINE OP2
C     OUTPUT - WING ALONE AND BODY CARRY-OVER
      COMMON CF,A,ELAMB,ALPH,X,Y,CL1EV,ALPHEV,ALPHB,C,THETB,TAU,TAUBAR,
     1 THETBR,BOC,BCO,THET1,THET,XB,CEFV,ALPHWB,OUTPUT,  BETA,PI,AR,TR,
     2 S,M,M1,M2,M3,N,ALPHA,CLTOT,MM1,XW,ZW,ELB,THETA,XWB,EMACH,ALAM,
     3 ALAMQC,ALAMB,BAR,CL,CLWB,XCP
      DIMENSION CF(50,50),ELAMB(50),ALPH(100,50),X(101),Y(101),CL1EV(50)
     1 ,ALPHEV(50),ALPHB(100),A(100),C(100),THETB(101),TAU(50),BOC(50),
     2 TAUBAR(50),THETBR(50),BCO(50),THET1(99),THET(101),XB(101),
     3 CEFV(50),ALPHWB(50),OUTPUT(50)
 1013 FORMAT (1H1,20X,45HCHORDWISE LIFT DISTRIBUTION ON THE WING ALONE//
     1//1H ,29X,1HX,20X,10H(1/Q)DL/DX//)
 1014 FORMAT (1H ,19X,F15.4,F25.4)
 1015 FORMAT (1H0//1H ,20X,32HLIFT COEFFICIENT (WING ALONE) = ,F10.4//1H
     1 ,20X,32HCHORDWISE CENTER OF PRESSURE =  F10.4)
 1016 FORMAT (1H2,20X,46HCHORDWISE DISTRIBUTION OF BODY CARRY-OVER LIFT/
     1/1H ,29X,1HX,20X,10H(1/Q)DL/DX//)
 1017 FORMAT (1H0//1H ,20X,37HLIFT COEFFICIENT (BODY CARRY-OVER) = ,F10.
     14)
      PRINT 1013
      DO 6 J=1,M
      THEA=THETB(J)*BETA*S
 6    PRINT 1014, THEA, OUTPUT(J)
      PRINT 1015, CL, XCP
      PRINT 1016
      DO 7 J=1,M
      THEA=THETB(J)*BETA*S
 7    PRINT 1014, THEA, BCO(J)
      CLBCO=CLWB-CL
      PRINT 1017, CLBCO
      RETURN
      END
```

122

Approved for Public Release

```
      SUBROUTINE   OP3  (XLEEFV,XTEEFV)
      COMMON CF,A,ELAMB,ALPH,X,Y,CL1EV,ALPHEV,ALPHB,C,THETB,TAU,TAUBAR,
     1 THETBR,BOC,BCO,THET1,THET,XB,CEFV,ALPHWB,OUTPUT,   BETA,PI,AR,TR,
     2 S,M,M1,M2,M3,N,ALPHA,CLTOT,MM1,XW,ZW,ELB,THETA,XWB,EM\CH,ALAM,
     3 ALAMQC  ,ALAMB  ,BAR , DUM1,DUM2
      DIMENSION CF(50,50),ELAMB(50),ALPH(100,50),X(101),Y(101),CL1EV(50)
     1 ,ALPHEV(50),ALPHB(100),A(100),C(100),THETB(101),TAU(50),BOC(50),
     2 TAUBAR(50),THETBR(50),BCO(50),THET1(99),THET(101),XB(101),
     3 CEFV(50),ALPHWB(50),OUTPUT(50)
C     OUTPUT - EFFECTIVE WING GEOMETRY
      DIMENSION XLEEFV(50),XTEEFV(50)
      PRINT 1018
      PRINT 1019
      DO 1 J=1,N
      YT=ELAMB(J)*S
      XLEV=XLEEFV(J)*S*BETA
      XTE=XTEEFV(J)*S*BETA
      CT=CEFV(J)*S*BETA
      ALPHT=ALPHEV(J)
    1 PRINT 1020,YT,XLEV,XTE,CT,ALPHT
      RETURN
 1018 FORMAT (1H1,25X,23HEFFECTIVE WING GEOMETRY//1H ,20X,50HGEOMETRY OF
     1 THE EFFECTIVE WING, WHICH APPROXIMATES//1H ,20X,49HTHE REAL WING
     2BY RECTANGULAR BOXES.  AN EFFECTIVE//1H ,20X,51HSPANWISE ANGLE OF
     3ATTACK DISTRIBUTION IS CALCULATED//1H ,20X,49HFROM THE GIVEN ANGLE
     4 OF ATTACK DISTRIBUTION.  THE //1H ,20X,48HFOLLOWING DEFINITIONS A
     5PPLY.  ALL DIMENSIONS ARE//1H ,20X,43HMEASURED FROM THE ROOT OF TH
     6E LEADING EDGE.///)
 1019 FORMAT (1H ,20X,1HY,9X,46HSPANWISE DISTANCE TO CENTER OF CHORDWISE
     1 STRIP//1H ,20X,3HXLE,7X,44HCHORDWISE DISTANCE TO EFFECTIVE LEADIN
     2G EDGE//1H ,20X,    3HXTE,7X,45HCHORDWISE DISTANCE TO EFFECTIVE TR
     3AILING EDGE//1H ,20X,1HC,9X,15HEFFECTIVE CHORD/////1H ,25X,1HY,10X
     4,3HXLE,10X,3HXTE,10X,1HC,9X,5HALPHA//)
 1020 FORMAT (20X,5(F11.4,1X))
      END
```

123

```
      SUBROUTINE   OP4 (CL,YCP,KEY)
C     WING OUTPUT
      COMMON CF,A,ELAMB,ALPH,X,Y,CL1EV,ALPHEV,ALPHB,C,THETB,TAU,TAUBAR,
     1 THETBR,BOC,BCO,THET1,THET,XB,CEFV,ALPHWB,OUTPUT,  BETA,PI,AR,TR,
     2 S,M,M1,M2,M3,N,ALPHA,CLTOT,MM1,XW,ZW,ELB,THETA,XWB,EMACH,ALAM,
     3 ALAMOC  ,ALAMB
      DIMENSION CF(50,50),ELAMB(50),ALPH(100,50),X(101),Y(101),CL1EV(50)
     1 ,ALPHEV(50),ALPHB(100),A(100),C(100),THETB(101),TAU(50),BOC(50),
     2 TAUBAR(50),THETBR(50),BCO(50),THET1(99),THET(101),XB(101),
     3 CEFV(50),ALPHWB(50),OUTPUT(50)
      DIMENSION CL(50)
      IF (KEY-1) 10,10,11
10    PRINT 1021
      GO TO 12
11    PRINT 1022
12    PRINT 1023
      DO 2 J=1,N
      CLB=CL(J)/BETA
      CL1EFB=CL1EV(J)/BETA
2     PRINT 1024, ELAMB(J), CLB,CL1EFB, ALPHEV(J)
      CLTOTB=CLTOT/BETA
      PRINT 1025, CLTOTB, YCP
      RETURN
1021  FORMAT (1H1,25X,22HLIFT ON PHYSICAL WING //1H ,20X,55HSPANWISE LIF
     1T DISTRIBUTION ON THE PHYSICAL WING ALONE. /1H ,20X,28HCCL IS THE
     2SPANWISE LOADING.//////)
1022  FORMAT (1H1,25X,32HLIFT ON PHYSICAL WING WITH BODY //1H ,20X,55HSP
     2ANWISE LIFT DISTRIBUTION ON THE PHYSICAL WING IN THE /1H ,20X,21HP
     3RESENCE OF THE BODY.//////)
1023  FORMAT (1H ,25X,1HY,11X,2HCL,9X,3HCCL,9X,5HALPHA//)
1024  FORMAT (20X,4(F11.4,1X))
1025  FORMAT (1H0//1H ,20X,16HLIFT COEFFICIENT,12X,2H= ,F10.4/1H ,20X,30
     1HSPANWISE CENTER OF PRESSURE = ,F10.4)
      END
```

124

```
      SUBROUTINE OP5(DLDX,GAM,RT1,EIT1,ALPHO,CL1,CL2,CL3,XCP1,XCP2,XCP3)
C     OUTPUT - BODY CARRY OVER AFT
      COMMON CF,A,ELAMB,ALPH,X,Y,CL1EV,ALPHEV,ALPHB,C,THETB,TAU,TAUBAR,
     1 THETBR,BOC,BCO,THET1,THET,XB,CEFV,ALPHWB,OUTPUT,  BETA,PI,AR,TR,
     2 S,M,M1,M2,M3,N,ALPHA,CLTOT,MM1,XW,ZW,ELB,THETA,XWB,EMACH,ALAM,
     3 ALAMOC  ,ALAMB
      DIMENSION CF(50,50),ELAMB(50),ALPH(100,50),X(101),Y(101),CL1EV(50)
     1 ,ALPHEV(50),ALPHB(100),A(100),C(100),THETB(101),TAU(50),BOC(50),
     2 TAUBAR(50),THETBR(50),BCO(50),THET1(99),THET(101),XB(101),
     3 CEFV(50),ALPHWB(50),OUTPUT(50)
      DIMENSION RT1(50),EIT1(50),DLDX(50)
      PRINT 1026
      MP1=M+1
      DO 2 J=MP1,MM1
       T=THETB(J)*BETA*S
      XI=RT1(J)*S
      ETA=EIT1(J)*S
      OPT=DLDX(J)/BETA
2     PRINT 1027, T, XI,ETA, OPT
      PRINT 1028
       PRINT 1029,CL1,XCP1,CL2,XCP2,CL3,XCP3,ALPHO,GAM
      RETURN
1026  FORMAT (1H1,25X,24HLIFT ON BODY DUE TO WING//1H ,2 X,50HCHORDWISE
     1DISTRIBUTION OF BODY CARRY-OVER LIFT AFT/1H ,20X,55HOF THE TRAILIN
     2G EDGE OF THE ROOT CHORD.  (DISTRIBUTION /1H ,20X,50HFORWARD OF TR
     3AILING EDGE GIVEN ABOVE).  TOTAL LIFT/1H ,20X,47HCOEFFICIENTS (BAS
     4ED ON WING AREA) AND CHORDWISE/1H ,20X,50HCENTERS OF PRESSURE ARE
     5GIVEN FOR EACH SEGMENT OF THE BODY,/21X,57HAND FOR THE ENTIRE BODY
     6. (XI AND ETA GIVE POSITION OF THE/1H ,20X,17HROLLED-UP VORTEX.///
     7//1H ,25X,1HX,11X,2HXI,9X,3HETA,7X,10H(1/Q)DL/DX//)
1027  FORMAT (1H ,19X,4(F11.4,1X))
1028  FORMAT (1H0//1H ,46X,2HCL,9X,3HXCP//)
1029  FORMAT (1H ,20X,17HFORWARD PORTION  ,2F12.4//1H ,2 X,17HAFT PORTIO
     1N       ,2F12.4//1H ,20X,17HCOMPLETE BODY    ,2F12.4//1H ,20X,31HAV
     2ERAGE BODY ANGLE OF ATTACK = ,F10.4,8H RADIANS//   21X,31HSTRENGTH
     3 OF ROLLED-UP VORTEX = ,F10.4)
      END
```

```
       SUBROUTINE MATINV(N,B,M,DETERM)
       COMMON A
C
C          SUBROUTINE TO SOLVE THE MATRIX EQUATION AX=B, WHERE A IS
C      AN N X N SQUARE MATRIX, B IS A KNOWN M X N MATRIX, AND X IS
C      AN UNKNOWN M X N MATRIX. UPON RETURN THE INVERSE OF A IS PLACED
C      IN A, AND X IS PLACED IN B. BY SETTING M=0 THE SUBROUTINE MAY
C      BE USED FOR MATRIX INVERSION ALONE.  FOR FURTHER DETAILS SEE
C        IBM SHARE NO. 664.
C
       DIMENSION IPIVOT(50), A(50,50), B(50,1), INDEX(50,2), PIVOT(50)
       EQUIVALENCE (IROW,JROW),(ICOLUM,JCOLUM),(AMAX,T,SWAP)
10     DETERM=1.0
15     DO 20 J=1,N
20     IPIVOT(J)=0
30     DO 550 I=1,N
40     AMAX=0.0
45     DO 105 J=1,N
50     IF (IPIVOT(J)-1) 60,105,60
60     DO 100 K=1,N
70     IF (IPIVOT(K)-1) 80,100,740
80     IF (ABSF(AMAX)-ABSF(A(J,K)))85,100,100
85     IROW=J
90     ICOLUM=K
95     AMAX=A(J,K)
100    CONTINUE
105    CONTINUE
110    IPIVOT(ICOLUM)=IPIVOT(ICOLUM)+1
130    IF (IROW-ICOLUM) 140,260,140
140    DETERM=-DETERM
150    DO 200 L=1,N
160    SWAP=A(IROW,L)
170    A(IROW,L)=A(ICOLUM,L)
200    A(ICOLUM,L)=SWAP
205    IF (M) 260,260,210
210    DO 250 L=1,M
220    SWAP=B(IROW,L)
230    B(IROW,L)=B(ICOLUM,L)
250    B(ICOLUM,L)=SWAP
260    INDEX(I,1)=IROW
270    INDEX(I,2)=ICOLUM
310    PIVOT(I)=A(ICOLUM,ICOLUM)
320    DETERM=DETERM*PIVOT(I)
330    A(ICOLUM,ICOLUM)=1.0
340    DO 350 L=1,N
350    A(ICOLUM,L)=A(ICOLUM,L)/PIVOT(I)
355    IF (M) 380,380,360
360    DO 370 L=1,M
370    B(ICOLUM,L)=B(ICOLUM,L)/PIVOT(I)
380    DO 550 L1=1,N
390    IF (L1-ICOLUM) 400,550,400
400    T=A(L1,ICOLUM)
420    A(L1,ICOLUM)=0.0
```

```
430      DO 450 L=1,N
450      A(L1,L)=A(L1,L)-A(ICOLUM,L)*T
455      IF (M) 550,550,460
460      DO 500 L=1,M
500      B(L1,L)=B(L1,L)-B(ICOLUM,L)*T
550      CONTINUE
600      DO 710 I=1,N
610      L=N+1-I
620      IF (INDEX(L,1)-INDEX(L,2)) 630,710,630
630      JROW=INDEX(L,1)
640      JCOLUM=INDEX(L,2)
650      DO 705 K=1,N
660      SWAP=A(K,JROW)
670      A(K,JROW)=A(K,JCOLUM)
700      A(K,JCOLUM)=SWAP
705      CONTINUE
710      CONTINUE
740      RETURN
         END
```

127

```
          FAP
          ENTRY     RCP                                          00010
          ENTRY     FICP                                         00020
          ENTRY     RCMT                                         00030
          ENTRY     FICMT                                        00040
          ENTRY     RCM                                          00041
          ENTRY     FICM                                         00042
          ENTRY     RCD                                          00043
          ENTRY     FICD                                         00044
          ENTRY     RCS                                          00045
          ENTRY     FICS                                         00046
          ENTRY     RCC                                          00047
          ENTRY     FICC                                         00048
          ENTRY     RCSR                                         00049
          ENTRY     FICSR                                        00050
RCP       CLA*      1,4                                          00051
          FAD*      3,4                                          00060
          TRA       5,4                                          00070
FICP      CLA*      2,4                                          00080
          FAD*      4,4                                          00090
          TRA       5,4                                          00100
RCMT      LDQ*      2,4                                          00110
          FMP*      4,4                                          00120
          STO       TERM1                                        00130
          LDQ*      1,4                                          00140
          FMP*      3,4                                          00150
          FSB       TERM1                                        00160
          TRA       5,4                                          00170
FICMT     LDQ*      2,4                                          00180
          FMP*      3,4                                          00190
          STO       TERM1                                        00200
          LDQ*      4,4                                          00210
          FMP*      1,4                                          00220
          FAD       TERM1                                        00230
          TRA       5,4                                          00240
TERM1     PZE                                                    00250
RCM       CLA*      1,4                                          00260
          FSB*      3,4                                          00270
          TRA       5,4                                          00280
EICM      CLA*      2,4                                          00290
          FSB*      4,4                                          00300
          TRA       5,4                                          00310
RCD       LDQ*      1,4                                          00320
          FMP*      3,4                                          00330
          STO       TERM1                                        00340
          LDQ*      2,4                                          00350
          FMP*      4,4                                          00360
          FAD       TERM1                                        00370
          STO       NUM                                          00380
          LDQ*      3,4                                          00390
          FMP*      3,4                                          00400
          STO       TERM1                                        00410
          LDQ*      4,4                                          00420
```

128

```
        FMP*    4,4                                         00430
        FAD     TERM1                                       00440
        STO     DEN                                         00450
        CLA     NUM                                         00460
        FDP     DEN                                         00470
        XCA                                                 00480
        TRA     5,4                                         00490
NUM     PZE                                                 00500
DEN     PZE                                                 00510
EICD    LDQ*    1,4                                         00520
        FMP*    4,4                                         00530
        STO     TERM1                                       00540
        LDQ*    3,4                                         00550
        FMP*    2,4                                         00560
        FSB     TERM1                                       00570
        STO     NUM                                         00580
        LDQ*    3,4                                         00590
        FMP*    3,4                                         00600
        STO     TERM1                                       00610
        LDQ*    4,4                                         00620
        FMP*    4,4                                         00630
        FAD     TERM1                                       00640
        STO     DEN                                         00650
        CLA     NUM                                         00660
        FDP     DEN                                         00670
        XCA                                                 00680
        TRA     5,4                                         00690
RCS     LDQ*    2,4                                         00700
        FMP*    2,4                                         00710
        STO     TERM1                                       00720
        LDQ*    1,4                                         00730
        FMP*    1,4                                         00740
        FSB     TERM1                                       00750
        TRA     3,4                                         00760
FICS    LDQ*    1,4                                         00770
        FMP*    2,4                                         00780
        STO     TERM1                                       00790
        FAD     TERM1                                       00800
        TRA     3,4                                         00810
RCC     LDQ*    2,4                                         00820
        FMP*    2,4                                         00830
        XCA                                                 00840
        FMP*    2,4                                         00850
        XCA                                                 00860
        FMP*    1,4                                         00870
        STO     TERM1                                       00880
        FAD     TERM1                                       00890
        FAD     TERM1                                       00900
        STO     TERM1                                       00910
        LDQ*    1,4                                         00920
        FMP*    1,4                                         00930
        XCA                                                 00940
        FMP*    1,4                                         00950
```

129

```
          FSB      TERM1                                        00960
          TRA      3,4                                          00970
FICC      LDQ*     2,4                                          00980
          FMP*     2,4                                          00990
          XCA                                                   01000
          FMP*     2,4                                          01010
          STO      TERM2                                        01020
          LDQ*     2,4                                          01030
          FMP*     1,4                                          01040
          STO      TERM1                                        01050
          FAD      TERM1                                        01060
          FAD      TERM1                                        01070
          FSB      TERM2                                        01080
          TRA      3,4                                          01090
TERM2     PZE                                                   01100
RCSR      LDQ*     1,4                                          01110
          FMP*     1,4                                          01120
          STO      TERM1                                        01130
          LDQ*     2,4                                          01140
          FMP*     2,4                                          01150
          FAD      TERM1                                        01160
          SXA      XR4,4                                        01170
          TSX      $SQRT,4                                      01180
          STO      R                                            01190
XR4       AXT      **,4                                         01200
          CLA*     2,4                                          01210
          FDP*     1,4                                          01220
          XCA                                                   01230
          SXA      XR42,4                                       01240
          TSX      $ATAN,4                                      01250
          STO      THET                                         01260
XR42      AXT      **,4                                         01270
          CLA      THET                                         01280
          TPL      *+9                                          01281
          CLA*     1,4                                          01282
          TPL      *+4                                          01283
          CLA      =3.14159                                     01284
          FAD      THET                                         01285
          TRA      *+10                                         01286
          CLA      =6.28318                                     01287
          FAD      THET                                         01288
          TRA      *+7                                          01289
          CLA*     1,4                                          01290
          TPL      *+4                                          01291
          CLA      =3.14159                                     01292
          FAD      THET                                         01293
          TRA      *+2                                          01294
          CLA      THET                                         01295
          FDP      =2.                                          01296
          XCA                                                   01300
          SXA      XR43,4                                       01310
          TSX      $COS,4                                       01320
XR43      AXT      **,4                                         01330
```

```
           STO      COSTH                                    01340
           CLA      R                                        01350
           SXA      XR44,4                                   01360
           TSX      $SQRT,4                                  01370
           STO      R2                                       01380
XR44       AXT      **,4                                     01390
           LDQ      R2                                       01400
           FMP      COSTH                                    01410
           TRA      3,4                                      01420
R          PZE                                               01430
R2         PZE                                               01440
THET       PZE                                               01450
COSTH      PZE                                               01460
EICSR      LDQ*     1,4                                      01470
           FMP*     1,4                                      01480
           STO      TERM1                                    01490
           LDQ*     2,4                                      01500
           FMP*     2,4                                      01510
           FAD      TERM1                                    01520
           SXA      XR45,4                                   01530
           TSX      $SQRT,4                                  01540
           STO      R                                        01550
XR45       AXT      **,4                                     01560
           CLA*     2,4                                      01570
           FDP*     1,4                                      01580
           XCA                                               01590
           SXA      XR46,4                                   01600
           TSX      $ATAN,4                                  01610
           STO      THET                                     01620
XR46       AXT      **,4                                     01630
           CLA      THET                                     01640
           TPL      *+9                                      01641
           CLA*     1,4                                      01642
           TPL      *+4                                      01643
           CLA      =3.14159                                 01644
           FAD      THET                                     01645
           TRA      *+10                                     01646
           CLA      =6.28318                                 01647
           FAD      THET                                     01648
           TRA      *+7                                      01649
           CLA*     1,4                                      01650
           TPL      *+4                                      01651
           CLA      =3.14159                                 01652
           FAD      THET                                     01653
           TRA      *+2                                      01654
           CLA      THET                                     01655
           FDP      =2.                                      01656
           XCA                                               01660
           SXA      XR47,4                                   01670
           TSX      $SIN,4                                   01680
XR47       AXT      **,4                                     01690
           STO      SINTH                                    01700
           CLA      R                                        01710
```

131

```
        SXA     XR4B,4                                  01720
        TSX     $SQRT,4                                 01730
        STO     R2                                      01740
XR43    AXT     **,4                                    01750
        LDQ     R2                                      01760
        FMP     SINTH                                   01770
        TRA     3,4                                     01780
SINTH   PZE                                             01790
        END                                             01800
```

SAMPLE INPUT

```
      49.83      3.8935      .16314        12.88 57.295779          0.0          .90
       24    12    13      13    20    0
        13.137              0.0       36.15
   1.461        1.461        0.
   1.468        1.468        0.
   1.477        1.477        0.
   1.488        1.488        0.
   1.502        1.502        0.
   1.517        1.517        0.
   1.533        1.533        0.
   1.549        1.549        0.
   1.563        1.563        0.
   1.578        1.578        0.
   1.589        1.589        0.
   1.599        1.599        0.
   1.602        1.602        0.
   1.606        1.606        0.
   1.604        1.604        0.
   1.601        1.601        0.
   1.596        1.596        0.
   1.589        1.589        0.
   1.580        1.580        0.
   1.572        1.572        0.
   1.563        1.563        0.
   1.557        1.557        0.
   1.551        1.551        0.
   1.549        1.549        0.
   1.519        1.519        0.
   1.485        1.485        0.
   1.441        1.441        0.
   1.395        1.395        0.
   1.338        1.338        0.
   1.275        1.275        0.
   1.210        1.210        0.
   1.138        1.138        0.
   1.053        1.053        0.
   0.961        0.961        0.
   0.680        0.680        0.
   0.750        0.750        0.
```

134

SAMPLE OUTPUT

LINEAR AERODYNAMIC LOADS PROGRAM

LINEAR AERODYNAMIC LOAD DISTRIBUTIONS, INCLUDING

THE EFFECTS OF WING-BODY INTERFERENCE HAVE BEEN

CALCULATED ON THE FOLLOWING CONFIGURATION AT

SUBSONIC SPEEDS.

WING GEOMETRY

ASPECT RATIO = 3.893

TAPER RATIO = .163

LEADING EDGE SWEEP ANGLE = 49.830 DEGREES

DIHEDRAL ANGLE = 0. DEGREES

EXPOSED WING SEMI-SPAN = 12.880

WING ANGLE OF ATTACK DISTRIBUTION

(ORIGIN IS AT ROOT OF LEADING EDGE)

X/S	Y/S	ALPHA
.00348	.99846	57.29578
.00348	.99230	57.29578
.00348	.98003	57.29578
.00348	.96171	57.29578
.00348	.93747	57.29578
.00348	.90744	57.29578
.00348	.87182	57.29578
.00348	.83083	57.29578
.00348	.78471	57.29578
.00348	.73376	57.29578
.00348	.67828	57.29578
.00348	.61862	57.29578
.00348	.55514	57.29578
.00348	.48824	57.29578
.00348	.41834	57.29578
.00348	.34585	57.29578
.00348	.27123	57.29578
.00348	.19494	57.29578
.00348	.11745	57.29578

.00348	.03923	57.29578
.01387	.99846	57.29578
.01387	.99230	57.29578
.01387	.98003	57.29578
.01387	.96171	57.29578
.01387	.93747	57.29578
.01387	.90744	57.29578
.01387	.87182	57.29578
.01387	.83083	57.29578
.01387	.78471	57.29578
.01387	.73376	57.29578
.01387	.67828	57.29578
.01387	.61862	57.29578
.01387	.55514	57.29578
.01387	.48824	57.29578
.01387	.41834	57.29578
.01387	.34585	57.29578
.01387	.27123	57.29578
.01387	.19494	57.29578
.01387	.11745	57.29578
.01387	.03923	57.29578
.03101	.99846	57.29578
.03101	.99230	57.29578
.03101	.98003	57.29578
.03101	.96171	57.29578
.03101	.93747	57.29578
.03101	.90744	57.29578
.03101	.87182	57.29578
.03101	.83083	57.29578
.03101	.78471	57.29578
.03101	.73376	57.29578
.03101	.67828	57.29578
.03101	.61862	57.29578
.03101	.55514	57.29578
.03101	.48824	57.29578
.03101	.41834	57.29578
.03101	.34585	57.29578
.03101	.27123	57.29578
.03101	.19494	57.29578
.03101	.11745	57.29578
.03101	.03923	57.29578
.05463	.99846	57.29578
.05463	.99230	57.29578
.05463	.98003	57.29578
.05463	.96171	57.29578
.05463	.93747	57.29578
.05463	.90744	57.29578
.05463	.87182	57.29578
.05463	.83083	57.29578
.05463	.78471	57.29578
.05463	.73376	57.29578
.05463	.67828	57.29578
.05463	.61862	57.29578
.05463	.55514	57.29578
.05463	.48824	57.29578
.05463	.41834	57.29578
.05463	.34585	57.29578
.05463	.27123	57.29578
.05463	.19494	57.29578
.05463	.11745	57.29578
.05463	.03923	57.29578

.08434	.99846	57.29578
.08434	.99230	57.29578
.08434	.98003	57.29578
.08434	.96171	57.29578
.08434	.93747	57.29578
.08434	.90744	57.29578
.08434	.87182	57.29578
.08434	.83083	57.29578
.08434	.78471	57.29578
.08434	.73376	57.29578
.08434	.67828	57.29578
.08434	.61862	57.29578
.08434	.55514	57.29578
.08434	.48824	57.29578
.08434	.41834	57.29578
.08434	.34585	57.29578
.08434	.27123	57.29578
.08434	.19494	57.29578
.08434	.11745	57.29578
.08434	.03923	57.29578
.11970	.99846	57.29578
.11970	.99230	57.29578
.11970	.98003	57.29578
.11970	.96171	57.29578
.11970	.93747	57.29578
.11970	.90744	57.29578
.11970	.87182	57.29578
.11970	.83083	57.29578
.11970	.78471	57.29578
.11970	.73376	57.29578
.11970	.67828	57.29578
.11970	.61862	57.29578
.11970	.55514	57.29578
.11970	.48824	57.29578
.11970	.41834	57.29578
.11970	.34585	57.29578
.11970	.27123	57.29578
.11970	.19494	57.29578
.11970	.11745	57.29578
.11970	.03923	57.29578
.16012	.99846	57.29578
.16012	.99230	57.29578
.16012	.98003	57.29578
.16012	.96171	57.29578
.16012	.93747	57.29578
.16012	.90744	57.29578
.16012	.87182	57.29578
.16012	.83083	57.29578
.16012	.78471	57.29578
.16012	.73376	57.29578
.16012	.67828	57.29578
.16012	.61862	57.29578
.16012	.55514	57.29578
.16012	.48824	57.29578
.16012	.41834	57.29578
.16012	.34585	57.29578
.16012	.27123	57.29578
.16012	.19494	57.29578
.16012	.11745	57.29578
.16012	.03923	57.29578
.20499	.99846	57.29578

.20499	.99230	57.29578
.20499	.98003	57.29578
.20499	.96171	57.29578
.20499	.93747	57.29578
.20499	.90744	57.29578
.20499	.87182	57.29578
.20499	.83083	57.29578
.20499	.78471	57.29578
.20499	.73376	57.29578
.20499	.67828	57.29578
.20499	.61862	57.29578
.20499	.55514	57.29578
.20499	.48824	57.29578
.20499	.41834	57.29578
.20499	.34585	57.29578
.20499	.27123	57.29578
.20499	.19494	57.29578
.20499	.11745	57.29578
.20499	.03923	57.29578
.25359	.99846	57.29578
.25359	.99230	57.29578
.25359	.98003	57.29578
.25359	.96171	57.29578
.25359	.93747	57.29578
.25359	.90744	57.29578
.25359	.87182	57.29578
.25359	.83083	57.29578
.25359	.78471	57.29578
.25359	.73376	57.29578
.25359	.67828	57.29578
.25359	.61862	57.29578
.25359	.55514	57.29578
.25359	.48824	57.29578
.25359	.41834	57.29578
.25359	.34585	57.29578
.25359	.27123	57.29578
.25359	.19494	57.29578
.25359	.11745	57.29578
.25359	.03923	57.29578
.30516	.99846	57.29578
.30516	.99230	57.29578
.30516	.98003	57.29578
.30516	.96171	57.29578
.30516	.93747	57.29578
.30516	.90744	57.29578
.30516	.87182	57.29578
.30516	.83083	57.29578
.30516	.78471	57.29578
.30516	.73376	57.29578
.30516	.67828	57.29578
.30516	.61862	57.29578
.30516	.55514	57.29578
.30516	.48824	57.29578
.30516	.41834	57.29578
.30516	.34585	57.29578
.30516	.27123	57.29578
.30516	.19494	57.29578
.30516	.11745	57.29578
.30516	.03923	57.29578
.35888	.99846	57.29578
.35888	.99230	57.29578

.35888	.98003	57.29578
.35888	.96171	57.29578
.35889	.93747	57.29578
.35888	.90744	57.29578
.35888	.87182	57.29578
.35988	.83083	57.29578
.35888	.78471	57.29578
.35888	.73376	57.29578
.35888	.67828	57.29578
.35888	.61862	57.29578
.35888	.55514	57.29578
.35888	.48824	57.29578
.35888	.41834	57.29578
.35888	.34585	57.29578
.35888	.27123	57.29578
.35888	.19494	57.29578
.35888	.11745	57.29578
.35988	.03923	57.29578
.41390	.99846	57.29578
.41390	.99230	57.29578
.41390	.98003	57.29578
.41390	.96171	57.29578
.41390	.93747	57.29578
.41390	.90744	57.29578
.41390	.87182	57.29578
.41390	.83083	57.29578
.41390	.78471	57.29578
.41390	.73376	57.29578
.41390	.67828	57.29578
.41390	.61862	57.29578
.41390	.55514	57.29578
.41390	.48824	57.29578
.41390	.41834	57.29578
.41390	.34585	57.29578
.41390	.27123	57.29578
.41390	.19494	57.29578
.41390	.11745	57.29578
.41390	.03923	57.29578
.46936	.99846	57.29578
.46936	.99230	57.29578
.46936	.98003	57.29578
.46936	.96171	57.29578
.46936	.93747	57.29578
.46936	.90744	57.29578
.46936	.87182	57.29578
.46936	.83083	57.29578
.46936	.78471	57.29578
.46936	.73376	57.29578
.46936	.67828	57.29578
.46936	.61862	57.29578
.46936	.55514	57.29578
.46936	.48824	57.29578
.46936	.41834	57.29578
.46936	.34585	57.29578
.46936	.27123	57.29578
.46936	.19494	57.29578
.46936	.11745	57.29578
.46936	.03923	57.29578
.52438	.99846	57.29578
.52438	.99230	57.29578
.52438	.98003	57.29578

.52438	.96171	57.29578
.52438	.93747	57.29578
.52438	.90744	57.29578
.52438	.87182	57.29578
.52438	.83083	57.29578
.52438	.78471	57.29578
.52438	.73376	57.29578
.52438	.67828	57.29578
.52438	.61862	57.29578
.52438	.55514	57.29578
.52438	.48824	57.29578
.52438	.41834	57.29578
.52438	.34585	57.29578
.52438	.27123	57.29578
.52438	.19494	57.29578
.52438	.11745	57.29578
.52438	.03923	57.29578
.57810	.99846	57.29578
.57810	.99230	57.29578
.57810	.98003	57.29578
.57810	.96171	57.29578
.57810	.93747	57.29578
.57810	.90744	57.29578
.57810	.87182	57.29578
.57810	.83083	57.29578
.57810	.78471	57.29578
.57810	.73376	57.29578
.57810	.67828	57.29578
.57810	.61862	57.29578
.57810	.55514	57.29578
.57810	.48824	57.29578
.57810	.41834	57.29578
.57810	.34585	57.29578
.57810	.27123	57.29578
.57810	.19494	57.29578
.57810	.11745	57.29578
.57810	.03923	57.29578
.62967	.99846	57.29578
.62967	.99230	57.29578
.62967	.98003	57.29578
.62967	.96171	57.29578
.62967	.93747	57.29578
.62967	.90744	57.29578
.62967	.87182	57.29578
.62967	.83083	57.29578
.62967	.78471	57.29578
.62967	.73376	57.29578
.62967	.67828	57.29578
.62967	.61862	57.29578
.62967	.55514	57.29578
.62967	.48824	57.29578
.62967	.41834	57.29578
.62967	.34585	57.29578
.62967	.27123	57.29578
.62967	.19494	57.29578
.62967	.11745	57.29578
.62967	.03923	57.29578
.67827	.99846	57.29578
.67827	.99230	57.29578
.67827	.98003	57.29578
.67827	.96171	57.29578

.67827	.93747	57.29578
.67827	.90744	57.29578
.67827	.87182	57.29578
.67827	.83083	57.29578
.67827	.78471	57.29578
.67827	.73376	57.29578
.67827	.67928	57.29578
.67827	.61862	57.29578
.67827	.55514	57.29578
.67827	.48824	57.29578
.67827	.41834	57.29578
.67827	.34585	57.29578
.67827	.27123	57.29578
.67827	.19494	57.29578
.67827	.11745	57.29578
.67827	.03923	57.29578
.72313	.99846	57.29578
.72313	.99230	57.29578
.72313	.98003	57.29578
.72313	.96171	57.29578
.72313	.93747	57.29578
.72313	.90744	57.29578
.72313	.87182	57.29578
.72313	.83083	57.29578
.72313	.78471	57.29578
.72313	.73376	57.29578
.72313	.67828	57.29578
.72313	.61862	57.29578
.72313	.55514	57.29578
.72313	.48824	57.29578
.72313	.41834	57.29578
.72313	.34585	57.29578
.72313	.27123	57.29578
.72313	.19494	57.29578
.72313	.11745	57.29578
.72313	.03923	57.29578
.76355	.99846	57.29578
.76355	.99230	57.29578
.76355	.98003	57.29578
.76356	.96171	57.29578
.76356	.93747	57.29578
.76356	.90744	57.29578
.76356	.87182	57.29578
.76356	.83083	57.29578
.76356	.78471	57.29578
.76356	.73376	57.29578
.76356	.67828	57.29578
.76356	.61862	57.29578
.76355	.55514	57.29578
.76355	.48824	57.29578
.76356	.41834	57.29578
.76356	.34585	57.29578
.76356	.27123	57.29578
.76356	.19494	57.29578
.76356	.11745	57.29578
.76356	.03923	57.29578
.79891	.99846	57.29578
.79891	.99230	57.29578
.79891	.98003	57.29578
.79891	.96171	57.29578
.79891	.93747	57.29578

.79891	.90744	57.29578
.79891	.87182	57.29578
.79891	.83083	57.29578
.79891	.78471	57.29578
.79891	.73376	57.29578
.79891	.67828	57.29578
.79891	.61862	57.29578
.79891	.55514	57.29578
.79891	.48824	57.29578
.79891	.41834	57.29578
.79891	.34585	57.29578
.79891	.27123	57.29578
.79891	.19494	57.29578
.79891	.11745	57.29578
.79891	.03923	57.29578
.82863	.99846	57.29578
.82863	.99230	57.29578
.82863	.98003	57.29578
.82863	.96171	57.29578
.82863	.93747	57.29578
.82863	.90744	57.29578
.82863	.87182	57.29578
.82863	.83083	57.29578
.82863	.78471	57.29578
.82863	.73376	57.29578
.82863	.67828	57.29578
.82863	.61862	57.29578
.82863	.55514	57.29578
.82863	.48824	57.29578
.82863	.41834	57.29578
.82863	.34585	57.29578
.82863	.27123	57.29578
.82863	.19494	57.29578
.82863	.11745	57.29578
.82863	.03923	57.29578
.85225	.99846	57.29578
.85225	.99230	57.29578
.85225	.98003	57.29578
.85225	.96171	57.29578
.85225	.93747	57.29578
.85225	.90744	57.29578
.85225	.87182	57.29578
.85225	.83083	57.29578
.85225	.78471	57.29578
.85225	.73376	57.29578
.85225	.67828	57.29578
.85225	.61862	57.29578
.85225	.55514	57.29578
.85225	.48824	57.29578
.85225	.41834	57.29578
.85225	.34585	57.29578
.85225	.27123	57.29578
.85225	.19494	57.29578
.85225	.11745	57.29578
.85225	.03923	57.29578
.86938	.99846	57.29578
.86938	.99230	57.29578
.86938	.98003	57.29578
.86938	.96171	57.29578
.86938	.93747	57.29578
.86938	.90744	57.29578

.86938	.87182	57.29578
.86938	.83083	57.29578
.86938	.78471	57.29578
.86938	.73376	57.29578
.86938	.67828	57.29578
.86938	.61862	57.29578
.86938	.55514	57.29578
.86938	.48824	57.29578
.86938	.41834	57.29578
.86938	.34585	57.29578
.86938	.27123	57.29578
.86938	.19494	57.29578
.86938	.11745	57.29578
.86938	.03923	57.29578
.87978	.99846	57.29578
.87978	.99230	57.29578
.87978	.98003	57.29578
.87978	.96171	57.29578
.87978	.93747	57.29578
.87978	.90744	57.29578
.87978	.87182	57.29578
.87978	.83083	57.29578
.87978	.78471	57.29578
.87978	.73376	57.29578
.87978	.67828	57.29578
.87978	.61862	57.29578
.87978	.55514	57.29578
.87978	.48824	57.29578
.87978	.41834	57.29578
.87978	.34585	57.29578
.87978	.27123	57.29578
.87978	.19494	57.29578
.87978	.11745	57.29578
.87978	.03923	57.29578
.92090	.99846	57.29578
.92090	.99230	57.29578
.92090	.98003	57.29578
.92090	.96171	57.29578
.92090	.93747	57.29578
.92090	.90744	57.29578
.92090	.87182	57.29578
.92090	.83083	57.29578
.92090	.78471	57.29578
.92090	.73376	57.29578
.92090	.67828	57.29578
.92090	.61862	57.29578
.92090	.55514	57.29578
.92090	.48824	57.29578
.92090	.41834	57.29578
.92090	.34585	57.29578
.92090	.27123	57.29578
.92090	.19494	57.29578
.92090	.11745	57.29578
.92090	.03923	57.29578
.99619	.99846	57.29578
.99619	.99230	57.29578
.99619	.98003	57.29578
.99619	.96171	57.29578
.99619	.93747	57.29578
.99619	.90744	57.29578
.99619	.87182	57.29578

.99619	.83083	57.29578
.99619	.78471	57.29578
.99619	.73376	57.29578
.99619	.67828	57.29578
.99619	.61862	57.29578
.99619	.55514	57.29578
.99619	.48824	57.29578
.99619	.41834	57.29578
.99619	.34585	57.29578
.99619	.27123	57.29578
.99619	.19494	57.29578
.99619	.11745	57.29578
.99619	.03923	57.29578
1.07148	.99846	57.29578
1.07148	.99230	57.29578
1.07148	.98003	57.29578
1.07148	.96171	57.29578
1.07148	.93747	57.29578
1.07148	.90744	57.29578
1.07148	.87182	57.29578
1.07148	.83083	57.29578
1.07148	.78471	57.29578
1.07148	.73376	57.29578
1.07148	.67828	57.29578
1.07148	.61862	57.29578
1.07148	.55514	57.29578
1.07148	.48824	57.29578
1.07148	.41834	57.29578
1.07148	.34585	57.29578
1.07148	.27123	57.29578
1.07148	.19494	57.29578
1.07148	.11745	57.29578
1.07148	.03923	57.29578
1.14677	.99846	57.29578
1.14677	.99230	57.29578
1.14677	.98003	57.29578
1.14677	.96171	57.29578
1.14677	.93747	57.29578
1.14677	.90744	57.29578
1.14677	.87182	57.29578
1.14677	.83083	57.29578
1.14677	.78471	57.29578
1.14677	.73376	57.29578
1.14677	.67828	57.29578
1.14677	.61862	57.29578
1.14677	.55514	57.29578
1.14677	.48824	57.29578
1.14677	.41834	57.29578
1.14677	.34585	57.29578
1.14677	.27123	57.29578
1.14677	.19494	57.29578
1.14677	.11745	57.29578
1.14677	.03923	57.29578
1.22206	.99846	57.29578
1.22206	.99230	57.29578
1.22206	.98003	57.29578
1.22206	.96171	57.29578
1.22206	.93747	57.29578
1.22206	.90744	57.29578
1.22206	.87182	57.29578
1.22206	.83083	57.29578

1.22206	.78471	57.29578
1.22206	.73376	57.29578
1.22206	.67828	57.29578
1.22206	.61862	57.29578
1.22206	.55514	57.29578
1.22206	.48824	57.29578
1.22206	.41834	57.29578
1.22206	.34585	57.29578
1.22206	.27123	57.29578
1.22206	.19494	57.29578
1.22206	.11745	57.29578
1.22206	.03923	57.29578
1.29735	.99846	57.29578
1.29735	.99230	57.29578
1.29735	.98003	57.29578
1.29735	.96171	57.29578
1.29735	.93747	57.29578
1.29735	.90744	57.29578
1.29735	.87182	57.29578
1.29735	.83083	57.29578
1.29735	.78471	57.29578
1.29735	.73376	57.29578
1.29735	.67828	57.29578
1.29735	.61862	57.29578
1.29735	.55514	57.29578
1.29735	.48824	57.29578
1.29735	.41834	57.29578
1.29735	.34585	57.29578
1.29735	.27123	57.29578
1.29735	.19494	57.29578
1.29735	.11745	57.29578
1.29735	.03923	57.29578
1.37264	.99846	57.29578
1.37264	.99230	57.29578
1.37264	.98003	57.29578
1.37264	.96171	57.29578
1.37264	.93747	57.29578
1.37264	.90744	57.29578
1.37264	.87182	57.29578
1.37264	.83083	57.29578
1.37264	.78471	57.29578
1.37264	.73376	57.29578
1.37264	.67828	57.29578
1.37264	.61862	57.29578
1.37264	.55514	57.29578
1.37264	.48824	57.29578
1.37264	.41834	57.29578
1.37264	.34585	57.29578
1.37264	.27123	57.29578
1.37264	.19494	57.29578
1.37264	.11745	57.29578
1.37264	.03923	57.29578
1.44792	.99846	57.29578
1.44792	.99230	57.29578
1.44792	.98003	57.29578
1.44792	.96171	57.29578
1.44792	.93747	57.29578
1.44792	.90744	57.29578
1.44792	.87182	57.29578
1.44792	.83083	57.29578
1.44792	.78471	57.29578

146

1.44792	.73375	57.29573
1.44792	.67923	57.29573
1.44792	.61852	57.29573
1.44792	.55514	57.29573
1.44792	.43824	57.29573
1.44792	.41234	57.29573
1.44792	.34535	57.29573
1.44792	.27123	57.29573
1.44792	.19494	57.29573
1.44792	.11745	57.29573
1.44792	.03923	57.29573
1.52321	.99345	57.29573
1.52321	.99230	57.29578
1.52321	.98003	57.29578
1.52321	.96171	57.29578
1.52321	.93747	57.29578
1.52321	.90744	57.29578
1.52321	.87192	57.29578
1.52321	.83083	57.29578
1.52321	.78471	57.29578
1.52321	.73376	57.29578
1.52321	.67828	57.29578
1.52321	.61862	57.29573
1.52321	.55514	57.29578
1.52321	.43824	57.29578
1.52321	.41334	57.29578
1.52321	.34535	57.29578
1.52321	.27123	57.29578
1.52321	.19494	57.29579
1.52321	.11745	57.29578
1.52321	.03923	57.29573
1.59850	.99846	57.29578
1.59850	.99230	57.29578
1.59850	.98003	57.29578
1.59850	.96171	57.29578
1.59850	.93747	57.29578
1.59850	.90744	57.29578
1.59850	.87192	57.29578
1.59850	.83083	57.29578
1.59850	.78471	57.29578
1.59850	.73376	57.29578
1.59850	.67828	57.29578
1.59850	.61862	57.29578
1.59850	.55514	57.29578
1.59850	.43824	57.29578
1.59850	.41834	57.29578
1.59850	.34585	57.29578
1.59850	.27123	57.29578
1.59850	.19494	57.29578
1.59850	.11745	57.29578
1.59850	.03923	57.29578
1.67379	.99846	57.29578
1.67379	.99230	57.29578
1.67379	.98003	57.29578
1.67379	.96171	57.29578
1.67379	.93747	57.29578
1.67379	.90744	57.29578
1.67379	.87192	57.29578
1.67379	.83083	57.29578
1.67379	.78471	57.29578
1.67379	.73376	57.29578

147

1.67379	.67828	57.29578
1.67379	.61862	57.29578
1.67379	.55514	57.29578
1.67379	.49824	57.29578
1.67379	.41834	57.29578
1.67379	.34585	57.29578
1.67379	.27123	57.29578
1.67379	.19494	57.29578
1.67379	.11745	57.29578
1.67379	.03923	57.29578
1.74908	.99846	57.29578
1.74908	.99230	57.29578
1.74908	.98003	57.29578
1.74908	.96171	57.29578
1.74908	.93747	57.29578
1.74908	.90744	57.29578
1.74908	.87182	57.29578
1.74908	.83083	57.29578
1.74908	.78471	57.29578
1.74908	.73376	57.29578
1.74908	.67828	57.29578
1.74908	.61862	57.29578
1.74908	.55514	57.29578
1.74908	.48824	57.29578
1.74908	.41834	57.29578
1.74908	.34585	57.29578
1.74908	.27123	57.29578
1.74908	.19494	57.29578
1.74908	.11745	57.29578
1.74908	.03923	57.29578

BODY GEOMETRY

BODY LENGTH = 36.150

ELLIPTICAL CROSS SECTIONS

X (DISTANCE FROM NOSE)	HORIZONTAL AXIS	VERTICAL AXIS	ANGLE OF ATTACK
13.22671	1.46100	1.46100	0.
13.40471	1.46800	1.46800	0.
13.66818	1.47700	1.47700	0.
14.01306	1.48800	1.48800	0.
14.43372	1.50200	1.50200	0.
14.92366	1.51700	1.51700	0.
15.47514	1.53300	1.53300	0.
16.07946	1.54900	1.54900	0.
16.72708	1.56300	1.56300	0.
17.40779	1.57800	1.57800	0.
18.11086	1.58900	1.58900	0.
18.82518	1.59900	1.59900	0.
19.53951	1.60200	1.60200	0.
20.24258	1.60600	1.60600	0.
20.92328	1.60400	1.60400	0.
21.57091	1.60100	1.60100	0.
22.17523	1.59600	1.59600	0.
22.72671	1.58900	1.58900	0.
23.21667	1.58000	1.58000	0.
23.63737	1.57200	1.57200	0.
23.98218	1.56300	1.56300	0.
24.24567	1.55700	1.55700	0.
24.42365	1.55100	1.55100	0.
24.51337	1.54900	1.54900	0.
25.48309	1.51900	1.51900	0.
26.45281	1.48500	1.48500	0.
27.42253	1.44100	1.44100	0.
28.39225	1.39500	1.39500	0.
29.36197	1.33800	1.33800	0.
30.33168	1.27500	1.27500	0.
31.30140	1.21000	1.21000	0.
32.27112	1.13800	1.13800	0.
33.24084	1.05300	1.05300	0.
34.21056	.96100	.96100	0.
35.18028	.86000	.68000	0.
36.15000	.75000	.75000	0.

WING-BODY COMBINATION GEOMETRY

    WING LOCATION ON BODY

        LEADING EDGE DISTANCE FROM NOSE = 13.137

        HEIGHT OF ROOT CHORD ABOVE BODY CENTERLINE = 0.

FLIGHT CONDITIONS

        ANGLE OF ATTACK = 57.2958 DEGREES

        MACH NUMBER = .900

THE FOLLOWING NUMERICAL PARAMETERS HAVE BEEN USED IN THE CALCULATIONS

PARAMETER	USE	VALUE
M	NUMBER OF STATIONS ON BODY BETWEEN WING LEADING AND TRAILING EDGES	24
M1	NUMBER OF STATIONS ON BODY BETWEEN WING TRAILING EDGE AND AFT END OF BODY	12
M2	NUMBER OF INTERVALS USED IN THE NUMERICAL INTEGRATIONS EMPLOYED IN THE LAWRENCE PROCEDURE	13
M3	NUMBER OF INTERVALS USED IN THE NUMERICAL INTEGRATIONS EMPLOYED IN THE WEISSINGER PROCEDURE	13
N	NUMBER OF STATIONS ON THE WING SEMI-SPAN	20

LIFT ON WING-BODY COMBINATION

CHORDWISE LIFT DISTRIBUTION ON THE BODY, INCLUDING
THE LIFT OF THE WING. THE FOLLOWING DEFINITIONS APPLY.

X   DISTANCE FROM ROOT OF LEADING EDGE
        TO CENTER OF SPANWISE STRIP

B   EFFECTIVE SEMI-SPAN OF STRIP

DX   WIDTH OF SPANWISE STRIP

Q   DYNAMIC PRESSURE

X	B	DX	$(1/Q)DL/DX$
.0449	.0000	.0897	-.8666
.1737	.0000	.1780	.1144
.3904	.0000	.2635	-.0189
.7036	1.0106	.3448	.4886
1.0863	1.0106	.4207	-.2541
1.5417	1.0106	.4900	.9199
2.0624	2.0149	.5515	.7724
2.6403	2.0149	.6043	1.1050
3.2663	3.0068	.6476	1.3994
3.9304	3.0068	.6807	1.2631
4.6223	3.9801	.7031	2.5711
5.3310	4.9290	.7143	1.5871
6.0453	4.9290	.7143	2.0111
6.7540	5.8474	.7031	2.0870
7.4459	5.8474	.6807	2.0039
8.1101	6.7298	.6476	3.0317
8.7361	7.5707	.6043	2.0813
9.3140	7.5707	.5515	2.2607
9.8347	8.3649	.4900	2.0986
10.2900	8.3649	.4207	1.8208
10.6728	9.1075	.3448	1.8946
10.9769	9.1075	.2635	1.0639
11.1977	9.7940	.1780	1.3407
11.3315	9.7940	.0897	-1.2101

LIFT COEFFICIENT (WING-BODY COMBINATION) =   2.6605

CHORDWISE CENTER OF PRESSURE =   .5948
(PERCENT OF ROOT CHORD)

CHORDWISE LIFT DISTRIBUTION ON THE WING ALONE

X	(1/Q)DL/DX
.0449	-.4865
.1787	.0394
.3994	.1658
.7036	.7347
1.0863	-.2866
1.5417	1.0447
2.0624	.8605
2.6403	1.1062
3.2663	1.3793
3.9304	1.1971
4.6223	2.4025
5.3310	1.4586
6.0453	1.8435
6.7540	1.8879
7.4459	1.8136
8.1101	2.7179
8.7361	1.8691
9.3140	2.0162
9.8347	1.8759
10.2900	1.6163
10.6728	1.6892
10.9769	.9353
11.1977	1.1936
11.3315	-1.1120

LIFT COEFFICIENT (WING ALONE) = 2.4825

CHORDWISE CENTER OF PRESSURE = .5798

CHORDWISE DISTRIBUTION OF BODY CARRY-OVER LIFT

X	$(1/Q)DL/DX$
.0449	-.3801
.1787	.0750
.3994	-.1847
.7036	-.2462
1.0863	.0326
1.5417	-.1248
2.0624	-.0882
2.6403	-.0012
3.2663	.0201
3.9304	.0660
4.6223	.1686
5.3310	.1285
6.0453	.1676
6.7540	.1991
7.4459	.1903
8.1101	.3138
8.7361	.2122
9.3140	.2445
9.8347	.2227
10.2900	.2044
10.6728	.2054
10.9769	.1286
11.1977	.1471
11.3315	-.0981

LIFT COEFFICIENT (BODY CARRY-OVER) =   .1780

154

EFFECTIVE WING GEOMETRY

GEOMETRY OF THE EFFECTIVE WING, WHICH APPROXIMATES THE REAL WING BY RECTANGULAR BOXES. AN EFFECTIVE SPANWISE ANGLE OF ATTACK DISTRIBUTION IS CALCULATED FROM THE GIVEN ANGLE OF ATTACK DISTRIBUTION. THE FOLLOWING DEFINITIONS APPLY. ALL DIMENSIONS ARE MEASURED FROM THE ROOT OF THE LEADING EDGE.

Y   SPANWISE DISTANCE TO CENTER OF CHORDWISE STRIP

XLE   CHORDWISE DISTANCE TO EFFECTIVE LEADING EDGE

XTE   CHORDWISE DISTANCE TO EFFECTIVE TRAILING EDGE

C   EFFECTIVE CHORD

Y	XLE	XTE	C	ALPHA
12.8601	15.2552	17.1047	1.8495	1.0000
12.7809	15.2552	17.0694	1.8142	1.0000
12.6228	15.2552	16.9990	1.7437	1.0000
12.3869	14.2855	16.8939	2.6084	1.0000
12.0746	14.2855	16.7548	2.4693	1.0000
11.6879	14.2855	16.5825	2.2970	1.0000
11.2291	13.3158	16.3782	3.0624	1.0000
10.7011	12.3461	16.1430	3.7969	1.0000
10.1071	12.3461	15.8784	3.5323	1.0000
9.4508	11.1087	15.5861	4.4774	1.0000
8.7362	10.5004	15.2678	4.7674	1.0000
7.9678	9.5897	14.9255	5.3358	1.0000
7.1502	8.4339	14.5613	6.1274	1.0000
6.2886	7.7863	14.1775	6.3912	1.0000
5.3882	6.4025	13.7764	7.3739	1.0000
4.4546	4.9739	13.3606	8.3867	1.0000
3.4935	4.2708	12.9325	8.6617	1.0000
2.5108	2.9425	12.4948	9.5523	1.0000
1.5127	1.7867	12.0502	10.2635	1.0000
.5053	.5312	11.6014	11.0703	1.0000

LIFT ON PHYSICAL WING

SPANWISE LIFT DISTRIBUTION ON THE PHYSICAL WING ALONE.
CCL IS THE SPANWISE LOADING.

Y	CL	CCL	ALPHA
.9985	.7979	.2256	1.0000
.9923	2.3131	.6741	1.0000
.9800	3.6092	1.1147	1.0000
.9617	4.6032	1.5417	1.0000
.9375	5.2745	1.9488	1.0000
.9074	5.6512	2.3303	1.0000
.8718	5.7912	2.6832	1.0000
.8308	5.7627	3.0085	1.0000
.7847	5.6262	3.3095	1.0000
.7338	5.4261	3.5889	1.0000
.6783	5.1915	3.8477	1.0000
.6186	4.9405	4.0855	1.0000
.5551	4.6837	4.3008	1.0000
.4882	4.4270	4.4913	1.0000
.4183	4.1736	4.6542	1.0000
.3459	3.9251	4.7867	1.0000
.2712	3.6820	4.8859	1.0000
.1949	3.4448	4.9497	1.0000
.1174	3.2142	4.9770	1.0000
.0392	2.9944	4.9741	1.0000

LIFT COEFFICIENT   = 4.0483
SPANWISE CENTER OF PRESSURE =   .4319

156

LIFT ON PHYSICAL WING WITH BODY

SPANWISE LIFT DISTRIBUTION ON THE PHYSICAL WING IN THE
PRESENCE OF THE BODY.

Y	CL	CCL	ALPHA
.9985	.8146	.2303	1.0024
.9923	2.3619	.6884	1.0025
.9800	3.6862	1.1385	1.0026
.9617	4.7031	1.5751	1.0027
.9375	5.3917	1.9920	1.0029
.9074	5.7804	2.3836	1.0032
.8718	5.9285	2.7468	1.0036
.8308	5.9055	3.0831	1.0040
.7847	5.7729	3.3958	1.0047
.7338	5.5762	3.6882	1.0055
.6783	5.3451	3.9615	1.0066
.6186	5.0980	4.2157	1.0082
.5551	4.8459	4.4498	1.0104
.4882	4.5952	4.6620	1.0136
.4183	4.3494	4.8503	1.0183
.3459	4.1105	5.0128	1.0259
.2712	3.8797	5.1482	1.0387
.1949	3.6579	5.2559	1.0628
.1174	3.4473	5.3380	1.1160
.0392	3.2484	5.3960	1.2706

LIFT COEFFICIENT = 4.2389
SPANWISE CENTER OF PRESSURE = .4272

157

LIFT ON BODY DUE TO WING

CHORDWISE DISTRIBUTION OF BODY CARRY-OVER LIFT AFT
OF THE TRAILING EDGE OF THE ROOT CHORD. (DISTRIBUTION
FORWARD OF TRAILING EDGE GIVEN ABOVE). TOTAL LIFT
COEFFICIENTS (BASED ON WING AREA) AND CHORDWISE
CENTERS OF PRESSURE ARE GIVEN FOR EACH SEGMENT OF THE BODY,
AND FOR THE ENTIRE BODY. XI AND ETA GIVE POSITION OF THE
ROLLED-UP VORTEX.

X	XI	ETA	(1/Q)DL/DX
11.8612	11.5792	.9697	.0196
12.8309	11.5792	1.9394	.0257
13.8007	11.5792	2.9092	.0273
14.7704	11.5792	3.8789	.0303
15.7401	11.5792	4.8486	.0302
16.7098	11.5792	5.8183	.0279
17.6795	11.5792	6.7881	.0262
18.6493	11.5792	7.7578	.0250
19.619	11.5792	8.7275	.0220
20.5887	11.5792	9.6972	.0247
21.5584	11.5792	1 .6669	.0105
22.5281	11.5792	11.6366	-.0038

	CL	XCP
FORWARD PORTION	.178	.8043
AFT PORTION	. 476	1.2694
COMPLETE BODY	.2257	.9 22
AVERAGE BODY ANGLE OF ATTACK =	1. 0 RADIANS	
STRENGTH OF ROLLED-UP VORTEX =	1.3918	

APPENDIX II

EVALUATION OF CONTOUR INTEGRALS

It is necessary to evaluate the following complex contour integral:

$$\oint_{B(x)} \bar{\Phi}(\theta) \frac{d\Psi}{d\theta} d\theta$$

where the contour $B(x)$ in the θ-plane is shown below

$$\theta = y + iz$$
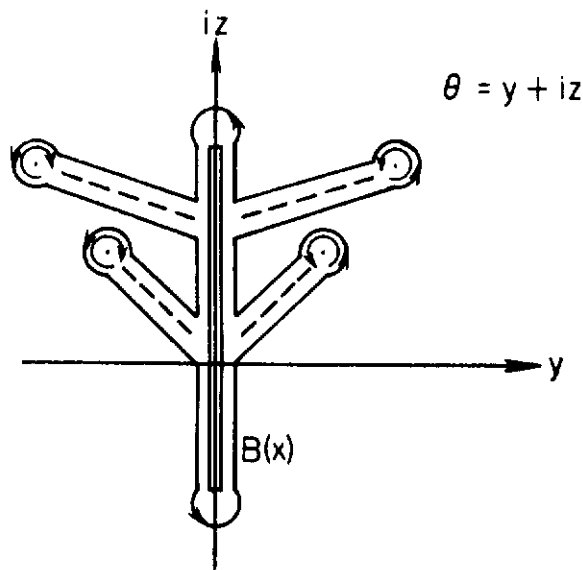
The integral may be evaluated in two parts, by separating the terms due to the vortices from the terms due to the free stream. Thus Eq. (162) may be written:

$$\oint_{B(x)} \bar{\Phi}(\Psi) d\Psi = \oint_{B(x)} \bar{\Phi}_{VORTICES}(\theta) \frac{d\Psi}{d\theta} d\theta + \oint_{B(x)} \bar{\Phi}_{FREE-STREAM}(\theta) \frac{d\Psi}{d\theta} d\theta \tag{II-1}$$

where

$$\bar{\Phi}_{VORTICES}(\theta) = -\frac{i\Gamma_0}{2\pi} \ln\left(\frac{\theta - \theta_0}{\theta + \bar{\theta}_0}\right) - \frac{i\Gamma_1}{2\pi} \ln\left(\frac{\theta - \theta_1}{\theta + \bar{\theta}_1}\right) \tag{II-2}$$

159

and

$$\Phi_{FREE\text{-}STREAM}(\theta) = -i \, U_\infty \sin \alpha \, \theta \qquad \text{(II-3)}$$

The integral containing the terms due to the vortices may be evaluated by the use of Cauchy's integral theorem, which states that if a function $f(z)$ is analytic inside and on a closed curve C, then

$$\oint_C f(z) \, dz = 0 \qquad \text{(II-4)}$$

Thus we may write that

$$\oint_C \Phi_{VORTICES}(\theta) \frac{d\mathcal{G}}{d\theta} = 0 \qquad \text{(II-5)}$$

where the contour $C = C_1 + C_2$ is shown in the following sketch
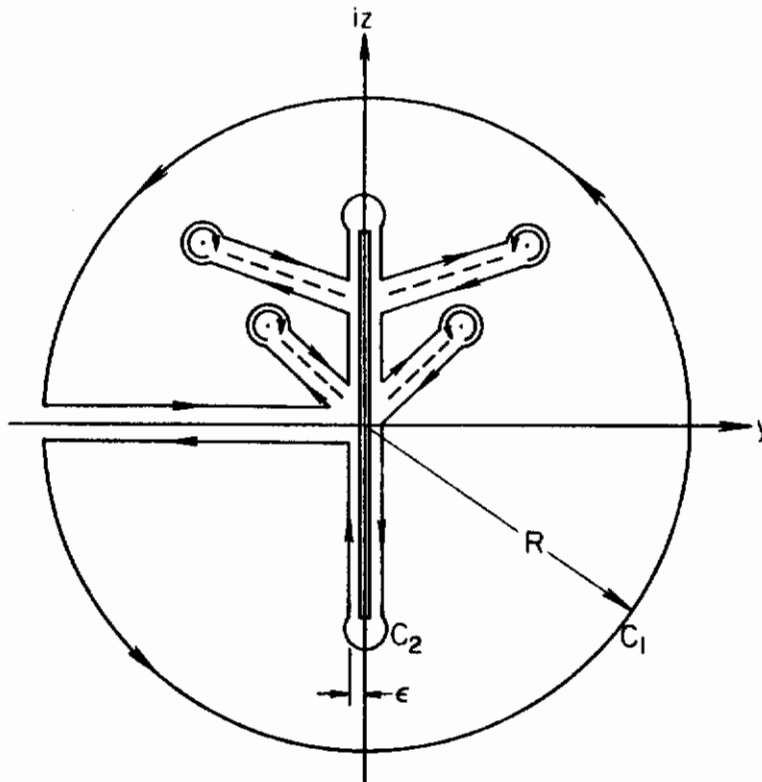
Equation (II-5) may be written

$$\lim_{\substack{R \to \infty \\ \epsilon \to 0}} \left\{ \int_{-\epsilon}^{-R} \Phi \frac{d\mathcal{G}}{d\theta} \, d\theta + \int_{\theta = Re^{-i\pi}}^{\theta = Re^{i\pi}} \Phi \frac{d\mathcal{G}}{d\theta} \, d\theta + \int_{-R}^{-\epsilon} \Phi \frac{d\mathcal{G}}{d\theta} \, d\theta \right\} = \oint_{C_2 = \mathcal{B}(X)} \Phi \, d\mathcal{G}/d\theta$$

$$\text{(II-6)}$$

160

where C_1 is the segment of the contour C consisting of the large circle of arbitrary radius R, and C_2 is the segment around the transformed wing-body combination, vortices and feeding sheets as shown.

It is possible to show that the first and third terms, taken along the horizontal branches of the contour, cancel in the following manner.

$$\int_{-\epsilon}^{-R} \oint \frac{d\varphi}{d\theta}\, d\theta = \int_{-\epsilon}^{-R} \left\{ \frac{-i\Gamma_0}{2\pi} \ln\left(\frac{\theta-\theta_0}{\theta+\bar{\theta}_0}\right) - \frac{i\Gamma_1}{2\pi} \ln\left(\frac{\theta-\theta_1}{\theta+\theta_1}\right) \right\}$$

$$\left\{ \left(\frac{k^2+r^2}{2r^2}\right)\left(\frac{\theta}{\sqrt{\theta^2+s'^2+4r^2}}\right) - \left(\frac{k^2+r^2}{2r^2}\right)\left(\frac{\theta}{\sqrt{\theta^2+s'^2}}\right) \right\} d\theta \qquad \text{(II-7)}$$

which may be evaluated in four parts. Since the four resulting integrals are nearly identical in form, only the first will be evaluated in complete detail, as an illustration.

$$\int_{-\epsilon}^{-R} -\frac{i\Gamma_0}{2\pi} \ln\left(\frac{\theta-\theta_0}{\theta+\bar{\theta}_0}\right)\left(\frac{k^2+r^2}{2r^2}\right)\left(\frac{\theta}{\sqrt{\theta^2+s'^2+4r^2}}\right) d\theta$$

$$= -\frac{i\Gamma_0}{2\pi}\left(\frac{k^2+r^2}{2r^2}\right)\int_{-\epsilon}^{-R} \left[\ln(\theta-\theta_0) - \ln(\theta+\bar{\theta}_0)\right]\left[\frac{\theta}{\sqrt{\theta^2+s'^2+4r^2}}\right] d\theta$$

$$= -\frac{i\Gamma_0}{2\pi}\left(\frac{k^2+r^2}{2r^2}\right)\left\{ \int_{-\epsilon}^{-R} \left[\ln|\theta-\theta_0| + i\arg(\theta-\theta_0)\right]\left[\frac{\theta}{\sqrt{\theta^2+s'^2+4r^2}}\right] d\theta \right.$$

$$\left. - \int_{-\epsilon}^{-R} \left[\ln|\theta+\bar{\theta}_0| + i\arg(\theta+\bar{\theta}_0)\right]\left[\frac{\theta}{\sqrt{\theta^2+s'^2+4r^2}}\right] d\theta \right\}$$

$$\text{(II-8)}$$

161

$$= \frac{-i\mathcal{S}_o}{2\pi}\left(\frac{k^2+r^2}{2r^2}\right)\left\{\int_{-\epsilon}^{-R} \ln(y-y_o)\left(\frac{y}{\sqrt{y^2+s'^2+4r^2}}\right)dy\right.$$

$$+ i\int_{-\epsilon}^{-R} \tan^{-1}\left(\frac{z_o}{y-y_o}\right)\left(\frac{y}{\sqrt{y^2+s'^2+4r^2}}\right)dy$$

$$-\int_{-\epsilon}^{-R} \ln(y+y_o)\left(\frac{y}{\sqrt{y^2+s'^2+4r^2}}\right)dy - i\int_{-\epsilon}^{-R}\tan^{-1}\left(\frac{z_o}{y+y_o}\right)\left(\frac{y}{\sqrt{y^2+s'^2+4r^2}}\right)dy\right\}$$

$$\text{(II-9)}$$

since $\theta = y$ and $d\theta = dy$ on the real axis. The third term of Eq. (II-6) may be written

$$\int_{-R}^{-\epsilon} \oint \frac{d\mathcal{S}}{d\theta}\, d\theta = \int_{-R}^{-\epsilon}\left\{-\frac{i\mathcal{S}_o}{2\pi}\ln\left(\frac{\theta-\theta_o}{\theta+\theta_o}\right) - \frac{i\mathcal{S}_o}{2\pi}\ln\left(\frac{\theta-\theta_1}{\theta+\bar{\theta}_1}\right)\right\}$$

$$\times \left\{\left(\frac{k^2+r^2}{2r^2}\right)\left(\frac{\theta}{\sqrt{\theta^2+s'^2+4r^2}}\right) - \left(\frac{k^2-r^2}{2r^2}\right)\left(\frac{\theta}{\sqrt{\theta^2+s'^2}}\right)\right\}d\theta$$

$$\text{(II-10)}$$

which again may be evaluated in four parts. Considering the term corresponding to the integral evaluated in Eq. (II-8) and Eq. (II-9).

$$\int_{-R}^{-\epsilon} -\frac{i\mathcal{S}_o}{2\pi}\ln\left(\frac{\theta-\theta_o}{\theta+\bar{\theta}_o}\right)\left(\frac{k^2+r^2}{2r^2}\right)\left(\frac{\theta}{\sqrt{\theta^2+s'^2+4r^2}}\right)d\theta$$

$$= -\frac{i\mathcal{S}_o}{2\pi}\left(\frac{k^2+r^2}{2r^2}\right)\int_{-R}^{-\epsilon}\left[\ln(\theta-\theta_o)-\ln(\theta+\bar{\theta}_o)\right]\left[\frac{\theta}{\sqrt{\theta^2+s'^2+4r^2}}\right]d\theta$$

$$= -\frac{iL_o}{2\pi}\left(\frac{t^2+r^2}{2r^2}\right)\left\{\int_{-\ell}^{-\epsilon}\left[\ln|\theta-\theta_o|+i\,arg(\theta-\theta_o)+2\pi i\right]\left[\frac{\theta}{\sqrt{\theta^2+s'^2+4r^2}}\right]d\theta\right.$$

$$\left.-\int_{-\ell}^{-\epsilon}\left[\ln|\theta+\bar\theta_o|+i\,arg(\theta+\bar\theta_o)+2\pi i\right]\left[\frac{\theta}{\sqrt{\theta^2+s'^2+4r^2}}\right]d\theta\right\} \tag{II-11}$$

since the arguments of $\ln(\theta-\theta_o)$ and $\ln(\theta+\bar\theta_o)$ gain an additional 2π when the function is evaluated around the portion of the contour C_1. Equation (II-11) may now be rewritten by letting $\theta=y$. Taking the opposite sign and reversing the limits of integration:

$$\int_{-\ell}^{-\epsilon}-\frac{iL_o}{2\pi}\ln\left(\frac{\theta-\theta_o}{\theta+\theta_o}\right)\left(\frac{t^2+r^2}{2r^2}\right)\left(\frac{\theta}{\sqrt{\theta^2+s'^2+4r^2}}\right)d\theta$$

$$=\frac{iL_o}{2\pi}\left(\frac{t^2+r^2}{2r^2}\right)\left\{\int_{-\epsilon}^{-\ell}\ln(y-y_o)\left(\frac{y}{\sqrt{y^2+s'^2+r^2}}\right)dy\right.$$

$$+i\int_{-\epsilon}^{-\ell}\tan^{-1}\left(\frac{z_o}{y-y_o}\right)\left(\frac{y}{\sqrt{y^2+s'^2+4r^2}}\right)dy+\int_{-\epsilon}^{-\ell}2\pi i\left(\frac{y}{\sqrt{y^2+s'^2+4r^2}}\right)dy$$

$$-\int_{-\epsilon}^{-\ell}\ln(y+y_o)\left(\frac{y}{\sqrt{y^2+s'^2+4r^2}}\right)dy$$

$$\left.-i\int_{-\epsilon}^{-\ell}\tan^{-1}\left(\frac{z_o}{y+y_o}\right)\left(\frac{y}{\sqrt{y^2+s'^2+4r^2}}\right)dy-\int_{-\epsilon}^{-\ell}2\pi i\left(\frac{y}{\sqrt{y^2+s'^2+4r^2}}\right)dy\right\} \tag{II-12}$$

which is just the negative of the right-hand side of Eq. (II-9), since the terms containing $2\pi i$ will cancel. It may be easily seen that the other three integrals contained in Eq. (II-7) will just be cancelled by the other three integrals contained in Eq. (II-10). Thus the first and third terms of Eq. (II-6) just cancel.

163

The second term of Eq. (II-6) will now be evaluated on the large circle C_1. Making a substitution of variables let $\theta = Re^{i\omega}$. Then $d\theta = iRe^{i\omega}d\omega$, and:

$$I_1 = \lim_{R \to \infty} \int_{\theta=Re^{-i\pi}}^{\theta=Re^{i\pi}} \bar{\phi} \frac{d\Psi}{d\theta} d\theta = \oint_{\theta(\gamma)} \bar{\phi}_{VORTICES}(\theta) \frac{d\Psi}{d\theta} d\theta$$

$$= \lim_{R \to \infty} \int_{-\pi}^{\pi} \left\{ -\frac{i\Gamma_0}{2\pi} \ln\left(\frac{Re^{i\omega}-\theta_0}{Re^{i\omega}+\bar{\theta}_0}\right) - \frac{i\Gamma_1}{2\pi} \ln\left(\frac{Re^{i\omega}-\theta_1}{Re^{i\omega}+\bar{\theta}_1}\right) \right\}$$

$$\times \left\{ \left(\frac{k^2+r^2}{2r^2}\right) \frac{Re^{i\omega}}{\sqrt{R^2 e^{2i\omega}+s'^2+4r^2}} - \left(\frac{k^2-r^2}{2r^2}\right) \frac{Re^{i\omega}}{\sqrt{R^2 e^{2i\omega}+s'^2}} \right\} iRe^{i\omega} d\omega \tag{II-13}$$

Since:

$$\lim_{R \to \infty} (R^2 e^{2i\omega}) \approx \lim_{R \to \infty} (R^2 e^{2i\omega}+s'^2+4r^2) \approx \lim_{R \to \infty} (R^2 e^{2i\omega}+s'^2) \tag{II-14}$$

we may combine terms to give:

$$I_1 \approx \lim_{R \to \infty} \int_{-\pi}^{\pi} i(\bar{R}_1 + \bar{R}_2) \left\{ \left(\frac{k^2+r^2}{2r^2}\right) - \left(\frac{k^2-r^2}{2r^2}\right) \right\} Re^{i\omega} d\omega \tag{II-15}$$

where

$$\bar{R}_1 = -\frac{i\Gamma_0}{2\pi} \ln\left(\frac{Re^{i\omega}-\theta_0}{Re^{i\omega}+\bar{\theta}_0}\right) \tag{II-16}$$

and

$$\bar{R}_2 = -\frac{i\Gamma_0}{2\pi} \ln\left(\frac{Re^{i\omega}-\theta_1}{Re^{i\omega}+\bar{\theta}_1}\right) \tag{II-17}$$

Now:

$$\bar{R}_1 = -\frac{i\Gamma_0}{2\pi} \ln\left[\frac{1-\theta_0/Re^{i\omega}}{1+\bar{\theta}_0/Re^{i\omega}}\right]$$

$$= -\frac{i\Gamma_0}{2\pi} \ln\left[\left(1-\frac{\theta_0}{R} e^{i\omega}\right)\left(1-\frac{\bar{\theta}_0}{Re^{i\omega}}+\cdots \theta\left(\frac{1}{R^2}\right)+\cdots\right)\right] \tag{II-18}$$

164

Neglecting terms of order $1/R^2$ or greater:

$$\bar{R}_1 \approx -\frac{i\Omega_0}{2\pi} \ln\left[1 - \frac{e^{-i\omega}}{R}(\theta_0 + \bar{\theta}_0) \right]$$

(II-19)

$$\approx \frac{i\Omega_0}{2\pi}\left[\frac{e^{-i\omega}}{R}(\theta_0 + \bar{\theta}_0) \right]$$

Similarly:

$$\bar{R}_2 \approx \frac{i\Omega_1}{2\pi}\left[\frac{e^{-i\omega}}{R}(\theta_1 + \bar{\theta}_1) \right]$$

(II-20)

Finally, then:

$$I_1 = -\int_{-\pi}^{\pi}\left\{ \frac{\Omega_0}{2\pi}(\theta_0 + \bar{\theta}_0) + \frac{\Omega_1}{2\pi}(\theta_1 + \bar{\theta}_1) \right\} d\omega$$

$$= -\Omega_0(\theta_0 + \bar{\theta}_0) - \Omega_1(\theta_1 + \bar{\theta}_1)$$

(II-21)

The integral containing the terms due to the free stream in Eq. (II-1) should be evaluated directly on the contour $B(x)$. However, since the function $\bar{\phi}_{\text{free stream}}(\theta)\frac{d\bar{\phi}}{d\theta}$ is analytic inside the portions of the contour which go around the vortices and their feeding sheets, the contour may be collapsed to one around a vertical line between the end points of the transformed wing-body combination, as shown in the sketch below:
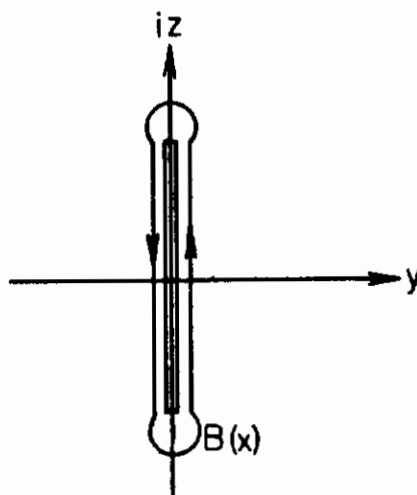
Thus

$$I_2 = \oint_{\mathcal{B}(x)} \Phi_{FREE\text{-}STREAM}(\theta)\,\frac{d\mathcal{S}}{d\theta}\,d\theta = \lim_{\epsilon \to 0}\left\{ \int_{-i(\sqrt{s'^2+4r^2}-\epsilon)}^{i(\sqrt{s'^2+4r^2}-\epsilon)} \Phi(\theta)\frac{d\mathcal{S}}{d\theta}\,d\theta \right.$$

$$\left. + \oint_{C_3} \Phi(\theta)\frac{d\mathcal{S}}{d\theta}\,d\theta + \int_{i(\sqrt{6'^2+4r^2}-\epsilon)}^{-i(\sqrt{s'^2+4r^2}-\epsilon)} \Phi(\theta)\frac{d\mathcal{S}}{d\theta}\,d\theta + \oint_{C_4} \Phi(\theta)\frac{d\mathcal{S}}{d\theta}\,d\theta \right\} \qquad \text{(II-22)}$$

where C_3 and C_4 are the portions of the contour around the end points at $\pm i(\sqrt{s'^2+4r^2})$ as shown in the close-up view below
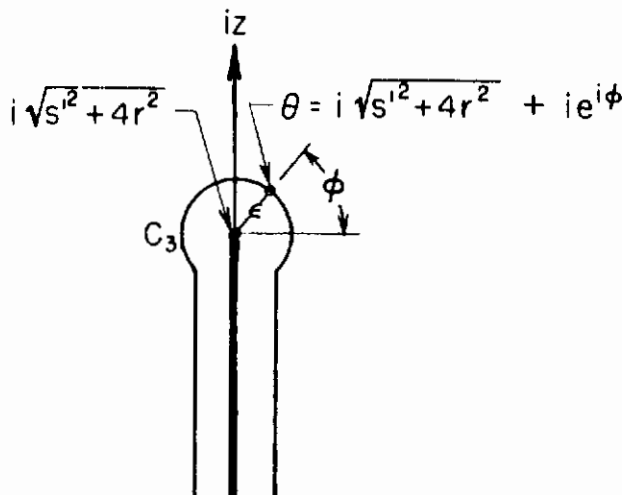
The first term may be evaluated in the two parts as follows:

$$\lim_{\epsilon \to 0} \int_{-i(\sqrt{s'^2+4r^2}-\epsilon)}^{i(\sqrt{s'^2+4r^2}-\epsilon)} \Phi(\theta)\frac{d\mathcal{S}}{d\theta}\,d\theta = \lim_{\epsilon \to 0} \int_{-i(\sqrt{s'^2+4r^2}-\epsilon)}^{i(\sqrt{s'^2+4r^2}-\epsilon)} -i\,U_\infty \sin\alpha\,\theta\left(\frac{k^2 r^2}{2r^2}\right)\frac{\theta}{\sqrt{\theta^2+s'^2+4r^2}}\,d\theta$$

$$-\lim_{\epsilon \to 0} \int_{-i\left(\sqrt{S'^2 + 4r^2} - \epsilon\right)}^{i\left(\sqrt{S'^2 + 4r^2} - \epsilon\right)} -iU_\infty \sin\alpha \; \theta \left(\frac{t^2 - r^2}{2r^2}\right) \frac{\theta}{\sqrt{\theta^2 + S'^2}} \, d\theta \qquad \text{(II-23)}$$

The first integral has a branch point at the end points of the contour, $\pm i\sqrt{S'^2 + 4r^2}$. The second integral has branch points at $\pm is'$. The function is analytic at the end points. The integrals may thus be evaluated as real integrals provided that the branch points are treated carefully. The limits of the second integral may be replaced by $\pm is'$, since the function is analytic on the portions of the contour between the branch points and the end points. Since $\theta = iz$ and $d\theta = idz$ Eq. (II-23) may be written

$$\lim_{\epsilon \to 0} \int_{-i\left(\sqrt{S'^2 + 4r^2} - \epsilon\right)}^{i\left(\sqrt{S'^2 + 4r^2} - \epsilon\right)} f(\theta) \frac{df}{d\theta} d\theta = \lim_{\epsilon \to 0} \int_{-\sqrt{S'^2 + 4r^2} - \epsilon}^{\sqrt{S'^2 + 4r^2} - \epsilon} -iU_\infty \sin\alpha \, (iz) \left(\frac{t^2 - r^2}{2r^3}\right) \frac{iz}{\sqrt{S'^2 + 4r^2 - z^2}} \, idz$$

$$-\lim_{\epsilon \to 0} \int_{-s'}^{s'} -iU_\infty \sin\alpha \, (iz)\left(\frac{t^2 - r^2}{2r^2}\right) \frac{iz}{\sqrt{S'^2 - z^2}} \, idz \qquad \text{(II-24)}$$

$$= -U_\infty \sin\alpha \left(\frac{t^2 + r^2}{2r^2}\right) \left[-\frac{z}{2}\sqrt{S'^2 + 4r^2 - z^2} + \frac{S'^2 + 4r^2}{2}\sin^{-1}\left(\frac{z}{\sqrt{S'^2 + 4r^2}}\right) \right]_{-\sqrt{S'^2 + 4r^2}}^{\sqrt{S'^2 + 4r^2}}$$

$$+ U_\infty \sin\alpha \left(\frac{t^2 - r^2}{2r^2}\right) \left[-\frac{z}{2}\sqrt{S'^2 - z^2} + \frac{S'^2}{2}\sin^{-1}\left(\frac{z}{S'}\right) \right]_{-s'}^{s'}$$

$$= -U_\infty \sin\alpha \left\{ \left(\frac{t^2 + r^2}{2r^2}\right)\left(\frac{S'^2 + 4r^2}{2}\right)\pi - \left(\frac{t^2 - r^2}{2r^2}\right)\left(\frac{S'^2}{2}\right)\pi \right\} \qquad \text{(II-25)}$$

The third term in Eq. (II-22) contains exactly the same integrals as the first term, with the limits reversed. Since the integrals are to be evaluated on the opposite side of the branch cut (line joining the branch points) however, the square roots contribute an additional minus sign to each term.

Thus the third term in Eq. (II-22) has exactly the same value as the first term, and is also given by the right-hand side of Eq. (II-25).

The integrals around the branch points may be evaluated in the following manner:

$$\oint_{C_3} \frac{d\Gamma}{d\theta}(\theta) d\theta \oint_{C_3} -i U_\infty \sin\alpha\, \theta \left\{ \left(\frac{k^2+r^2}{2r^2}\right) \frac{\theta}{\sqrt{\theta^2+s'^2+4r^2}} - \left(\frac{k^2-r^2}{2r^2}\right) \frac{\theta}{\sqrt{\theta^2+s'^2}} \right\} d\theta$$

$$= \oint_{C_3} -i U_\infty \sin\alpha\, \theta \left(\frac{k^2+r^2}{2r^2}\right) \frac{\theta}{\sqrt{\theta^2+s'^2+4r^2}} d\theta - \oint_{C_3'} -i U_\infty \sin\alpha\, \theta \left(\frac{k^2-r^2}{2r^2}\right) \frac{\theta}{\sqrt{\theta^2+s'^2}} d\theta$$

(II-26)

where the contour C_3' is that around the branch point at is'. Letting $\theta = i\sqrt{s'^2+4r^2} + \epsilon e^{i\phi}$ in the first integral

$$\oint -i U_\infty \sin\theta \left(\frac{k^2+r^2}{2r^2}\right) \frac{\theta}{\sqrt{\theta^2+s'^2+4r^2}} d\theta =$$

$$\lim_{\epsilon \to 0} \int_{\phi=\pi/2}^{\phi=3\pi/2} \frac{(-iU_\infty \sin\alpha)(-s'^2-4r^2+2i\sqrt{s'^2+4r^2}\,\epsilon e^{i\phi}+\ldots)}{(\sqrt{2i\sqrt{s'^2+4r^2}\,\epsilon e^{i\phi/2}}+\ldots)} \left(\frac{k^2+r^2}{2r^2}\right) i\epsilon e^{i\phi} d\phi = 0$$

(II-27)

In a similar manner, letting $\theta = is' + \epsilon e^{i\phi}$

$$\oint_{C_3'} -i U_\infty \sin\alpha\, \theta \left(\frac{k^2-r^2}{2r^2}\right) \frac{\theta}{\sqrt{\theta^2+s'^2}} d\theta$$

$$= \lim_{\epsilon \to 0} \int_{\phi=\pi/2}^{\phi=3\pi/2} \frac{(-iU_\infty \sin\alpha)(-s'^2+2i\,s'\epsilon e^{i\phi}+\ldots)}{(\sqrt{2is'\epsilon}\,e^{i\phi/2}+\ldots)} \left(\frac{k^2-r^2}{2r^2}\right) i\epsilon e^{i\phi} dp = 0$$

(II-28)

168

Thus the integrals around both upper branch points are zero in the limit as $\epsilon \rightarrow 0$. The integrals around the lower branch points are similarly zero.

Thus the free stream integral may be written:

$$I_2 = -U_\infty \sin \alpha \, \pi \left\{ \left(\frac{k^2+r^2}{2r^2} \right) \left(s'^2 + 4r^2 \right) - \left(\frac{k^2-r^2}{2r^2} \right) s'^2 \right\} \qquad \text{(II-29)}$$

Finally, then

$$\oint_{s(\lambda)} \bar{p}(\theta) \frac{ds}{d\theta} \, d\theta = -\Omega_2^2 (\theta_o + \bar{\theta}_o) - \Omega_1 (\theta_1 + \bar{\theta}_1)$$

$$-U_\infty \sin \alpha \, \pi \left\{ \left(\frac{k^2+r^2}{2r^2} \right) \left(s'^2 + 4r^2 \right) - \left(\frac{k^2-r^2}{2r^2} \right) s'^2 \right\}$$

$$\text{(II-30)}$$

REFERENCES

1. Schindel, L.H., <u>An Evaluation of Procedures for Calculating Aerodynamic Loads</u>, Air Force Flight Dynamics Laboratory Technical Report 65-18, February, 1965.

2. Ellison, D.E., Malthan, L.V., et al, <u>USAF Stability and Control DATCOM</u>, Air Force Flight Dynamics Laboratory, October 1960 (Revised).

3. Spreiter, J.R., <u>Aerodynamic Properties of Slender Wing-Body Combinations at Subsonic, Transonic, and Supersonic Speeds</u>, NACA Technical Note 1662, 1948.

4. Pitts, W.C., Nielsen, J.N., and Kaattari, G.E., <u>Lift and Center of Pressure of Wing-Body-Tail Combinations at Subsonic, Transonic, and Supersonic Speeds</u>, NACA Report 1307, 1957.

5. Gray, W.L., and Schenk, K.M., <u>A Method for Calculating the Subsonic Steady-State Loading on an Airplane with a Wing of Arbitrary Plan Form and Stiffness</u>, NACA Technical Note 3030, 1953.

6. Lawrence, H.R., and Flax, A.H., "Wing-Body Interference at Subsonic and Supersonic Speeds-Survey and New Development", <u>Journal of Aero. Sci.</u>, Vol. 21, No. 5, May, 1954.

7. Ferrari, C., "Interaction Problems" Section C of <u>Aerodynamic Components of Aircraft at High Speeds</u>, Edited by A.F. Donovan and H.R. Lawrence, Vol. VII of <u>High Speed Aerodynamics and Jet Propulsion</u>, Princeton University Press, 1957.

8. Lennertz, J., <u>On the Mutual Reaction of Wings and Body</u>, NACA Technical Memo 400, 1927.

9. Lawrence, H.R., "The Lift Distribution on Low Aspect Ratio Wings at Subsonic Speeds", <u>Journal of Aero. Sci.</u>, Vol. 19, No. 10, October, 1951.

10. Ashley, H., Widnall, S., and Landahl, M.T., "New Directions in Lifting Surface Theory", <u>Journal of A.I.A.A.</u>, Vol. 3, No. 1, January, 1965.

11. Weissinger, J., <u>The Lift Distribution of Swept-Back Wings</u>, NACA Technical Memo 1120, 1947, Translation of "Über die Auftriebsverteilung von Pfeilflugeln", ZWB, Forschungsbericht, Nr. 1553, Berlin-Adlershof, 1942.

12. Jones, R.T., Properties of Low-Aspect Ratio Pointed Wings at Speeds Below and Above the Speed of Sound, NACA Report 835, 1946.

13. Schindel, L.H., Effect of Vortex Separation on Lifting Bodies of Elliptic Cross Section, M.I.T. Aerophysics Laboratory Technical Report 118, September, 1965.

14. DeYoung, J., and Harper, C.W., Theoretical Symmetric Span Loading at Subsonic Speeds for Wings Having Arbitrary Planform, NACA Report 921, 1948.

15. Chamberlain, T.E., Methods of Calculating Aerodynamic Loads on Aircraft Structures: Part II-Nonlinear Effects, Air Force Flight Dynamics Laboratory Technical Report 66-37, Part II, April, 1966.

16. Brown, C.E., and Michael, W.H., Jr., "Effect of Leading-Edge Separation on the Lift of a Delta Wing", Journal of Aero. Sci., Vol. 21, No. 10, October, 1954.

17. Allen, H.J., Estimation of the Forces and Moments on Inclined Bodies of Revolution of High Fineness Ratio, NACA Research Memo A9I26, 1949.

18. Kelly, H.R., The Estimation of Normal Force and Pitching Moment Coefficients for Blunt-Based Bodies of Revolution at Large Angles of Attack, Naval Ordnance Test Station Report TM-998, 1953.

19. Hill, J.A.F., "A Nonlinear Theory of the Lift on Slender Bodies of Revolution", Proceedings of U.S. Navy Symposium on Aeroballistics, Navord Report 5338, October, 1954.

20. Bryson, A.E., Jr., "Symmetric Vortex Separation on Circular Cylinders and Cones", Journal of Appl. Mech., Vol. 26, No. 4, December, 1959.

21. Schindel, L.H., Separated Flow About Lifting Bodies, M.I.T. Aerophysics Laboratory Technical Report 80, September, 1963

22. Friberg, E.G., Measurement of Vortex Separation Part I: Two-Dimensional Circular and Elliptic Bodies, M.I.T. Aerophysics Laboratory Technical Report 114, July, 1965.

23. Friberg, E.G., Measurement of Vortex Separation Part II: Three-Dimensional Circular and Elliptic Bodies, M.I.T. Aerophysics Laboratory Technical Report 115, August, 1965.

24. Sutton, F.B., and Lautenberger, J.W., Jr., The Effect of Body Contouring on the Longitudinal Characteristics at Mach Numbers up to 0.92 of a Wing-Fuselage-Tail and Several Wing-Fuselage Combinations Having Sweptback Wings of Relatively High Aspect Ratio, NACA Research Memo A56J08, 1957.

25. Fischetti, T.L., Investigation at Mach Numbers from 0.80 to 1.43 of Pressure and Load Distributions Over a Thin 45° Sweptback Highly Tapered Wing in Combination with Basic and Indented Bodies, NACA Research Memo L57O29a, 1957.

26. Kelly, T.C., Transonic Wind-Tunnel Investigation of Aerodynamic-Loading Characteristics of a 2-Percent-Thick Trapezoidal Wing in Combination with Basic and Indented Bodies, NACA Research Memo L56J12a, 1957.

27. Nielsen, J.N., Katzen, E.D., and Tang, K.K., Lift and Pitching-Moment Interference Between a Pointed Cylindrical Body and Triangular Wings of Various Aspect Ratios at Mach Numbers of 1.50 and 2.02, NACA Technical Note 3795, 1956.

28. Maskell, E.C., On the Asymptotic Structure of a Conical Leading-Edge Vortex, presented at Symposium on Concentrated Vortex Motions in Fluids, International Union of Theoretical and Applied Mechanics, Ann Arbor, July, 1964.

29. Smith, J.H.B., The Improved Calculation of the Mangler-Smith Model of Leading-Edge Separation from a Slender Delta Wing at Incidence, presented at Symposium on Concentrated Vortex Motions in Fluids, International Union of Theoretical and Applied Mechanics, Ann Arbor, July, 1964.

30. Lighthill, M.J., "Higher Approximations" Section E of General Theory of High Speed Aerodynamics, Edited by W.R. Sears, Vol. VI of High Speed Aerodynamics and Jet Propulsion, Princeton University Press, 1954.

31. Ferri, A., "The Method of Characteristics", Section G of General Theory of High Speed Aerodynamics, Edited by W.R. Sears, Vol. VI of High Speed Aerodynamics and Jet Propulsion, Princeton University Press, 1954.

32. Pershing, B., Separated Flow Past Slender Delta Wings with Secondary Vortex Simulation, Aerospace Corp. Report No. TDR-269(4560-10)-4, August, 1964.

REFERENCES (Concluded)

33. Chou, D. C., Methods of Calculating Aerodynamic Loads on Aircraft Structures: Part III – Effects of Engines, Stores, and Wing-Tail Interference, Air Force Flight Dynamics Laboratory Technical Report 66-37, Part III, May, 1966.
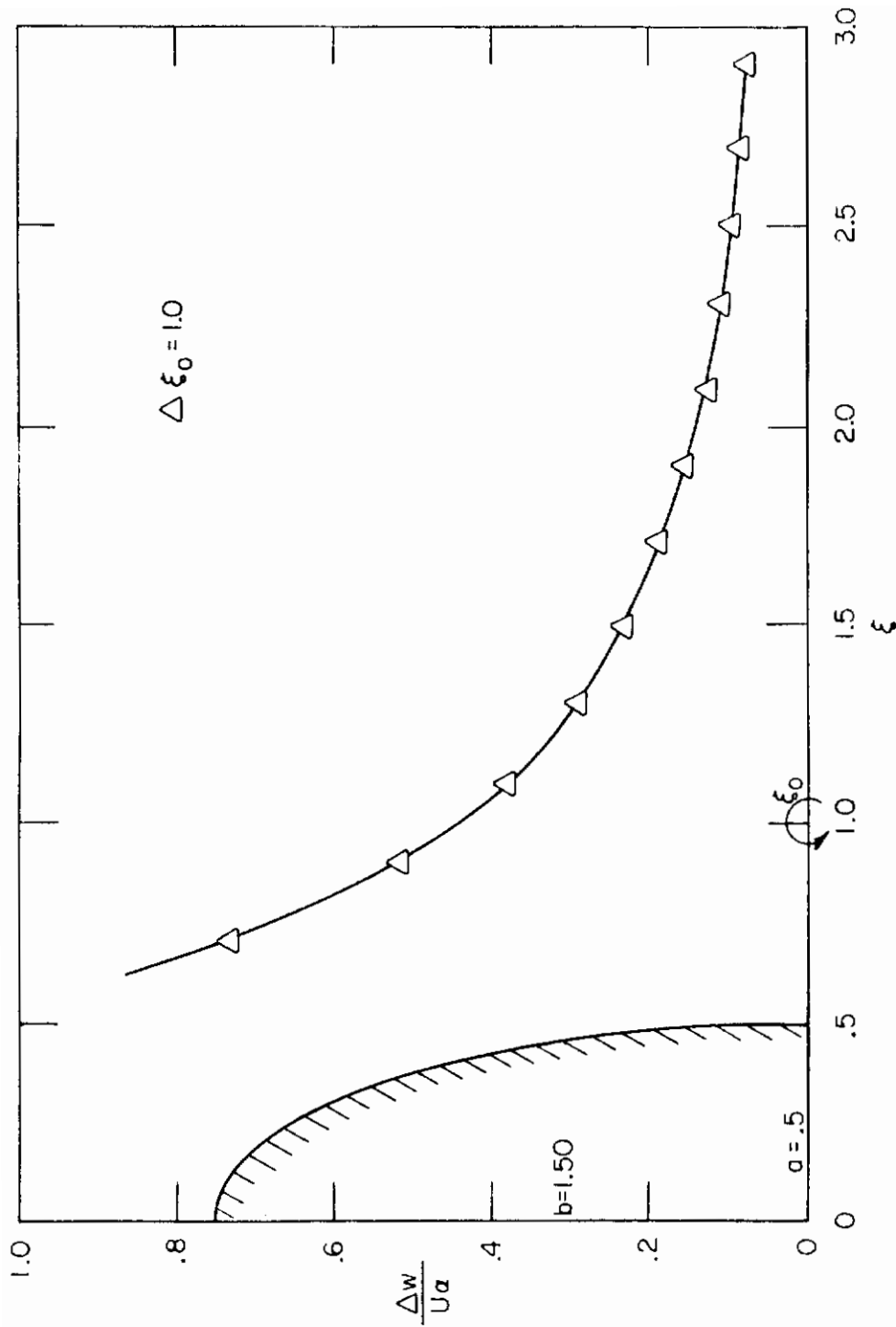
Figure 1. Error in Downwash for an Ellipse with b/a = 3
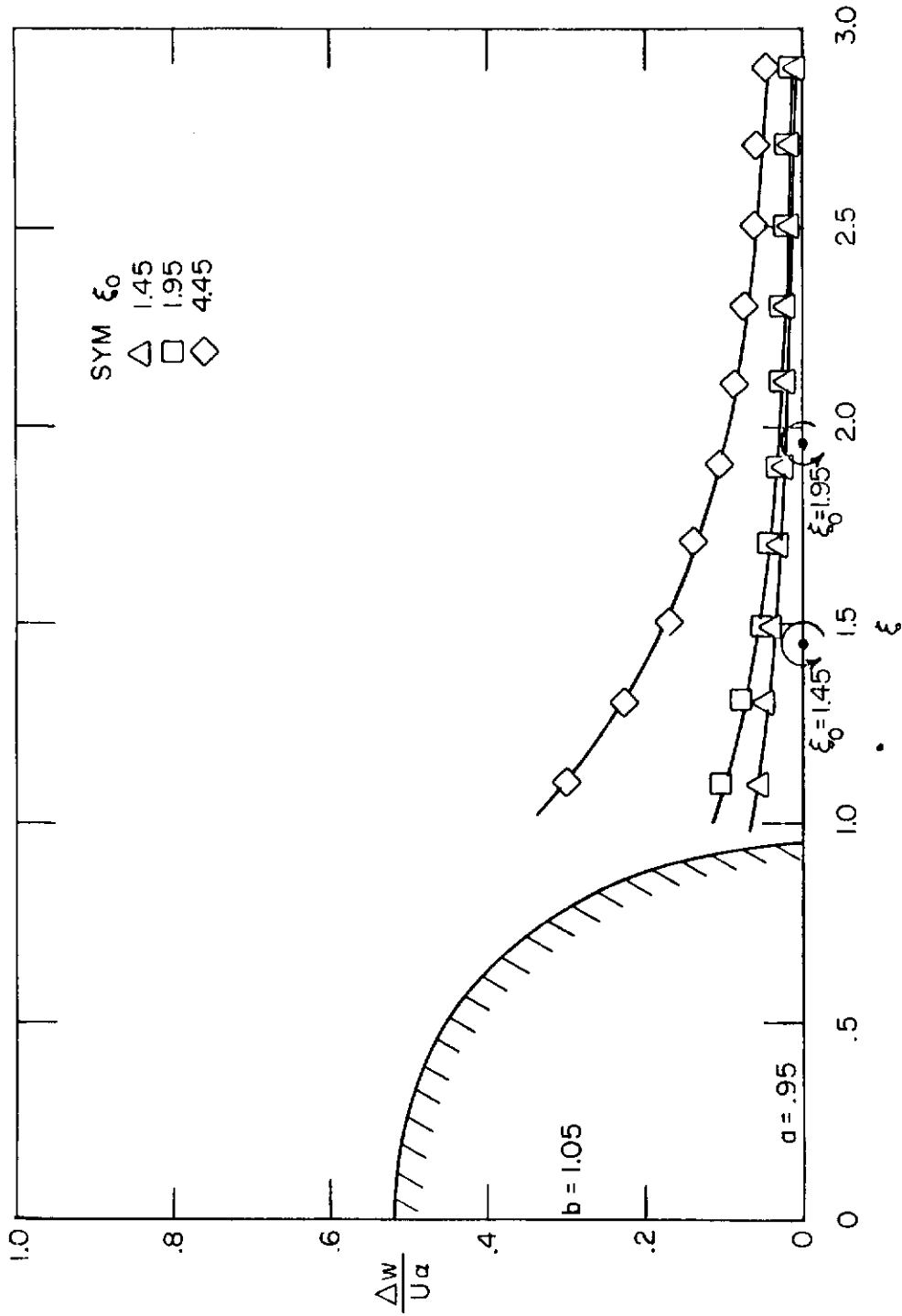
Figure 2. Error in Downwash for an Ellipse with $b/a = 1.1$
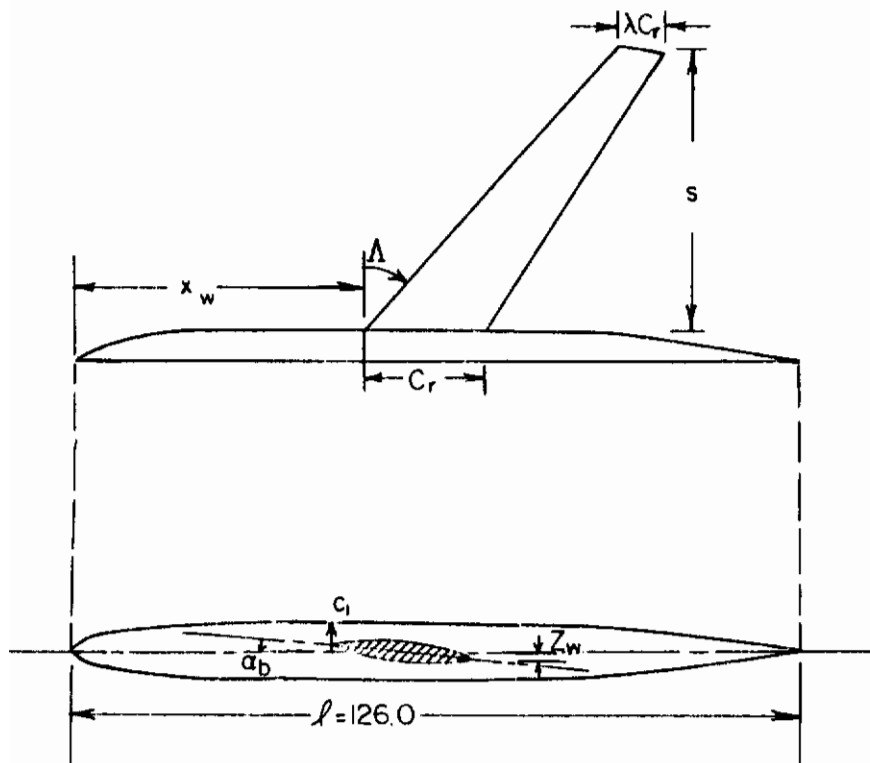
CONFIGURATION	Λ	AR	λ	s	x_w	Z_w	α_b
1	42.0°	6.619	.423	49.61	49.58	-.63	-3.00
2	46.9°	5.669	.425	45.41	48.01	-.62	-2.95
3	51.9°	4.709	.428	40.82	46.67	-.62	-2.90

$$a_1 = c_1 = 5.0$$

$$\theta = 0.$$

$$M = .60 \longrightarrow .92$$

Figure 3. Typical Model of Ref. 24

177
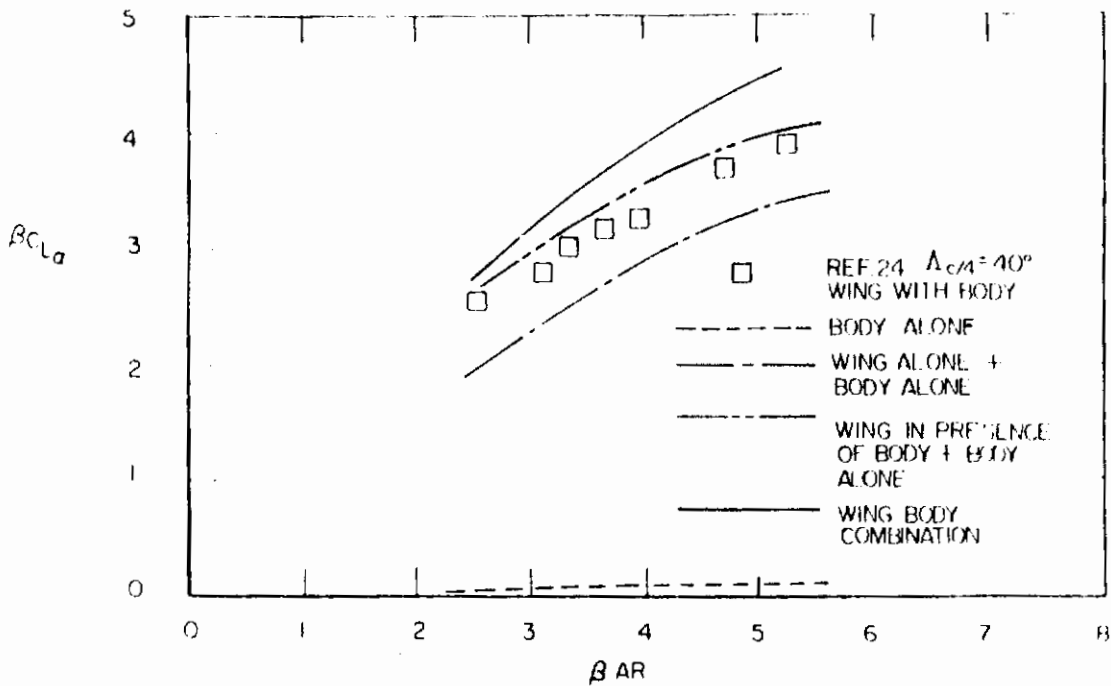
Figure 4. Reduced Lift Curve Slopes for the $\Lambda_{c/4} = 40°$ High Aspect Ratio Wing-Body Combination at Various Mach Numbers. Comparison with Theory
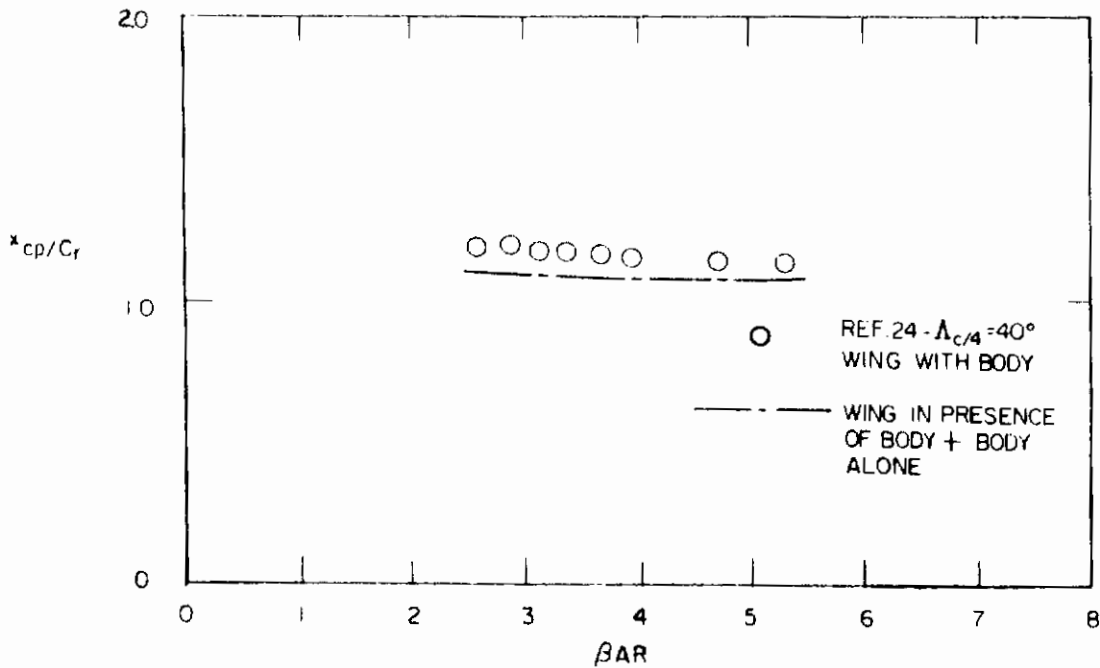
Figure 5. Center of Pressure Location for the $\Lambda_{c/4} = 40°$ High Aspect Ratio Wing-Body Combination at Various Mach Numbers. Comparison with Theory
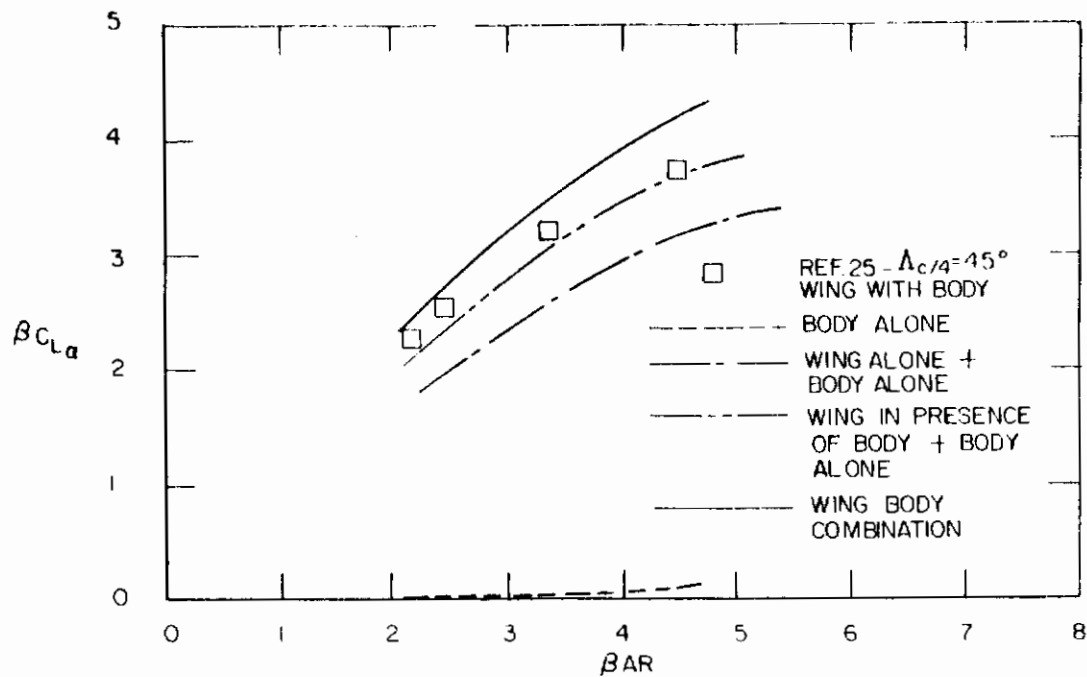
Figure 6. Reduced Lift Curve Slopes for the $\Lambda_{c/4} = 45°$ High Aspect Ratio Wing-Body Combination at Various Mach Numbers. Comparison with Theory
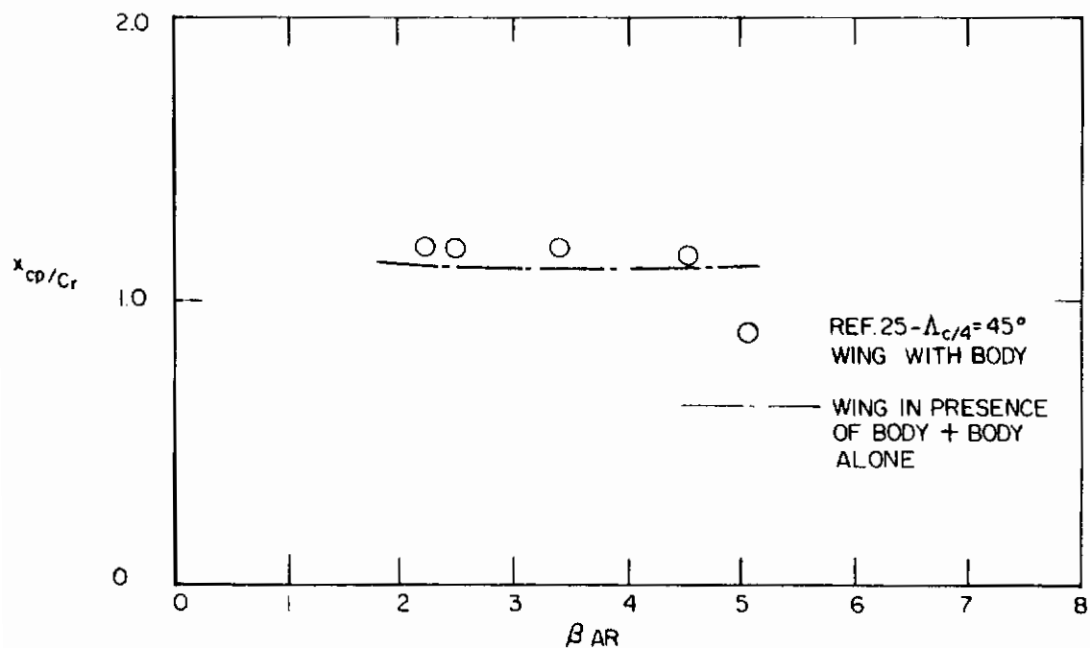
Figure 7. Center of Pressure Location for the $\Lambda_{c/4} = 45°$ High Aspect Ratio Wing-Body Combination at Various Mach Numbers. Comparison with Theory

179
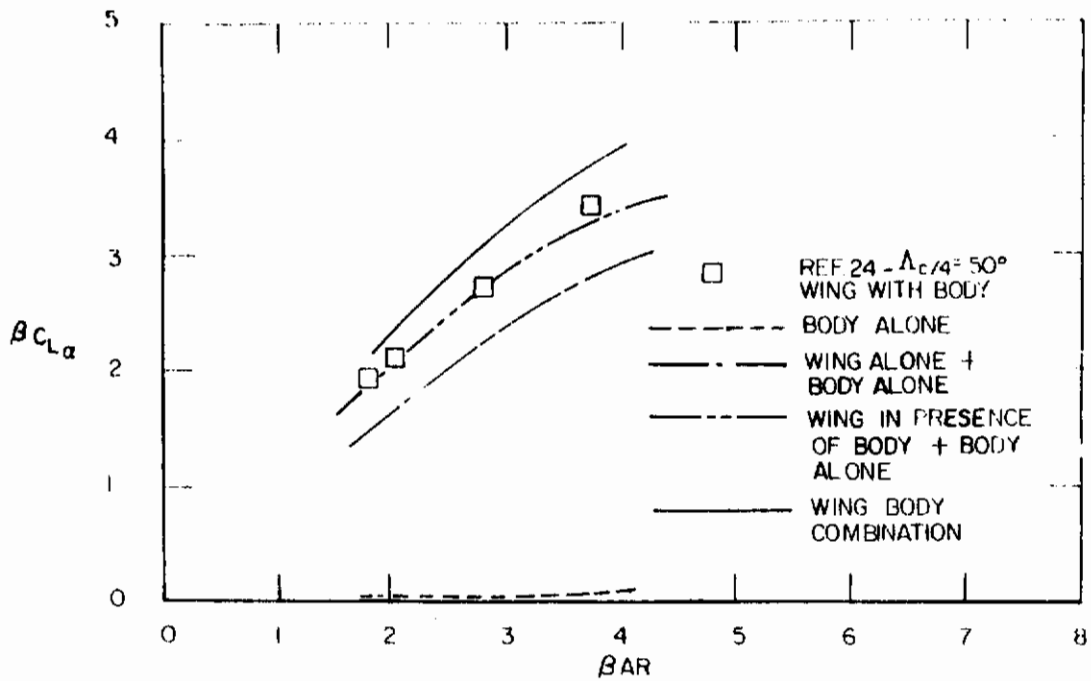
Figure 8.   Reduced Lift Curve Slopes for the $\Lambda_{c/4} = 50°$ High Aspect
Ratio Wing-Body Combination at Various Mach Numbers.
Comparison with Theory
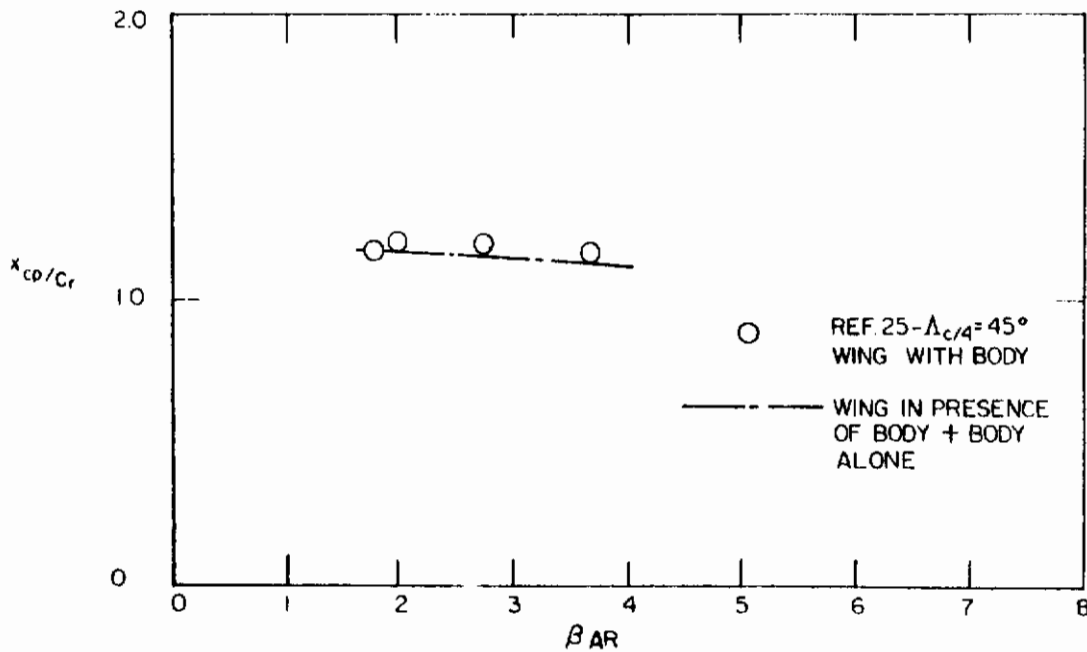
Figure 9.   Center of Pressure Location for the $\Lambda_{c/4} = 50°$ High
Aspect Ratio Wing-Body Combination at Various Mach
Numbers.   Comparison with Theory
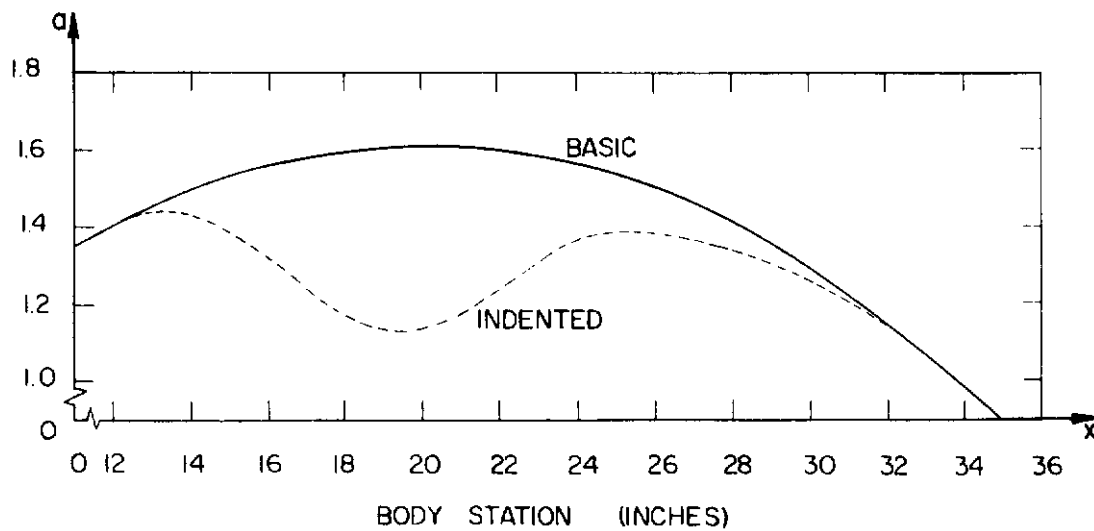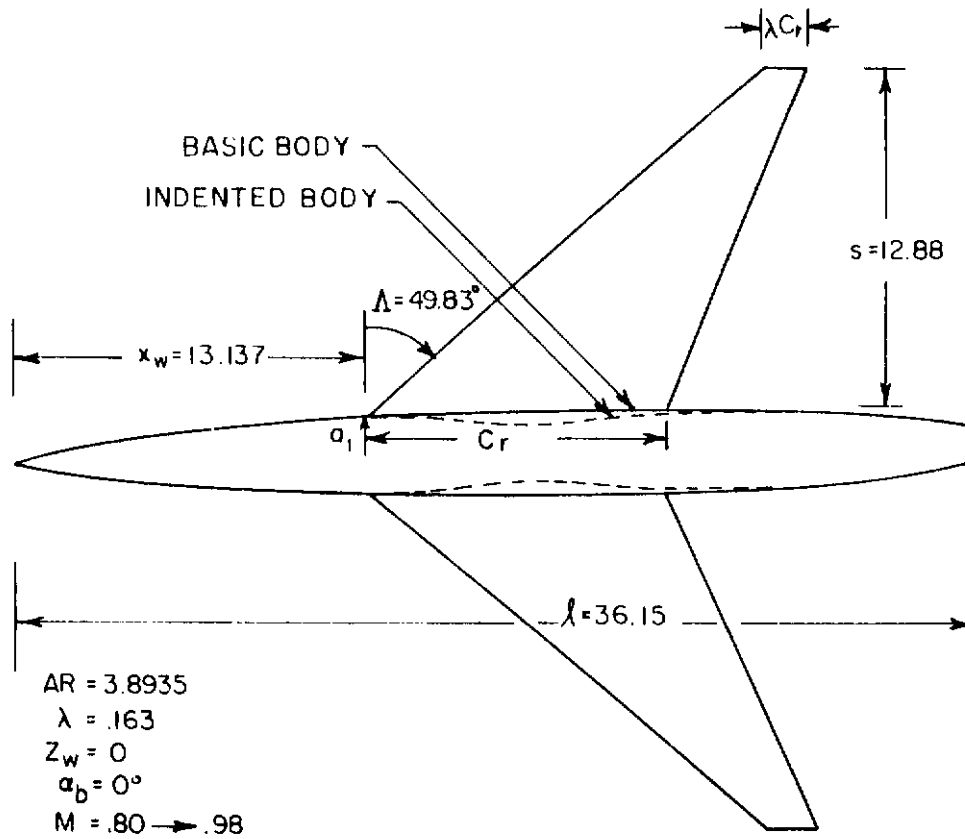
Figure 10.   Model of Ref. 25
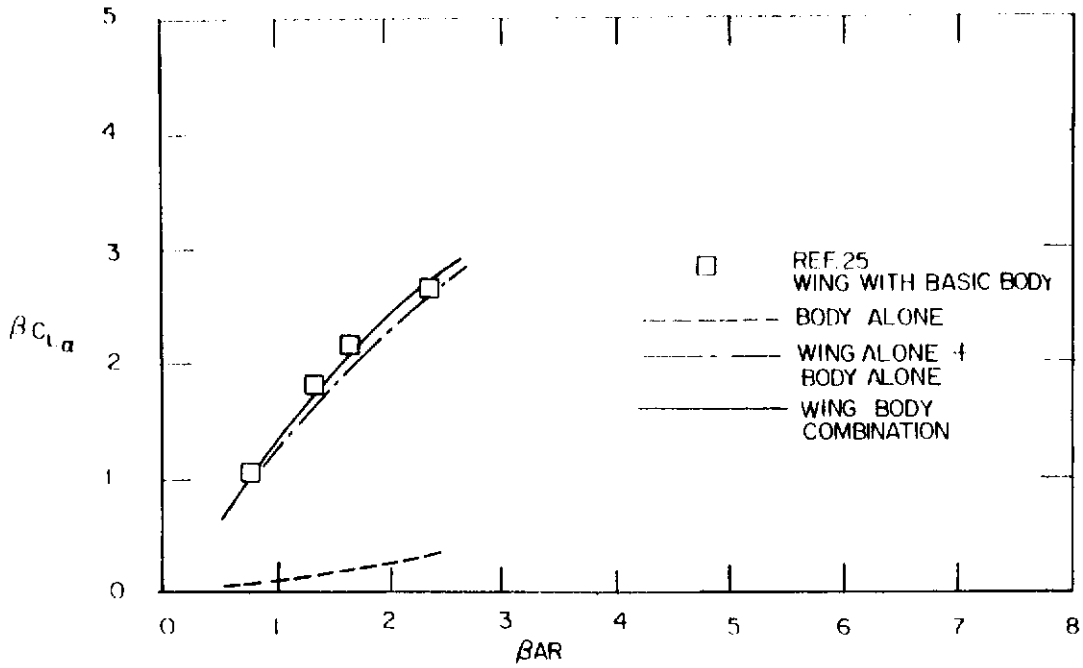
Figure 11. Reduced Lift Curve Slopes for the Medium Aspect Ratio Highly Swept Wing-Basic Body Combination. Comparison with Theory
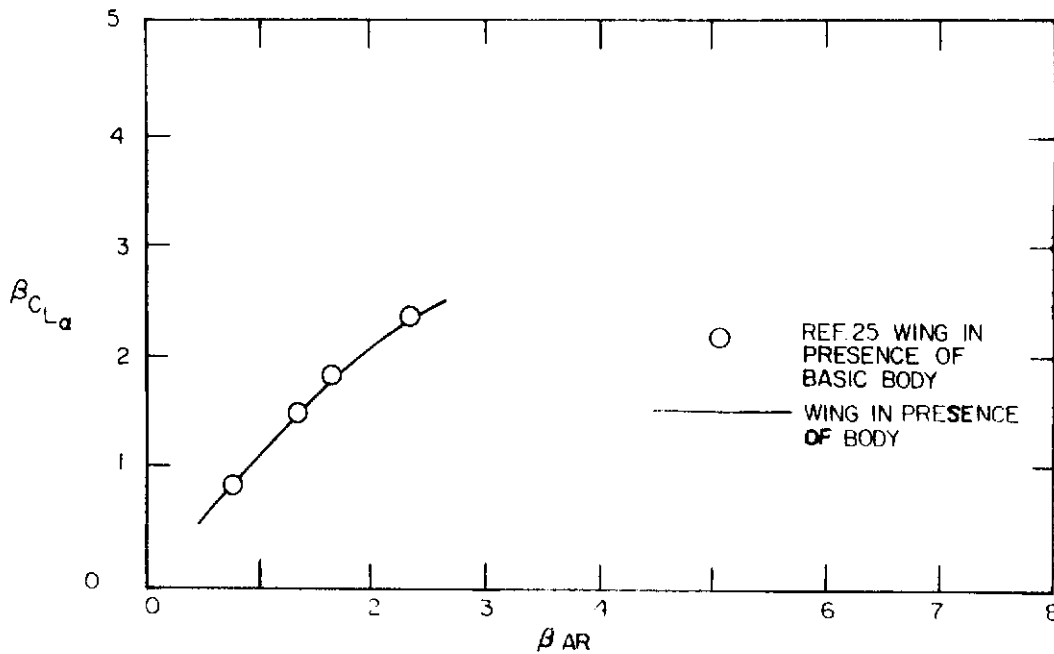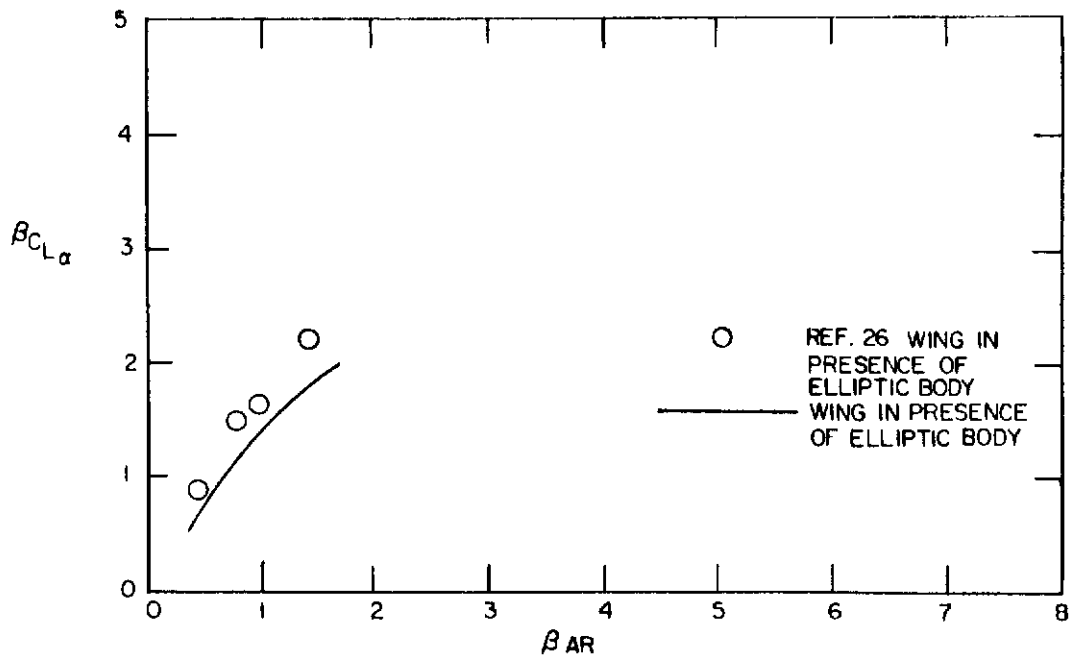

Figure 12. Reduced Lift Curve Slopes for the Medium Aspect Ratio Highly Swept Wing in the Presence of the Basic Body. Comparison with Theory

182
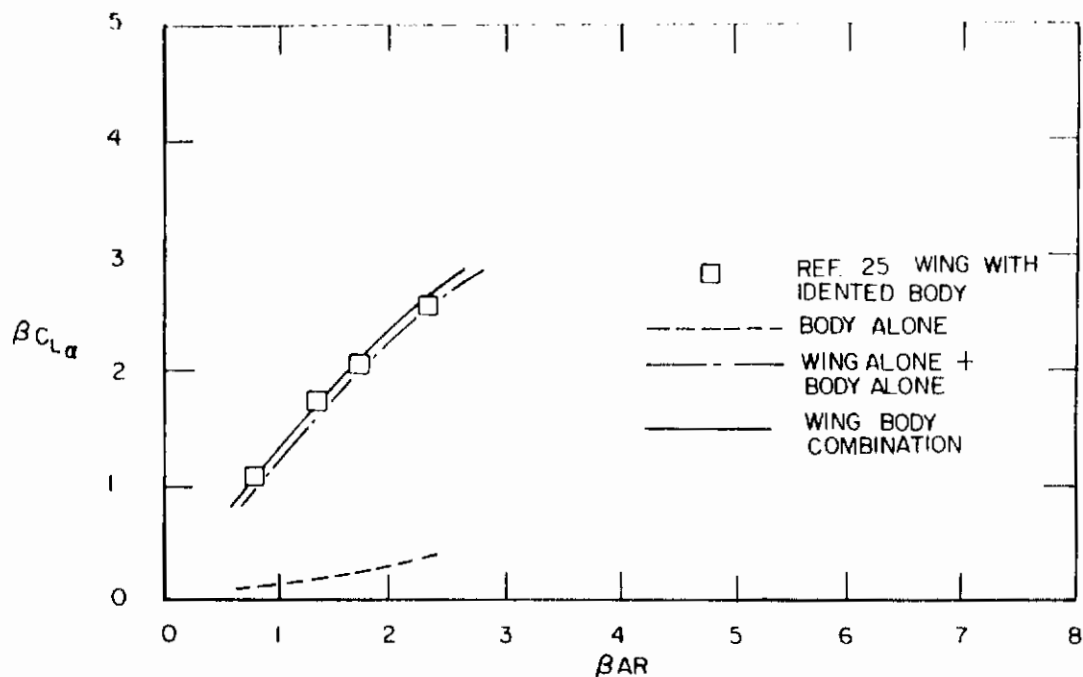
Figure 13. Reduced Lift Curve Slopes for the Medium Aspect Ratio
Highly Swept Wing-Indented Body Combination. Com-
parison with Theory
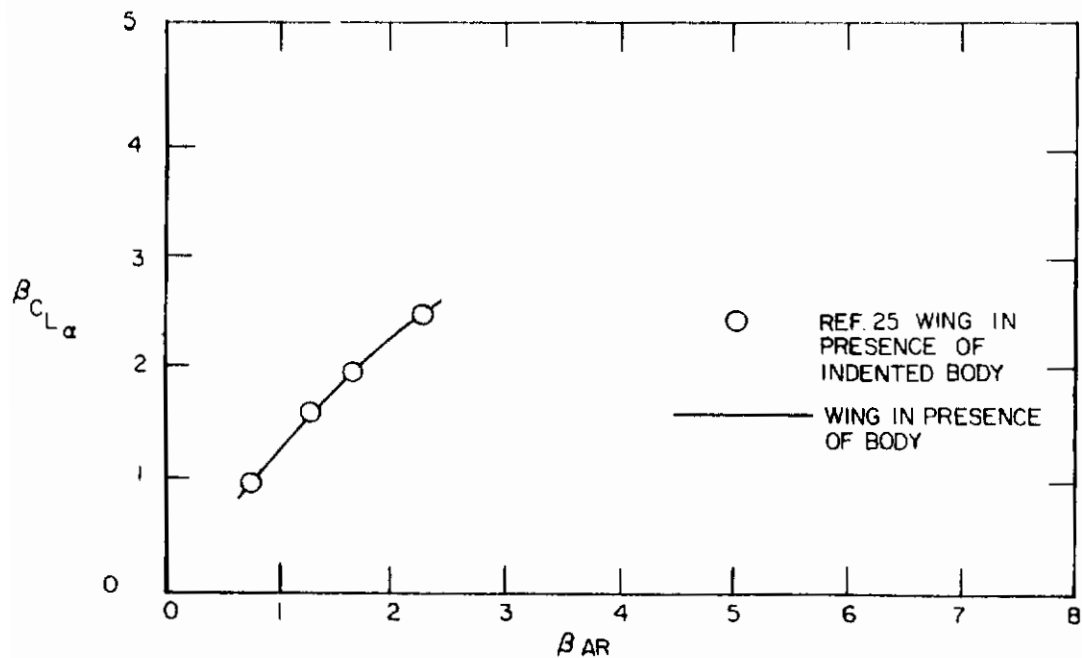
Figure 14. Reduced Lift Curve Slopes for the Medium Aspect Ratio
Highly Swept Wing in the Presence of the Indented Body.
Comparison with Theory

183
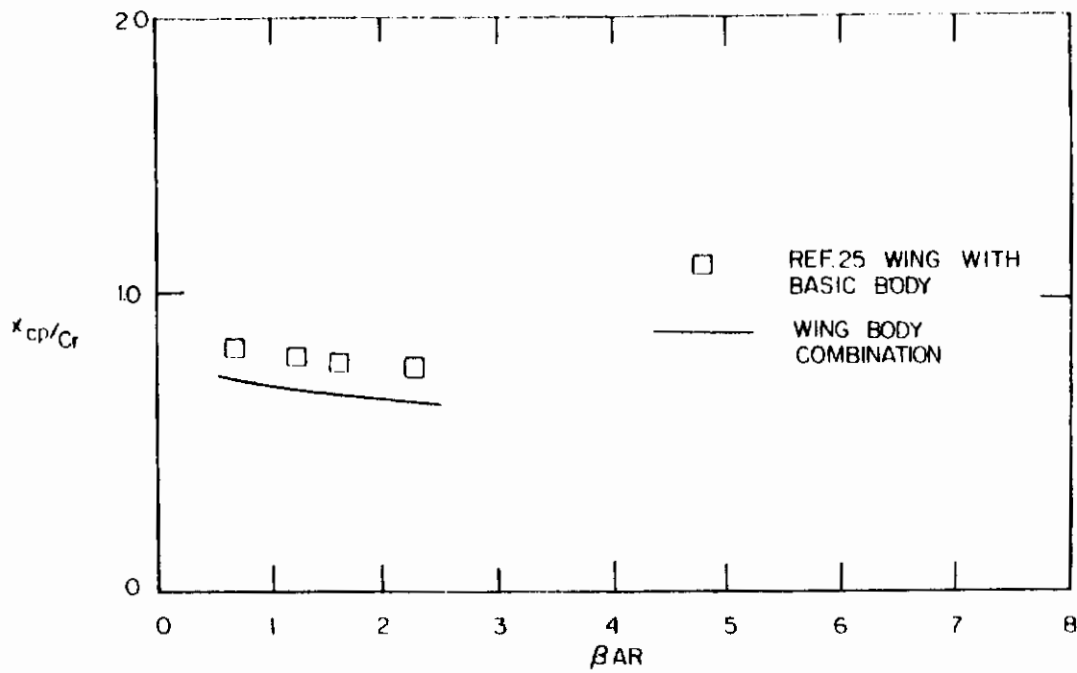
Figure 15.   Center of Pressure Location for the Medium Aspect Ratio
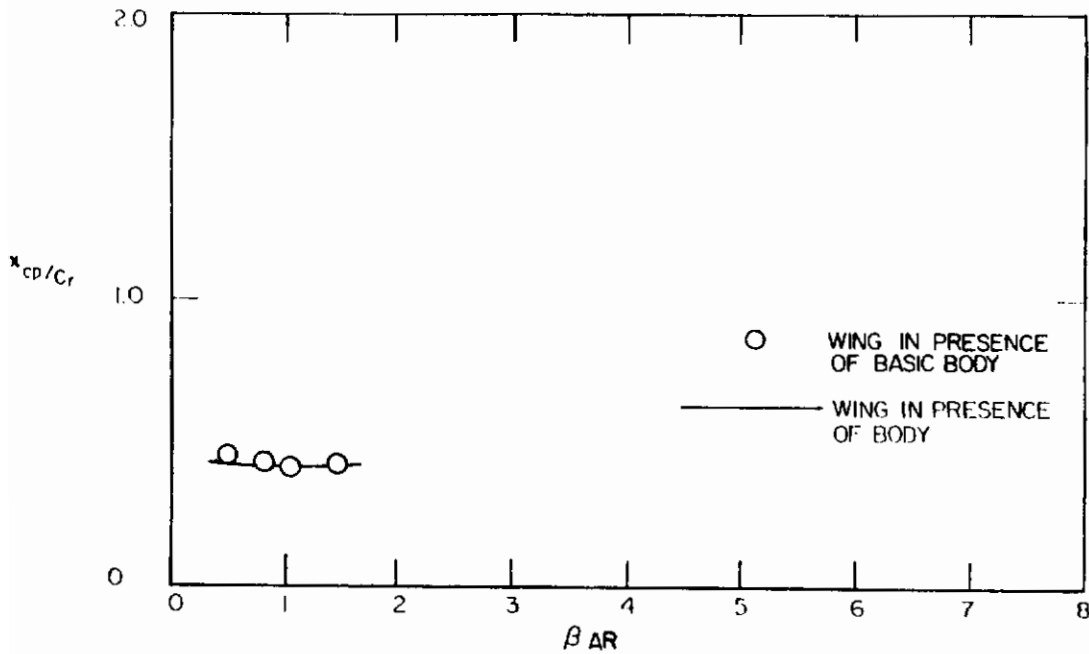Highly Swept Wing-Basic Body Combination.   Compari-
son with Theory
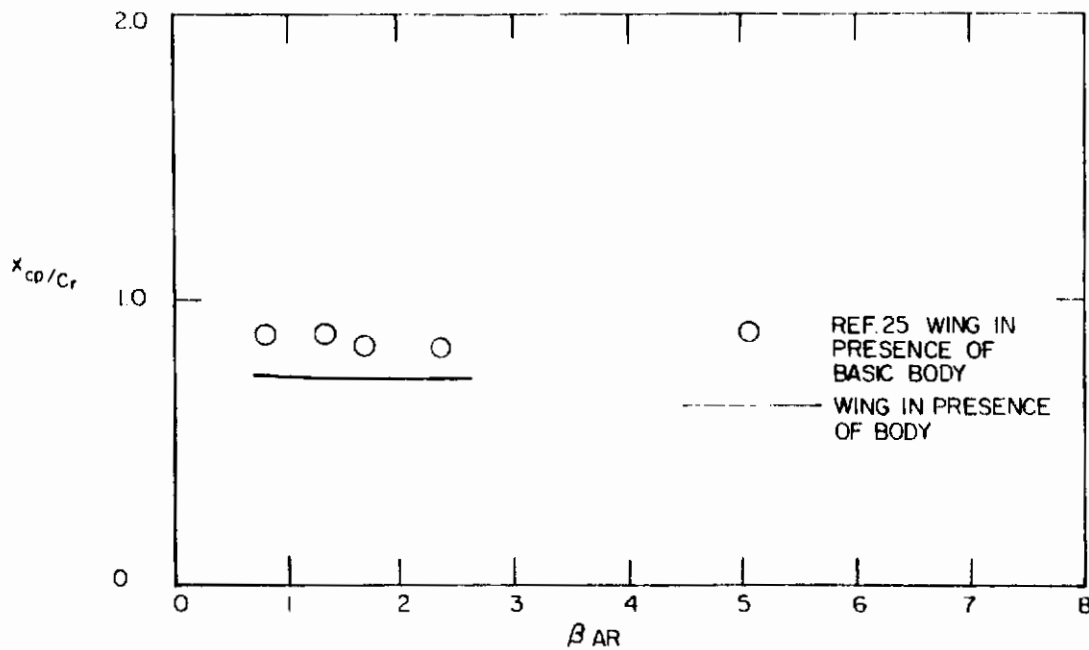
Figure 16.   Center of Pressure Location for the Medium Aspect Ratio
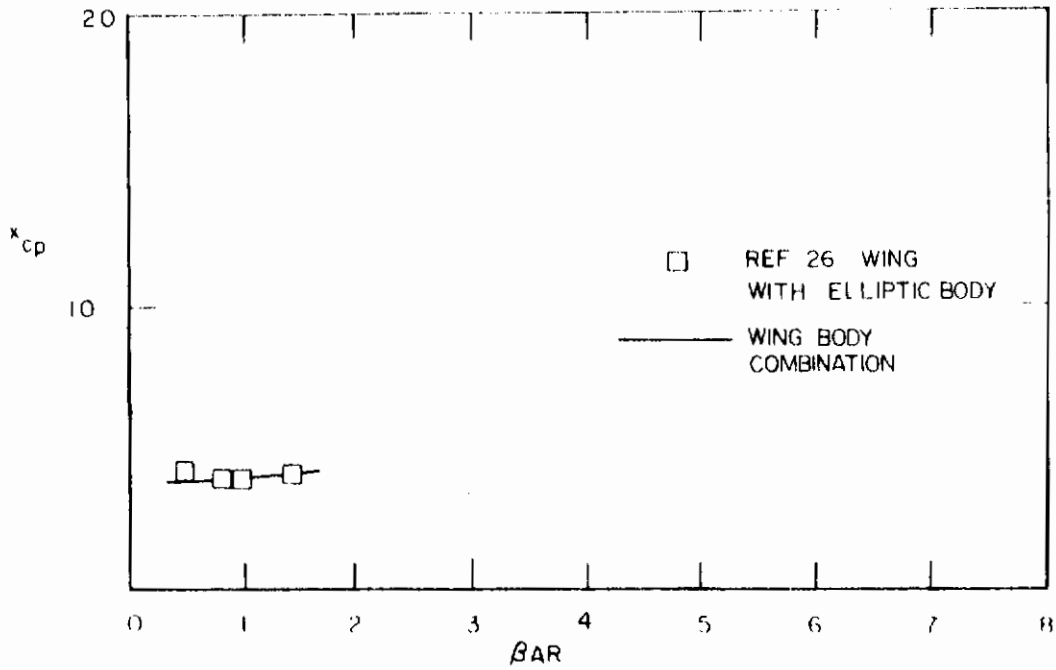Highly Swept Wing in the Presence of the Basic Body.
Comparison with Theory
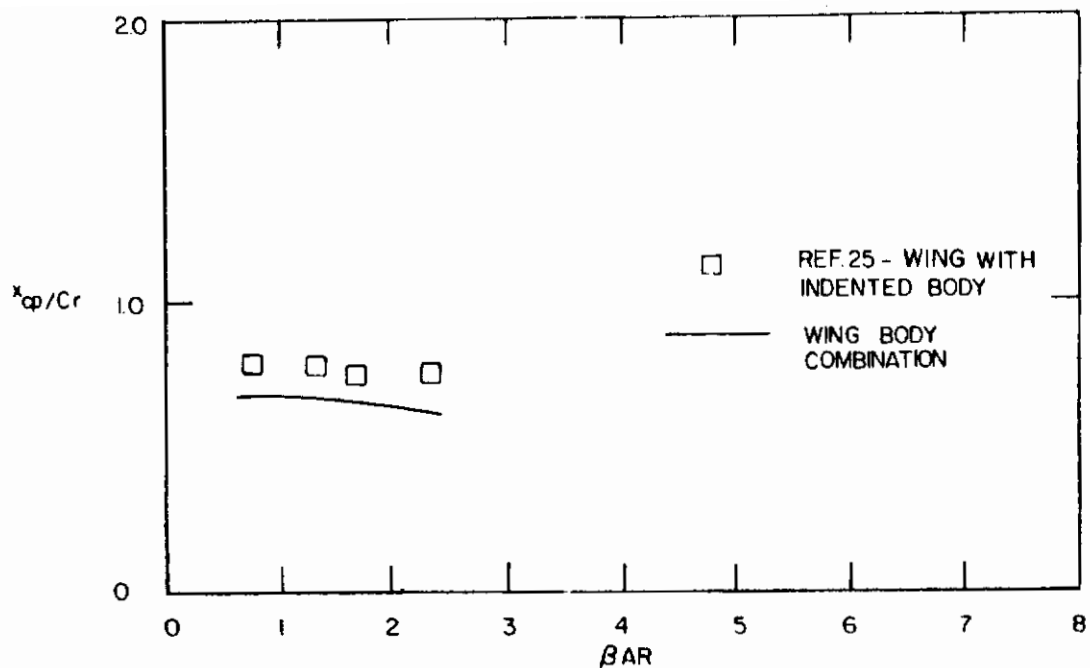
Figure 17. Center of Pressure Location for the Medium Aspect Ratio Highly Swept Wing-Indented Body Combination. Comparison with Theory
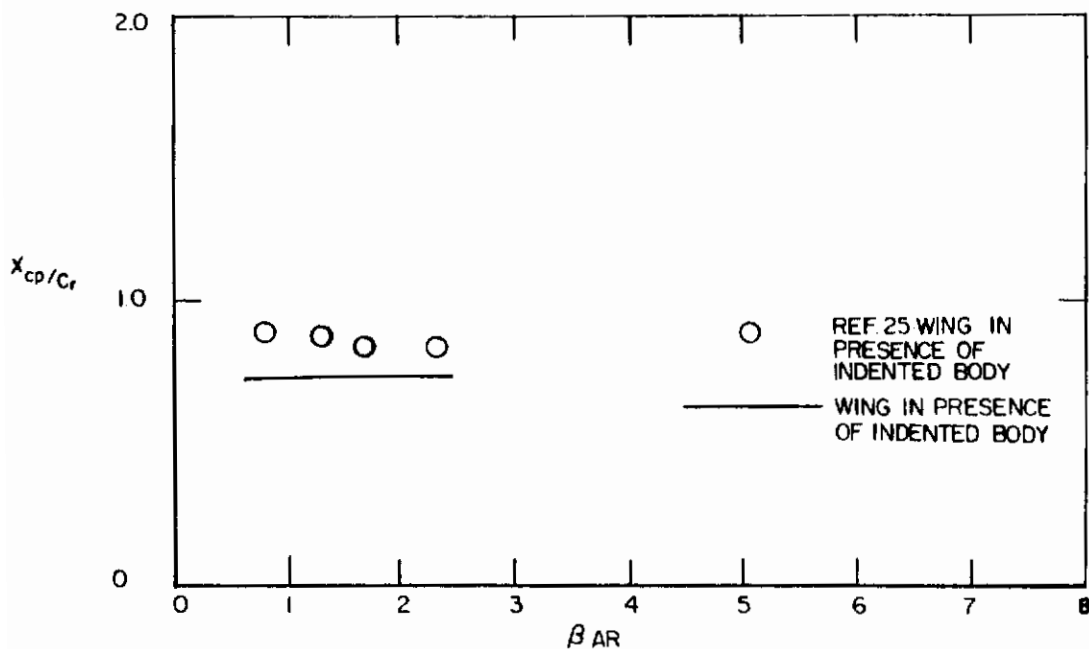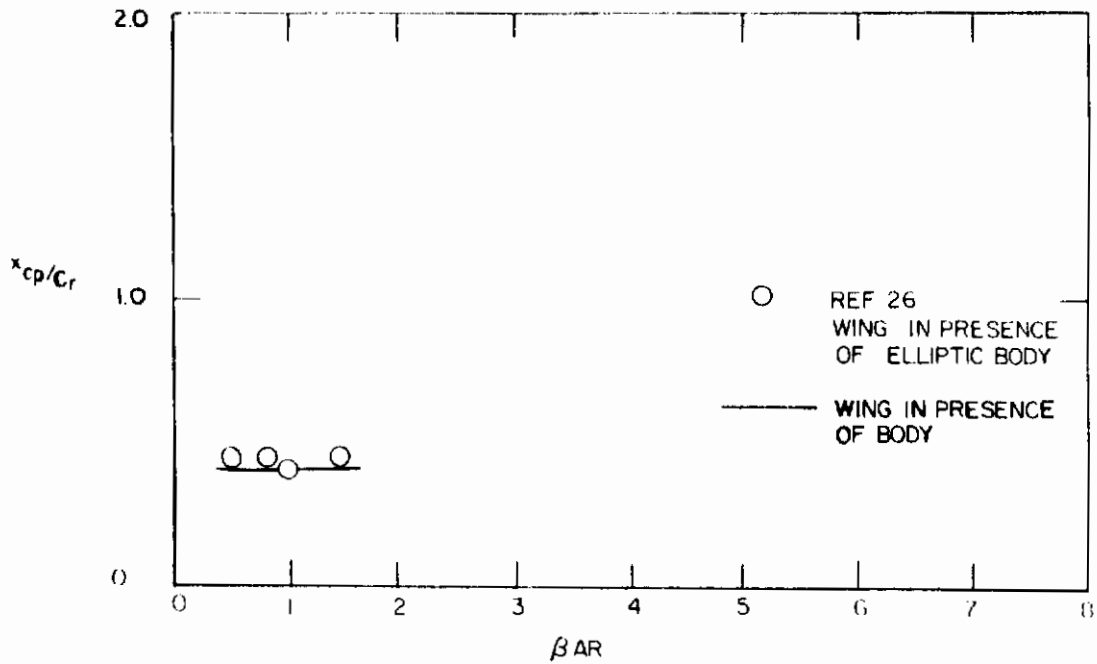

Figure 18. Center of Pressure Location for the Medium Aspect Ratio Highly Swept Wing in the Presence of the Indented Body. Comparison with Theory

185
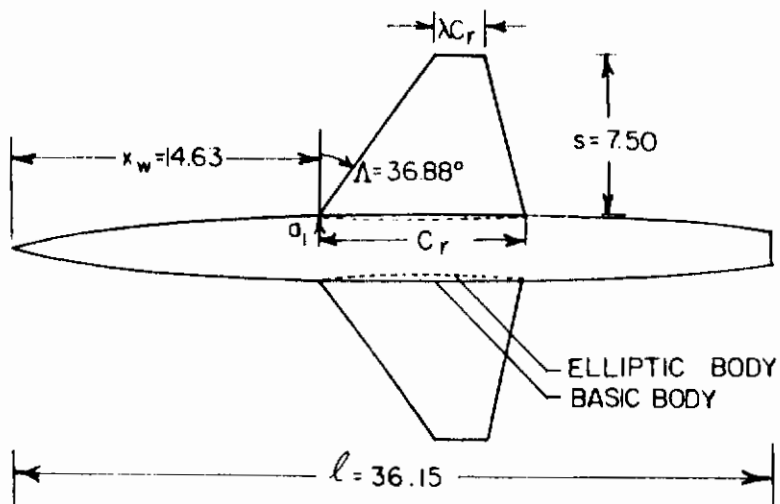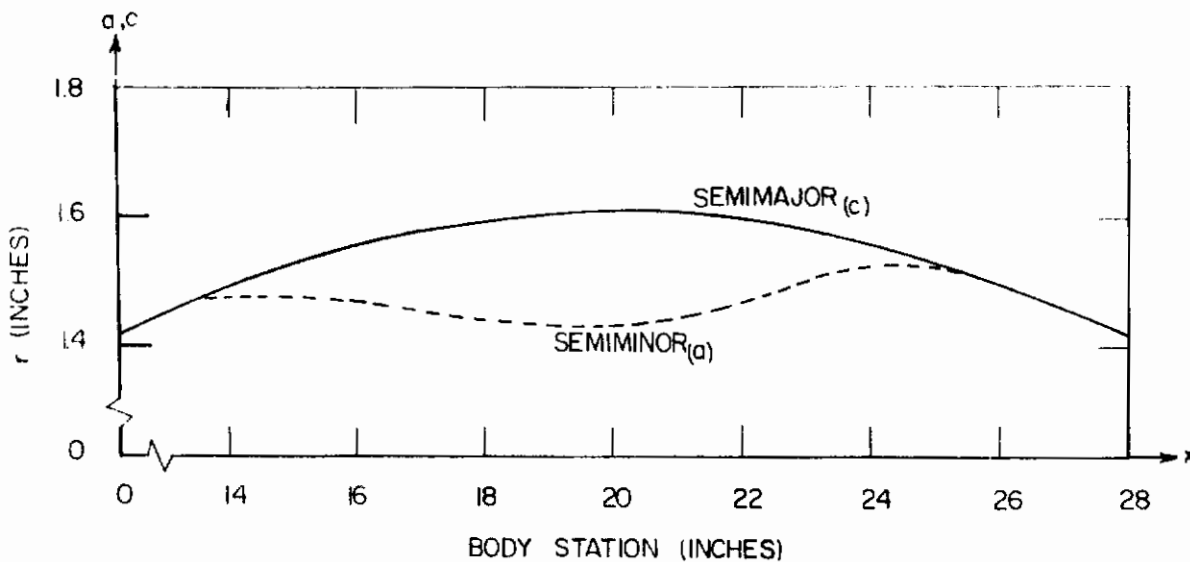
Figure 19. Model of Ref. 26

186
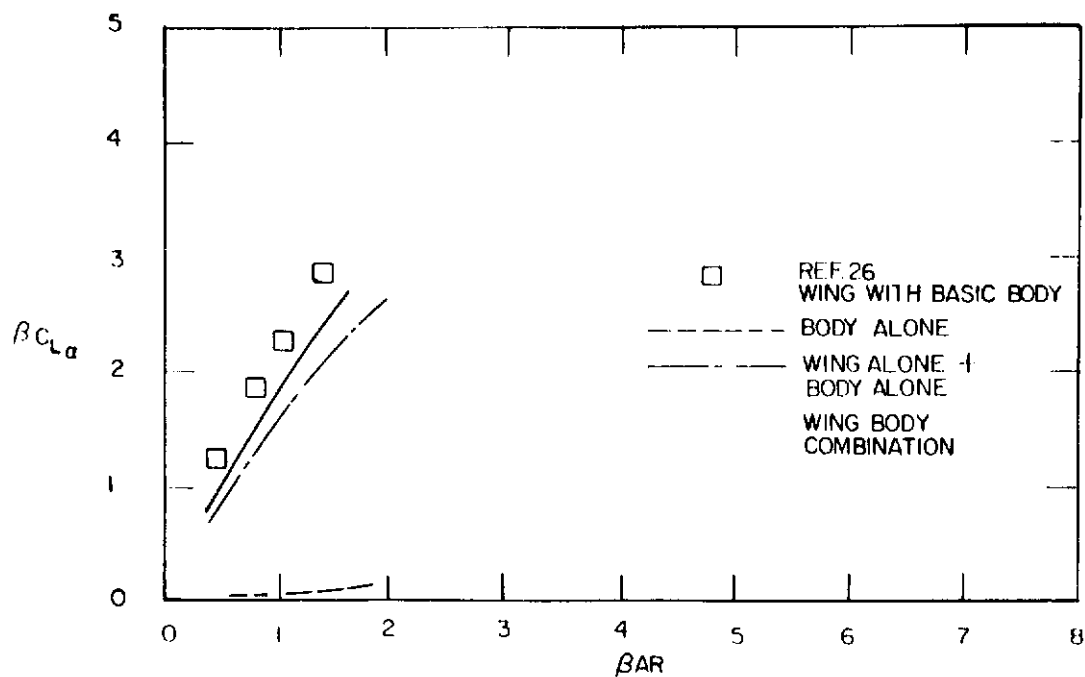
Figure 20. Reduced Lift Curve Slopes for the Medium Aspect
Ratio Relatively Unswept Wing-Basic Body Com-
bination. Comparison with Theory
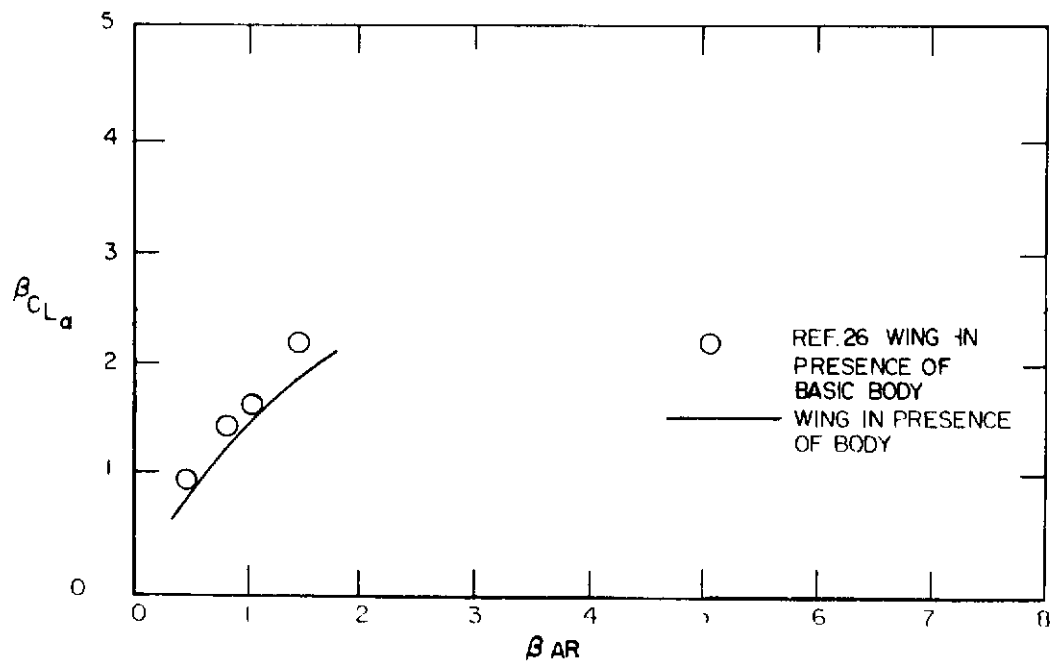
Figure 21. Reduced Lift Curve Slopes for the Medium Aspect
Ratio Relatively Unswept Wing in the Presence of
the Basic Body

187
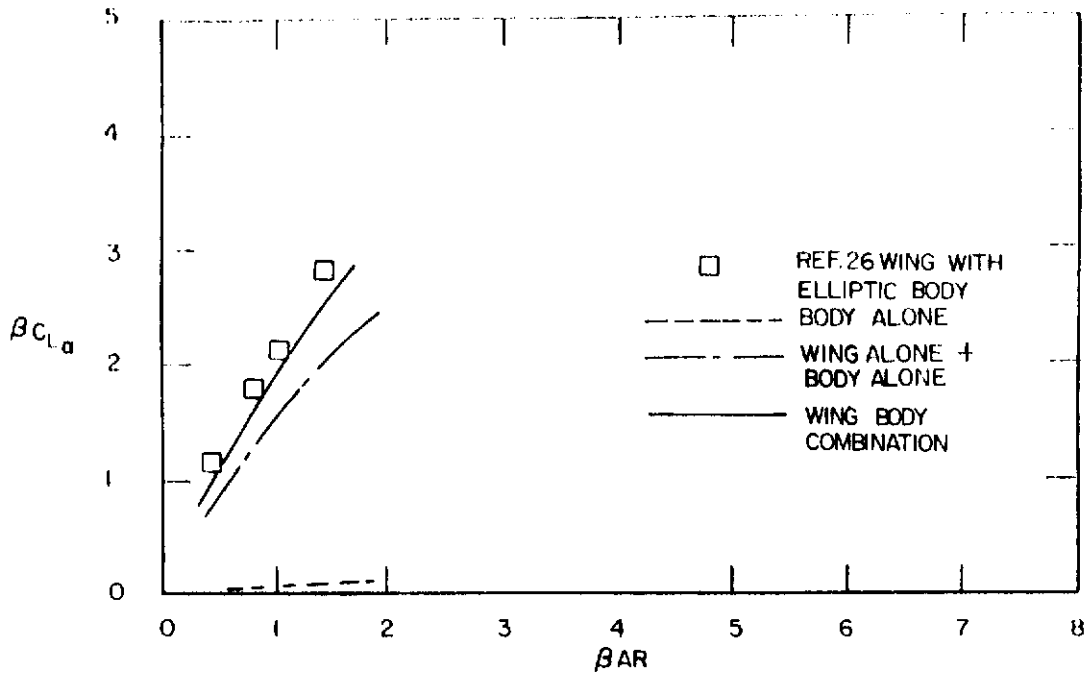
Figure 22. Reduced Lift Curve Slopes for the Medium Aspect Ratio Relatively Unswept Wing-Elliptical Body Combination. Comparison with Theory

Figure 23. Reduced Lift Curve Slopes for the Medium Aspect Ratio Relatively Unswept Wing in the Presence of the Elliptical Body

188
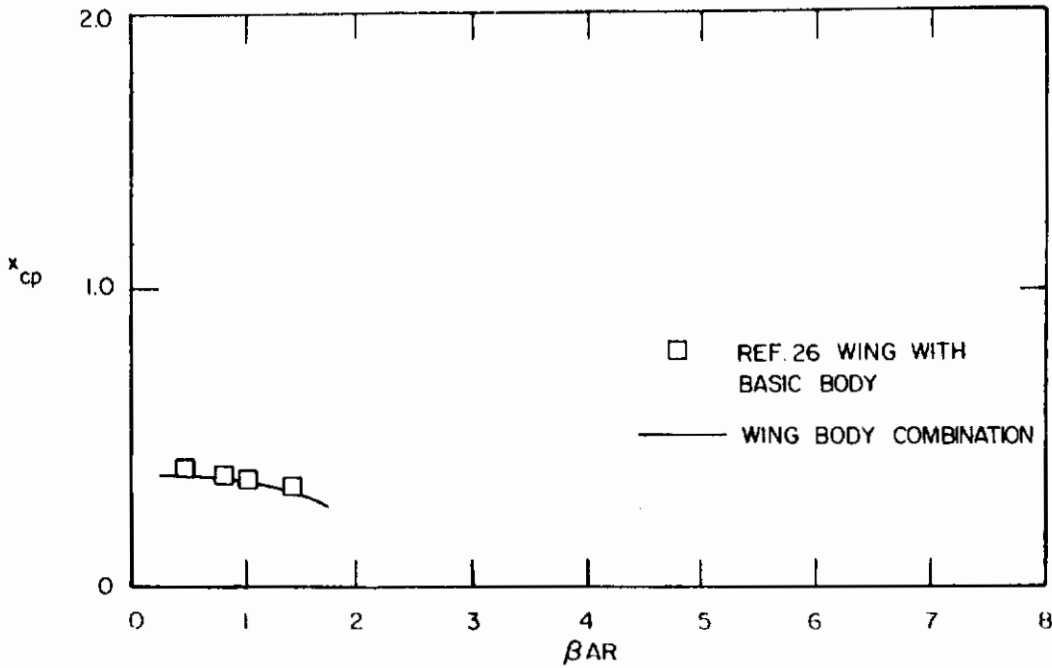
Figure 24. Center of Pressure Location for the Medium Aspect Ratio Relatively Unswept Wing-Basic Body Combination. Comparison with Theory

Figure 25. Center of Pressure Location for the Medium Aspect Ratio Relatively Unswept Wing in the Presence of the Basic Body

189

Figure 26.   Center of Pressure Location for the Medium Aspect Ratio
Relatively Unswept Wing-Elliptical Body Combination.
Comparison with Theory

Figure 27.   Center of Pressure Location for the Medium Aspect Ratio
Relatively Unswept Wing in the Presence of the Elliptical
Body

190
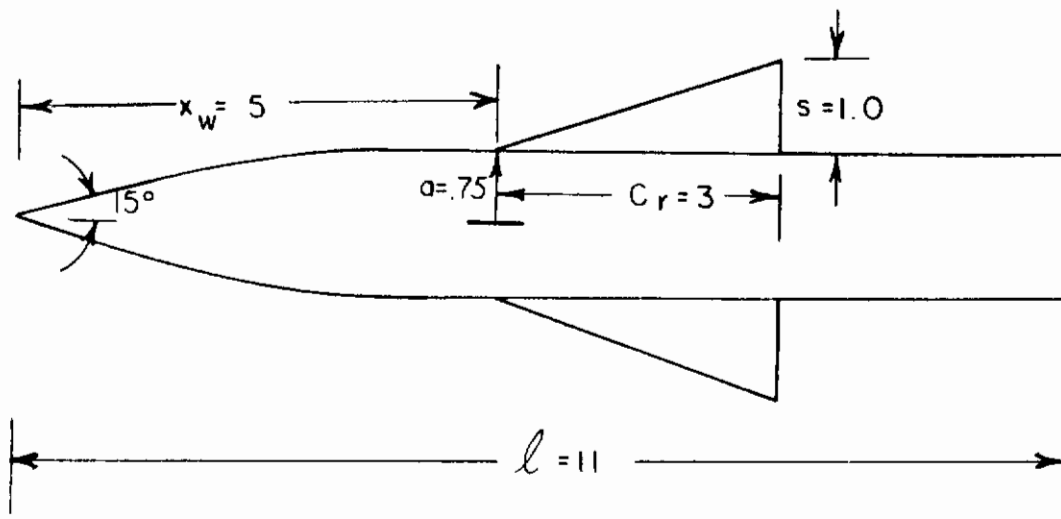
Figure 28.   Model of Ref. 26
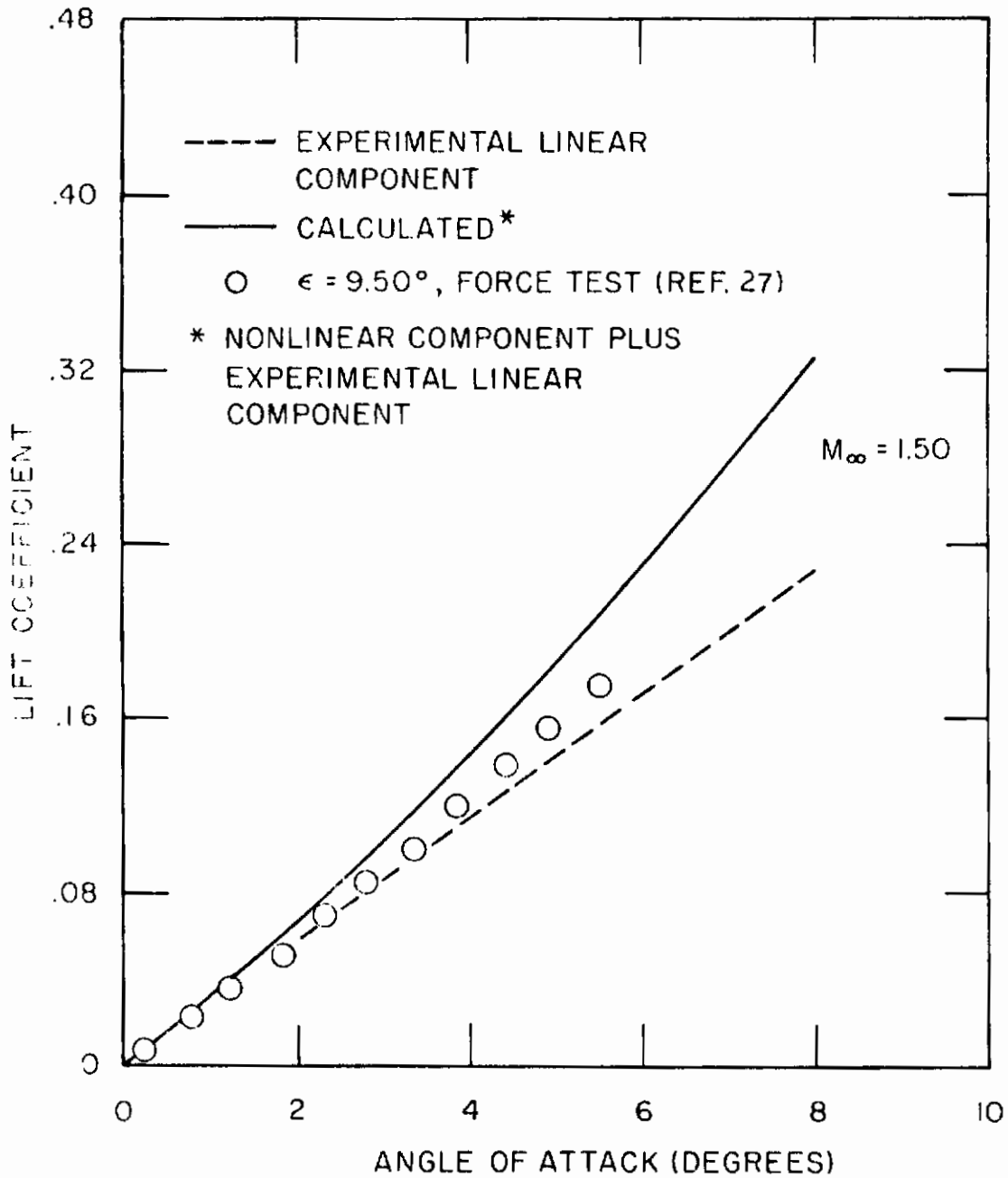
Figure 29.   Variation of Lift Coefficient with Angle of Attack for
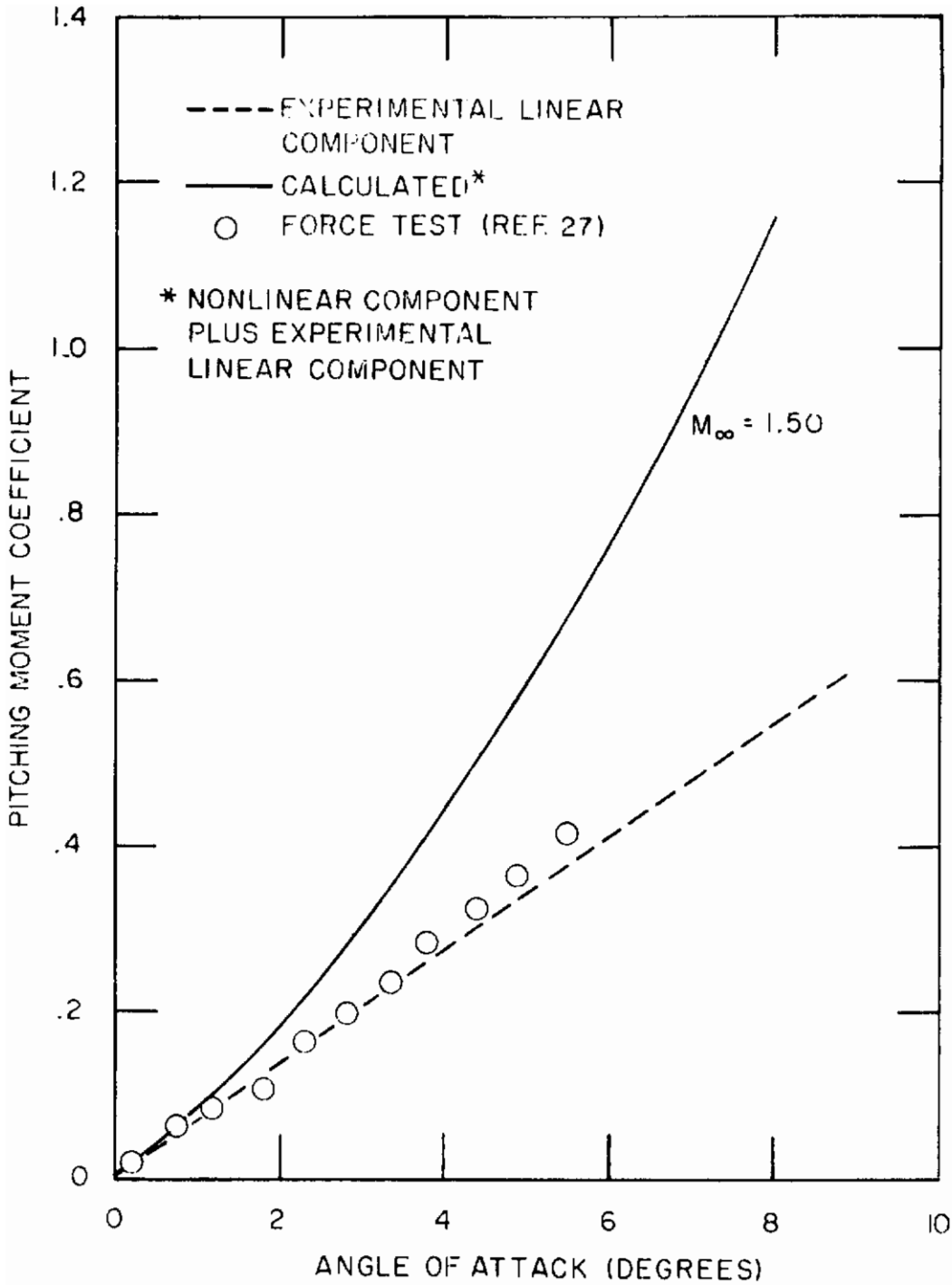a Low Aspect Ratio Wing-Tangent Ogive Cylinder
Combination.   Comparison with Theory

Figure 30. Variation of Pitching Moment Coefficient with Angle of Attack for a Low Aspect Ratio Wing-Tangent Ogive Cylinder Combination. Comparison with Theory
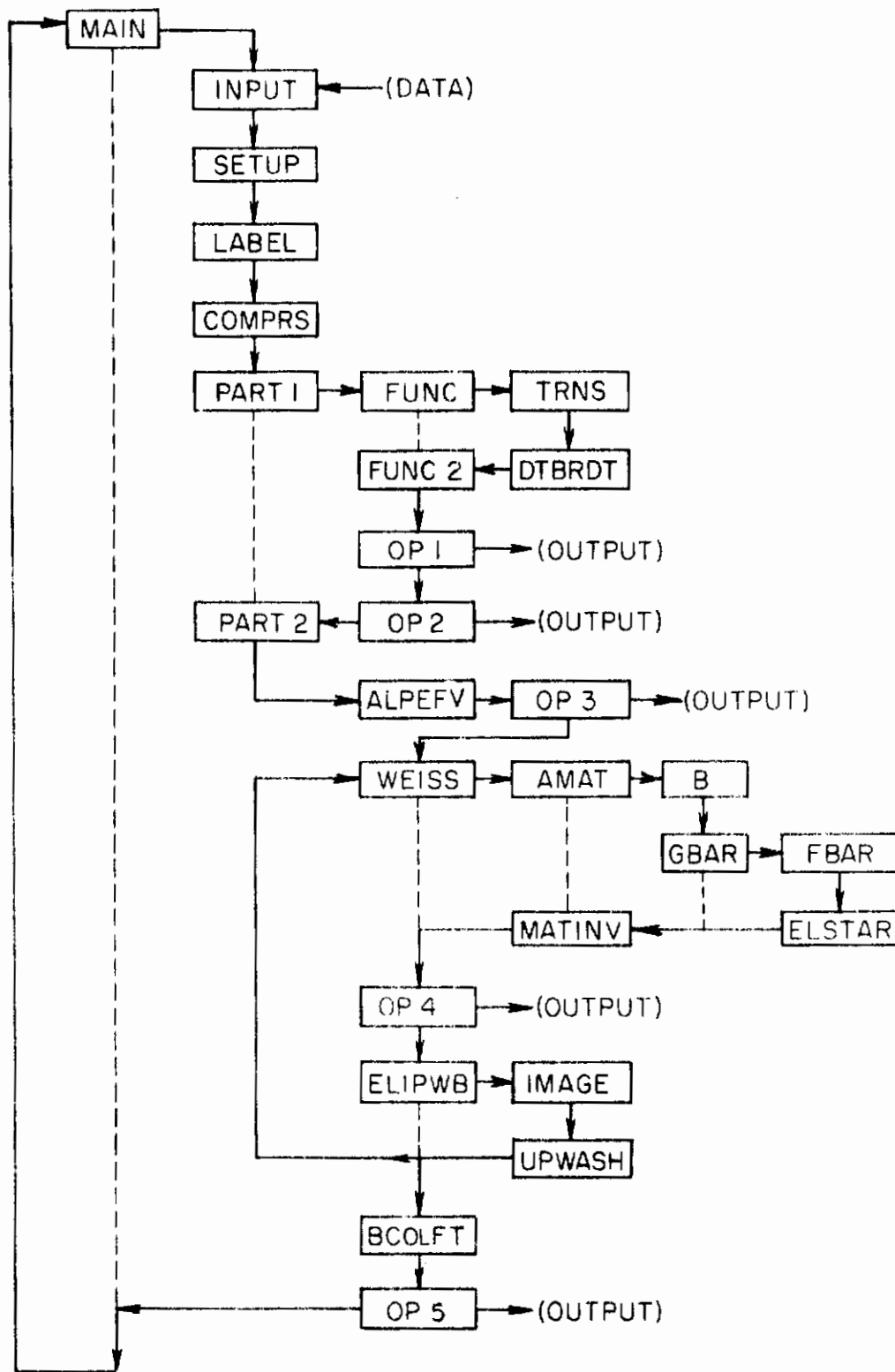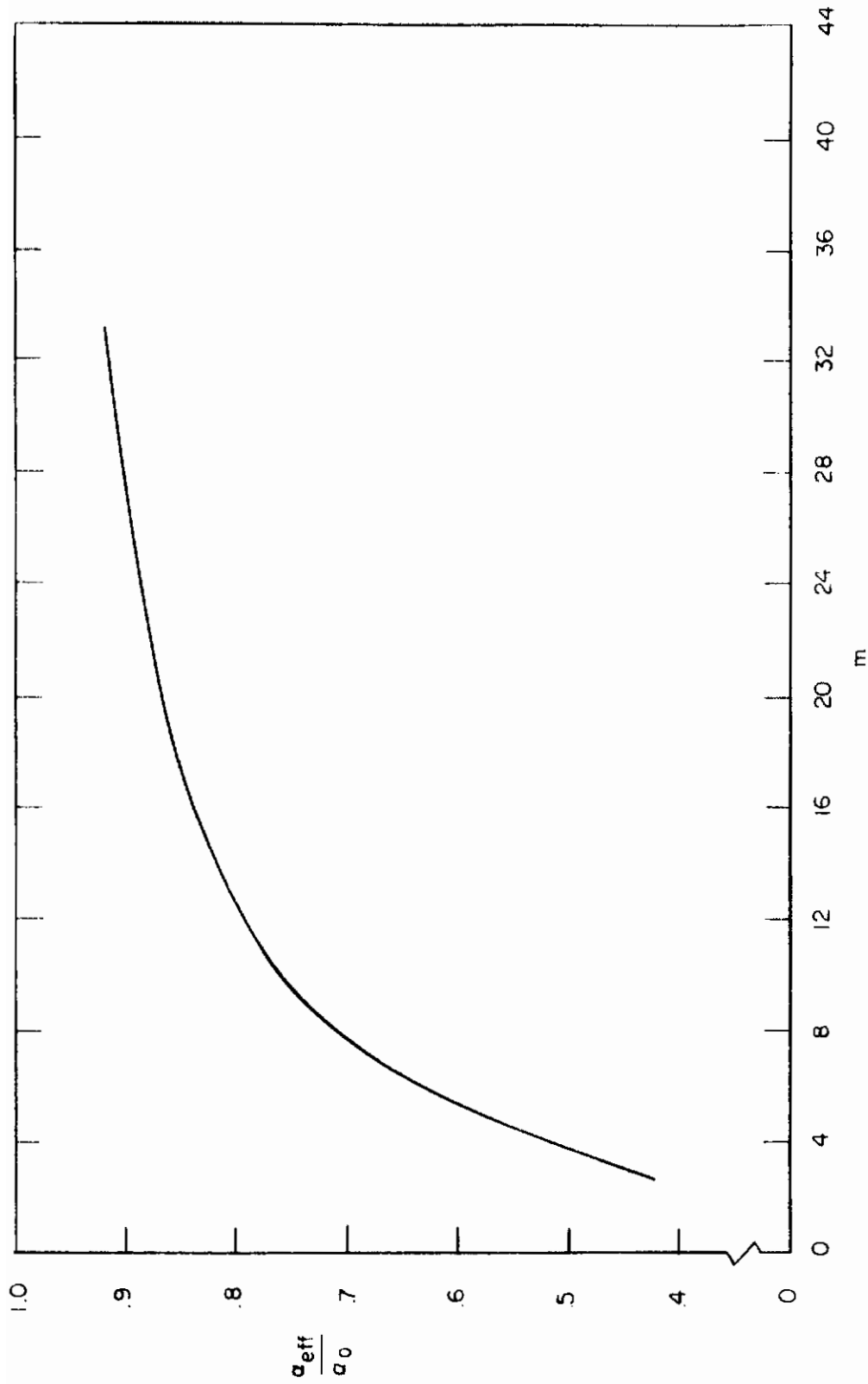
Figure 31. Computer Program Flow Chart

Figure 32. Results of Numerical Approximation to Cauchy
Principal Value Integral

DOCUMENT CONTROL DATA - R&D

(Security classification of title body of abstract and indexing annotation must be entered when the overall report is classified)

1 ORIGINATING ACTIVITY (Corporate author)	2a REPORT SECURITY CLASSIFICATION
Massachusetts Institute of Technology 560 Memorial Drive Cambridge 39, Massachusetts	Unclassified
	2b GROUP

3. REPORT TITLE

METHODS OF CALCULATING AERODYNAMIC LOADS ON AIRCRAFT STRUCTURES: PART I – WING-BODY INTERFERENCE EFFECTS

4 DESCRIPTIVE NOTES (Type of report and inclusive dates)

Final Report; January 4, 1965 – January 3, 1966

5 AUTHOR(S) (Last name, first name, initial)

Borland, Christopher J.

6. REPORT DATE	7a. TOTAL NO. OF PAGES	7b. NO. OF REFS
August 1966	195 + xiv	33

8a. CONTRACT OR GRANT NO. AF 33(615)-2291 b. PROJECT NO. 1367 c. Task No. 136715 d.	9a. ORIGINATOR'S REPORT NUMBER(S) AFFDL-TR-66-37, Part I 9b. OTHER REPORT NO(S) (Any other numbers that may be assigned this report) TR 120

10 AVAILABILITY/LIMITATION NOTICES

This document is subject to special export controls and each transmittal to foreign governments or foreign nationals may be made only with prior approval of Air Force Flight Dynamics Laboratory(FDTR), Wright-Patterson AFB, Ohio

11. SUPPLEMENTARY NOTES	12. SPONSORING MILITARY ACTIVITY Air Force Flight Dynamics Laboratory (FDTR), Wright-Patterson AFB, Ohio

13 ABSTRACT

Methods are proposed for calculating the distribution of aerodynamic loads due to mutual interference effects between wings and bodies The methods fall into two ranges of applicability: linear, and nonlinear, with angle of attack.

Applicability of the linear loads methods to aeroelastic calculations is discussed. A computer program is presented which may be used to calculate interference loads at subsonic Mach numbers on a configuration consisting of (1) a body of any varying elliptic cross section and camber distribution, and (2) a wing with straight leading and trailing edges of any sweep angle, twist distribution, and camber distribution, located above or below the body centerline. Extension to the supersonic case is indicated. Generally good agreement with experimental data is found.

Nonlinear wing-body interference loads are also considered. Several possible methods of representing the separated flow about a wing-body combination are proposed, and analyzed by the slender body theory. Numerical procedures are outlined, and some comparisons with experimental data are made. Agreement is somewhat less than satisfactory.

Recommendations are made for further analytic extensions and improvements, and for additional experimental studies.

.14 KEY WORDS	LINK A		LINK B		LINK C	
	ROLE	WT	ROLE	WT	ROLE	WT

INSTRUCTIONS

1. ORIGINATING ACTIVITY: Enter the name and address of the contractor, subcontractor, grantee, Department of Defense activity or other organization (corporate author) issuing the report.

2a. REPORT SECURITY CLASSIFICATION: Enter the overall security classification of the report. Indicate whether "Restricted Data" is included. Marking is to be in accordance with appropriate security regulations.

2b. GROUP: Automatic downgrading is specified in DoD Directive 5200.10 and Armed Forces Industrial Manual. Enter the group number. Also, when applicable, show that optional markings have been used for Group 3 and Group 4 as authorized.

3. REPORT TITLE: Enter the complete report title in all capital letters. Titles in all cases should be unclassified. If a meaningful title cannot be selected without classification, show title classification in all capitals in parenthesis immediately following the title.

4. DESCRIPTIVE NOTES: If appropriate, enter the type of report, e.g., interim, progress, summary, annual, or final. Give the inclusive dates when a specific reporting period is covered.

5. AUTHOR(S): Enter the name(s) of author(s) as shown on or in the report. Enter last name, first name, middle initial. If military, show rank and branch of service. The name of the principal author is an absolute minimum requirement.

6. REPORT DATE: Enter the date of the report as day, month, year; or month, year. If more than one date appears on the report, use date of publication.

7a. TOTAL NUMBER OF PAGES: The total page count should follow normal pagination procedures, i.e., enter the number of pages containing information.

7b. NUMBER OF REFERENCES: Enter the total number of references cited in the report.

8a. CONTRACT OR GRANT NUMBER: If appropriate, enter the applicable number of the contract or grant under which the report was written.

8b, 8c, & 8d. PROJECT NUMBER: Enter the appropriate military department identification, such as project number, subproject number, system numbers, task number, etc.

9a. ORIGINATOR'S REPORT NUMBER(S): Enter the official report number by which the document will be identified and controlled by the originating activity. This number must be unique to this report.

9b. OTHER REPORT NUMBER(S): If the report has been assigned any other report numbers (either by the originator or by the sponsor), also enter this number(s).

10. AVAILABILITY/LIMITATION NOTICES: Enter any limitations on further dissemination of the report, other than those

imposed by security classification, using standard statements such as:

(1) "Qualified requesters may obtain copies of this report from DDC."

(2) "Foreign announcement and dissemination of this report by DDC is not authorized."

(3) "U. S. Government agencies may obtain copies of this report directly from DDC. Other qualified DDC users shall request through

_____."

(4) "U. S. military agencies may obtain copies of this report directly from DDC. Other qualified users shall request through

_____."

(5) "All distribution of this report is controlled. Qualified DDC users shall request through

_____."

If the report has been furnished to the Office of Technical Services, Department of Commerce, for sale to the public, indicate this fact and enter the price, if known.

11. SUPPLEMENTARY NOTES: Use for additional explanatory notes.

12. SPONSORING MILITARY ACTIVITY: Enter the name of the departmental project office or laboratory sponsoring (paying for) the research and development. Include address.

13. ABSTRACT: Enter an abstract giving a brief and factual summary of the document indicative of the report, even though it may also appear elsewhere in the body of the technical report. If additional space is required, a continuation sheet shall be attached.

It is highly desirable that the abstract of classified reports be unclassified. Each paragraph of the abstract shall end with an indication of the military security classification of the information in the paragraph, represented as (TS), (S), (C), or (U).

There is no limitation on the length of the abstract. However, the suggested length is from 150 to 225 words.

14. KEY WORDS: Key words are technically meaningful terms or short phrases that characterize a report and may be used as index entries for cataloging the report. Key words must be selected so that no security classification is required. Identifiers, such as equipment model designation, trade name, military project code name, geographic location, may be used as key words but will be followed by an indication of technical context. The assignment of links, rules, and weights is optional.

GPO 886-551